Live-Cell Imaging of Human Oocytes and Regulation of Cohesin Removal in Meiosis II

Mahdi Lamb
Biosciences Institute, Newcastle University

A thesis submitted for the degree of Doctor of Philosophy, April 20

Abstract

The “maternal age effect” describes the striking increase in risk of miscarriage and chromosomally abnormal embryos and children from women older than 35. Studies in mice have shown that the protein complex Cohesin is reduced in an age-dependent manner. This protein complex ensures accurate segregation during both rounds of meiosis, by holding the chromosomes together and providing a counteracting force to spindle microtubules.

Despite a wealth of knowledge generated from human oocytes, there are few live-cell studies, in part due to the paucity of material. This thesis uses human oocytes specifically donated for research to assess the effect of age on alignment of chromosomes at metaphase I and -II, which is a predictor of missegregation. Using high-resolution live-cell microscopy, it is clear that increased age is associated with chromosomes that are misaligned in metaphase I and -II.

At metaphase II, eggs arrest until they are fertilised by sperm. The regulation of how chromosomes separate at this point is poorly understood. While the bulk of Cohesin is removed in anaphase I, a small amount is “protected” by Shugoshin 2 and remains between the centromeres to allow for faithful segregation in meiosis II. Currently, there is poor experimental work to support the hypotheses proposed to explain how the mechanisms that protect Cohesin in meiosis I are removed in meiosis II. One of these hypotheses is the requirement of spindle tension to separate the protector, Shugoshin 2, from Cohesin in meiosis II. Here, I show that spindle tension is not required for deprotection and that alternative models should be considered, such as one which suggests that higher-order regulation around meiosis II resumption is orchestrated by the Anaphase Promoting Complex and its coactivator Cdc20, APC/C^{Cdc20}, a protein complex that is active at anaphase onset.

Acknowledgements

I would like to thank Prof Mary Herbert for providing the opportunity to perform the work in this thesis. Dr Wolfgang Zachariae has been a guiding light during my time in research, and I owe a lot to him for his guidance in my professional and personal development. I would also like to thank Dr Jo Elson for her time in supervising my studies.

I am grateful to Prof Jon Higgins, Prof David Elliot, and Dr Alison Tyson-Capper, who have been a cornerstone of support throughout. Naturally, I would like to thank members of the Herbert group. Especially Barbora Badurova, Abigail Hedquist-Hall, Jordan Marley, Dr Yuko Takeda, and Dr Linlin Wang (in no specific order), for helping me stay level-headed during this process and reminding me of the importance of symbiotic, nurturing relationships.

The staff at the Newcastle Fertility Centre have recruited and supported patients/donors, without whom I would not have been able to study human oocytes for this thesis. Of course, I am very grateful to the patients and donors themselves. Without the staff at the Functional Genomics Unit, the mouse work could not have been performed, so I am also grateful for their tireless efforts in looking after the many mice that have been sacrificed for this study. I would also like to thank Prof Hanhui Ma for providing the ß-satellite sgRNA sequence, and Dr Anna Kuznetsova for helpful discussions on working with mouse oocytes and eggs.

From a personal point, I have learnt a huge amount of humility and endless other lessons from friends and family, both near and far. Dr Kristine Oleinika is one of my oldest friends and strongly encouraged me to return to academia when I felt ready to move on. Imants Latkovskis has been a great confidant for the better part of a decade.

Friends during my undergraduate degree in Glasgow – Carlo van den Heuvel, Andrew McCartan, Sophie Williams – showed me what it was to have a place I could call *my* home. Returning to my hometown, I was worried I could never claim my parents' home as my own, so I am grateful for my friends here – Natalie Miles, Lander Velazquez, Sam Bolton – for the warmth that showed me this was not true. This list of friends is by no means exhaustive – I have been lucky enough to cross paths with many people along the way and I am grateful to have travelled this journey with them.

Statement of Originality

All work contained in this thesis was performed by myself except for the clinical procedures involved in the retrieval of human oocytes, which were carried out by the clinical team at Newcastle Fertility Centre (see 3.4), and a few technical tasks when experiments were run in parallel (Dr Lisa Lister who assisted in removing cumulus cells from human oocytes; Liliana Martin Guillen who assisted in dish set-up; and Abigail Hedquist-Hall who assisted in *in vitro* transcription). An early confocal time-lapse microscopy experiment was assisted by Dr Alex Laude (Bioimaging Unit, Newcastle University). The groundwork for setting up the Zeiss LSM880 microscope with Airyscan was provided by Dr Nicolas Sergent (Carl Zeiss microscopy), who further assisted through discussions about macro development for the microscope.

Where work has been carried out by others, citations have been provided either in the main text or figure legends, where appropriate. When copyrighted materials have been used, an attribution has been provided in the figure legend in accordance with the respective licences. Minimal alterations, in line with copyright licences, have been made in a small number of figures; this entails the removal of small elements of figures not relevant to the text of the thesis.

Table of Contents

List of Figures and Tables

List of Figures

List of Tables

Abbreviations

Abbreviation	Definition
ACA	Anti-Centromere Antibody
aCGH	array-Comparative Genomic Hybridisation
AF	Alexa-Fluor
APC/C	Anaphase-Promoting Complex/Cyclosome
Aurkb	Aurora Kinase B
Bub1	Budding Uninhibited by Benzimidazoles 1
Bub3	Budding Uninhibited by Benzimidazoles 3
BubR1	Bub1-related kinase
CamKII	Ca^{2+}/Calmodulin-dependent protein Kinase II
cAMP	3',5'-cyclic Adenosine Monophosphate
Cas9	CRISPR-associated protein 9
Cdc20	Cell-Division Cycle protein 20
Cdc25	Cell-Division Cycle protein 25
Cdc7	Cell-Division Cycle protein 7
Cdh1	CDC20 Homolog 1
Cdk1	Cyclin-Dependent Kinase 1
Cdk2	Cyclin-Dependent Kinase 2
CENP-C	Centromere Protein C 1
CK1	Casein Kinase 1
CLSM	Confocal Laser-Scanning Microscope
c-Mad2	Closed Mad2
CRISPR	Clustered Regularly Interspaced Short Palindromic Repeats
crRNA	CRISPR RNA
CSF	Cytostatic Factor
Csm1	Chromosome Segregation in Meiosis 1
D-box	Destruction box
dCas9	dead Cas9
DEPC	Diethyl Pyrocarbonate
DIC	Differential Interference Contrast
DMSO	Dimethyl Sulfoxide
DNA	Deoxyribonucleic Acid
DoG	Difference of Gaussians
DTT	DiThioThreitol
EDTA	Ethylenediaminetetraacetic Acid
EGFP	Enhanced Green Fluorescent Protein
EGTA	Ethylene Glycol-bis(ß-aminoethyl ether)-N,N,N′,N′-Tetraacetic Acid
Emi2	Endogenous Meiotic Inhibitor 2
Esco1/Esco2	Establishment of Sister Chromatid Cohesion N-Acetyltransferase 1/2
FIJI	Fiji Is Just ImageJ

Abbreviation	Definition
fRNP	fluorescent Ribonucleoprotein
FSH	Follicle Stimulating Hormone
GaAsP	Gallium Arsenide Phosphide
GC	Granulosa Cells
GV	Germinal Vesicle
GVBD	Germinal Vesicle Breakdown
H2A	Histone 2A
H2B	Histone 2B
hCG	Human Chorionic Gonadotropin
HCl	Hydrochloric Acid
HEPES	4-(2-Hydroxyethyl)-1-Piperazineethanesulfonic acid
HFEA	Human Fertilisation and Embryology Authority
HTTP	HyperText Transfer Protocol
I2PP2A	Inhibitor of PP2A
IBMX	3-Isobutyl-1-Methylxanthine
ICSI	Intracytoplasmic Sperm Injection
INCENP	Inner Centromere Protein
IQR	Inter-quartile range
ITK	Insight Toolkit
IVF	*In Vitro* Fertilisation
IVT	*In Vitro* Transcription
KDE	Kernel Density Estimation
Knl1	Kinetochore Scaffold 1
KSOM	Kalium (K+) Simplex Optimized Medium
LAP	Linear Assignment Problem
LB	Lysogeny Broth
LED	Light Emitting Diode
LH	Luteinising Hormone
LoG	Laplacian of Gaussian
Lrs4	Loss of rDNA silencing 4
Mad2	Mitotic Arrest Deficient 2
Mam1	Monopolar microtubule Attachment during Meiosis I 1
MAP4	Microtubule-Associated Protein 4
MAPK	Mitogen-Activated Protein Kinase
MAPKK	MAPK Kinase
Mau2	MAU2 Sister Chromatid Cohesion Factor
MCAK	Mitotic Centromere-Associated Kinesin
MCC	Mitotic Checkpoint Complex
MCP	MS2 Capping Protein
Meikin	Meiosis I-specific Kinetochore protein
MFI	Mean Fluorescence Intensity
MG132	Carbobenzoxy-Leu-Leu-leucinal
MI	Meiosis I

Abbreviation	Definition
MII	Meiosis II
MIM	Mad2-Interacting Mutant
Mos	Proto-oncogene serine/threonine-protein kinase mos
MPF	Maturation-Promoting Factor
Mps1	Monopolar Spindle 1
Msk1	Mitogen- and Stress-activated protein Kinase-1
MTBD	Microtubule-binding Domain
MTOC	Microtubule Organising Centre
MWU	Mann-Whitney U-test
MyPic	My Pipeline Constructor
N22	RNA binding domain of the bacteriophage protein N
NaCl	Sodium Chloride
NaOH	Sodium Hydroxide
Ndc80	Highly expressed in cancer protein
NEBD	Nuclear Envelope Break Down
NFC	Newcastle Fertility Centre
Nipbl	Nipped-B-Like Protein
NLS	Nuclear Localisation Sequence
Noco	Nocodazole
NP-40	Nonionic Polyoxyethylene surfactant 40
o-Mad2	Open Mad2
PAM	Protospacer-Adjacent Motif
PB	Polar Body
PBE	Polar Body Extrusion
PBS	Phosphate-buffered solution
PCP	PP7 Capping Protein
PCR	Polymerase Chain Reaction
Pds5	Precocious Dissociation of Sisters protein 5
PFA	Paraformaldehyde
pGEMHE	pGEM High Expression
Pias1	Protein Inhibitor of Activated STAT 1
PLK	Polo-like Kinase
Plk1	Polo-like Kinase 1
PMT	Photo-Multiplier Tube
PN	Pronuclear/Pronucleus/Pronuclei
PP1	Protein Phosphatase 1
PP2A	Protein Phosphatase 2A
pRB	Retinoblastoma protein
Prdm9	PR domain zinc finger protein 9
pRN3	pBluescript (KS+) RN3
PUF	RNA binding domain of Pumilio/FBF proteins
Q1	Quartile 1
Q3	Quartile 3

Abbreviation	Definition
Rad21	Double-strand-break repair protein rad21 homolog
Rec8	REC8 Meiotic Recombination Protein
Rev	Reversine
RNA	Ribonucleic Acid
ROI	Region of Interest
Rsk	Ribosomal S6 kinase
Rts1	Serine/threonine-protein phosphatase 2A 56 kDa regulatory subunit delta isoform
RVD	Repeat Variable Diresidue
S. pyogenes	*Streptococcus pyogenes*
SAC	Spindle Assembly Checkpoint
SCF	Skp, Cullin, F-box containing complex
SDS	Sodium dodecyl sulphate
Sgol1	Shugoshin-like 1
Sgol2	Shugoshin-like 2
sgRNA	single guide RNA
Smc1	Structural Maintenance of Chromosomes 1
Smc3	Structural Maintenance of Chromosomes 3
SNR	Signal:Noise Ratio
SP6	SP6 RNA polymerase
S-phase	Synthesis phase
Spo11	SPOrulation protein 11
Spo13	SPOrulation protein 13
$SrCl_2$	Strontium Chloride
SUMO	Small Ubiquitin-like Modifier
SV40	Simian Virus 40
T3	T3 RNA polymerase
T7	T7 RNA polymerase
TALE	dead TALEN
TALEN	Transcription Activator-Like Effector Nucleases
TE	Tris:Edta
Topo II	Topoisomerase II
tracrRNA	trans-activating crRNA
Trim21	Tripartite motif-containing protein 21
Ttk	Threonine/Tyrosine Kinase
VBA	Visual Basic for Applications
Wapl	Wings-apart Like
WT	Wild-type
X. laevis	*Xenopus laevis*

Chapter 1: Introduction

Fertilisation is the process by which a female gamete ("egg") and a male gamete ("sperm") fuse to form the zygote, a single cell that gives rise to all the tissues of a developing embryo. In order to maintain the correct number of chromosomes after these two gametes fuse, their chromosome number must be halved through a process called meiosis (Handel & Schimenti, 2010; Herbert et al., 2015). Meiosis and fertilisation are important processes for sexually reproducing organisms as it is the means by which genetic information is passed on from one generation to the next. However, the other cells of the body ("the somatic cells") undergo another form of cell division, called mitosis.

1.1 The Cell Cycle and Inheritance of Genetic Information

The etymology of mitosis is derived from the Greek work μίτος (mitos) meaning "thread". Observations by Walther Fleming in the 1880s led to the coinage of this term. He was able to observe cell division in the fins and gills of salamanders and saw thread-like chromosomes undergoing segregation on a spindle formed from two poles (Flemming, 1882) (Figure 1). Since then, our understanding of somatic cell division has been dramatically enhanced by determining the molecular details underpinning this process, but it was these early cytological observations that laid the foundations to our understanding of the cell cycle today.

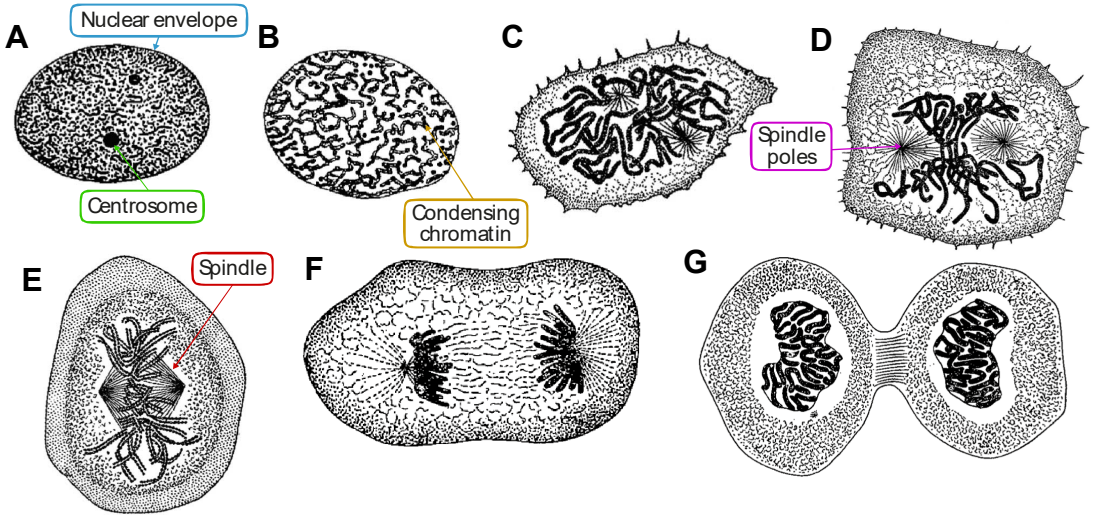

Figure 1 Illustration of the Phases of Mitosis as Drawn by Walther Flemming

Some of the earliest depictions of mitosis as drawn by Walther Flemming. ***A*** *An interphase nucleus containing decondensed chromatin.* ***B-D*** *The nuclear envelope breaking down and the DNA condensing into thread-like chromosomes as the cell advances from prophase into prometaphase.* ***E*** *The chromosomes*

*aligning on a metaphase plate, equidistant from two spindle poles. **F** The chromosomes separating, and segregating as chromatids, reaching the spindle poles during anaphase. **G** A new cell membrane forming around the decondensing chromatin during telophase. Figure reproduced from (Flemming, 1882).*

Cells spend relatively little time in mitosis compared to time spent in interphase (Figure 2). After cells divide ("cytokinesis"), the interphase nucleus of the cell contains decondensed chromatin, which allows the transcriptional machinery access to the DNA (Hübner et al., 2013). Enhanced transcriptional activity is important for the growth of the cell in this first gap phase, G_1 phase, as the cell can sense the completeness of growth and hinders entry into S-phase, where DNA replication occurs, until sufficient growth has occurred (Bertoli et al., 2013). This "checkpoint" also ensures that DNA damage is repaired in advance of replication. E2F is a transcription factor that is involved in promoting the expression of S-phase genes (Müller et al., 1997), but in early G_1 phase is prevented from binding to the promoters of such genes as it is inhibited by Retinoblastoma protein (pRb) (Bertoli et al., 2013); pRb only binds to E2F in its unphosphorylated form. Phosphorylation by Cyclin-Dependent Kinase (Cdk) 4/6-Cyclin D then Cdk2-Cyclin E alleviates this inhibition thereby allowing entry into S-phase. Aside from the DNA replication that occurs in S-phase, the centrosome, the poles from which microtubules will emanate to form the mitotic spindle, will also duplicate (Stearns, 2001). Once this has completed, the cell undergoes another gap phase, G_2 phase, in preparation of mitosis (Figure 2) (Hochegger et al., 2008).

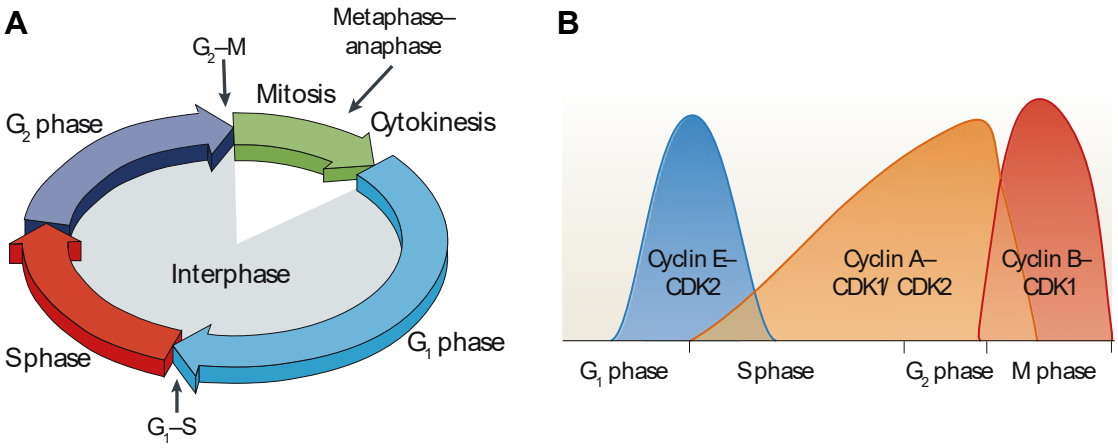

Figure 2 Cell-Cycle Control is Provided by Cyclins and Cyclin-Dependent Kinases

***A** An illustration of the cell cycle phases showing the journey from the first gap phase (G_1) into DNA replication (in S-phase) and then chromosome segregation (M-phase) followed by splitting into two daughter cells (cytokinesis); black arrows show the presence of important cell cycle transitions, which are regulated by checkpoint mechanisms. **B** The transitions between cell cycles phases are highly regulated to ensure the unidirectionality of the cell cycle. Key to this is the activity of Cyclins and Cyclin-Dependent Kinases. The graph illustrates the change in activity of different Cyclin and Cyclin-Dependent Kinases over one round of the cell cycle. Figure reproduced with permission from Springer Nature Customer Service Centre GmbH: (Hochegger et al., 2008).*

1.2 Mitosis and Chromosome Segregation into Identical Daughter Cells

Cells begin mitosis with replicated DNA and duplicated centrosomes; the DNA is still decondensed in the nucleus. The early stages of mitosis are governed by Cdk1-Cyclin B1, also known as Maturation Promoting Factor (MPF) (Smith & Ecker, 1971; Masui & Markert, 1971; Domingo-Sananes et al., 2011). Prior to mitosis, MPF is inhibited by phosphorylation of the T14/Y15 residues by the kinases Wee1 and Myt1 (Fattaey & Booher, 1997; Nurse & Thuriaux, 1980). These sites are then dephosphorylated by Cdc25 (Cell Division Cycle 25) to initiate mitosis, activating MPF (Gould et al., 1990). Reliant on MPF, mitosis beings with Nuclear Envelope Break Down (NEBD); DNA condensation into "X"-shaped chromosomes; and organisation of microtubules into a bipolar spindle structure by microtubular assembly originating from the centrosomes (Nigg, 2001) (Figure 3). However, accurate segregation during anaphase only occurs once chromosomes align correctly, with each replicated sister facing opposite poles of the spindle (Musacchio & Salmon, 2007) (Figure 4). For this to happen, the centromere, the point where the two chromatids join, will recruit proteins to form a kinetochore (Musacchio & Desai, 2017). These multi-subunit complexes will form on the centromeres of each chromatid and contain binding sites for microtubules of the spindle to attach (Petry, 2016). The cell uses the spindle and its attachments to kinetochores to sense if chromosome have aligned correctly ("bi-oriented"), as only spindle fibres from opposite poles will generate tension between sister kinetochores (Li & Nicklas, 1997; Maresca & Salmon, 2009; Musacchio & Salmon, 2007). Once attachments are correct, the Anaphase Promoting Complex/Cyclosome (APC/C)

becomes active and mediates the degradation of MPF and a myriad of other proteins to enable anaphase and sister chromatid separation (Peters, 2006). Subsequent cytokinesis results in daughter cells with an equal, or euploid, number of chromosomes.

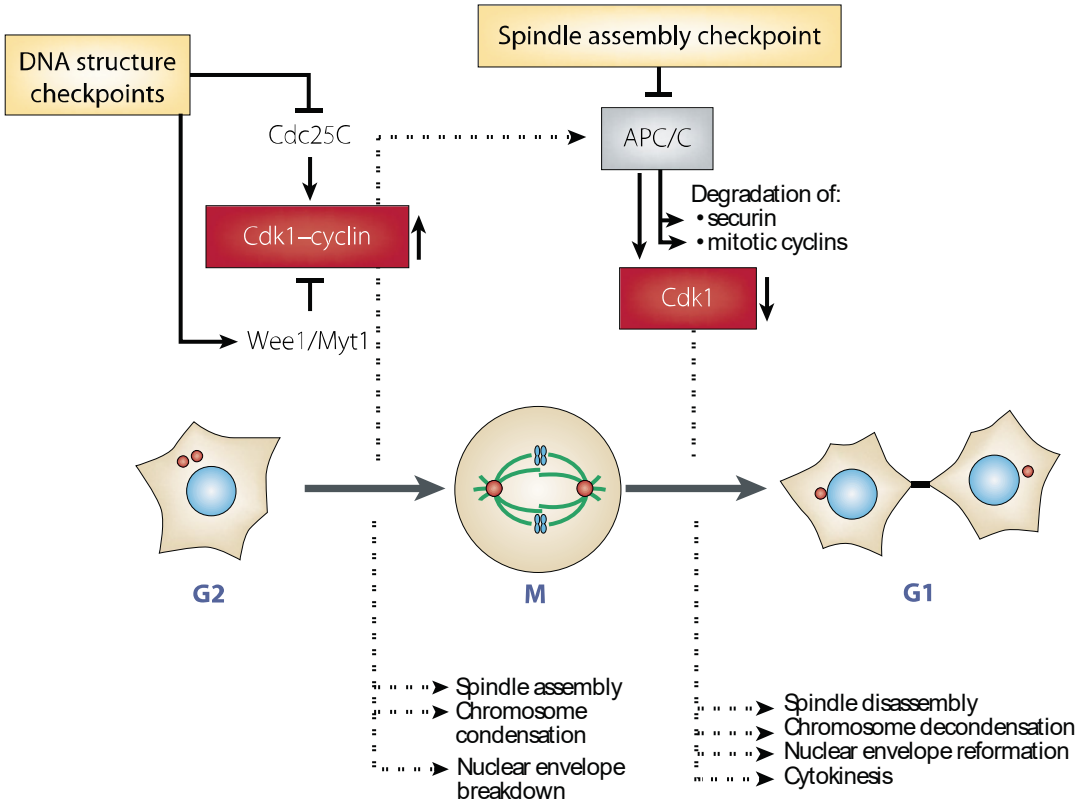

Figure 3 Cdk1-Cyclin B1 and APC/C Control Entry and Exit from Mitosis, Respectively

Cyclin Dependent Kinase 1 (Cdk1)-Cyclin B1, also known as Maturating Promoting Factor (MPF), is a kinase that regulates entry into mitosis by promoting Nuclear Envelope Break Down (NEBD), chromosome condensation and spindle assembly. Exit from mitosis is promoted via the Anaphase Promoting Complex (APC/C), which is a ubiquitin-ligase activated by high MPF activity. Once the APC/C becomes active, it degrades Cyclin B1, thereby inactivating MPF. The relationship between the APC/C and MPF underlies the cyclical nature of mitosis. Figure reproduced with permission from Springer Nature Customer Service Centre GmbH: (Nigg, 2001).

The APC/C is a large protein complex which ubiquitinates lysine residues of proteins (Mattiroli & Sixma, 2014), marking them for proteasome-mediated degradation. Its specificity is defined by binding of coactivators Cdc20 (Cell Division Cycle 1) or Cdh1 (Cdc20 Homologue 1) (Peters, 2006), which allow the APC/C to bind

sequence motifs such as the D-box and KEN-box in its substrates (Davey & Morgan, 2016). The APC/C binds different coactivators at different stages in the cell cycle, but APC/C^{Cdc20} is active in early anaphase and is the form which resolves sister chromatids (Rieder et al., 1994). The APC/C is itself activated by the MPF and (Golan et al., 2002), following correct alignment, will inactivate MPF through destruction of Cyclin B1 in order to form an oscillatory system that gives rise to the cyclical nature of cell cycle control (Sudakin et al., 1995; Mochida et al., 2016). Further regulation of the APC/C is provided by the Mitotic Checkpoint Complex (MCC). The MCC is a protein complex that works with the cells "tension-sensing" ability to ensure accurate chromosome segregation (Musacchio, 2015a). Mad2 (Mitotic Arrest Deficient 2), is a core component of the MCC and has two main conformations, an open (o-Mad2) and closed one (c-Mad2) (Musacchio & Desai, 2017). c-Mad2 binds the APC/C co-activator Cdc20 and forms the MCC by also binding to a Bub3-BubR1 heterodimer. The MCC is recruited to kinetochores that are not yet attached to the spindle and generates a "wait-anaphase" signal, until correct attachments have been made (Figure 4). This process is catalysed by the master regulatory kinase of the MCC, Mps1 (Monopolar Spindle 1, also known as Ttk, Dual Threonine/Tyrosine Kinase), which phosphorylates and recruits to the kinetochores many of the MCC components (Ji et al., 2017; Pachis & Kops, 2018).

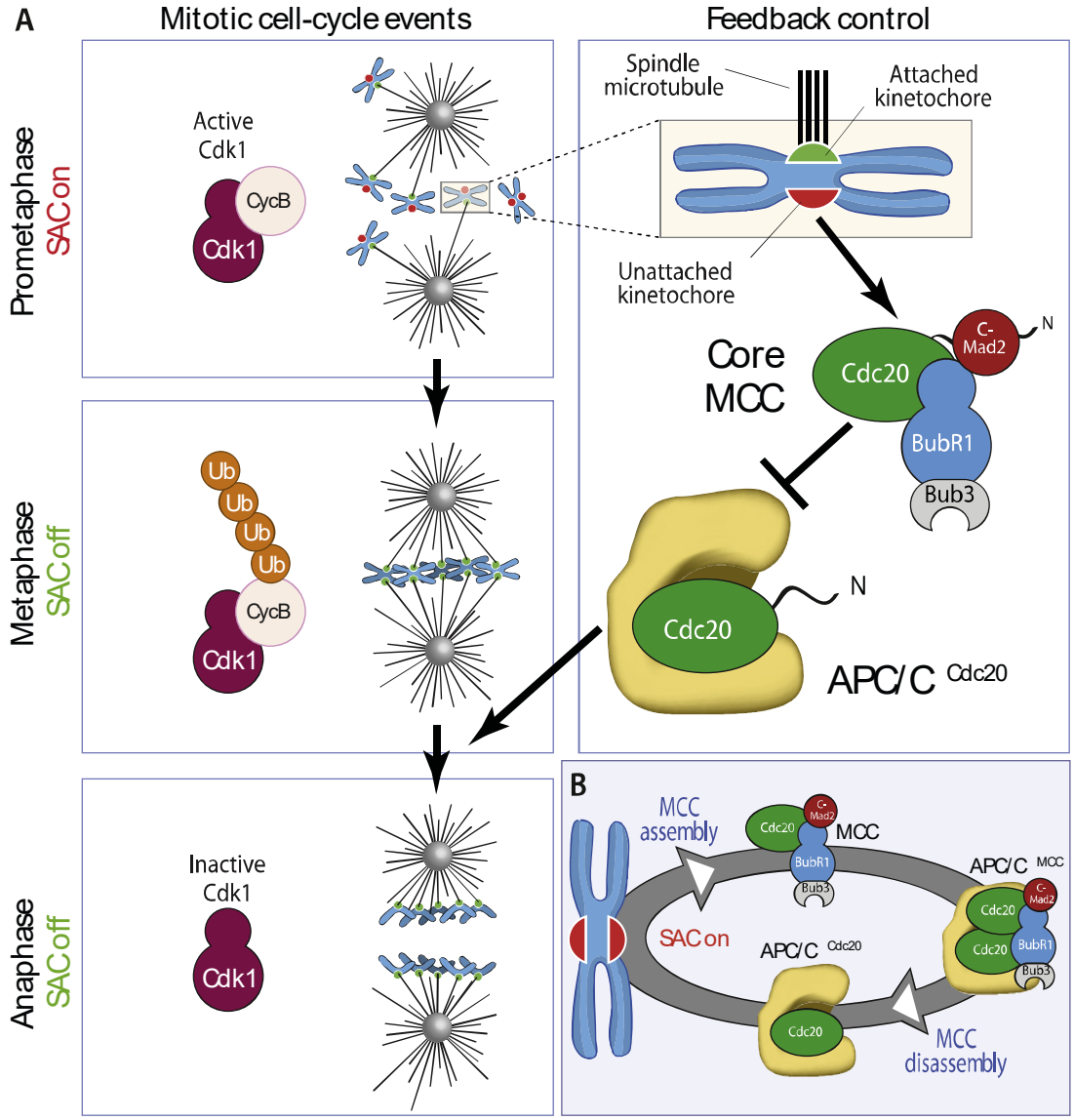

Figure 4 Formation of the Mitotic Checkpoint Complex Blocks the Cell from Undergoing Anaphase Until All Chromosomes Align

A *Shows the Spindle Assembly Checkpoint (SAC) being activated in prometaphase as sister kinetochores haven't yet bi-oriented, this occurs through the assembly of the Mitotic Checkpoint Complex (MCC). The SAC is off when all chromosomes have aligned in metaphase; the absence of the MCC, an APC/C inhibitor, allows for APC/C^{Cdc20} activation and ubiquitination of its substrates, including Cyclin B1. By anaphase, Cyclin B1 has been degraded and thus Cdk1 becomes inactive.* ***B*** *The cycle of MCC assembly and disassembly is important for continued monitoring of attachments during prometaphase. Figure reproduced with permission from Elsevier Ltd.: (Musacchio, 2015b).*

As mentioned, bi-orientation can be sensed by the cell as it generates tension between sister kinetochores. This resulting tension causes a change in the fine

balance between phosphatases and kinases at the kinetochore (Figure 5). Prior to attachments, kinetochore components are highly phosphorylated by Aurora Kinase B (Aurkb) localised at the inner centromere (Bishop et al., 2002). Upon bi-orientation, substrates are pulled away from Aurkb leading to decreased phosphorylation that is further ensured by active dephosphorylation by Protein Phosphatase 1 (PP1) at the kinetochore-microtubule interface (Emanuele et al., 2008; Lampson & Cheeseman, 2011). This dephosphorylation, as well as other checkpoint silencing processes (Jia et al., 2011), prevent recruitment of the MCC to correctly attached kinetochores. Once all kinetochores are correctly attached, the cell is able to progress to anaphase. Otherwise, inaccurate chromosome segregation would occur, leading to aneuploidy. If cells are unable to form all correct attachments, the cell will arrest due to the Spindle Assembly Checkpoint (SAC).

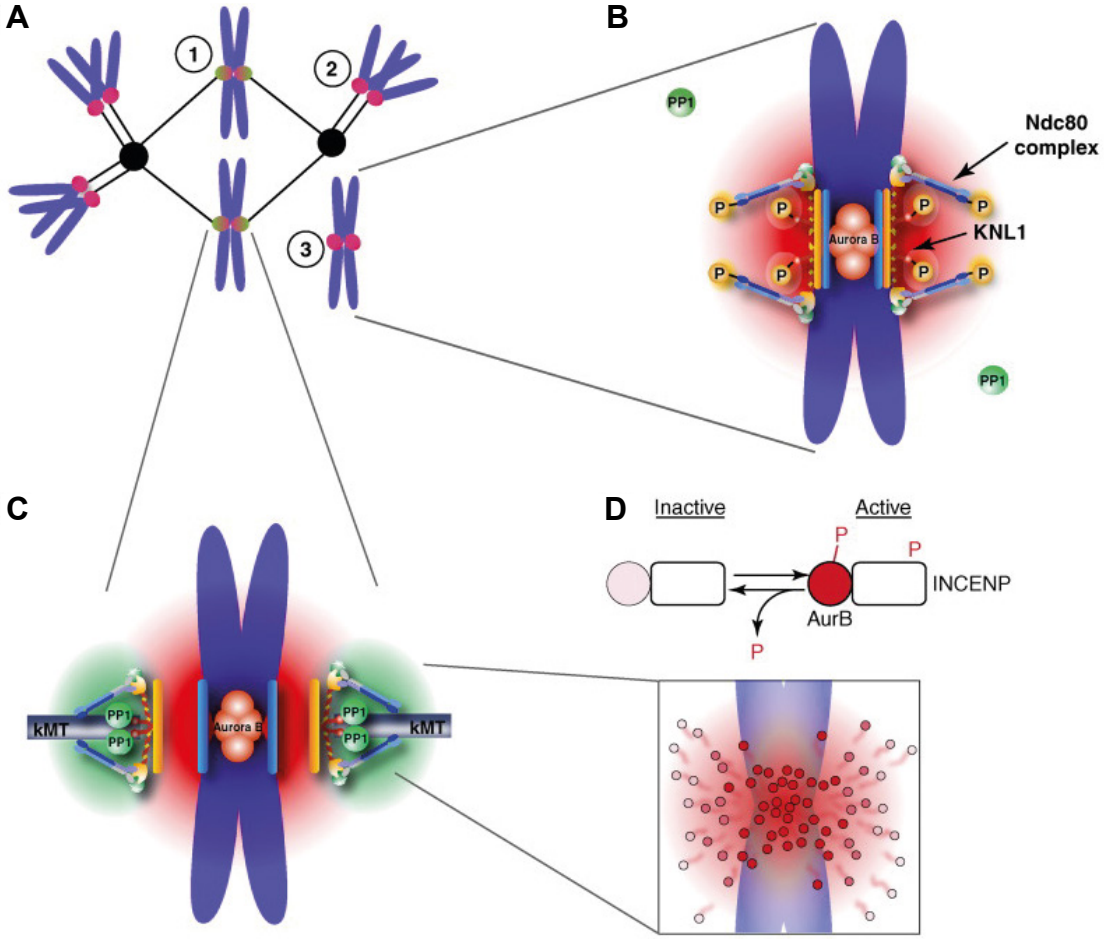

Figure 5 Correct Attachments are Ensured in Mitosis Through Sensing for Bi-orientation of Sister Kinetochores

__A__ Prometaphase showing (1) a bi-oriented chromosome, (2) mono-oriented and (3) unattached sister kinetochores. __B__ Shows Aurora Kinase B (Aurkb) at the inner centromere, phosphorylating kinetochore components such as Knl1 and Ndc80. __C__ Shows bi-oriented sister kinetochores that are under tension,

resulting in kinetochores being moved away from Aurora Kinase B's region of phosphorylation and being actively dephosphorylated by PP1. ***D*** *An Aurora Kinase B gradient showing inner substrates, such as INCENP (Inner Centromere Protein), as phosphorylated, and outer substrates as dephosphorylated. Figure reproduced with permission from Elsevier Ltd.: (Lampson & Cheeseman, 2011).*

1.3 Cohesin and its Regulation in the Cell Cycle

Tension at the kinetochores can only be provided by a counteracting force to that generated by the spindle. This is provided by the protein complex Cohesin (Peters & Nishiyama, 2012), which is found primarily at the centromeres in metaphase, giving chromosomes their characteristic "X"-shape (Haarhuis et al., 2014). This protein complex is composed of a central "ring" made up of three core proteins (Smc1α or ß, Smc3, and an α-kleisin (Michaelis et al., 1997)) that physically entrap sister chromatids and hold them together until they disengage at anaphase (Figure 6). Sister chromatid cohesion is established during DNA replication (Peters & Nishiyama, 2012), and it is thought that replication forks might be able to progress through the Cohesin ring (Sherwood et al., 2010). In this model, Cohesin is loaded onto DNA prior to replication, automatically entangling sister chromatids in preparation for cell division (Uhlmann & Nasmyth, 1998). Though Cohesin can load after DNA replication, "cohesive" Cohesin that holds sister chromatids together is thought to load only during replication (and DNA damage repair, reviewed in (Lyons & Morgan, 2011)) and holds sister chromatids together until anaphase. Once all attachments are correct, the α-kleisin of Cohesin, Rad21 in mitosis, is cleaved by the protease Separase (Uhlmann et al., 2000), opening the Cohesin ring and separating sister chromatids. In order to prevent Cohesin removal before this point, Separase is kept inactive by inhibitory binding of Securin (Kumada et al., 1998), and phosphorylation by Cdk1-Cyclin B1 (Stemmann et al., 2001). Both Securin and Cyclin B1 are degraded at anaphase onset as they contain D-boxes in their N-termini, making them substrates of the APC/C^{Cdc20} (Figure 6A) (Schwab et al., 1997; Yamano et al., 2004).

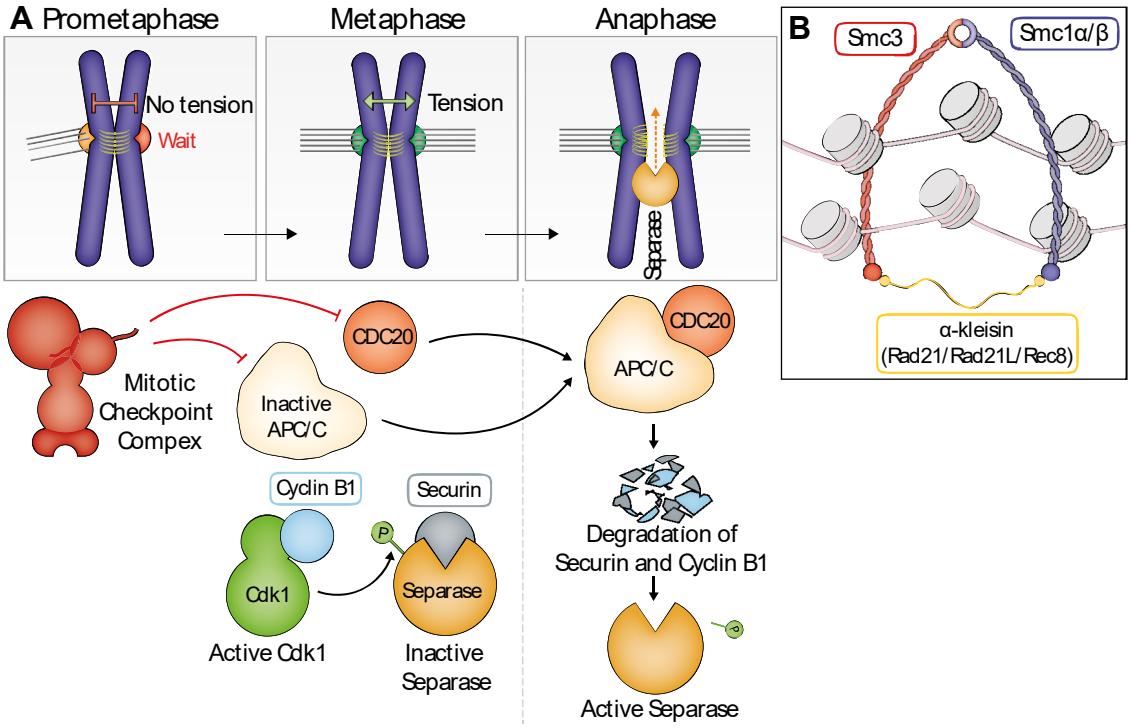

Figure 6 Regulation of Cohesin Removal by Separase-Mediated Cleavage in Mitosis

A Cohesin at the kinetochores functions in the cell's ability to detect erroneous attachments by counteracting spindle forces in prometaphase. The Spindle Assembly Checkpoint (SAC) ensures that all kinetochores are correctly attached, recruiting the MCC (Mitotic Checkpoint Complex) to unattached kinetochores, which generates a wait-anaphase signal. This wait signal is silenced once all kinetochores have made tension-generating attachments. Only once all attachments are correct can Cdc20 activate the APC/C. APC/C^{Cdc20} degrades Securin and Cyclin B, activating Separase, thus removing Cohesin during anaphase, and allowing sister chromatids to segregate. ***B*** *Cohesin is a tripartite ring made up of two core Smcs and a bridging a-kleisin, that creates cohesion between sister chromatids.*

Cohesin is first loaded onto DNA during G_1 phase by a protein complex called Adherin (sometimes called Kollerin) consisting of Nipbl and Mau2 (Ciosk et al., 2000; Peters & Nishiyama, 2012) (Figure 7). This DNA-Cohesin interaction is dynamic as Cohesin loading is counteracted by binding of the Cohesin-releasing factor Wapl (Wings Apart-like) to one of Cohesin's accessory subunits Pds5 (Precocious Dissociation of Sisters protein 5) (Nishiyama et al., 2010). In order to stabilise Cohesin, this Wapl-interaction needs to be inhibited, as performed by binding of

Sororin to Pds5. This occurs following acetylation of the Cohesin subunit Smc3 by Esco1/Esco2 (Skibbens et al., 1999), establishing sister chromatid cohesion.

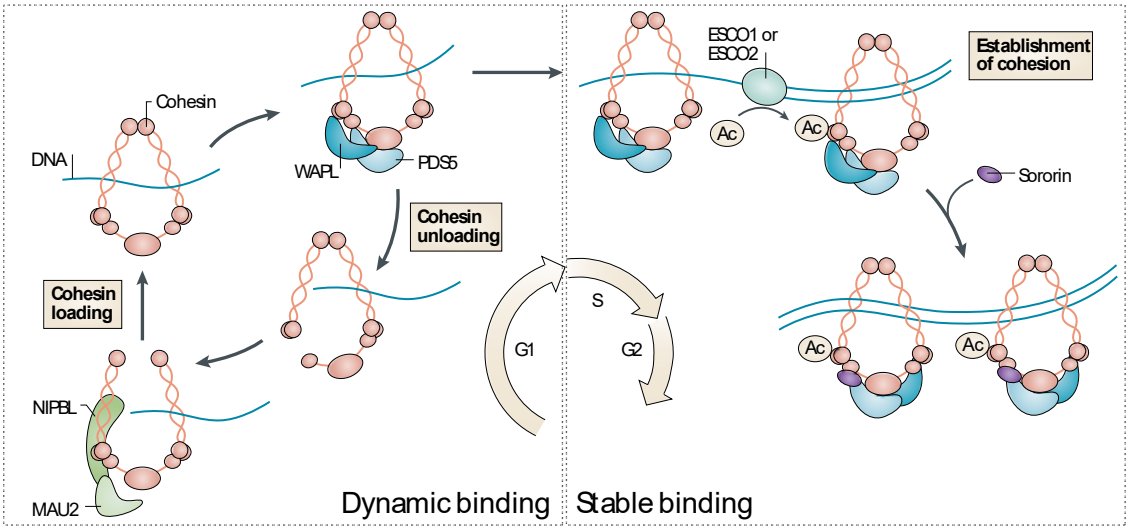

Figure 7 Establishment of Cohesion Occurs During S-phase

Adherin, composed of Nipbl and Mau2, enables the binding of Cohesin to DNA during G_1 phase. However, this association is dynamic as Wapl releases Cohesin such that Cohesin's binding is dynamic at this stage. It is not until S-phase, when Cohesin is stabilised, and sister chromatid cohesion established, in advance of DNA replication. This is performed by preventing Wapl from binding to Cohesin, a function performed by Sororin following Smc3 acetylation by Esco1/Esco2. Figure reproduced with permission from Elsevier Ltd.: (Losada, 2014).

The bulk of Cohesin is removed in prophase in a process called the "prophase pathway" (Figure 8) (Haarhuis et al., 2014). The prophase pathway is the phosphorylation of Cohesin accessory factors by mitotic kinases. Such accessory factors include Sororin, whose phosphorylation leads to its removal from Cohesin (Figure 8A) (Nishiyama et al., 2010; Haarhuis et al., 2014). As a result, Cohesin's interaction with DNA is no longer stabilised and Wapl is again able to bind Pds5, leading to the removal of arm (non-centromeric) Cohesin in prophase (Gandhi et al., 2006). However, centromeric Cohesin must be "protected" from this removal in order to maintain a counteracting force at the kinetochores against spindle microtubules in prometaphase. Protection from this pathway is provided by recruitment of the phosphatase PP2A (Protein Phosphatase 2A) which is associated with Shugoshin 1 (Sgol1) (Kitajima et al., 2004), one of two orthologues of the yeast Shugoshin in mammals (Gutiérrez-Caballero et al., 2012). PP2A dephosphorylates

centromeric Cohesin accessory factors thereby providing protection (Xu et al., 2009). Sgol1 is itself recruited to Cohesin first by binding to a Bub1 (Budding Uninhibited by Benzimidazoles 1, a SAC kinase) phosphorylated H2A mark at the centromeres (Kawashima et al., 2010), and then by Cdk1-Cyclin B1 phosphorylation of Sgol1 that mediates its binding to Cohesin (Liu et al., 2015; Liu, Jia, et al., 2013) (Figure 8B).

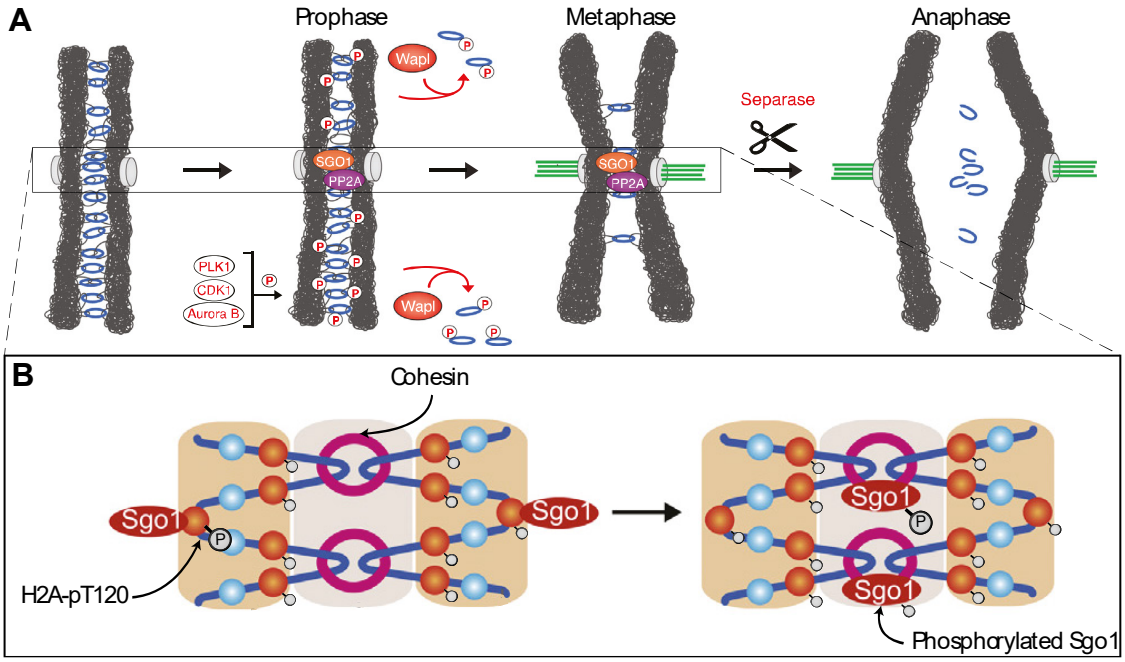

Figure 8 Separase-Independent Removal of Cohesin, and Recruitment of Sgol1, in Mitosis

A *In prophase, Cohesin accessory factors are phosphorylated by mitotic kinases (Plk1, Cdk1, Aurora Kinase B), allowing Wapl to release Cohesin from the chromosomes, in a process called the "prophase pathway". Centromeric Cohesin is protected through dephosphorylation by PP2A, which requires the recruitment of Sgol1 to the centromere. Figure reproduced with permission from Elsevier Ltd.: (Haarhuis et al., 2014).* ***B*** *Sgol1 is first recruited by Bub1-mediated phosphorylation of the histone subunit H2A, a prerequisite for Cdk1-mediated loading onto Cohesin. Figure reproduced with permission from Elsevier Ltd.: (Liu et al., 2015).*

In summary, Cohesin is first loaded onto DNA in G_1-phase, but only becomes stabilised in S-phase, resulting in sister chromatid cohesion. Most Cohesin is removed early in mitosis through the prophase pathway, but centromeric Cohesin must be protected and maintained for it to counteract spindle forces in prometaphase. Only in anaphase is this remaining pool of Cohesin removed. Timely removing of Cohesin in mitosis is critical for accurate chromosome segregation, which is dependent upon

the balance between Cdk1-Cyclin B1 and the APC/C^{Cdc20}. This balance ensures accurate alignment during metaphase by working with the MCC during prometaphase, and removal of Cohesin, through activation of Separase, during anaphase so that daughter cells maintain correct ploidy.

1.4 Chromosome Segregation in Meiosis: From Diploid to Haploid

Gametes, on the other hand, need to halve their chromosome number, such that fertilisation brings this back to the normal chromosomal complement. Without this, the chromosome number would double with each round of fertilisation. The specialised type of cell division required for this necessitate several modifications to the cell cycle logic as described in mitosis (Petronczki et al., 2003).

Differences in meiosis begin even before DNA replication. In fact, modifications of DNA replication enable meiosis to function differently. Firstly, in addition to Rad21-containing Cohesin, the α-kleisin subunit of Cohesin is exchanged for the meiosis-specific Rec8 and Rad21L (Watanabe et al., 2001; Uhlmann, 2011). DNA replication then occurs, followed by the formation of double-strand breaks (Hunter, 2015). Typically, double strand breaks are repaired by the cell's DNA-repair machinery: the ends are resected; the sister chromatid is found to provide a template to repair from; and then repair commences (though there are alternative methods of DNA double-strand break repair as reviewed in (Featherstone & Jackson, 1999)). However in meiosis, these occur in site-specific hotspots defined by the histone methyltransferase Prdm9 (PR domain zinc finger protein 9) (Grey et al., 2018). The meiosis-specific endonuclease Spo11 is then recruited to these sites to intentionally generate double-strand breaks (Lam & Keeney, 2015). The purpose of which, is not for it to be repaired by sister chromatids, but by a homologous chromosome, in a process called homologous recombination. While some of these repairs lead to gene conversion, i.e. the swapping of short fragments of DNA in one homologous chromosome for the other, others form "crossovers" (reciprocal exchange). Crossovers are physical linkages that join homologous chromosomes, maternal and paternal, into one larger structure called a "bivalent". Use of homologous chromosomes over sister chromatids for repair is promoted by two meiosis-specific structures: lateral elements which are rod-like, proteinaceous structures along the axis of each homologue; and the synaptonemal complex, a ribbon-like structure connecting the lateral elements so that homologues are held in close proximity (Page & Hawley, 2004). Accurate chromosome segregation requires

that at least one crossover is formed (Wang et al., 2015). This bivalent structure is important as the homologous chromosomes will segregate in a reductional manner in meiosis I, and then equationally in meiosis II.

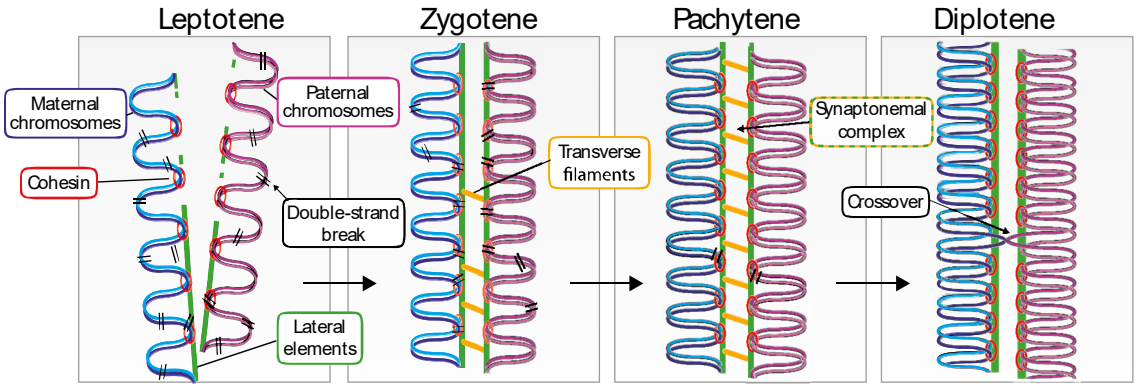

Figure 9 Prophase I in Meiosis Forms Physical Linkages Between the Maternal and Paternal genomes

In leptotene (early prophase I), double-strand breaks are formed by the endonuclease Spo11 throughout both genomes. The generation of a synaptonemal complex during prophase I, made up of lateral elements and transverse filaments, keeps the two genomes aposed and leads to preferential repair of these double-strand breaks by homologous chromosomes rather than sister chromatids. This leads to several outcomes: some will form physical linkages with the homologous chromosome, called "crossovers"; and others repair with the homologous chromosome to genereate "non-crossover" sites (small portions of the genome will be "shuffled" with the other so that one chromosome contains portions of the other). Chromosomes containing crossovers are called bivalents and are unique to mieosis I and important for the faithful segregation of homologous chromosomes in meiosis I.

As homologous chromosomes segregate in meiosis I, sister chromatids must face the same spindle pole, rather than opposite poles as in mitosis. This process is called mono-orientation (Nasmyth, 2015). While crucial to meiosis, the molecular mechanism of mono-orientation remains poorly understood. The most well-characterised model comes from budding yeast (Petronczki et al., 2006), where the Monopolin complex (consisting of Hrr25 [also known as Casein Kinase 1, CK1], Mam1, Csm1 and Lrs4) has been postulated to act as a clamp to crosslink sister kinetochores (Corbett & Harrison, 2012). X-ray crystallography shows it as having a "V" shape, in support of this model (Corbett et al., 2010). Alternatively, Monopolin might act as a

recruiting device for CK1, which then changes the properties of yet to be identified kinetochore components. However, with the exception of CK1, homologues of Monopolin subunits have only been identified in budding yeast. Interestingly, recent work revealed that mono-orientation requires a family of proteins represented by Spo13 in yeast and Meikin (Meiosis-specific Kinetochore factor) in mammals (Kim et al., 2014). While poorly conserved at the primary sequence level, these proteins share the ability to bind kinetochores and associate with Polo-like kinases (PLK). Thus, Spo13/Meikin might elicit mono-orientation by recruiting PLK to kinetochores at entry into meiosis I. Mono-orientation allows for homologous chromosomes to segregate during anaphase I, but to ensure accurate chromosomes segregation in meiosis II, Cohesin must persist between sister centromeres.

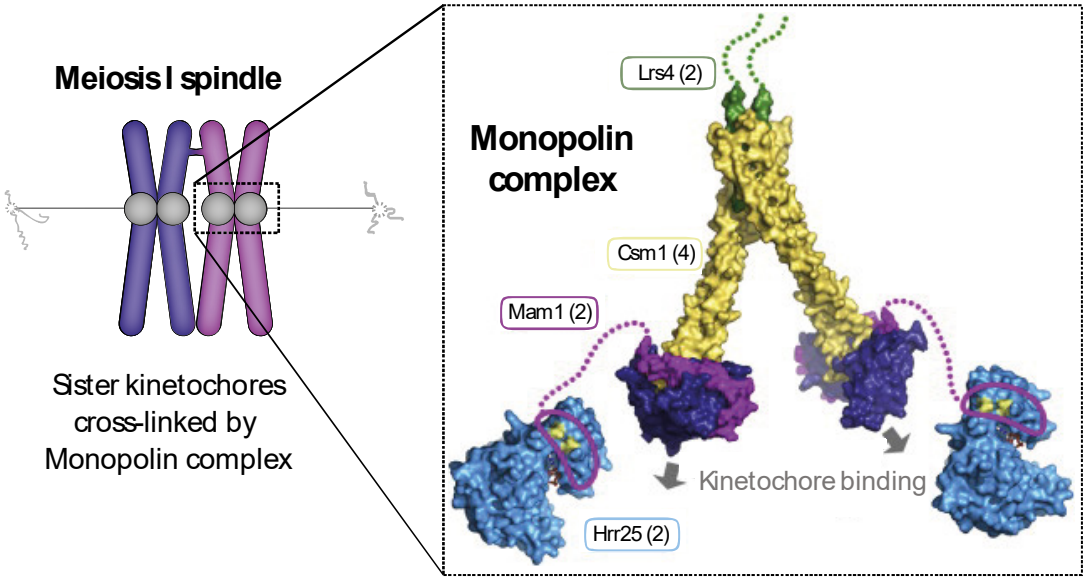

Figure 10 Mono-orientation in Meiosis I in Budding Yeast is Mediated by the Monopolin Complex, Which Crosslinks Sister Kinetochores

In order for bivalents to segregate faithfully in meiosis I, sister kinetochores must face the same spindle pole, unlike in mitosis or meiosis II where each sister kinetochore is attached to different poles. In budding yeast, the Monopolin complex is thought to crosslink sister kinetochores so they function as a single unit, in order to attach to the same spindle pole, enabling faithful segregation in meiosis I. Inset figure reproduced with permission from Elsevier Ltd.: (Corbett et al., 2010).

This fraction of Cohesin, at the centromeres, is "protected" against Separase-mediated cleavage in meiosis I, so that chromosomes (or "dyads") can realign and segregate in meiosis II. The mechanisms governing protection in meiosis

were first elucidated in yeast where Casein Kinase 1 (CK1) and the Cdc7-Dbf4 kinase phosphorylate Rec8 to prime it for cleavage (Katis et al., 2010). Centromeric Rec8 is dephosphorylated by PP2A, thereby protecting centromeric Cohesin until meiosis II (Riedel et al., 2006). PP2A is also recruited to the centromere by a Shugoshin orthologue, Shugoshin 2 (Sgol2) in mammals (Kitajima et al., 2004) (Figure 11). In mouse oocytes, knockdown (Lee et al., 2008) or knockout (Llano et al., 2008) of Sgol2 leads to separation of sister chromatids rather than separation of homologous chromosomes at anaphase I, indicating that Sgol2 is the protective Shugoshin in meiosis I.

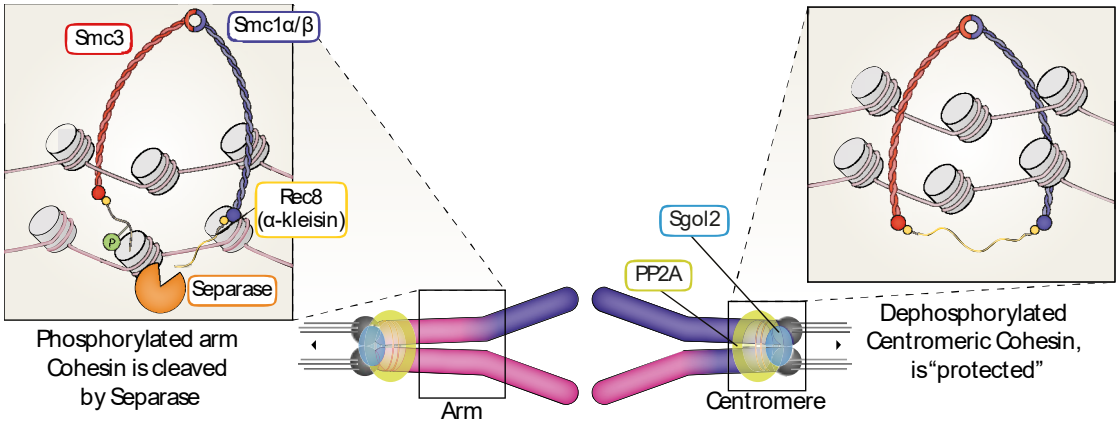

Figure 11 "Protection" of Centromeric Cohesin During Anaphase I

Arm Cohesin is phosphorylated, which is a prerequisite for Separase-mediated cleavage during anaphase I. Centromeric Cohesin is protected from cleavage through dephosphorylation by the phosphatase PP2A, whose localisation to Cohesin is dependent on Sgol2. This ensures Cohesin remains at the centromeres, preventing sister chromatids from separating, and therefore allowing alignment of dyads in meiosis II.

While wild-type Sgol2 can rescue the Sgol2 knockout phenotype, a mutant form of Sgol2 that cannot bind PP2A is unable to prevent premature separation of sister chromatids (Rattani et al., 2013). PP2A is a holoenzyme consisting of three components, namely the scaffold A and catalytic C components, and a regulatory B component that confers its specificity (Xu et al., 2009). In meiosis, it is B56 (or Rts1 in yeast) that provides this function (Slupe et al., 2011). However, how protection is removed in meiosis II is a process that is as of yet only poorly understood (Herbert & Toth, 2017). This is, in part, due to the difficulty in establishing yeast cultures that are synchronous enough to analyse events specific to meiosis II. As a result, two models have been suggested in mouse oocytes: one that predicts that spindle tension

is required for deprotection (Lee et al., 2008), exploiting that sister kinetochores do not have tension between them in meiosis I but do in meiosis II; and another that suggests that PP2A is itself inhibited differently between meiosis I and -II (Chambon et al., 2013). More recently, yeast have been successfully synchronised in meiosis II and this has led to a new model that shows the APC/C^{Cdc20} not only degrades Securin to activate Separase and therefore Cohesin cleavage, but concomitantly degrades Shugoshin to remove protection (Argüello-Miranda et al., 2017; Jonak et al., 2017).

On completion of meiosis II, the cell will then undergo a gap-phase followed by DNA replication in S-phase, as is the case for exit from mitosis. Exit from meiosis I, on the other hand, must not be accompanied by DNA replication (Petronczki et al., 2003). The model for how this occurs comes from *Xenopus laevis (X. laevis)*, where Cyclin B1 levels are not completely depleted during anaphase I (Hutchins et al., 2003). This persistent MPF activity is compatible with spindle disassembly and cytokinesis but prevents entry into S-phase. A further factor is the Mos/MAPK cascade, which works to maintain this reduced level of Cyclin B1 in the presence of the APC/C^{Cdc20} (Hochegger et al., 2001). It is also thought that APC/C^{Cdh1} remains inactive subsequent to APC/C^{Cdc20} activity in anaphase I (Karabinova et al., 2011), unlike in mitotic anaphase. Whether the absence of an APC/C^{Cdh1} is involved in preventing complete destruction of Cyclin B1 has not been investigated, though Cyclin B1 is also a substrate of APC/C^{Cdh1} (Thornton & Toczyski, 2003).

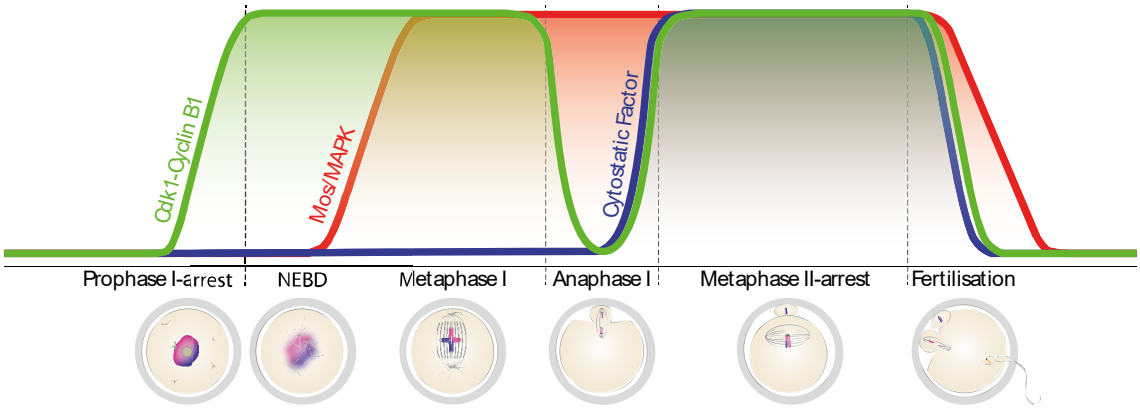

Figure 12 Dynamics of MPF, Mos/MAPK, and CSF Activity During Meiosis I and -II in Mouse Oocytes

Mos/MAPK activity is required for the suppression of DNA replication after exit from meiosis I and to maintain Cytostatic-Factor (CSF)-arrest in eggs at metaphase II. Accordingly, prior to Nuclear Envelope Break Down (NEBD, or GVBD in oocytes), oocytes have low Mos/MAPK activity, as well as low MPF

activity. Upon resumption of meiosis I, MPF activity increases and peaks before anaphase I, when the APC/C^{Cdc20} is active, and Cyclin B1 is degraded; MPF activity then reaccumulates in meiosis II. Eggs arrest due to inhibition of the APC/C^{Cdc20} by the Cytostatic Factor. Fertilisation then leads to release from CSF-arrest and a drop in both MPF and Mos/MAPK activity, allowing for exit from meiosis II. Graph adapted from (Dupré et al., 2011)[1] and (Madgwick & Jones, 2007)[2].

Finally, meiosis is coordinated with gametogenesis. Gametogenesis is the process by which meiotic cells differentiate into highly specialised cells capable of recognising and fusing with a gamete of the opposite sex to form a zygote. While meiotic chromosome segregation is an evolutionarily conserved process, gametogenesis differs markedly between species and, in animals and plants, between the sexes. In mammals, for example this is the differentiation of male gametic cells into spermatocytes, and in females ito eggs.

1.5 Meiosis in Mammalian Oocytes

In mammalian males, sperm are produced from precursor spermatogonial stem cells that are continuously replenished after puberty. Females, on the other hand, are born with a limited stock of millions of oocytes that have already started meiosis (~2.5 million in human (Wallace & Kelsey, 2010)), but arrest until a select few resume meiosis at puberty and more continue to do so each menstrual cycle until menopause (Handel & Schimenti, 2010). Female mammalian meiosis starts *in utero*, where DNA replication occurs in oocyte precursor cells in foetal ovaries (Sirlin & Edwards, 1959). As mentioned, homologous recombination follows DNA replication and homologous chromosomes form into bivalents. Oocytes then arrest in prophase I containing a large nucleus (Albertini & Carabatsos, 1998), called a "germinal vesicle" (GV) (Wagner & Barry, 1836) (Figure 13). These oocytes are surrounded by a layer of flattened Granulosa Cells (GCs) that can transport proteins to the oocyte via gap junctions (Eppig, 2018), including cyclic-AMP (cAMP). High levels of intracellular cAMP maintains prophase I-arrest by keeping MPF activity low (Williams & Erickson, 2000; von Stetina & Orr-Weaver, 2011). This GC-oocyte complex is called a primordial

[1] Reproduced in accordance with CC BY 3.0. https://creativecommons.org/licenses/by/3.0/
[2] Reproduced in accordance with CC BY 2.0. https://creativecommons.org/licenses/by/2.0/

follicle (Richards & Pangas, 2010). Hormonal stimulation, by Follicle Stimulating Hormone (FSH), after sexual maturity, allows for further development of the follicle (Gougeon, 1996). FSH stimulates GCs to proliferate and produce oestradiol, which then trigger a surge of Luteinising Hormone (LH) (Chian et al., 2004). The LH surge results in the closing of gap junctions, and therefore depletes cAMP levels within the oocytes, enabling GV-arrested oocytes to resume meiosis I (Mehlmann, 2005). The GV breaks down (GVBD, akin to Nuclear Envelope Breakdown, NEBD), followed by assembly of the first meiotic spindle and segregation of bivalents in the first meiotic division. Unlike in mitosis, oocyte spindle assembly occurs in the absence of centrosomes (Namgoong & Kim, 2018). This acentriolar spindle assembly is instead coordinated by several Microtubule Organising Centres (MTOC), which begin as multiple foci that eventually accumulate as two poles (Schuh & Ellenberg, 2007). Upon completion of anaphase I, and unlike in most other cell divisions, the oocyte produces a non-viable polar body (PB1) (Conklin, 1915). The oocyte will begin to form a spindle for meiosis II, but arrests at metaphase II, at which stage it is ovulated as an egg and is ready for fertilisation (Tunquist, 2003; Mehlmann, 2005).

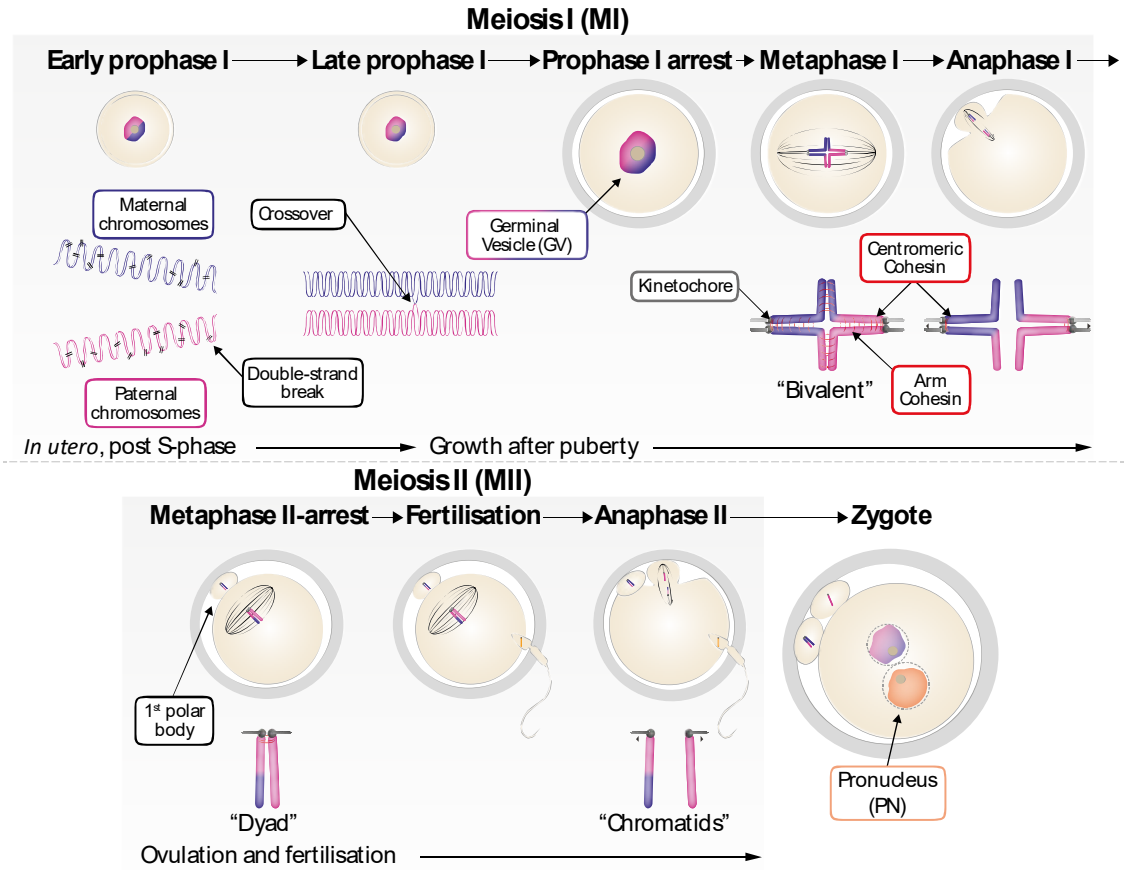

Figure 13 Meiosis in Mammalian Oocytes

Oocyte meiosis begins in utero, with the formation of crossovers, generating a bivalent stabilised by Cohesin. Upon sexual maturity, a subset of oocytes

continue maturation each menstrual cycle. The hormonal stimulation leads to follicular growth and eventually release of the oocyte from prophase I arrest; marked by the break-down of the nuclear envelope (or Germinal Vesicle Break-Down in oocytes). An acentriolar spindle forms to generate attachments to mono-oriented kinetochores, in preparation for alignment of homologous chromosomes in metaphase I. Arm Cohesin is removed at anaphase I, resolving the bivalent into two dyads; one set of dyads is extruded to the first polar body and the second remains in the oocyte. Cohesin remains at the centromere so that dyads can realign on the metaphase II spindle, at which point the oocyte is ovulated and is referred to as an egg. The egg then arrests until sperm entry when it resumes meiosis II, removing centromeric Cohesin and extruding the second polar body. The fertilised egg, now a zygote, undergoes several rounds of mitosis to form an embryo.

Ovulated eggs are arrested at metaphase II, also known as Cytostatic Factor-arrest (CSF-arrest), which is maintained through partial inhibition of the APC/C (Kornbluth & Fissore, 2015). While the APC/C^{Cdc20} is still active at low levels during the arrest (McGuinness et al., 2009), it is not active in such a way that allows for progression into anaphase II. This inhibition is performed by Emi2 (Endogenous Meiotic Inhibitor 2) (Madgwick et al., 2006), through direct binding of the APC/C via its C-terminus (Shoji et al., 2014; Ohe et al., 2010) (Figure 14). It also specifically inhibits the APC/C^{Cdc20} through binding of Cdc20 (Shoji et al., 2006, 2014). Emi2 is itself regulated through a number of kinases and phosphatases, as has been shown in *X. laevis* (Isoda et al., 2011) (Figure 14). As part of a feedback loop between itself and Cdk1-Cyclin B1 to maintain low APC/C^{Cdc20} activity, Cdk1-Cyclin B1-phosphorylation destabilises Emi2. Were this destabilisation allowed to go to completion, Emi2 would no longer be able to inhibit the APC/C, and eggs would spontaneously activate. The destabilising Cdk1-Cyclin B1 phosphorylation is counteracted by PP2A-B56, which is recruited to Emi2 via Rsk (p90 S6 kinase)-mediated phosphorylation. Rsk is itself recruited to Emi2 through a signalling cascade that is triggered by Mos, a MAPKK kinase (Inoue et al., 2007; Wu et al., 2007). The orthologous phosphorylation sites on Emi2 are also important for stabilisation of Emi2 in mouse eggs (Suzuki et al., 2010), though they are phosphorylated by Msk1 (Nuclear

Mitogen- and Stress-activated protein Kinase 1) rather than Rsk (Miyagaki et al., 2011) (Figure 14).

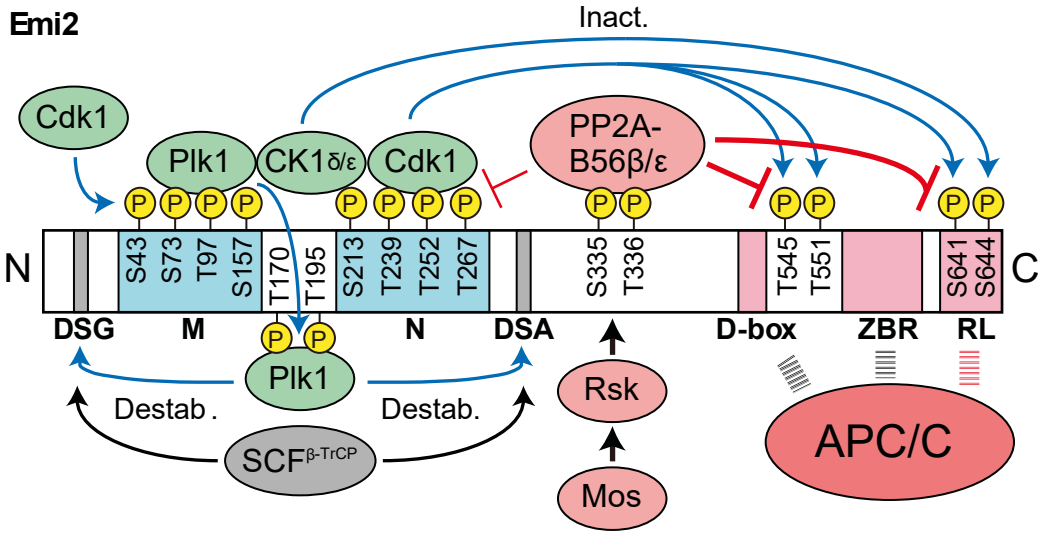

Figure 14 Regulation of Emi2, Which Inhibits the APC/C During Metaphase II-arrest

A schematic showing the regulation of Emi2, which inhibits the APC/C^{Cdc20} in metaphase II of eggs by interacting with the APC/C via its C-terminus. Emi2 stability is negatively regulated by phosphorylation on its N-terminus by a number of kinases. These are counteracted by PP2A-B56, which itself is recruited via Rsk-mediated phosphorylation, as part of the Mos/MAPK cascade. Plk1 (Polo-like Kinase 1) further acts to destabilise Emi2 by phosphorylating the degrons (DSG/DSA) that are recognised by the ubiquitin ligase SCF. Figure reproduced with permission from Elsevier Ltd.: (Isoda et al., 2011).

This mechanism of inhibition is alleviated upon sperm entry. Sperm entry causes a change in intracellular calcium levels, which the egg senses through CamKII (Calmodulin-Dependent Protein Kinase II) (Chang et al., 2009). CamKII directly phosphorylates Emi2, leading to the generation of a polo binding site (Hansen et al., 2006). Plk1 (Polo-like Kinase 1) then hyper-phosphorylates these sites, which enhances degradation of Emi2 by the ubiquitin ligase SCF (Skp, Cullin, F-box containing complex) leading to release from CSF-arrest and entry into anaphase II (Jia et al., 2015).

1.6 "Maternal Age Effect": Age-Associated Increase in Aneuploidy in Oocytes

The process of meiotic resumption and ovulation normally occurs once a month in women, thus many oocytes have been arrested in prophase I for many decades before

they are ovulated. This extended period of time greatly increases the risk of infertility, miscarriages and of having children with chromosomal abnormalities, with a dramatic increase after the age of 35 (Nagaoka et al., 2012) (Figure 15). Many of these chromosomal abnormalities are due to an incorrect number of chromosomes, called aneuploidy. A study of over 20,000 human oocytes found the rate of aneuploidy more than doubled in patients of *in vitro* fertilisation (IVF) over 40 compared to those under 35 years where the rate is ~20% (Kuliev et al., 2011). Few chromosomal abnormalities are compatible with live birth, exceptions include trisomy of chromosome 18 or 21 (which cause Edwards and Downs syndromes, respectively) (Savva et al., 2010), characterised by severe developmental abnormalities (Down, 1887; Edwards et al., 1960). Early work suggested that these chromosomal abnormalities are caused by chromosome non-disjunction at meiosis I, i.e. gain or loss of whole, dyad chromosomes (Bugge et al., 1998; Hassold et al., 1991). However, research from Roslyn Angell showed the major cause of abnormalities was the gain or loss of a chromatid, or of prematurely separated sister chromatids (Angell, 1991). "Prematurely separated sister chromatids" describes the process of dyads separating into two sister chromatids while in the egg, effectively making them euploid, but these chromatids segregate randomly upon resumption of meiosis II.

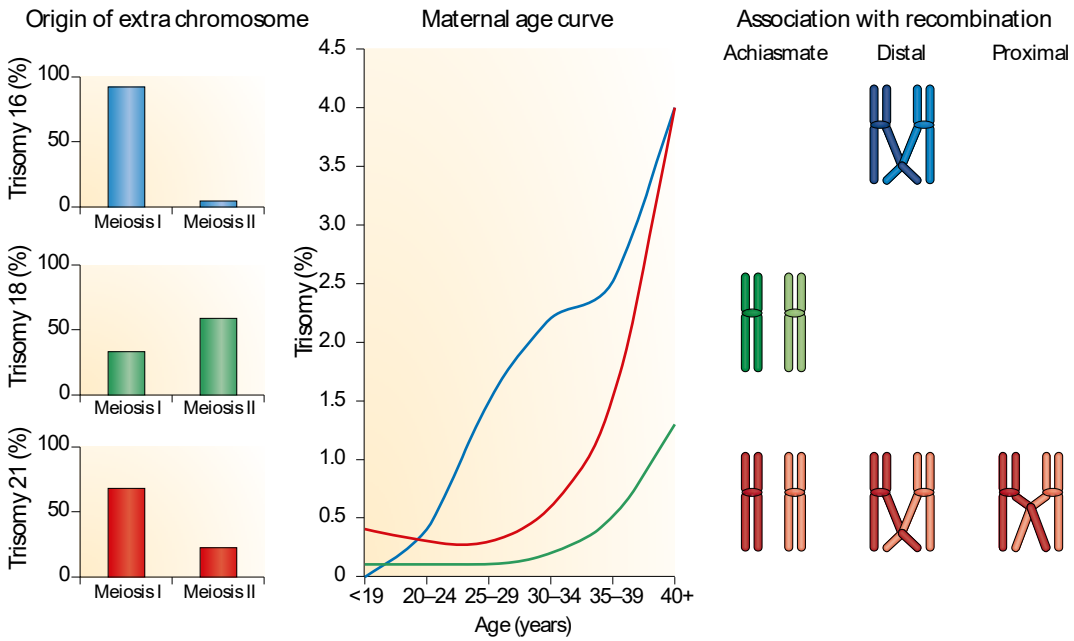

Figure 15 The "Maternal Age" Effect

Advanced maternal age increases the risk of meiosis I and -II errors, with a dramatic increase after the age of 35 years. While the relationship between age and specific chromosomes are different, there is a general exponential

increase at 35. Shown are the three autosomal trisomies: trisomy 16 is incompatible with live birth and results in miscarriage; and trisomy 18 (Edwards syndrome) and 21 (Downs syndrome), which can result in live births but cause developmental disorders. Each trisomy displays different proportions of meiosis I and -II errors and are associated with different error-prone crossover configurations (achiasmate refers to chromosomes lacking crossovers; distal as those with a crossover near the telomere; and proximal as those near the centromere). Figure reproduced with permission from Springer Nature Customer Service Centre GmbH: (Nagaoka et al., 2012).

A major contributor to chromosome missegregation is the absence of crossovers or a crossover location that increases susceptibility to aneuploidy (Nagaoka et al., 2012). As previously mentioned, meiotic cells require a single crossover per homologue pair for faithful chromosome segregation in meiosis I. Therefore, chromosomes without crossovers segregate as "univalents" rather than bivalents in meiosis I (Baker et al., 1996). Some chromosomes appear to have a greater tendency to fail to form crossovers than others, such as chromosomes 18 and 21 (Lamb et al., 1996; Fisher et al., 1995; Bugge et al., 1998; Hassold et al., 1995; Oliver et al., 2008; Lamb et al., 1997).

Chiasmata are the physical manifestation of crossovers, which are stabilised by Cohesin (Maguire, 1974, 1985). As mentioned, removal of Cohesin in anaphase I separates homologous chromosomes, and removal of centromeric Cohesin in meiosis II separates sister chromatids. Therefore in anaphase I, only the Cohesin below (distal to) the chiasma needs to be removed to allow for faithful chromosome segregation in meiosis I (Moore & Orr-Weaver, 1997; Petronczki et al., 2003). This means that the amount of Cohesin distal to the chiasmata is important for faithful segregation. As a result, chiasmata nearer the telomeres have less Cohesin distal to the chiasma and therefore a less stabilised bivalent. Crossovers are generally prevented from occurring near the centromere (Lambie & Shirleen Roeder, 1988). However, when this does happen, it compromises centromeric Cohesin, which is required for faithful segregation in meiosis II. It is therefore likely that the lack of a chiasma, or a single distal chiasma leads to errors in meiosis I; and chiasmata nearer the centromere leads to errors in meiosis II. Location of crossovers can be inferred by comparing a child's DNA to their parents' (Lamb et al., 1997; Oliver et al., 2008, 2012). In children

with trisomy 21, configurations without crossovers were the most common cause of aneuploidy of chromosome 21. Children with aneuploidy of chromosome 21 who were born to younger mothers were more likely to have crossovers nearer the distal end (telomeric) of the long arm (also known as the 'q' arm) of chromosome 21. However, such children born to older mothers had crossovers nearer the centromere (Lamb et al., 2005; Oliver et al., 2008). This shows that distal crossovers are overall more prone to aneuploidy, but as women age even the more stable configurations (such as crossovers nearer the centromere) become susceptible.

Studies using mice have shown that Cohesin itself is reduced with advanced age (>14 months old) (Lister et al., 2010; Chiang et al., 2010). While both Lister et al. (2010) and Chiang et al. (2010) show that there is a reduction of chromosomally-associated Cohesin, Chiang et al. (2010) compare the overall amount of Rec8 in oocytes by Western blotting, and show that it is unchanged with age. That the overall amount of Cohesin isn't reduced with age suggests that Cohesin is mis-located rather than degraded, as would be the case were it to be degraded by Separase. Separase-cleavage of Rec8 results in N-end rule mediated degradation of the protein (Liu et al., 2016). This would predict a reduction of overall Cohesin, so the likely mechanism of Cohesin deterioration is through a cleavage-independent process. Exactly how Cohesin deterioration occurs is unknown, but this is also associated with a reduction in Sgol2 (Lister et al., 2010). Given that Sgol2 itself is recruited to Rec8, this shows that both proteins rely on each other for localisation and function in protection of centromeric Cohesin. Therefore, reduction in one is likely to lead to a reduction in the other in a positive feedback loop that accelerates Cohesin loss over time. Such a positive feedback loop may go some way to explain the shape of the maternal age effect curve, which is more exponential than linear. Studies looking at human oocytes suggest that Cohesin is also reduced in older women (Duncan et al., 2012; Tsutsumi et al., 2014). The result of Cohesin depletion is often seen cytologically as "distally-associated" chromosomes in meiosis I whereby, rather than cross-shaped bivalents, bivalents appear as two weakly joined chromosomes at the telomeric ends furthest away from the centromeres (Chiang et al., 2012).

Much of the research on aneuploidy in human oocytes comes from fixed unfertilised eggs, therefore assignment of the origin of chromosomal abnormalities to meiosis I or meiosis II is done *post hoc*. Assignment becomes more ambiguous as errors assigned to meiosis II may have originated in meiosis I but cannot be detected

due to the *post hoc* nature of analysis. Some chromosomes are more prone to errors that appear to be meiosis I origin rather than meiosis II. For example, trisomy of chromosome 16 and 21 appear to predominantly originate from meiosis I, whereas trisomy of chromosome 18 is more likely to originate from a meiosis II error (Handyside, 2012; Nagaoka et al., 2012) (Figure 15). Recent work in mouse oocytes using live-cell time-lapse microscopy suggests that chromosomes that are "distally-associated" separate before metaphase I, but then realign on the meiosis I spindle as "dyads" in advance of anaphase I, either mono- or bi- oriented (Sakakibara et al., 2015) (Figure 16). When both are bi-oriented, chromatids segregate equally, giving a "euploid" chromosome complement, but these chromatids then segregate randomly in meiosis II. This is sometimes called "balanced predivision". If only one is bi-oriented, this results in gain or loss of a chromatid depending on whether the mono-oriented homologous chromosomes ends up in the oocyte or polar body. Other work has suggested that separated chromatids appear in metaphase II-arrest of aged oocytes due to the separation of dyads shortly after anaphase I (Yun et al., 2014), suggesting meiosis II is the more susceptible division that leads to aneuploidy (Fragouli et al., 2010, 2013; Handyside et al., 2012) (Figure 16).

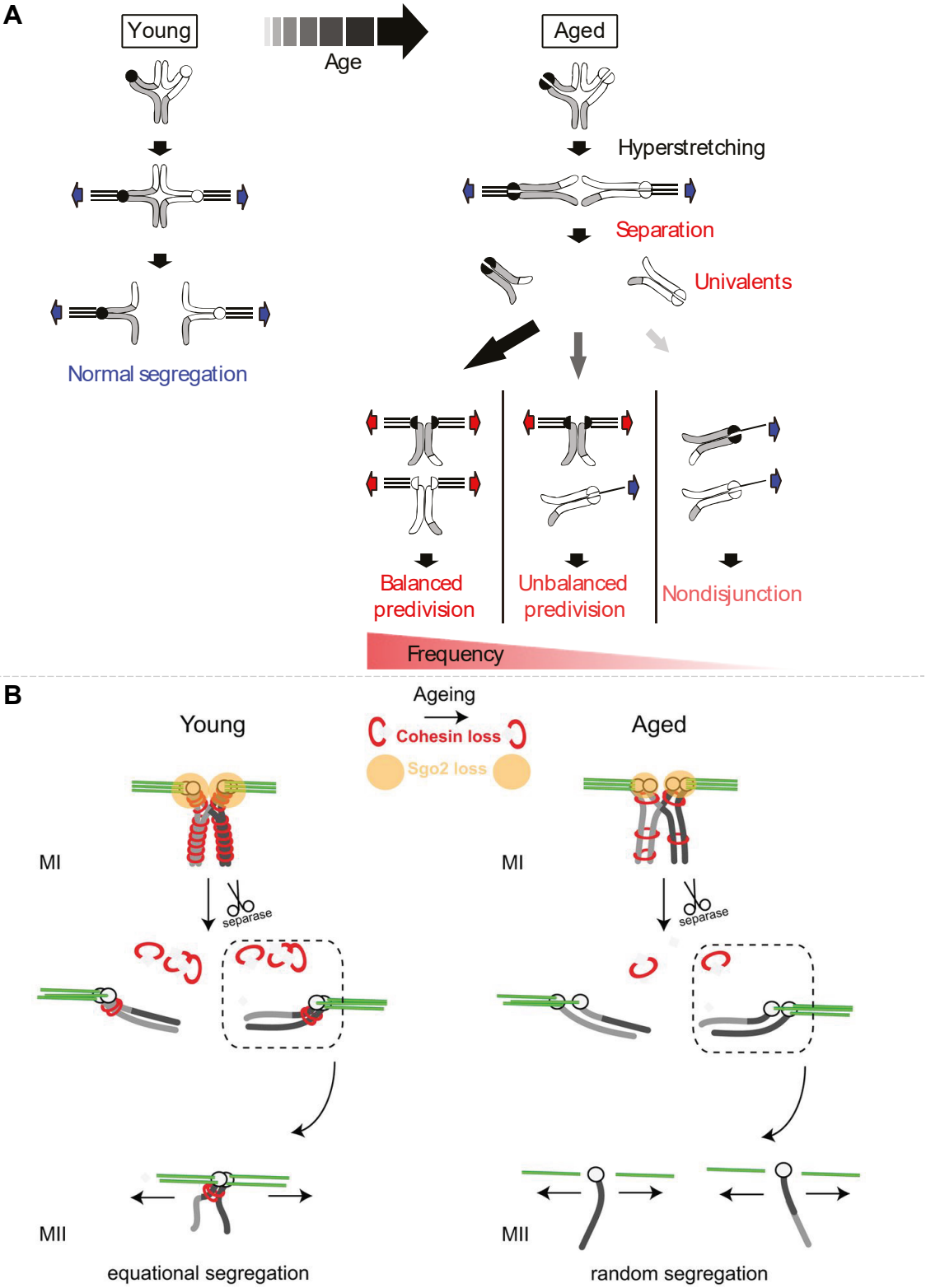

Figure 16 Generation of Aneuploidies in Oocytes of Older Mice

A A schematic showing the most common pathway for segregation errors in meiosis I of oocytes of older mice, as determined by live-cell imaging, was due to "balanced predivision": chromosomes become hyperstretched in prometaphase I, prematurely separate and then divide on the metaphase I

*spindle as "dyads". Figure reproduced from (Sakakibara et al., 2015)[3]. **B** Prematurely separated chromatids can also appear in meiosis II due to dyads separating prematurely shortly after anaphase I. Figure reproduced (Yun et al., 2014)[3].*

1.7 Monitoring Chromosome Segregation by Time-lapse Microscopy

Recent developments in microscopy and computational analyses have allowed for the finer elucidation of how aneuploid oocytes are generated. Unlike widefield microscopes, which typically use a fluorescence lamp to illuminate a large field of view that is captured by a camera, Confocal Laser Scanning Microscopes (CLSMs) work by increasing spatial resolution and reducing phototoxicity (Claxton et al., 2006) (Figure 17). While widefield microscopes can be modified to enhance resolution through super-resolution techniques such as Structural Interference Microscopy (SIM) and Total Internal Reflection Fluorescence (TIRF) (Schermelleh et al., 2010), resolution is typically limited by the out of focus light generated by the excitation of fluorescent proteins. This generates a Point Spread Function (PSF) with a characteristic profile called an "Airy disk" (Cole et al., 2011) (Figure 17). As all the fluorescent molecules are simultaneously excited by the large plane of light generated by the lamp, the rings of neighbouring Airy disks overlap and obscure the true signal. To counteract this, CLSMs use a point scanning detector, combined with a laser for excitation (Jonkman & Brown, 2015). This reduces the number of fluorescent molecules excited and the number of photons captured. Further, the light entering the detector can be restricted using a pinhole to a smaller part of the Airy disk so that, for example, only the strong central peak is captured (Claxton et al., 2006) (Figure 17). The hardware-based resolution of widefield microscopes is therefore restricted by a number of factors, but primarily the power (or magnification) of the objective lens. The point scanning detector of confocal microscopes, however, can be moved into the focal path to increase the magnification (Rietdorf & Stelzer, 2006). The ability for images of multiple resolutions to be taken from the same objective allows for fluorescence-based tracking without compromising the sample, e.g. to use a lower resolution for finding

[3] Reproduced in accordance with CC BY 4.0. https://creativecommons.org/licenses/by/4.0/

the sample and a higher resolution for acquiring high resolution images (Rabut & Ellenberg, 2004).

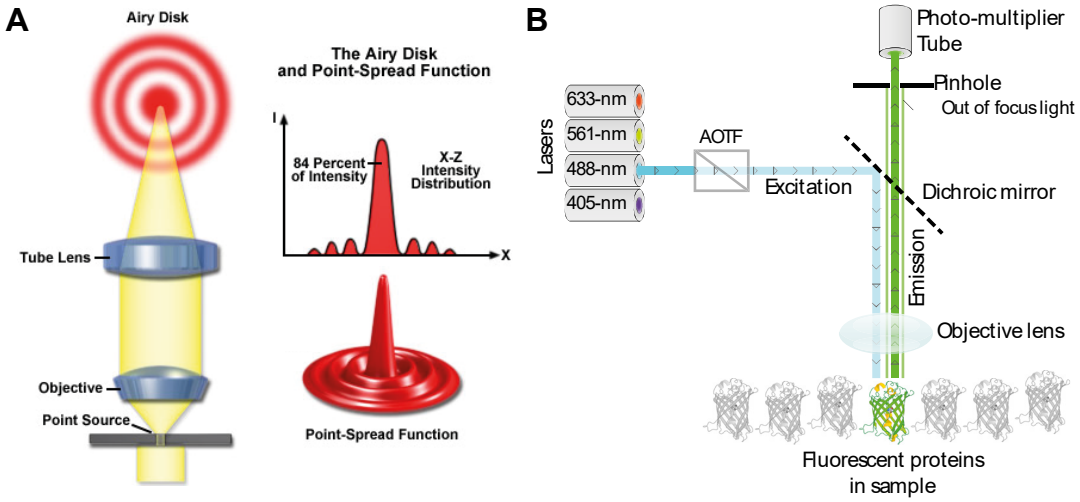

Figure 17 Confocal Laser Scanning Microscopes Increase Resolution by Rejecting Out-of-Focus Light

A *Light excites a point source that generates an optical path traveling through an objective and tube lens. Rather than generating a point, it is spread out with the majority of the light at the centre, surrounded by smaller rings. This optical pattern is called the Airy disk. Figure reproduced with permission from Carl Zeiss Ltd.: (Rottenfusser et al., 2006).* ***B*** *In Confocal Laser Scanning Microscopes, samples containing fluorescent particles are excited by a laser, whose fluorescence is detected by a point-scanning detector such as a Photo-multiplier Tube (PMT). For example, Enhanced Green Fluorescent Protein (EGFP) will be excited by a 488-nm laser. The intensity of light can be attenuated by an Acousto-optic tunable filter (AOTF), which allows for a reduction in the excitation light. The light will then be reflected by a dichroic mirror, through an objective lens, to the sample. Fluorescent probes are excited and will emit light of a different wavelength, which is transmitted through the dichroic mirror. Before reaching the detector, out of focus light can be removed by adjusting a pinhole. Illustration of GFP reproduced with permission from the Royal Society of Chemistry: (Frommer et al., 2009).*

The most common approach to chromosome tracking is to use the signal of a fluorescent-tagged abundant protein associated with chromosomes, such as Histone 2B (H2B) (Hadjantonakis & Papaioannou, 2004; Kitajima et al., 2011) (Figure 18). Even with low resolution and, therefore, lower overall excitation of the sample, a 3D image can be taken around the putative chromosome mass. A centre of mass can

be calculated by finding the weighted mean of each axis (van Assen et al., 2002). A 1D map is generated by walking along each axis to calculate the fluorescence distribution. For example, if a 1D map of the x-axis is generated, then the sum of intensities of the YZ plane starting at the beginning of the axis is calculated, and this process continues along that axis. The peak of this 1D map is then used to generate the x-coordinate. The same process is repeated for the remaining axes to generate an x, y and z coordinate for the microscope to use for refocusing. As the final position is a non-integer coordinate, this is considered a sub-pixel coordinate.

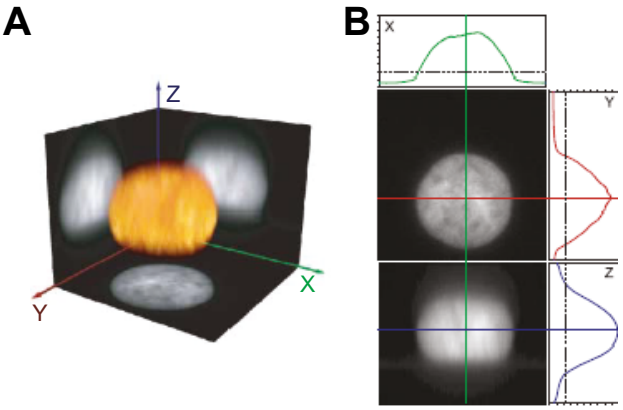

Figure 18 Centre of Mass Tracking

An example of centre of mass tracking using histone signal. ***A*** *Fluorescent-tagged histone is imaged by a confocal microscope in 3D.* ***B*** *A weighted mean of the signal is then produced for each axis and the peak in each axis is used to find the centre of mass. The graphs show the weighted mean of each axis. The top image shows a maximum intensity Z-projection; the bottom image shows a Y-projection. The centre of mass is found by using the peaks in each axis (as shown by the horizontal and vertical lines) and is passed to the microscope for recentring. Figure reproduced with permission from John Wiley and Sons: (Rabut & Ellenberg, 2004).*

High-resolution imaging is then performed of an experiment containing spot-like fluorescent feature such as kinetochores. Images are acquired for an extended period of time at a temporal resolution of ~1.5-5 minutes in mouse oocytes (Kitajima et al., 2011; Sakakibara et al., 2015), or ~2 seconds for mitotically dividing cells (Burroughs et al., 2015). Once captured, kinetochores are detected as spots-like features and assigned their own coordinates, in a process called spot-detection (Figure 19). There are a variety of both open-source (Tinevez et al., 2017; Obara et al., 2007; Vladimirou et al., 2013) and commercial solutions to spot-detection (Imaris

(Kitajima & EMBL Colleagues, 2011), and Arivis (Arivis ag, 2019)), but the overall concept is the same. First, the image is filtered for spot-like features. Image filtering is carried out by generating a small window, or kernel, on an image (e.g. a 3x3x3 pixel kernel) that scans across the image so that all regions are filtered independently (McReynolds & Blythe, 2005) (Figure 19A). Naturally, this window needs to be adjusted so that it is a size that includes a single spot-like feature to prevent generating extra spots (from a window too-small) or too few spots (from too large a window). The spot-like features are filtered using a Laplacian of Gaussian (LoG) function (Figure 19B). However, LoG filtering is computationally intensive and can be approximated using a Difference of Gaussians (DoG) filter (Lindeberg, 2015). A Gaussian filter reduces noise and enhances signal by acting as a short-pass filter, reducing the appearance of spots that are below a certain user-defined size (typically given by a sigma, σ, which is related to the radius, r, of a spot by the number of dimensions, d, through the equation $\sigma \approx \frac{r}{\sqrt{d}}$ (Spring et al., 2016)). A DoG filter, as the name implies, applies two Gaussian filters separately and takes the difference of these two images. This can either be used as a band-pass filter (retaining only features of a size between the two given Gaussian filters) (Spring et al., 2016), or as an approximation of the Laplacian of Gaussian when the ratio between sigma values is ~1.6 (Marr & Hildreth, 1980). The resulting image then needs to be converted to pixel coordinates. This is performed by further filtering the image, this time in order to find which pixel of the putative spot is the maximal intensity of its surrounding pixels, in a process called regional maxima filter (Lindeberg, 1994, 1993) (Figure 19). Pixels in the LoG- (or DoG-) transformed image that overlap with the regional maxima filtered image are taken as the centre of each spot. As this form of spot detection is intensity invariant, spurious spots are typically detected. These can be further filtered by setting a threshold for the minimum intensity. The centres of the spots can then be further resolved to sub-pixel coordinates for increased precision (Tinevez et al., 2017; Armond et al., 2016).

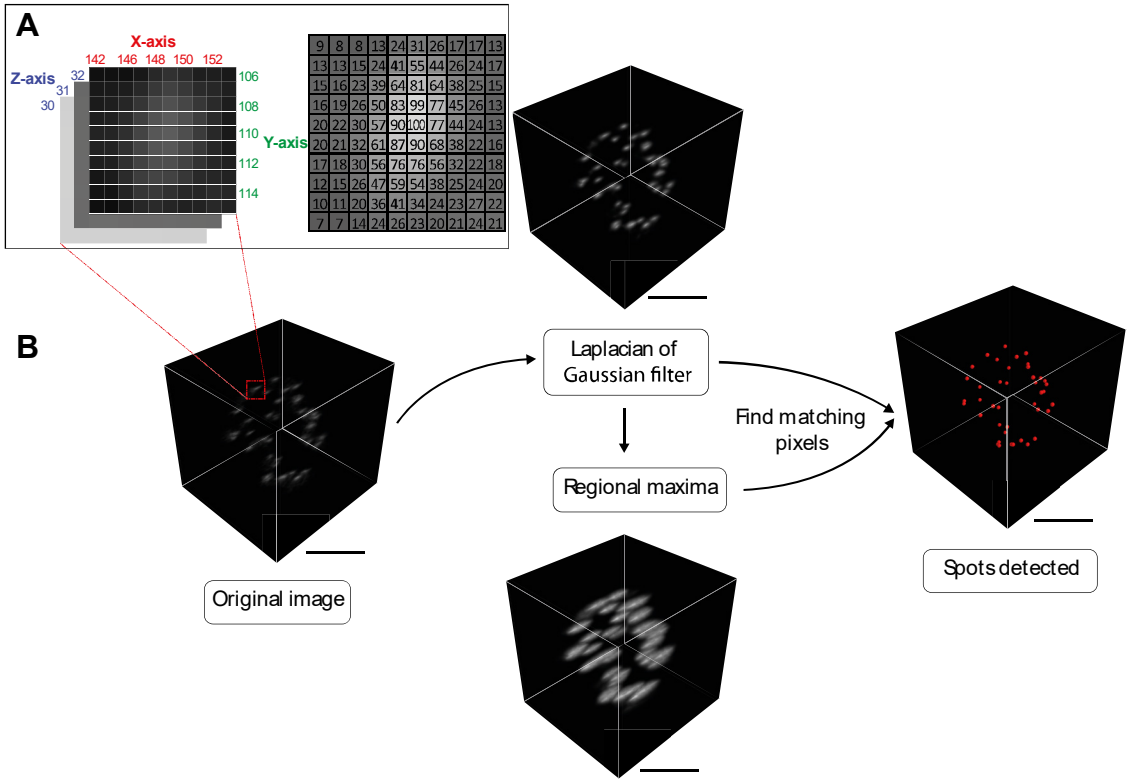

Figure 19 Automatic Spot Detection is Performed by Filtering for Spot-Like Features and Pinpointed by Finding a Regional Maximal Intensity

***A** Shows a sub-region around a putative spot in the 3D image as a series of **Z**-slices (Left) and then the top of this **Z**-slice as numeric values representing the intensities of those pixels (Right). **B** Such sub-regions are used as windows that scan across the image for filtering. For spot detection, this can be done by using a Laplacian of Gaussian (LoG) filter, followed by finding the pixels with the largest intensity in that region (regional maxima). The overlapping pixels between the LoG filtered image and regional maxima are considered to be the centre of spots as shown as red dots in "Spots detected". Black bar next to 3D images is a scale bar = 10 μm.*

Once spots at each time point have been detected, they need to be related between consecutive time points. This is performed by assuming that the movement of spots is minimal between time points. However, due to cellular/chromosome movement, this is typically not true. So, the points are translated (transformation whereby all the points are moved in the same direction) based on the centre of all points, making the points relative to the centre (Kitajima et al., 2011). Once this correction has been applied, spots need to be paired between time points. A "brute-force" (trial-and-error) approach is to look at all the combinations of spots between two consecutive time points and choose the combination that has the smallest global

movement, a variation of the Linear Assignment Problem (LAP) (Burkard et al., 2012). Solving LAPs can be computationally intensive, especially considering this needs to be repeated over all time points. Several algorithms have been proposed, the earliest of which is the Hungarian or Munkres-Kuhn algorithm to efficiently determine the combination with the smallest overall movement (Munkres, 1957; Kuhn, 2010). Further refinement of generating "tracks" is by predicting the next position of a spot based on its previous position, as can be done using a Kalman filter for movement with fairly constant speed (Armond et al., 2016; Jaqaman et al., 2008; Tinevez et al., 2017) or an autoregressive model when speeds change throughout the experiment (Elnagar & Gupta, 1998; Kitajima et al., 2011).

The Munkres-Kuhn algorithm can also be used to pair spots automatically within a time point, for example sister kinetochores, allowing for the measurements of forces applied to pairs of spots (Kitajima et al., 2011; Armond et al., 2015). As mentioned, this approach of using spot detection and generating tracks using the Munkres-Kuhn has already been applied to monitoring the dynamics of kinetochores in mouse oocyte meiosis I (Figure 20).

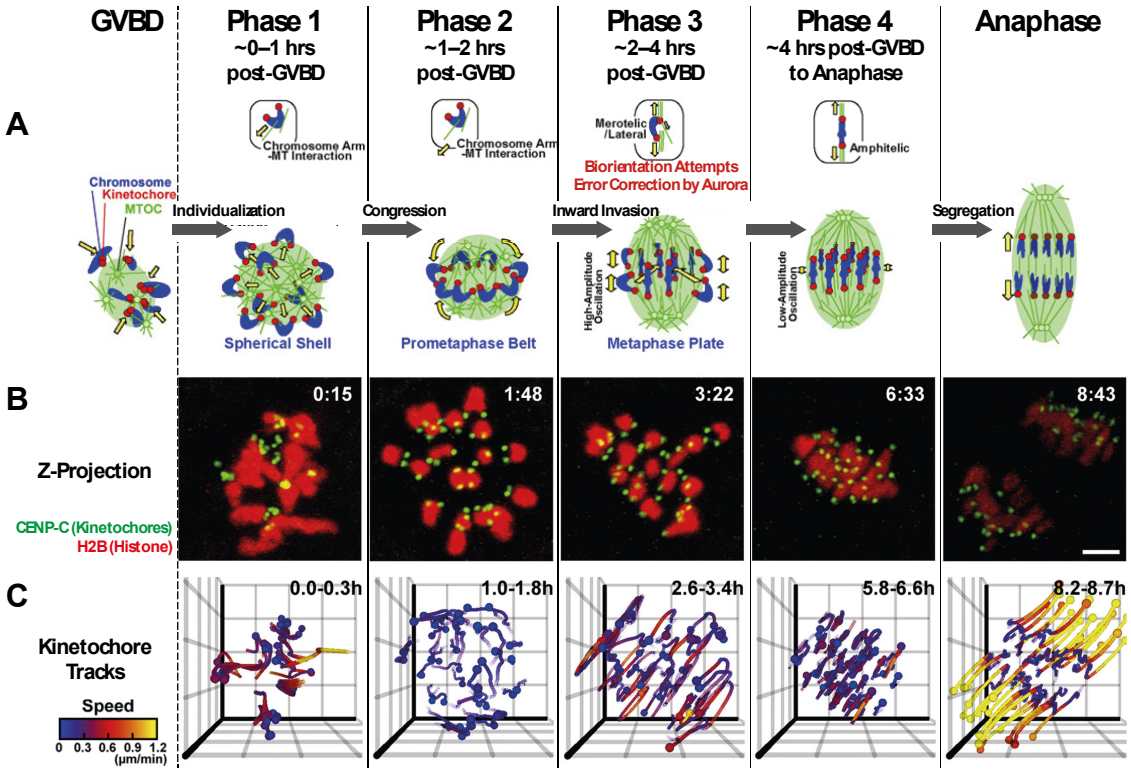

Figure 20 Kinetochore Tracking of Mouse Oocytes Reveals Their Dynamics in Meiosis I

Kinetochore dynamics change through four phases of mouse oocyte meiosis I, between GVBD and Anaphase. The first phase after GVBD, is where decondensed chromatin become individualised into chromosomes. Shortly

followed by the development of a prometaphase I belt, which the chromosomes move around on slowly. In phase 3, the chromosomes increase in pace and start to move laterally on a metaphase I plate in a process called "bivalent stretching". Finally, the chromosomes slow down on the metaphase I plate in advance of anaphase I when chromosomes will segregate rapidly. The approximate duration of each phase is shown under the headers at the top of the figure. ***A*** *A schematic showing the changes in spindle and chromosome morphology during meiosis I.* ***B*** *Shows meiosis I in a mouse oocyte that has been microinjected with RNAs encoding a fluorescent marker of the kinetochores (CENP-C) and histone (H2B). The 3D images from the time-lapse are shown as* ***Z****-projections.* ***C*** *Shows tracks generated from the movement of kinetochores after spot detection. Figure reproduced with permission from Elsevier Ltd.: (Kitajima et al., 2011).*

Chapter 2: Aims

The overall aim of this thesis is to investigate the mechanisms governing accurate chromosome segregation in female mammalian meiosis and to study the consequences of these mechanisms deteriorating, as is the case in oocytes of advanced age.

2.1 Regulation of Cohesin Removal in Meiosis II

The first aim is to elucidate the mechanisms that regulate Cohesin removal in meiosis II. As mentioned, Cohesin is "protected" in meiosis I, but the mechanisms by which protection is removed in meiosis II are poorly understood. In fact, only recently has this begun to be investigated in yeast, where much of our understanding of the fundamentals of meiosis come from. This is mostly due to the difficulty in synchronising yeast in metaphase II, something that eggs do naturally as they arrest in metaphase II in anticipation of fertilisation by the sperm. Meiosis II is often regarded as akin to mitosis since chromatids segregate, unlike in meiosis I where homologous chromosomes disjoin. However, there are a number of unique features; not least that meiosis II is the only round of chromosome segregation that is not preceded by a round of DNA replication. Further, it then leads into the process of embryogenesis, where cells become smaller and smaller in size, despite the usual need for cell growth before DNA replication. There are also unique features in eggs, such as CSF-arrest, that add an additional level of complexity to this stage of the cell cycle.

To shed light on the mechanisms underlying deprotection of centromeric Cohesin at meiosis II, I tested the functional significance of the prevailing model in mammalian eggs, namely that bipolar spindle forces are required for deprotection. While providing a seemingly simple solution to the deprotection problem, this model has not been experimentally tested in any meiotic system. Subsequently, I investigated to what extent aspects of another distinct deprotection model developed for yeast is applicable to mouse eggs. While this model has been proposed for an organism that does not show a natural arrest at meiosis II, it predicts that centromeric Cohesin is protected at metaphase II and is only deprotected upon activation of the APC/C^{Cdc20} at entry into anaphase II. Protection of centromeric Cohesin at metaphase II seems an attractive idea for mammalian oocytes, in which small amounts of centromeric Cohesin have to withstand bipolar spindle forces for extended periods of time.

In summary, I hypothesise that spindle tension is unlikely to be required for deprotection of Cohesin in meiosis II. This is because a mutant strain of budding yeast, where sister centromeres experience bipolar forces in metaphase I, do not segregate as chromatids in anaphase I (Petronczki et al., 2006).

2.2 Live-cell Imaging of Human Oocytes

Secondly, to further understand the cytological data underlying the concept of the maternal age effect, I developed tools for imaging of human centromeres in live-cell time-lapse microscopy. This included the establishment of molecular markers, microscopy techniques and analytical tools. A major aim was to detect and quantify chromosome missegregation in human oocytes, using oocytes that have been specifically donated for research, rather than using oocytes that have been rejected from IVF treatment. In developing these techniques, I aim to understand in more detail the impact of maternal age. In particular, I investigated the question of how bivalent and dyad chromosomes correctly align at metaphase I and –II, respectively, and how these processes are affected by advanced maternal age.

Previous work in mouse and human oocytes has shown that there is an age-associated increase in misalignment at metaphase I (Liu & Keefe, 2008; Lister et al., 2010; Chiang et al., 2010; Nakagawa & FitzHarris, 2017; Yun et al., 2014). Therefore, I would hypothesise that a similar effect would be observed but using an unbiased, quantitative approach.

Chapter 3: Materials & Methods

3.1 Media Used for Oocyte and Egg Culture

A variety of buffered media were used for the culture of oocytes and eggs. M2 medium was used for harvest and collection of oocytes from mice. It is HEPES (4-(2-hydroxyethyl)-1-piperazineethanesulfonic acid)-buffered and therefore enables handling without CO_2 while maintaining a neutral pH (Swain, 2010).

G-IVF™ PLUS medium (Vitrolife) is a complex medium that is typically used for *In Vitro* Fertilisation (IVF) of human gametes and is designed to support the functionality of eggs and sperm. G-IVF™ PLUS medium is bicarbonate-buffered and therefore needs to be equilibrated in a 6% CO_2 environment to maintain a pH of 7.35 (Swain, 2012). G-MOPS™ PLUS medium (Vitrolife) is a medium designed for handling of gametes and embryos outside of a CO_2 environment. It was typically used for handling procedures that occurred during the 16-hour culture of mouse oocytes to metaphase II-arrest, and handling procedures of human oocytes. Given that it is part of the same series of media as G-IVF™ PLUS medium (G-Series™, Vitrolife), it is the most appropriate medium for this purpose. KSOM medium (Millipore) is designed for mouse embryo culture, hence it was used following the resumption of meiosis II from metaphase II-arrest in mouse eggs (Kishigami & Wakayama, 2007).

G-IVF™ PLUS and KSOM media-containing dishes were pre-incubated for at least four hours, usually overnight, at 37 °C with 6% CO_2 and 5% O_2 reduced with N_2. All dishes were overlaid with mineral oil or OVOIL™ (Vitrolife).

G-TL™ PLUS medium was used following activation of human eggs, as it is typically used for time-lapse imaging following clinical *In Vitro* Fertilisation techniques.

3.2 Mouse Oocyte Harvest and Culture

Animals were housed at the Function Genomics Unit, Newcastle University and all procedures were approved by a local Ethical Review Committee and licenced by the Home Office under the Animal (Scientific Procedures) Act 1986.

CD1 Swiss mice were sacrificed by cervical dislocation or exposure to carbon dioxide. GV-stage oocytes were harvested by puncturing ovaries with 29G needles in M2 medium (Sigma) supplemented with 200 μM 3-isobutyl-1-methylxanthine (IBMX, Sigma), to maintain prophase I-arrest (Schultz et al., 1983). This arrest can then be released by culturing oocytes in IBMX-free media ("IBMX-release"). For meiosis I experiments, oocytes were cultured in G-IVF™ PLUS medium (Vitrolife) for

< 8.5 hours. Only oocytes that underwent germinal vesicle break-down (GVBD) within 90 minutes of IBMX-release were used. For meiosis II experiments, oocytes were cultured for 16 hours. Only eggs that extruded a polar body 12-14 hours after IBMX-release were used.

3.3 Mouse Egg Activation and Culture with Inhibitors

Release from IBMX causes resumption of meiosis I, but eggs then arrest in meiosis II (metaphase II-arrest). This arrest can be released by artificially "activating" eggs using a process that mimics the calcium signalling elicited by sperm entry (Kishigami & Wakayama, 2007; Han & Gao, 2013). Mouse egg activation was initiated after 15.5 hours of culture post-IBMX release by transfer to KSOM medium (Millipore) for 30 minutes, and subsequently to KSOM medium containing 5 mM $SrCl_2$ (Sigma) and 2 mM EGTA in KSOM (Millipore) (Kishigami & Wakayama, 2007), such that eggs were activated 16 hours after IBMX-release.

Nocodazole (Millipore) and Reversine (Cambridge Bioscience) were used at a final concentration of 1 μM in culture medium. Both inhibitors were diluted into the culture medium from stock solutions (1 mM) in DMSO (Sigma). MG132 (Carbobenzoxy-Leu-Leu-leucinal, Sigma) was used at a final concentration of 10 μM in culture medium, diluted from a 10 mM stock solution in DMSO.

DMSO concentration was controlled between experimental groups.

3.4 Human Oocyte Collection, Culture and Activation

The human oocyte study was approved by the Newcastle and North Tyneside Research Ethics Committee and licenced by the Human Fertilisation and Embryology Authority (HFEA). Informed consent was obtained from all donors and patients by research nurses. Oocytes were collected by the clinical team at the Newcastle Fertility Centre (NFC). Immature oocytes (lacking the first polar body) that were rejected for IVF treatment were transferred from the NFC in G-IVF™ PLUS medium. Once transferred, oocytes were kept in G-IVF™ PLUS medium at 37 °C with 6% CO_2 and 5% O_2, as recommended by the manufacturer.

Oocytes specifically donated for research were transferred from the NFC in G-MOPS™ PLUS medium. These oocytes were in tight Cumulus-Oocyte Complexes and were treated with hyaluronidase (HYASE™, Vitrolife) for 30 seconds in G-MOPS™ PLUS medium on a heated-stage set to 37 °C before being mechanically "stripped" of cumulus cells with a 146-155 μm glass pipette (Vitrolife) in G-MOPS™ PLUS medium.

Once cumulus cells had been removed, oocytes were further cultured in G-IVF™ PLUS medium.

Human eggs were artificially activated to resume meiosis II by treatment with 100 µM of the calcium ionophore A23187 (Sigma) in G-TL™ PLUS medium for at least 40 minutes (Nakagawa et al., 2001). Further culture was in G-TL™ PLUS medium without ionophore. In later experiments, eggs were kept in the G-TL™ PLUS medium with ionophore for imaging, but exposure was kept to < 3 hours.

3.5 Microinjection and Piezo-Actuated Microinjection

Microinjection pipettes were prepared by pulling capillary tubes on a Sutter P-97 instrument to form two straight microinjection pipettes. A microforge (Narishige MF-900) was used to introduce a 30° bend.

All microinjections were performed on an inverted Nikon TE2000U microscope, with micromanipulators for both a holding pipette and a microinjection pipette (Narishige) (Hayden A. Homer et al., 2005). A programmable pneumatic microinjector (Narishige IM-300) was used to produce specific microinjections corresponding to 2-3% of the volume of a mouse oocyte or 4-5% of that of a human oocyte (a larger pipette opening is usually required for larger microinjection volumes).

Piezo-actuated microinjections were developed for the work in this thesis, specifically for microinjections at the metaphase II-arrest of mouse eggs where traditional microinjection techniques compromise survival (Yoshida & Perry, 2007). The protocol was based on a previous publication (Yoshida & Perry, 2007), but modified to work without mercury, and for microinjection pipettes with smaller openings. Pipettes used for Intracytoplasmic Sperm Injection (ICSI) have a larger opening and are therefore less likely to block due to their contents. An alternative to mercury for piezo-actuation is Fluorinert FC-770 (Hermans-Borgmeyer, 2013). Accommodating microinjection pipettes with smaller openings was performed by reducing the impact of contaminants in the microinjection pipette. Large air pockets were removed by “flicking” the microinjection pipette; smaller air pockets were pushed out of the microinjection pipette by clearing the pipette after back-filling with Fluorinert FC-770. Bubbles can form when loading the aqueous microinjection mixture into the microinjection pipette containing Fluorinert FC-770. This was prevented by washing the microinjection pipette with the microinjection mixture through filling and expelling, prior to commencing microinjections.

Piezo-actuated microinjections were performed with a piezo-impact unit (PM150FU, Prime-tech). Microinjection pipettes were back-filled with 15-20 µl of Fluorinert FC-770 (Sigma), before being front-filled with the microinjection mixture. Once the microinjection pipette was in the oocyte or egg, a single piezo pulse of intensity ~5 was applied, followed by microinjection as described above. Piezo-actuated microinjections were performed on mouse eggs in G-MOPS™ PLUS medium. Once all oocytes/eggs had been microinjected, they were transferred to G-IVF™ PLUS medium. All human oocyte microinjections were cultured the same way. All mouse GV-stage oocytes were microinjected in M2 medium containing 200 µM IBMX and allowed to recover for 2-3 hours followed by culturing in G-IVF™ PLUS medium.

For "TrimAway" experiments (see 3.6 for a brief description), antibody microinjections were performed in G-MOPS™ PLUS medium supplemented with DMSO (Rec8 TrimAway in DMSO experiments), or G-MOPS™ PLUS medium supplemented with 1 µM nocodazole (Rec8 TrimAway in nocodazole experiments) before culture in KSOM medium (with supplements as for G-MOPS™ PLUS medium).

3.6 Concentration and Microinjection of Antibodies for TrimAway

"TrimAway" is a two-part system that enables the depletion of endogenous proteins (Clift et al., 2017, 2018). The first part is the microinjection of Trim21, a ubiquitin ligase that binds cytoplasmic antibodies. The second part is the microinjection of an antibody that targets the protein to be depleted. When these two components are provided, the antibody targets the protein, and the Trim21 targets the antibody leading to proteasome-mediated degradation of the target protein (Foss et al., 2015).

The Rec8 antibody used for TrimAway had already been affinity purified (a generous gift from Melina Schuh). The antibody was concentrated and exchanged into a buffer suitable for microinjection. Both processes were performed using an Amicon Ultra-0.5 Ultracel-50 filter (Merck), according to manufacturer's instructions. Briefly, sample was loaded onto the device and centrifuged at 14,000 x g for 10 minutes. Flow-through was discarded, and PBS (Gibco) appropriate for cell culture was then loaded onto the sample and centrifuged as before. Finally, the filter was inverted and placed into a new tube and centrifuged at 1,000 x g for 2 minutes.

Prior to microinjection, the concentrated antibody was diluted 1:1 in 1 x PBS containing 4 mg/ml Dextran-AF647 (Alexa-Fluor 647) (Molecular Probes) and 0.1% NP-40 (Sigma). This was centrifuged at maximum speed for 5 minutes at 4 °C. Dextran-AF647 was used to check for successful microinjection.

3.7 Air-Dried Chromosome Spreads of Oocytes and Eggs

Zonae pelucidae were removed by a brief exposure to warmed Acidified (pH 2.5) Tyrode's solution (Merck). Oocytes/eggs were pipetted up and down using a glass pipette to prevent oocytes/eggs adhering to the bottom of the dish, before being washed in M2 medium. *Zona*-free oocytes/eggs were placed in a hypotonic solution (0.5% sodium citrate) for 2 minutes (5 minutes for human oocytes/eggs) before being dropped along a poly-lysine-coated slide (Menzel Gläser) covered with a thin layer of fixing solution (1% formaldehyde, 0.14% Triton X-100 and 3 mM DTT, pH 9.2) (Hodges & Hunt, 2002; Susiarjo et al., 2009). A formaldehyde stock solution was prepared by dissolving paraformaldehyde with the help of NaOH (5 M) at 55-60 °C. For later spreads, sucrose was added to the fixative at a concentration of 100 mM ("Frozen spreads"). Slides were dried overnight at room temperature in a humidified chamber. A hydrophobic box was drawn around the region that contained spread chromosomes using a Pap-pen (ImmEdge). "Frozen spreads" were stored in the freezer (-20 °C) until staining. Other slides were washed twice for 2 minutes in 0.05% Photo-flo and twice for 2 minutes in PBS. These slides were then either stored in PBS at 4 °C or stained immediately.

Prior to staining, frozen slides were allowed to warm to room temperature (~5 minutes) followed by soaking in PBS for 15 minutes. Slides were then washed 2 x 2 minutes in 0.05% Photo-flo (Kodak) and 2 x 2 minutes in PBS.

3.8 Immunostaining of Chromosome Spreads

Slides containing chromosomes spreads were incubated in blocking solution (1 x PBS, 0.05% Triton X-100, 0.05% Tween-20, 10% Normal Goat Serum [Stratatech]) for 1 hour at room temperature. Slides were then incubated overnight at 4 °C with primary antibodies, diluted in blocking solution.

Slides were washed 1 x 10 minutes in PBS with 0.4% Photo-flo, 2 x 10 minutes in PBS with 0.1% Triton X-100, 1 x 10 minutes in PBS with 0.4% Photo-flo and 1 x 2 minutes in PBS. Slides were incubated with secondary antibodies, diluted in blocking solution, for 1 hour at room temperature. The aforementioned washes were then performed again, and the slides were mounted with Vectashield with DAPI

(Vectamount). Slides were covered with #1.5 coverslips (22 x 22 mm and 22 x 50 mm: Scientific Laboratory Suppliers, 22 x 40 mm: Deckgläser) and sealed with rubber glue.

Primary antibodies used in immunostaining of chromosome spreads in this thesis are listed in Table 1.

Table 1 Primary Antibodies Used for Immunostaining of Chromosome Spreads

Antibody	Host	Supplier	Dilution
ACA	Human	Antibodies Inc. #15-234/#15-235	1:50
Rec8	Rabbit	Gift from M. Schuh	1:100
Sgol2	Guinea-pig	Gift from C. Höög	1:100
Sgol2	Rabbit	Gift from J. Barbero	1:100
Topo II	Rabbit	Abcam #ab109524	1:100

*In combination with fluorophore-conjugated secondary antibodies, primary antibodies were used to characterise the localisation of proteins, on chromosome spreads prepared from oocytes and eggs, using fluorescence microscopy. The name of the antibody as they appear in this thesis is listed under **Antibody**, along with the **Host** species from which the antibody was generated; the secondary antibody targets the antibody based on the host of the primary antibody. The **Dilution** in blocking buffer and **Supplier** are also given. Anti-Centromere Antibody (ACA) was used to mark kinetochores (Moroi et al., 1980); anti-Topoisomerase II (Topo II) was used to mark the chromatid axis (Earnshaw & Heck, 1985); and anti-Sgol2, and anti-Rec8 were used to mark their respective proteins.*

AF488-conjugated goat anti-Rabbit (Molecular Probes, #A11008) and AF568-conjugated goat anti-Guinea pig (Molecular Probes, #A11075) secondary antibodies were used at a 1:800 dilution. AF647-conjugated goat anti-human (Molecular Probes, #A21445) and Cy5-conjugated goat anti-human (Stratatech, #109-175-003) secondary antibodies were used at a 1:400 dilution.

3.9 Image Acquisition of Chromosome Spreads and Live Cells

Imaging was performed on a Nikon A1R confocal microscope fitted with 2 GaAsP detectors (using NIS elements software (Nikon Instruments Inc., 2013)), a Zeiss LSM880 microscope with Airyscan (using Zen 2.3 software (Carl Zeiss Microscopy GmbH, 2019)) or a Nikon TE2000U microscope (using Metamorph (Molecular Devices, 2011)).

Care was taken to keep images quantifiable, where relevant, between experimental datasets. Microscope settings were optimised such that physical regions were exposed to the same low level of light between experiments of the same dataset. The lowest exposure to light (LED/lasers) was used to reduce phototoxicity and photobleaching. Phototoxicity is relevant for live-cell experiments where excess amounts of light (especially those of a lower wavelength) can damage cells (Icha et al., 2017). Photobleaching is the artefact of repeatedly or excessively exposing fluorescent probes (usually a fluorescent dye or protein) to light in such a way that it diminishes the fluorescent probe's ability to emit light upon further excitation (Ghauharali & Brakenhoff, 2000). To ensure that physical regions were exposed to the same level of light, the following microscope settings were kept consistent: scanner speed; laser power; detector gain; exposure time; and spatial resolution. Spatial resolution is chosen based on the knowledge that too high a resolution is likely to cause photobleaching/phototoxicity and too low resolution will give images of too poor quality to analyse. Laser power was kept as low as possible while ensuring that signal and noise could be visually distinguished. At this point, detector gain was modified so that a 12-bit histogram was ~20-50% full to ensure adequate dynamic range (~800-2000 grey values). If the higher gain resulted in considerably more noise, then gain was reduced, and the laser power increased instead. For experiments looking at reduction of proteins between experimental groups, optimisation was performed on the experimental group where signal was expected to be higher to prevent saturation if settings were optimised with the experimental group containing lower signal. The Nikon A1R confocal microscope contains an internal laser power meter, which can record and restore laser output between experiments. All imaging between controls and experimental groups were performed in the same session, though different repeats were imaged on different days. This was to ensure laser stability was similar and therefore relative for each repeat.

3.9.1 Imaging of Chromosome Spreads

Chromosome spreads were either imaged on a Nikon A1R confocal microscope, or a Zeiss LSM880 microscope with Airyscan. All chromosome spreads were imaged as Z-stacks by manually finding the best-focus and setting this as the centre position and taking the same number of Z-planes above and below this point. Imaging was performed from highest wavelength to shortest wavelength to prevent cross-talk,

which is the non-specific excitation of a different fluorescent protein/dye whose illumination is also captured (Bacia et al., 2012). Emission filters were used to further prevent the impact of cross-talk on images and detect specific signal. For eggs that had been spread shortly after nocodazole treatment, chromosomes often clumped into smaller groups (due to the lack of a spindle keeping all chromosomes together). These clumps were imaged individually in order to ensure that as many chromatids were captured as possible.

3.9.2 Imaging of Live Mouse Oocytes and Eggs

Mouse eggs were predominantly imaged on a Zeiss LSM880 microscope with Airyscan. To allow for imaging of eggs in different inhibitors in the same experiment, a 4-chamber glass-bottomed dish (CellVis) was used. Eggs were cultured in a 2 µl drop of media (typically KSOM medium), overlaid with mineral oil, all near the centre of the dish to reduce time taken for stage repositioning. To account for Z-drift during these experiments *Definite Focus.2* was used (Carl Zeiss Microscopy GmbH, 2017), which maintains focus relative to the coverslip. This was performed before each time point. All attempts to keep culture similar to incubator culture were taken (e.g. CO_2, O_2 and temperature were kept to the same standard as in incubators).

For monitoring TrimAway of Rec8 in mouse eggs, the experiment was performed on a Nikon TE2000U microscope using Metamorph software. A high-walled glass bottomed-dish was used (ibidi), and culture was performed in a 2 µl-drop of medium (KSOM medium), overlaid with mineral oil. 5 x 7.5 µm steps around the centre of the eggs were taken every 5 minutes.

For imaging of oocytes for CRISPR optimisation, oocytes were cultured on a Nikon A1R confocal microscope. Imaging was performed with atmospheric oxygen (20.9%), but CO_2 was kept as 6%. Time-lapse experiments were performed either with Nikon's ND-acquisition module (when imaging multiple oocytes) or with a custom macro to autofocus on chromosomes as described in 5.4. Imaging of mouse oocytes for CRISPR optimisation on a Zeiss LSM880 microscope with Airyscan was performed using the *AutoFocusScreen* or *MyPiC* macro (Kitajima et al., 2011; Politi et al., 2018). These two macros are written in the native Zen environment using Visual Basic for Applications (VBA), which were unable to calculate the centre of mass on raw Airyscan images, as each position in the image is represented by 32 intensities (one from each detector of the 32-detector array in the Airyscan detector (Huff, 2015)). As a result, chromosome tracking was performed in "Airyscan mode" using the "CO"

(Confocal) option. This enables tracking as all 32 detectors are used together to give one intensity per position, which allows for calculating the centre of mass in the Zen environment and minimally changes the optical path between tracking and acquisition of high-resolution images. The latter was performed in "Airyscan Fast" mode.

3.9.3 Imaging of Live Human Oocytes and Eggs

Human eggs were imaged on a Zeiss LSM880 microscope with Airyscan. High-resolution images were taken with the Airyscan detector using Fast mode. Imaging was performed in a high-walled glass-bottomed 35 mm dish (ibidi). Initially this was done in a 2 µl-drop. As low volume did not prevent movement of oocytes but could have a negative effect on culture conditions (human oocytes are recommended to be cultured with 10 µl medium per oocyte (Vitrolife Sweden AB, 2017)), this was changed to 60 µl for a maximum of six oocytes. To make such dishes, 200 µl of media was added to the base of the dish and spread around with a pipette tip to cover the floor of the dish. OVOIL™ was then used as an overlay. The dish was tilted on an angle so that media accumulated in one region and 140 µl was aspirated from this region to reduce the volume to 60 µl.

"Chromosome" tracking was performed as described in 5.8, 5.9 or 5.10.

3.10 Image Processing and Analysis, and Statistical Analysis

3.10.1 Image Processing

Image processing was performed in Zen Black 2.3 (for Airyscan processing) (Carl Zeiss Microscopy GmbH, 2019) or FIJI (all other processing) (Schindelin et al., 2012). Image processing was done in batches with a macro so that processing procedures could be traced (or *SpotCollectionManager* as described in 5.5). For many of the images with spot-like features, a Difference of Gaussian filter was applied using *SpotCollectionManager* to enhance signal and remove noise. Images in figures are maximum-intensity Z-projections unless otherwise stated. All measurements were performed on raw images in 3D where relevant. All scale bars are 10 µm.

3.10.2 Euclidian Distance, Munkres-Kuhn Algorithm, and Outlier Detection

Distances used throughout this thesis are Euclidian distances. That is, they are the square-root of the sum of the square of differences in each dimension (i.e. in X, Y and Z) (Anton & Rorres, 2013).

The Munkres-Kuhn algorithm is a solution to the Linear Assignment Problem (Burkard et al., 2012). It can be used to make assignments between two groups such that a corresponding measure between the members of each group are kept the smallest. For example, if a matrix of Euclidean distances is made between the members of each group, the Munkres-Kuhn algorithm will find assignments between the two groups to reduce the overall distances between each group. This process can be convenient for automatically pairing points.

Outlier detection was performed using Tukey's fences (Tukey, 1977). Briefly, univariate data were sorted and the difference between the first quartile (Q1, 25% of the number of data points, or the mean of the points above and below 25% if the number of data points is odd) and the third quartile (Q3, 75%) was defined as the interquartile range (IQR). Values below $Q1 - 1.5 \times IQR$ and above $Q3 + 1.5 \times IQR$ were defined as outliers.

3.10.3 Fluorescence Intensity Measurements

Fluorescence intensities were measured using a modified version of *SpotCollectionManager*. Firstly, spots were detected on the kinetochore channel, and curated so that they were in the correct position. As the Rec8 channel contains a lot of noise, spots were added manually. Each were saved as separate "spot collections".

Intensity measurements were made using TrackMate (Tinevez et al., 2017), which calculates the mean intensity of an ellipsoid around a given point (0.5 μm for signal measurement, 1 μm for background measurement). To compare signal to background, a mean background measurement was made and subtracted from the signal measurement. The background is a region in the image away from chromosomes.

For experiments where quantification was performed on multiple days, all fluorescence intensities were normalised to the mean of a "standard" for that day. E.g. for fluorescence intensity at metaphase II-arrest compared to anaphase II, mean intensities at metaphase II-arrest were used for normalisation. This normalisation was chosen over normalising to a different channel, as each channel was excited by independent lasers. Normalising to a different channel is often used when imaging is done with the same light source (e.g. a widefield microscope experiment that uses

a single fluorescence lamp) (Bhakdi & Thaicharoen, 2018). However, confocal systems tend to use independent lasers for each excitation and therefore the power output of each laser varies independently.

3.10.4 Kinetochore Counting from Chromosome Spreads

Kinetochore counting was performed manually. Staining of Topoisomerase II helped to further assign whether sisters were separated or not.

Eggs that were spread after nocodazole incubation occasionally resulted in chromosomes of the same egg being separated into smaller groups (due to the absence of a spindle). A FIJI macro was developed and used to extract the stage positions and map these relative to each other. This information was used with the number of chromatids, blind to separation levels, to reassign eggs *post-hoc*. Eggs that had fewer than 10 chromatids assigned to them were excluded from analysis.

3.10.5 Securin Mean Fluorescence Intensity

Securin Mean Fluorescence Intensity was calculated on mean-intensity Z projections of raw images. The images were then registered to account for drift using *StackReg* in FIJI (Thevenaz et al., 1998). Circular ROIs (Regions of Interest) were drawn around each egg (either the whole egg or a sub-region in eggs to account for part of the egg going out of view). The mean intensity of each ROI was then calculated using the FIJI plugin *Time Series Analyze*r (Balaji J, 2014). The mean of a region away from eggs ("background") was taken and subtracted from all positions. The resulting values were then set proportionate to the initial value to account for variation in expression levels. Mean and standard deviation were calculated by *numpy* in Python (Van Der Walt et al., 2011).

3.10.6 Spot Detection and Registration for Tracking Centromeres in Mouse Oocytes

Spot detection was performed using *SpotCollectionManager* (as described in 5.5). Using *SpotCollectionManager*, a Difference of Gaussian filter was performed on the channel containing spot-like features in each image from a time-lapse experiment and automatic spot detection was performed. These were then manually curated. Spots were paired using the Munkres-Kuhn algorithm (Munkres, 1957; Kuhn, 2010), and then also manually curated.

Once all spots had been identified for the time series, spot registration was performed using a custom FIJI script (as described in 5.6). The script first extracts

all paired spots from each image and performs tracking using the Linear Assignment tracker in TrackMate (Tinevez et al., 2017). Upon completion, any spots that were not linked throughout the experiment were collected and the same Linear Assignment tracker was used to assign these to tracks.

3.10.7 Nuclear:Cytoplasmic Ratio

Calculations of the nuclear:cytoplasmic ratio were performed in FIJI and Python. A circular ROI was drawn in a single Z-plane in a region of the dCas9-mNeonGreen channel that overlapped with strong H2B signal. The built-in "measure" function of FIJI was used to determine the mean grey value. The ROI was then moved away from the H2B signal and another measurement taken in the cytoplasm. As the area was kept the same, the ratio can be calculated from the ratio of these two mean grey values. A single Z-plane was used to prevent including the fluorescence of a cytoplasmic region from other Z-planes, as would be the case in a Z-projection.

3.10.8 Timing of Events in Human Oocytes Relative to hCG Time

To determine the time of cell-cycle events relative to hCG administration, a FIJI macro was developed and used to extract the acquisition time of each image and this was subtracted from the hCG time for each donor. Each image was then scored as GV-stage (nuclear membrane intact), prometaphase I (absence of a nuclear membrane, spindle not bipolar, chromosomes not aligned), metaphase I (bipolar spindle containing mostly aligned chromosomes), anaphase I (dyads separating), prometaphase II (stage between anaphase I and metaphase II), metaphase II (bipolar spindle containing mostly aligned chromosomes), anaphase II (chromatids separating). As imaging had to be restarted multiple times, if the stage before and after restarting was the same, the oocyte/egg was assumed to be the same during this period. Oocytes that had been observed to fail to progress beyond metaphase I were excluded from the displacement analysis.

3.10.9 Transformation of Images in 3D

For generating representative images of metaphase I and -II spindles, 3D Z-stacks were rotated in 3D such that the centre of the image was the centre of the chromosome mass and the X-axis is equivalent to the spindle axis (i.e. between the two poles of the spindle). This was carried out based on a previously published method using Eigenvalue decomposition of kinetochore pairs (Kitajima et al., 2011; Strang, 2016). First a variance-covariance matrix is generated for each axis (X, Y and

Z) of the centre of each pair of kinetochores. Eigenvalue decomposition of these points creates three new axes (Eigenvectors) that better represent the data (equivalent to the Spindle axis, Spindle equator, and a less prominent spindle axis). The variance-covariance matrix is performed on the centre of kinetochore pairs to reduce the variation in the spindle axis. In doing so, the Eigenvalue (or size) of the smallest size (i.e. that which has the lowest variance) is the spindle axis. The largest is then the spindle axis. The centre of all points is the mean x, y and z position of all kinetochore pairs.

Given this information, Eigenvectors are matched up to the corresponding X, Y and Z axes of the original image and a least squares fitting approach is used to transform images using a Rigid Body model fit calculated from corresponding points in the coordinate system from Eigenvalue Decomposition and the acquired image using modules in TrakEM2 (Cardona et al., 2012).

3.10.10 Displacement Measurements in Metaphase of Human Oocytes and Eggs

In the previous approach, the spindle axis was estimated by looking at the inter-kinetochore distances. It was assumed that a larger inter-kinetochore distance corresponded to a larger spindle force and therefore better represented the spindle axis. However, this does not consider crossover location or size of the chromosomes when this approach is done in meiosis I. Further, this approach relies on time-lapse data to stabilise the spindle axis estimation, which was often not available for the work in this thesis. As a result, an alternative approach was taken to estimate the metaphase plate. A mean unit vector was calculated using the unit vectors of each paired centromere (Strang, 2016). As some of these unit vectors may be similar but in the reverse direction, vector addition of the unit vector with the mean unit vector was performed and if the magnitude was reduced, the unit vector was reversed before being added to the spindle axis estimate (Strang, 2016). To account for chromosomes that were oriented in a direction different to the spindle axis estimate, those with outlying angles to the mean unit vector were removed and the mean unit vector was calculated as previously described.

Given the mean unit vector, the centre of all points, the equation of an infinite plane can be calculated (Strang, 2016). Projecting the centromeres (or mean position of centromeres, in the instance of paired centromeres) to this plane and calculating the Euclidean distance between these original and projected points is defined as the distance from the metaphase plate (Strang, 2016).

3.10.11 Displacement Measurements of Centromeres in Anaphase of Human Oocytes and Eggs

For single time points, it is not known which kinetochores/centromeres belong to the same chromosome. As a result, the process for measuring displacement in metaphase needs to be modified. First, to estimate the spindle axis, k-means clustering was performed to group each separating bulk of chromosomes/chromatids (Lloyd, 1982). A vector that passes through the centre of these was used as an estimate of the spindle axis (Strang, 2016). Each kinetochore/centromere was projected onto this vector to identify the front of each separating bulk, i.e. the kinetochore position relative to the spindle axis (referred to as the "anaphase front"). The points that were the furthest in each direction from the midpoint between each cluster was used, as before, to generate two planes, one for each cluster. The distance between centromeres projected to their respective planes and the original position was used to measure the extent of lagging (Strang, 2016).

3.10.12 Statistical Analysis

All statistical tests were performed in *SciPy* in Python and all graphs were plotted with *Plotly* in Python. Comparisons where there are two groups were performed using Mann-Whitney U test as a two-tailed test in *SciPy* using the `use_continuity` command to correct for ties. Comparisons of proportions were performed using Fisher's exact test in *SciPy* using default arguments. Where relevant, multiple test correction was performed using Bonferroni's procedure. Student's t-test was used when comparing mean and standard deviations, when comparisons were made to published datasets without raw data.

3.11 Molecular Cloning

Plasmids were generated by "traditional" restriction enzyme cloning or by ligation-independent cloning using the In-Fusion procedure (Takara Bio) according to manufacturer's instructions. Polymerase Chain Reaction (PCR) fragments were generated using Q5 PCR Kit (NEB) according to manufacturer's instructions. For some constructs, oligo annealing was used instead. Oligo annealing was performed by mixing 2 µg of each oligo in annealing buffer (10 mM Tris/HCl, pH 7.5-8.0, 50 mM NaCl, 1 mM EDTA), denaturing the oligos at 95 °C for 2 minutes and then linearly decreasing the temperature to 25 °C over 45 minutes. Once ligation of the vector and insert(s) was complete, 2.5 µl of each reaction was used to transform Stellar Competent Cells (Takara Bio) according to manufacturer's instructions and

then plated on LB agar plates with appropriate antibiotics (usually 100 µg/ml ampicillin or 50 µg/ml kanamycin). After 16-18 hours of culture at 37 °C, the plates were stored at 4 °C. Plates were either used to inoculate 2 ml of antibiotic-supplemented LB broth or used in colony screening. Colony screening was performed using the OneTaq polymerase kit (NEB) according to manufacturer's instructions. Only positive clones were used for inoculation.

After 16-18 hours of culture, cells we collected by centrifugation (5 minutes at 10,000 rpm in a bench-top centrifuge) and then processed through the Wizard SV Mini-prep kit (Promega) according to manufacturer's instructions but eluted in low EDTA TE buffer (ThermoFisher Scientific). To confirm correct generation of a plasmid, DNA was sent for Sanger sequencing at Source BioScience along with primers appropriate for the construct. Primers were chosen from the plasmid backbone (e.g. in pGEMHE-based plasmids: "T7F": 5'-TAATACGACTCACTATAGGG-3', is present in the T7 promoter upstream of the 5' start site of the coding sequence; "XL_BG_R": 5'-TTTATTAGGAGCAGATACGAATGG–3', which is downstream of the 3' stop site of the coding sequence) or internally (in instances of mutagenesis, for example). Source BioScience perform Sanger sequencing on an ABI 3730 DNA Sequencer (Applied Biosystems).

3.12 *In Vitro* Transcription

Plasmids used for *in vitro* transcription were subcloned into a pGEMHE vector, which contains a T7 promoter and linearisation sites 3' to a poly-A tailing sequence. The T7 promoter enables transcription using a T7 polymerase, which can be capped to mimic eukaryotic RNAs. In order to do this, plasmids with a pGEMHE backbone were linearised, as otherwise transcription would not terminate at the 3' end of the nascent chain.

The reaction was then digested with proteinase K (Roche), extracted with phenol:chloroform, followed by precipitation of the DNA with ethanol. Briefly, 2 µl of 10 mg/ml proteinase K and 5 µl of 10% SDS were added to the restriction digest reaction and incubated at 50 °C for 30 minutes. The reaction was brought to 150 µl with DEPC-treated water and thoroughly mixed with 150 µl of phenol:chloroform:isoamyl alcohol to form an emulsion before being centrifuged at maximum speed for 1 minute. The top phase was withdrawn and subsequently mixed with 150 µl of chloroform, followed by centrifugation at maximum speed for 1 minute. The upper phase was supplemented with 1 µl of glycogen (20 mg/ml), 5 µl

of 3 M sodium acetate (pH 5.2) and 300 µl of 100% ice-cold ethanol. This mixture was placed at -80 °C for 1 hour before being centrifuged for 15 minutes at room temperature. The supernatant was removed, and residual ethanol was removed again after a brief centrifugation. The DNA pellet was air-dried and resuspended in 6 µl of nuclease-free H_2O.

In vitro transcription was performed with phage T7 RNA polymerase using the mMessage mMachine T7 kit (Ambion) according to manufacturer's instructions. Plasmid DNA was removed by a 15 minute treatment with Turbo DNase (Ambion). The RNA was diluted to 100 µl with DEPC-treated water and purified with an RNeasy micro kit (Qiagen) according to manufacturer's instructions except it was eluted in 13 µl of RNase-free H_2O. The concentration of the RNA was determined with a NanoDrop device (Thermo-Fisher Scientific) and stored at either -20 °C or -80 °C until use.

In vitro transcribed RNAs used in this thesis are listed in Table 2.

Table 2 In vitro Transcribed RNAs Used for Microinjection

Plasmid	Source	RNA conc.	Dilution
bpSV40NLS-dCas9-mNeonGreen-c-mycNLS[4]	This work based on dCas9-mNeonGreen	250 ng/µl	1:4
Cdc20(MIM)	This work based on (Rattani et al., 2013)	2000 ng/µl	2:1
Cdc20(WT)	This work based on (Rattani et al., 2013)	2000 ng/µl	2:1
dCas9-EGFP	This work based on (Chen et al., 2013)	250 ng/µl	1:4
dCas9-mNeonGreen[4]	This work based on dCas9-EGFP	250 ng/µl	1:4
dCas9-mNeonGreen-NucleoplasminNLS[4]	This work based on dCas9-mNeonGreen	250 ng/µl	1:4
H2B-mCherry	(Schuh & Ellenberg, 2007)	1500 ng/µl	[1:4,1:1]

[4] See 5.2.1 for more details

Plasmid	Source	RNA conc.	Dilution
H2B-miRFP670	This work, based on H2B-mCherry	1500 ng/µl	[1:4,1:1]
H2B-mScarlet	This work, based on H2B-mCherry	1500 ng/µl	[1:4,1:1]
mEGFP-Trim21	(Clift et al., 2017)	800 ng/µl	1:1
mEGFP-Trim21(ΔC)	(Clift et al., 2017)	800 ng/µl	1:1
mSecurin-mNeonGreen	This work based on (Hayden A Homer et al., 2005)	1000 ng/µl	1:2
NLS-Flag-linker-dCas9-mNeonGreen[4]	This work based on dCas9-mNeonGreen	250 ng/µl	1:4

*Microinjection of oocytes and eggs with in vitro transcribed RNAs encoding a fluorescent-tagged version of a protein of interested can be used to investigate the localisation of that protein of interest. This also allows for the characterisation of that protein over time, and therefore during meiosis. Another use of microinjection is in understanding the effect of perturbing the function of a protein of interest, e.g. by using a dominant negative form of that protein to perturb the function of the endogenous protein. In vitro transcribed RNAs are produced from plasmid DNAs, the names of these appear in **Plasmid**. The **Source** of the DNA describes which authors created the plasmid or how the plasmids were made. After RNA was generated, they were diluted as in **RNA conc**. and stored at -20 °C or -80 °C until use. Prior to microinjection, a master mix of different RNAs for that experiment were made from these stocks. The final **Dilution** in such a mix is given; in some cases different dilutions were used, the range is shown in square brackets.*

3.13 sgRNA Synthesis

The DNA template for sgRNAs was generated through Q5 PCR of a stock plasmid containing the sgRNA backbone (pUC-sgRNA(FFE), derived from pSLQ1651-sgTelomere(F+E), a generous gift from Bo Huang, (Chen et al., 2013)). A forward primer was designed so that it contained a T7 promoter, followed by the targeting

sequence, and then a short region of homology to the plasmid (e.g. 5'-GATCACTAATACGACTCACTATAg-n_{20}-GTTTGAGAGCTATGCTGGAAAC-3', where n_{20} is a targeting sequence consisting of 20 nucleotides). A universal reverse primer was used (5'-AAAAAAAGCACCGACTCG-3') and PCR using Q5 polymerase was performed as recommended by the manufacturer. Upon completion, DNA was purified using a MinElute Reaction Cleanup Kit (Qiagen). The concentration was found using a NanoDrop device and 200 ng of DNA template was used as template for either a T7 mMessage Machine T7 kit, MAXIscript T7 Transcription Kit (Thermo Fisher Scientific), or T7 Quick High Yield RNA Synthesis Kit (New England Biolabs). All reactions were performed as recommended by the manufacturer, except that they were allowed to continue overnight. DNase I was added to terminate the reaction (as recommended by the manufacturer).

sgRNA was purified by phenol:chloroform extraction and precipitated with isopropanol. Briefly, the reaction was diluted to 135 µl with DEPC-treated water, 15 µl of 5 mM ammonium acetate/100 mM EDTA solution (Ambion) and 150 µl of phenol:chloroform:isoamyl alcohol (Sigma Aldrich) were added and mixed thoroughly. The emulsified mixture was centrifuged for 1 minute at maximum speed. The top phase was collected and added to 150 µl of chloroform (Sigma Aldrich). After mixing and centrifugation, the aqueous phase was moved to a new tube. 150 µl of isopropanol was added and mixed before precipitated for at least an hour at -20 °C (or for 30 minutes at -80 °C followed by 30 minutes at -20 °C). The sgRNA was collected by centrifugation at maximum speed for 15 minutes at 0-4 °C. After removal of the supernatant, the pellet was air-dried and resuspended in 60 µl of RNase-free H_2O. A NanoDrop device was used to determine the concentration of the sgRNA, which was stored at -80 °C until use.

sgRNA targeting sequences can be found in Table 3.

Table 3 sgRNA Targeting Sequences Used to Visualise Repeats in Oocytes

Species	Location	Target sequence	Source
Mouse	**Akap6 (chromosome 12)**	CACAGTGCTCAGGGGACC	(Fu et al., 2016)

Species	Location	Target sequence	Source
Human	**α-satellite (centromeres)**	GAATCTGCAAGTGGATATT	(Chen, Hu, et al., 2016)
Human	**ß-satellite (centromeres of chromosome 9, 13, 14, 15, 21, 22)**	GACAAGAGTTACATCACCT	(Chen, Hu, et al., 2016)
Mouse	**Chromosome 9 pericentromere**	GGCAGTCAGTCATCAC/ TCAGTCATCAC	This work[5]
Mouse	**Major satellite (peri-centromeres)**	CCACTGTAGGACGTGGAATA	(Deng et al., 2015)
Mouse	**Minor satellite (centromeres)**	ACACTGAAAAACACATTCGT	(Anton et al., 2014)
Human / Mouse	**Telomere**	GGTTAGGGTTAGGGTTAGGGTTA	(Chen et al., 2013)

*As part of a modified CRISPR system, where the Cas9 nuclease is replaced by a fluorescent-tagged, nuclease-dead version of the protein (dCas9-FP), sgRNAs can be used to target specific DNA sequences. A targeted locus must recruit enough dCas9-FPs that the signal is greater than the background. As a result, repetitive regions containing multiple target sites were used for visualising genomic loci. The **Location** of the chromosomes is given in the table along with the **Species** that contains that sequence. The specific **Target sequence** is also provided along with the **Source** of the sequence, or "This work" for the novel sgRNA targeting sequence.*

[5] Please see 5.3.2 for more details

Chapter 4: Understanding the Role of Spindle Tension in Cohesin Removal in Meiosis II

4.1 Introduction

Centromeric Cohesin is "protected" by dephosphorylation of Rec8 by PP2A, up until anaphase of meiosis I (Kitajima et al., 2004). PP2A's association with Rec8 is dependent on Sgol2 in mouse oocyte meiosis I (Llano et al., 2008; Lee et al., 2008). Whether this protective mechanism needs to be disabled, and how this happens, has only partially been investigated providing different models of how protection is removed in meiosis II.

4.1.1 Does Protection Need to be Removed Before Anaphase II?

Anaphase II is the process whereby sister chromatids separate, a process which would be prevented should the mechanisms of protection from meiosis I remain active in meiosis II. The question of whether "deprotection" is required can be considered by looking at how this process might occur in other stages of the cell cycle. In mitosis, protection is required against the prophase pathway, a non-catalytic removal of Cohesin. Preventing degradation of Sgol1 by the APC/C^{Cdc20} using a non-degradable mutant has provided inconsistent results, suggesting that it either causes alignment defects (Fu et al., 2007) or has no effect (Karamysheva et al., 2009). However, as previously mentioned, Sgol1 accumulation at centromeres is performed in a Cdk1-Cyclin B1-dependent manner (Liu, Jia, et al., 2013; Liu, Rankin, et al., 2013). As Cyclin B1 is degraded by the APC/C^{Cdc20} (Thornton & Toczyski, 2003), this degradation could prevent Sgol1 from being recruited to Cohesin, and thereby explain the lack of a phenotype. While expression of a non-degradable version of Sgol1 that can still bind to Cohesin in the absence of Cdk1-Cyclin B1 activity has not been tested in mitosis, it allows for a model for "deprotection" in mitosis.

Importantly, the requirements for and the molecular players in the protection of Cohesin in mitosis are different to those in meiosis. In meiosis, both rounds of Cohesin removal, during anaphase I and -II, are catalytic (Terret et al., 2003; Kitajima et al., 2003). In meiosis I, protection is dependent upon Sgol2, which performs a myriad of functions distinct from its role in protection (Rattani et al., 2013), and distinct from Sgol1 (Gutiérrez-Caballero et al., 2012).

Developments in studying anaphase II have been hampered by the inability to synchronise yeast in metaphase II; this is also the case in mouse spermatocytes. As

these cells do not naturally arrest in metaphase II, the lack of synchrony when performing experiments may explain why rigorous testing in meiosis II has led to a few poorly described hypotheses about deprotection. Whether protection is active at metaphase II-arrest in oocytes has only briefly been tested. Morpholino knockdown of Securin in metaphase II-arrested oocytes, when Separase is no longer inhibited by Cdk1-Cyclin B1 phosphorylation (Nabti et al., 2008), showed that Separase activation is sufficient for removal of Cohesin in meiosis II (Marangos & Carroll, 2008; Nabti et al., 2008). Both Marangos & Carroll (2008) and Nabti et al. (2008) relied on ovulated eggs which, depending on the time between hormonal stimulation and egg collection, can compromise APC/C^{Cdc20} activity and lead to spontaneous activation (Xu et al., 1997; Abbott et al., 1998). The combination of a compromised APC/C^{Cdc20} and the extended knockdown required for effective morpholino may have degraded other substrates, leading to what appeared to be onward development.

A study using an anti-Securin antibody microinjection found that this led to the depletion of Rec8 6 hours after microinjection (Huo et al., 2006). While Huo et al. (2006) would agree with the previously mentioned morpholino studies that protection is not required, removal of Rec8 did not lead to separation of chromatids. One interpretation of this study is that while anti-Securin antibody microinjection activated Separase, only the Cohesin that is not protected was degraded, i.e. Rec8 in the cytoplasm not involved in cohesion. Were this to be the case, the report would in fact suggest that protection is active at metaphase II-arrest, rather than inactive.

In line with a model of persistent protection until anaphase II, an orthogonal protection system is active during anaphase I, where Sgol2 drops to undetectable levels (Ding et al., 2018). Perturbation of centromeric Pias1, a SUMO2/3 E3 ligase, causes loss of centromeric Cohesin as seen by segregation of chromatids in anaphase I, rather than dyads, suggesting its role in protection when Sgol2 is undetectable (Ding et al., 2018). By metaphase II-arrest, Sgol2 levels accumulate again, providing a possible role in maintenance of protection up until resumption of meiosis II.

Active protection would indeed be important at metaphase II-arrest. Due to the duration of the metaphase II-arrest with an active APC/C^{Cdc20}, this could lead to premature removal of Rec8 should Separase be active. Recent reports suggest that Securin is itself reduced in metaphase II-arrest in an age-dependent manner in mouse oocytes (Nabti et al., 2017), potentially confounding the maternal age effect.

4.1.2 "Deprotection by Tension"

The earliest model of deprotection comes from studies in mouse spermatocytes where spindle tension applied in meiosis II was hypothesised to cause Sgol2 to relocate away from Rec8, therefore leaving it susceptible to Separase-mediated cleavage in anaphase II (Gómez et al., 2007) (Figure 21). This is an attractive model as spindle fibres from opposite poles attach to the kinetochores of a dyad in meiosis II, but the same kinetochores attach to fibres from the same pole in meiosis I (Figure 21). An initial study looking at this model in oocytes showed that Sgol2 localises differently between early and late metaphase II. In fixed early metaphase II oocytes, Sgol2 localised with Rec8 but moved towards the kinetochores by late metaphase II (Lee et al., 2008). However, Sgol2 was found to be present between the kinetochores on egg chromosome spreads prepared at late metaphase II in the region where Rec8 normally resides (Chambon et al., 2013; Rattani et al., 2017).

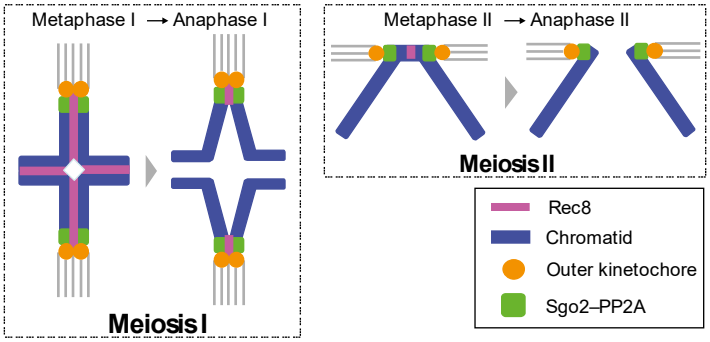

Figure 21 "Deprotection by Tension"

In the "deprotection by tension" model, Sgol2 is pulled away from Rec8 at metaphase II-arrest by spindle tension acting on sister kinetochores. This is in contrast to meiosis I, where sister kinetochores mono-orient and therefore lack tension. This relocalisation of Sgol2 then leaves Rec8 deprotected and allows cleavage by Separase upon Securin degradation at anaphase II. Figure reproduced with permission from Springer Nature Customer Service Centre GmbH: (Lee et al., 2008).

As well as Sgol2 relocalisation, it has been suggested that other proteins that relocate at this stage, such as MCAK (Mitotic Centromere-Associated Kinesin) and Aurora Kinase B, may also be involved in the "deprotection by tension" model (Gómez et al., 2007; Lee et al., 2008). Recent reports show that Sgol2 is itself a substrate of Aurora Kinase B/C, whose phosphorylation leads to the recruitment of MCAK to the centromeres in meiosis I (Rattani et al., 2013).

4.1.3 Deprotection by PP2A Inhibition

The second model suggests that I2PP2A, a putative inhibitor of PP2A, is required for sister chromatid segregation in meiosis II (Chambon et al., 2013). In this model, I2PP2A localises differently between meiosis I and -II; in meiosis I it does not colocalise with PP2A, but then colocalises in meiosis II to inhibit PP2A and allows phosphorylation of Rec8 (Figure 22).

Recent biochemical studies provide a possible mechanism of how I2PP2A might function. As previously described, PP2A is a holoenzyme made up of three components, the B component providing specificity. PP2A-B56, that is recruited to the centromeres in meiosis I, binds to substrates through a conserved motif (LxxIxE) (Hertz et al., 2016). Expression of a peptide containing this motif can act as an inhibitor of PP2A-B56 through competitive inhibition (Kruse et al., 2018; Wu et al., 2017). The motif is also present in I2PP2A, based on sequence alignments (ProViz & Davey Lab, 2019a). However, the relevance of PP2A inhibition is disputed as I2PP2A binds to Sgol2 (Krishnan et al., 2017; Qu et al., 2019). That Sgol2 is required for the localisation of PP2A and an inhibitor of PP2A is counterintuitive, given the crucial role of PP2A in meiosis I. This may suggest that there is an upstream regulator of I2PP2A that prevents it from functioning, or that it does not function in inhibiting PP2A.

Alternatively, I2PP2A may function without directly inhibiting PP2A's catalytic activity (Moshkin et al., 2013; Higgins & Herbert, 2013; Krishnan et al., 2017; Qu et al., 2019). However, the structure of I2PP2A suggests it is a histone chaperone (Eitoku et al., 2008; Das et al., 2010; Moshkin et al., 2013), and this could explain the results seen by over-expression or depletion/deletion of I2PP2A. Krishnan et al. (2017) show that I2PP2A interacts with Sgol2 in mitosis and knockdown of I2PP2A leads to mitotic delay and also persistence of Sgol2 in telophase (Sgol2 is otherwise not detected on chromosomes of control cells). Persistent Sgol2 is unlikely to be relevant for mitotic progression as knockdown of Sgol2 in mitosis does not result in premature separation of chromatids (Huang et al., 2007; Orth et al., 2011). The delay is in contrast to Qu et al. (2019), who performed knockdown of I2PP2A, and found that entry into metaphase was not affected, but chromosome segregation was impaired. Qu et al. (2019) looked in more detail at Sgol1, which associates with PP2A to provide protection to centromeric Cohesin during the prophase pathway (Kitajima et al., 2006). However, a mutant form of Sgol1 that cannot bind I2PP2A only shows slight delay in chromosome segregation, confirming that other observed major cell

cycle delays from over-expressing I2PP2A are independent of I2PP2A binding to Shugoshins. Given the difficulty in separating I2PP2A's functions as a histone chaperone and its binding to Shugoshins, it is difficult to directly infer if I2PP2A plays a role in mitosis.

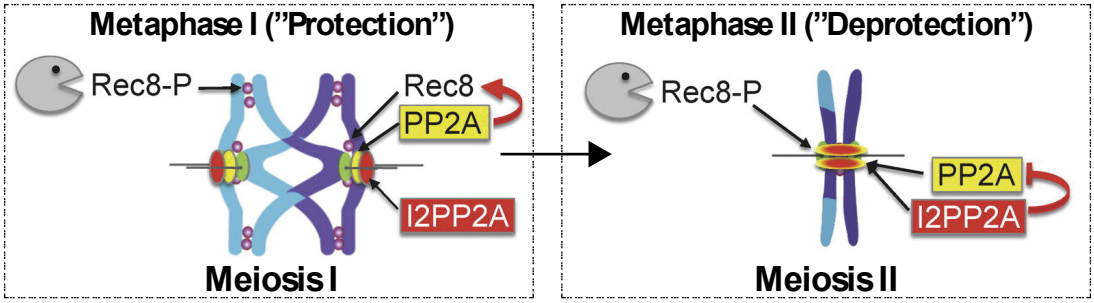

Figure 22 Deprotection by PP2A Inhibition

The deprotection by I2PP2A model suggests that I2PP2A localises differently between meiosis I and -II and is only active in meiosis II when it colocalises with and inhibits PP2A. This inhibition leads to dephosphorylation of Rec8 and cleavage upon Separase activation. Figure reproduced with permission from Elsevier Ltd.: (Chambon et al., 2013).

Studies examining the localisation of I2PP2A at metaphase II-arrest suggest that it is present either exclusively between the kinetochores (Qi et al., 2013), or additionally at the kinetochores (Chambon et al., 2013). This configuration of having I2PP2A both at and between the kinetochores is similar to that of Sgol2, presumably due to the binding of Sgol2 with I2PP2A. Morpholino knockdown of I2PP2A at metaphase II-arrest or during anaphase II does not appear to be any different from controls. When both orthologues of I2PP2A are knocked out in budding yeast, this did not prevent normal exit from meiosis II (Jonak et al., 2017), further suggesting that either deprotection is not conserved between yeast and mouse, or that I2PP2A does not play a role in deprotection.

4.1.4 Deprotection Mediated by APC/C^{Cdc20}

Though studies in budding yeast provided insights into protection of centromeric Cohesin in meiosis I, only after the development of a genetic system that artificially arrested yeast in metaphase II, could a more comprehensive model of deprotection be hypothesised (Herbert & Toth, 2017; Argüello-Miranda et al., 2017). Having developed a system to arrest yeast in metaphase II, a new model for deprotection was hypothesised whereby APC/C^{Cdc20} coordinates deprotection and cleavage of

Cohesin (Argüello-Miranda et al., 2017) (Figure 23). Here, the APC/C^{Cdc20} removes Cohesin by first degrading Shugoshin, priming Rec8 removal by allowing its phosphorylation, and degrading Securin to activate Separase and therefore cleavage of Cohesin. A further level of regulation comes from Casein Kinase 1 (CK1) which, as well as phosphorylating Rec8 (Katis et al., 2010), also regulates the removal of Shugoshin.

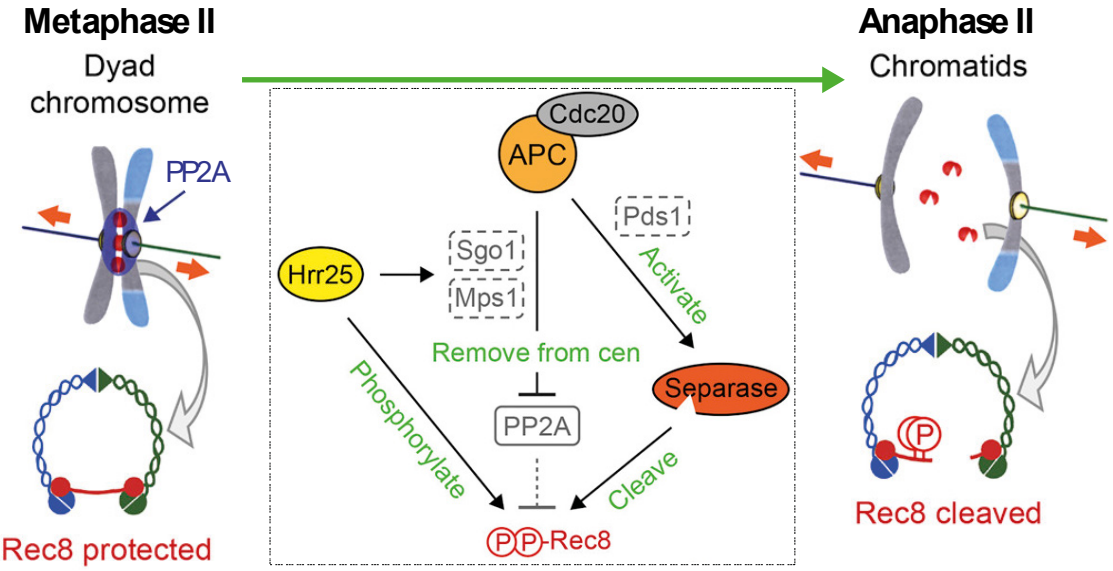

Figure 23 Deprotection Coordinated by APC/C^{Cdc20}

In yeast, Hrr25 (also known as Casein Kinase 1, CK1) induces deprotection by, in coordination with the APC/C^{Cdc20}, degrading Shugoshin and Securin. Shugoshin degradation allows for Rec8 phosphorylation by CK1, and Securin degradation leads to Separase activation. APC/C^{Cdc20}-mediated degradation of Mps1 degradation is also required for deprotection. Figure reproduced with permission from Elsevier Ltd.: (Argüello-Miranda et al., 2017).

As previously mentioned, CK1 is involved in CSF-release through phosphorylation of Emi2, at least in *X. laevis* (Isoda et al., 2011). Phosphorylation by CK1 prevents the binding of Emi2 to the APC/C. This CK1 phosphorylation site on Emi2 is conserved in mouse, and so a conserved role for CK1 in mammalian eggs is attractive because, as is the case with yeast, it would suggest that release from arrest and deprotection could be concurrent through a single kinase (Argüello-Miranda et al., 2017).

However, which kinase is involved in phosphorylation of Cohesin in mouse oocytes has yet to be determined. In yeast, this is CK1 and $Cdc7^{Dbf4}$, which work redundantly. CK1 inhibition or knockdown in mouse oocytes does not prevent normal

exit from meiosis I (Qi et al., 2015). However, even if CK1 is involved in phosphorylation of Rec8 in mouse oocytes, functional redundancy with another kinase may have prevented the observation of a phenotype.

Mps1 (Monopolar Spindle 1, also known as Ttk, dual-specificity Threonine/Tyrosine Kinase), another kinase involved in the model of deprotection coordinated by the APC/C^{Cdc20} (Argüello-Miranda et al., 2017), has also been shown to be involved in protection of centromeric Cohesin in meiosis I of mouse oocytes (El Yakoubi et al., 2017). Mps1 is also implicated in an alternative pathway to CSF, in *X. laevis*, where it works downstream of Cdk1-Cyclin E (Grimison et al., 2006).

4.2 Establishing a System for Meiosis II Resumption in the Absence of Spindle Tension

As the ability of an egg to maintain arrest at metaphase II can be compromised through *in vivo* maturation (Xu et al., 1997; Abbott et al., 1998), I tested whether oocytes harvested at the GV-stage and matured to metaphase II-arrest were able to resume meiosis upon treatment with $SrCl_2$ in calcium-free media. To test this, I monitored the ability of eggs to degrade fluorescent-tagged Securin, a substrate of the APC/C^{Cdc20}. Unactivated eggs (n = 20) accumulated exogenous fluorescent-tagged Securin, while eggs that had been activated (n = 17) predominantly degraded Securin (P = 1.3 x10^{-9}, Fisher's exact test) (Figure 24).

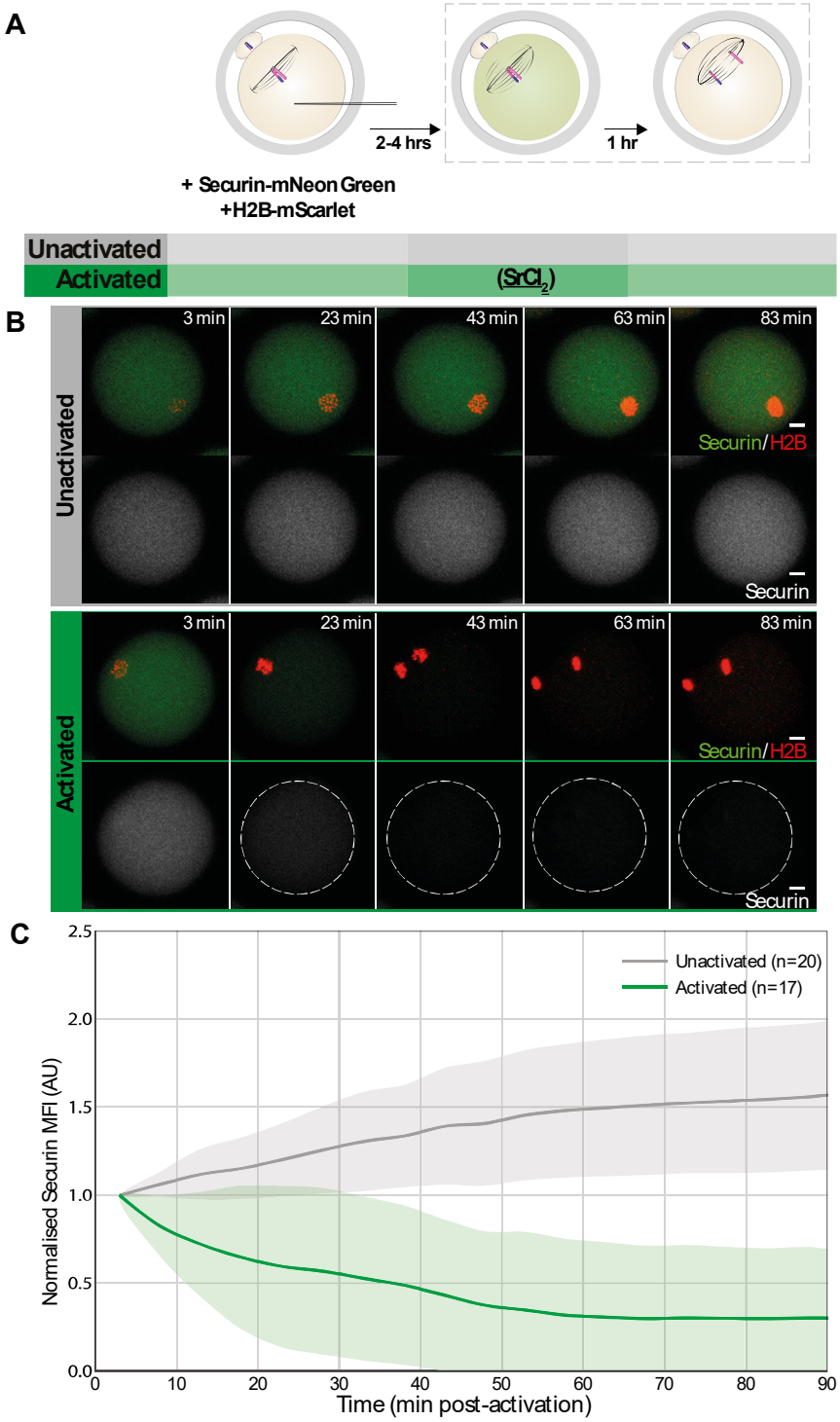

Figure 24 In vitro Matured Eggs Efficiently Activate with $SrCl_2$ in Calcium-free Media

In vitro matured eggs were microinjected with Securin-mNeonGreen, as a reporter of APC/C^{Cdc20} activity. Activated, but not unactivated, eggs were able to degrade fluorescent Securin. ***A*** *Experimental schematic (underlines highlight the differences between each experiment group, culture in brackets, '+' precedes microinjected components).* ***B*** *Example images from an experiment showing chromosomes (H2B) and Securin. Scale bar = 10 µm.* ***C*** *Line graph showing Mean (line) and Standard Deviation (light colour) of the*

background-subtracted Securin Mean Fluorescence Intensity (MFI), normalised to the background-subtracted fluorescence intensity at the first time point, after activation from each group.

Successful activation is judged by the resumption of meiosis II and therefore dyad chromosomes separating into sister chromatids. To determine the level of separation, chromosome spreads were prepared 1 hour after activation and stained with antibodies against kinetochores (Anti-Centromere Antibody, ACA) and Topoisomerase II (Topo II) (Figure 25). Topo II was used because it marks the peri-centromeric regions and chromatid axes (Li et al., 2013), assisting in identifying separation. Overall, the mean separation (±SD) for unactivated eggs was 0±1% (n = 34), compared to 94±24% (n = 32) in activated eggs (P = 6.5 x10^{-14}, two-tailed Mann-Whitney U test, MWU).

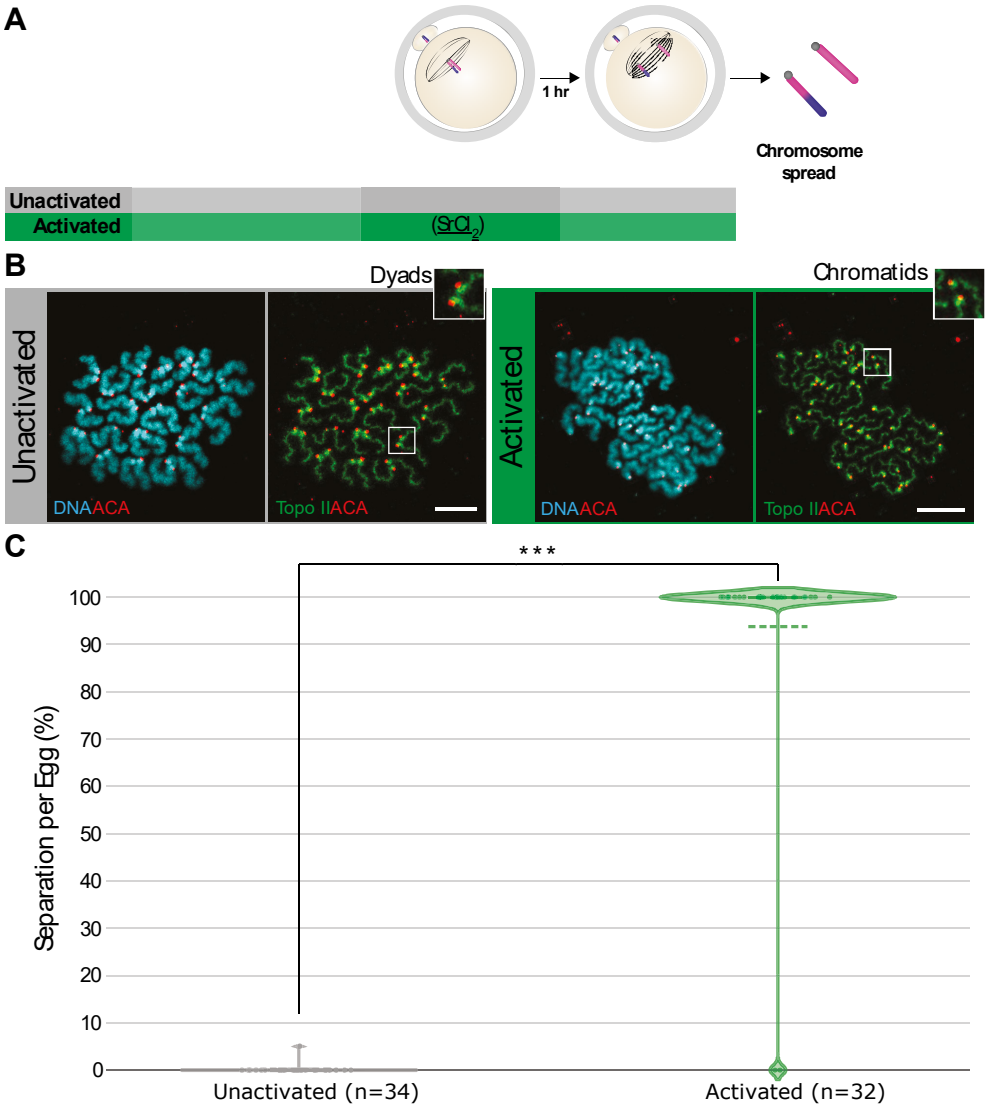

Figure 25 Successful APC/C^{Cdc20} Activation Leads to Separation of Dyads into Chromatids

***A** Experimental schematic. Differences are underlined and supplements to the culture medium are in brackets. **B** Example chromosome spreads stained with Topo II, showing the chromatid axis, and ACA, showing the kinetochores (insets show examples of dyads or chromatids, scale bar = 10 μm). **C** Violin plot showing separation of dyads per egg. Dots show the separation of individual eggs; boxplot shows the median and quartiles at 25% and 75%; dashed line shows mean; density plot is given by Kernel Density Estimation (KDE).*

Having established a system for reliably activating eggs, I worked on finding a way to remove spindle tension. Nocodazole is a potent microtubule depolymerising agent (Teusel et al., 2018), that causes the removal of the spindle. In removing the spindle, tension is also removed. However, the absence of correct attachments will cause arrest due to the Spindle Assembly Checkpoint (SAC). As a result, two different methods were used to allow for meiosis II resumption in the presence of SAC arrest and therefore in the absence of spindle tension.

4.3 Reversine-Bypass of Checkpoint Allows Centromere Separation in the Absence of Tension

The first approach was the use of reversine, a specific inhibitor of the master kinase of the SAC, Mps1 (Ciliberto & Hauf, 2017). Unlike in the presence of nocodazole alone (n = 12), activation with nocodazole and reversine (n = 19) resulted in Securin degradation (Figure 26) (P = 7.1 x10^{-9}, Fisher's exact test).

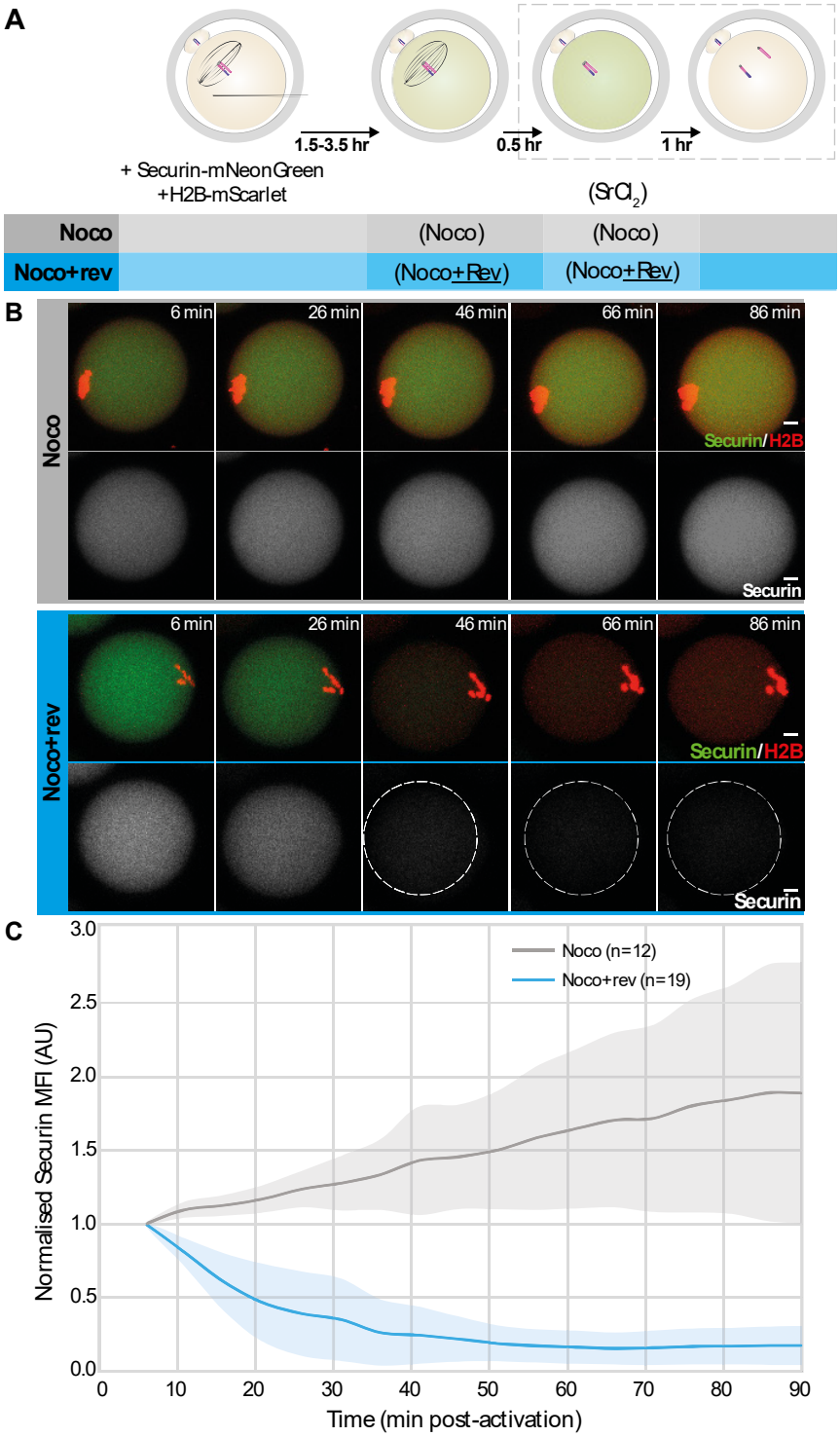

Figure 26 Mps1 Inhibition Lifts SAC arrest in the Presence of Nocodazole

Activation in the presence of nocodazole causes SAC-arrest, as can be seen by the accumulation of fluorescent-tagged Securin. Inhibition of Mps1 by reversine disables the formation of the MCC and therefore alleviates SAC-arrest, allowing for Securin degradation. ***A*** *Experimental schematic. Microinjected components are shown after a '+', culture media supplements in parentheses, and underlines highlight the differences between the two experimental groups.* ***B*** *Example images of Securin degradation, time shown is*

*post-activation. Scale bar = 10 µm. **C** Line graph showing the background-subtracted, normalised Securin MFI for each experimental group. MFI is normalised to the first time point. Thick line shows mean, light colour shows standard deviation.*

Separation when activated in the presence of nocodazole alone was almost absent, averaging at 0±1% (n = 36), while separation was greatly increased (P = 1.0 x10^{-13}, two-tailed MWU) to 46±15% (n = 29) when activation occurred in the presence of nocodazole and reversine (Figure 27).

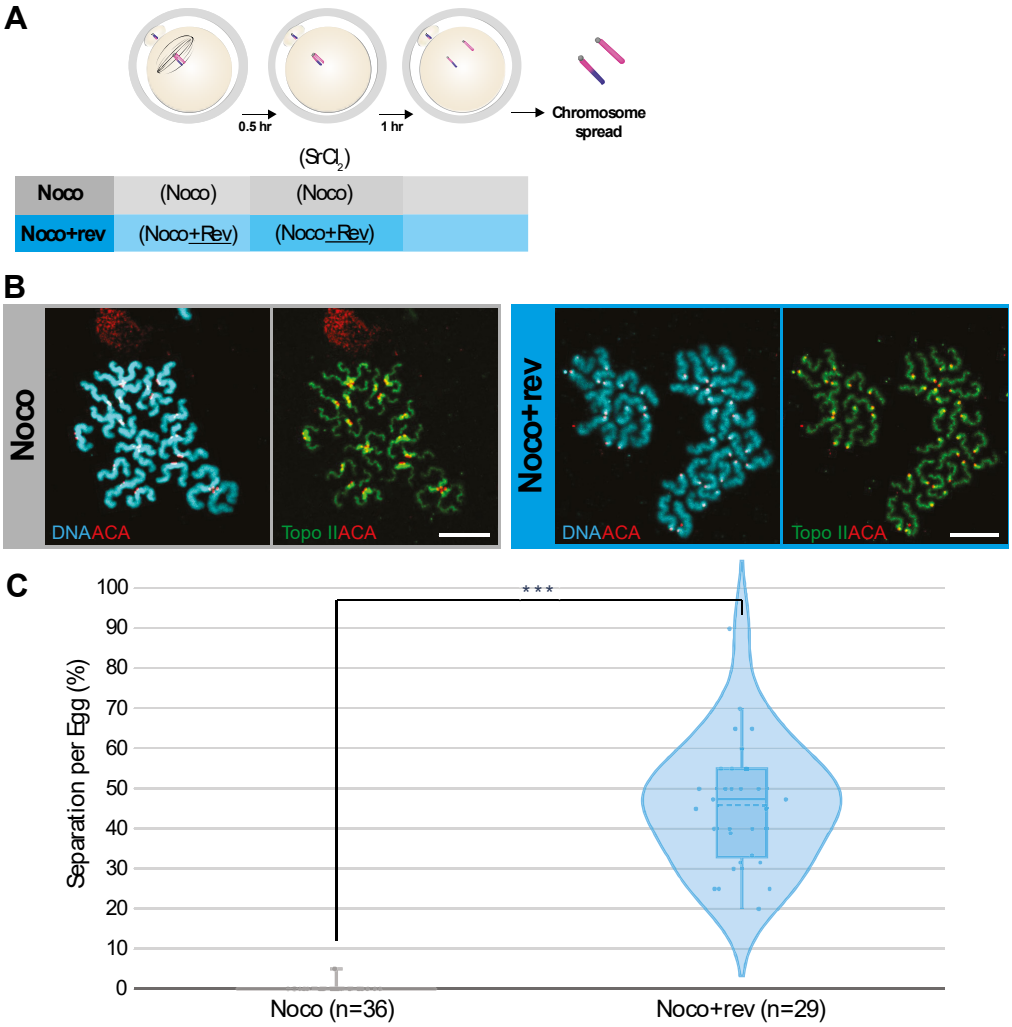

Figure 27 Chromatid Separation Occurs in the Absence of a Spindle, when SAC arrest is Bypassed by Reversine

*Chromosomes spreads prepared from eggs activated in the presence of nocodazole alone showed little to no separation, compared to an increase in separation when activation occurred in the presence of nocodazole and reversine. **A** Experimental schematic (difference between experimental groups are underlined). **B** Example chromosome spreads (scale bar = 10 µm). **C** Violin*

plot showing separation levels in each group: boxplot shows quartiles; dashed line shows mean; and density plot is KDE.

4.4 Direct Activation of the APC/C^{Cdc20} Enables Deprotection Without Tension

An alternative approach to allow for APC/C^{Cdc20} activation in the absence of spindle tension is the use of a mutant form of Cdc20, Cdc20(Mad2-Interaction Mutant, MIM), that is unable to bind the MCC but retains its ability to activate the APC/C (Izawa & Pines, 2012). This experiment is particularly important as recent reports suggest that Mps1 is involved in deprotection of Cohesin in yeast meiosis II (Argüello-Miranda et al., 2017; Jonak et al., 2017) and mouse oocyte meiosis I (El Yakoubi et al., 2017). For these experiments, GV-stage oocytes were cultured until early meiosis II (~12 hours post-IBMX release). At this point, eggs were microinjected with Cdc20(MIM) or Cdc20(WT) and exogenous Securin-mNeonGreen to test whether CDC20(MIM) was able to bypass the Spindle Assembly Checkpoint. As expected, Securin accumulated in eggs incubated with nocodazole that had been microinjected with Cdc20(WT) (n = 24) but not Cdc20(MIM) (n = 25) (P = 5.2 x10^{-11}, Fisher's exact test) (Figure 28).

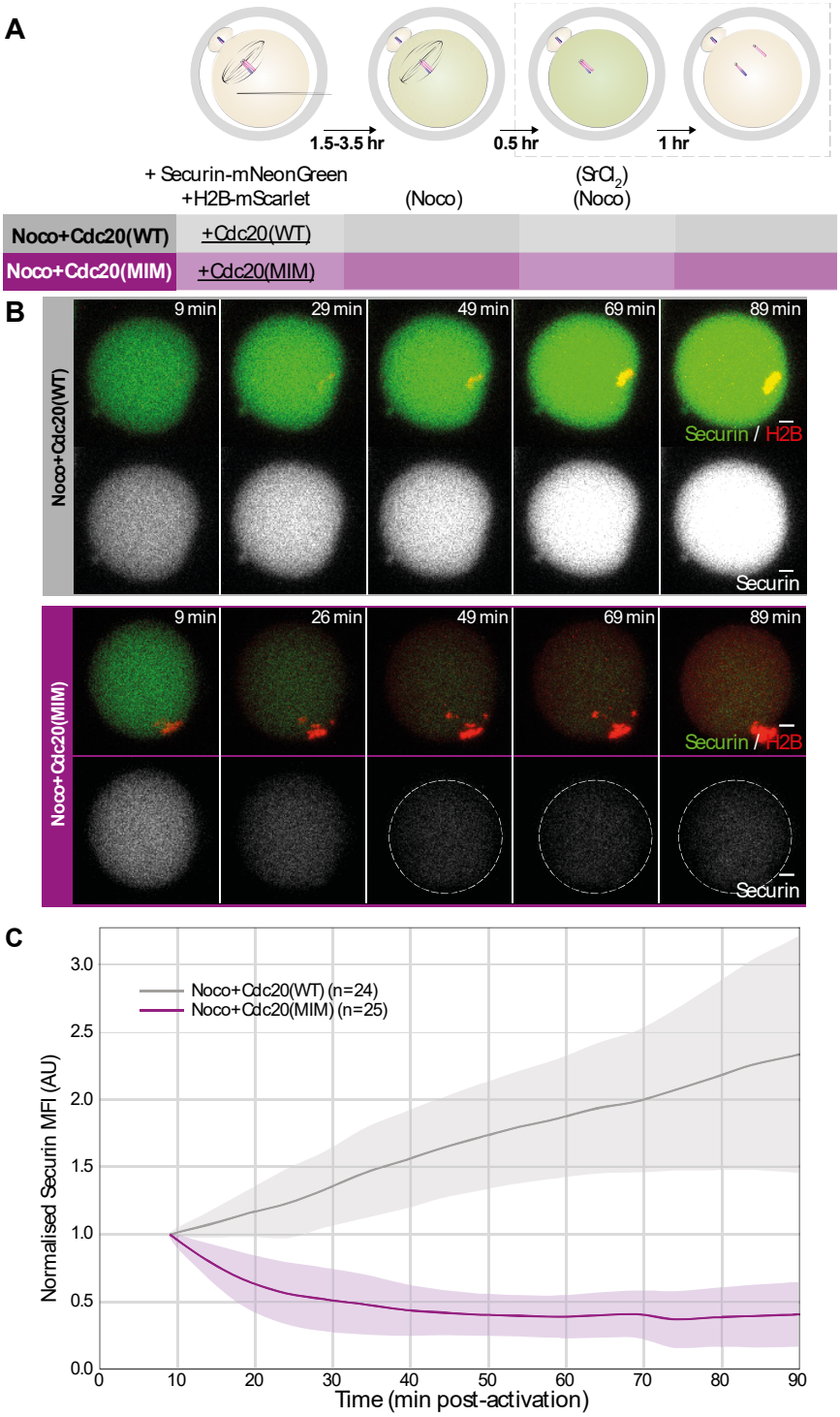

Figure 28 Direct Activation of the APC/C^{Cdc20} in the Absence Allows for Meiosis II Resumption

As an alternative to using reversine, Cdc20(MIM) was used to bypass the SAC-arrest induced by nocodazole treatment. Activation in the present of these components, allowed for Securin degradation. ***A*** *Experimental schematic.* ***B*** *Examples images from the time-lapse experiment. Scale bar = 10 µm.* ***C*** *Line graph showing the mean±SD of background-subtracted normalised Securin MFI for both experimental groups. MFI is normalised to the first time point.*

To determine the level of separation, chromosome spreads were prepared 1 hour after activation. As was the case with the treatment of eggs with nocodazole and reversine, eggs had separation in the absence of tension. Those that had been microinjected with Cdc20(WT) had 2±3% (n = 44) of separated chromatids compared to an increase (P = 2.7 x10^{-18}, two-tailed MWU) to 46±17% (n = 61) in those microinjected with Cdc20(MIM) (Figure 29).

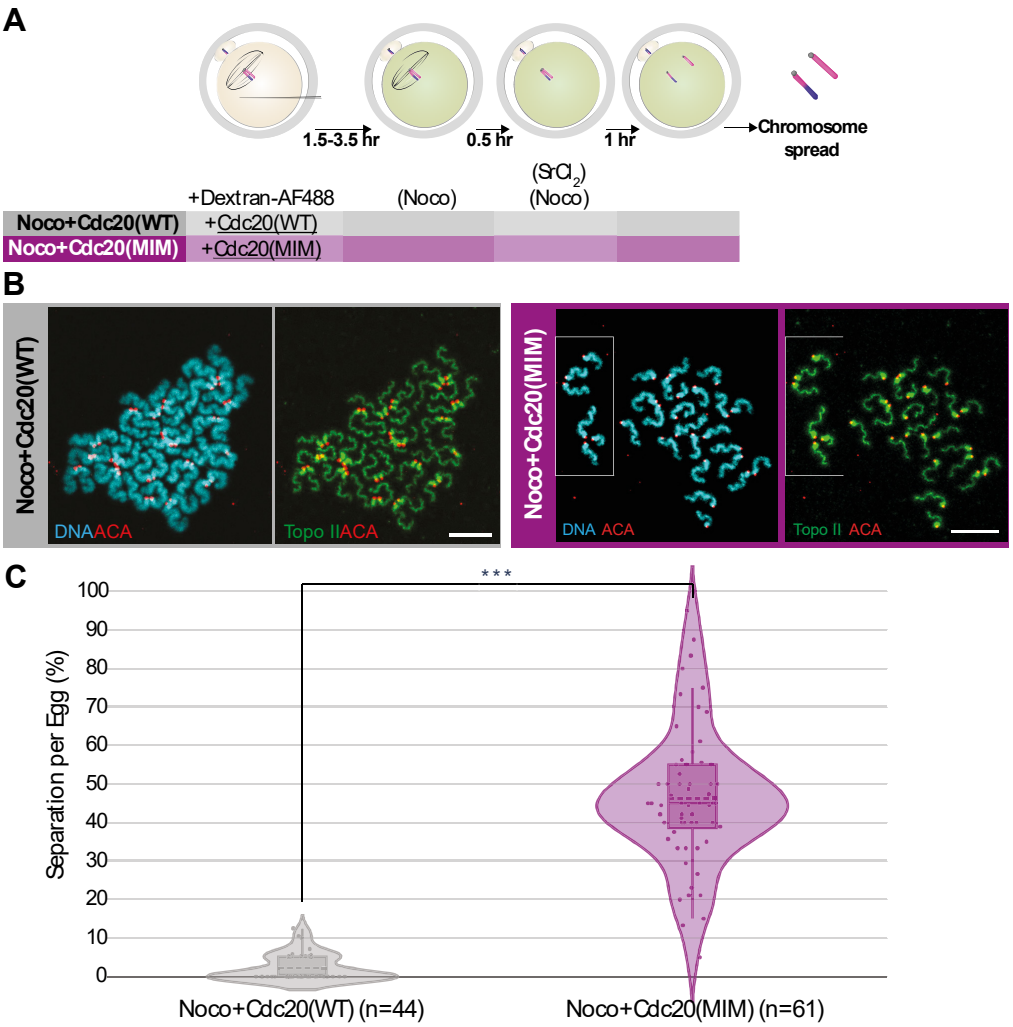

Figure 29 Direct Activation of the APC/C^{Cdc20} in the Absence of Spindle Tension Allows Sister Chromatid Separation

To test if sister chromatid separation could occur in the absence of spindle tension, Cdc20(MIM) was microinjected into eggs and then eggs were activated in the presence of nocodazole. ***A*** *Experimental schematic.* ***B*** *Examples of chromosome spreads.* ***C*** *Violin plot showing the distribution of separation levels between each group: boxplot shows quartiles; dashed line shows mean; and density plot is KDE.*

4.5 Absence of Spindle Tension Impairs Counting of Separated Chromatids

However, separation was not as high as eggs activated in the absence of nocodazole (P = 4.3 x10^{-10}, two-tailed MWU). This could mean that tension is still required for separation of some but not all chromosomes, or that tension is required for another process downstream of deprotection. It is known that sister chromatids form catenates during DNA replication and so, as well as Cohesin, sister chromatids are bound by small threads of DNA (Wang et al., 2008).

To test if spindle tension was required for a process other than deprotection, I used the "TrimAway" system to remove endogenous Rec8, as has been recently described (Clift et al., 2017), but in the absence of a spindle. To establish that the TrimAway system worked, I microinjected GV-stage oocytes with Trim21 and allowed them to progress to metaphase II-arrest. At this point the Rec8 antibody was microinjected which, combined with exogenous Trim21, causes proteasome-mediated degradation of Rec8 and therefore sister separation in the absence of activation (Figure 30). When this experiment was performed, there was 98±3% (n = 13) separation in eggs that had been microinjected with wild-type Trim21, but dramatically less (1±2%, n = 9) with a catalytically dead Trim21(ΔC) (P = 5.4 x10^{-5}, two-tailed MWU) (Figure 30).

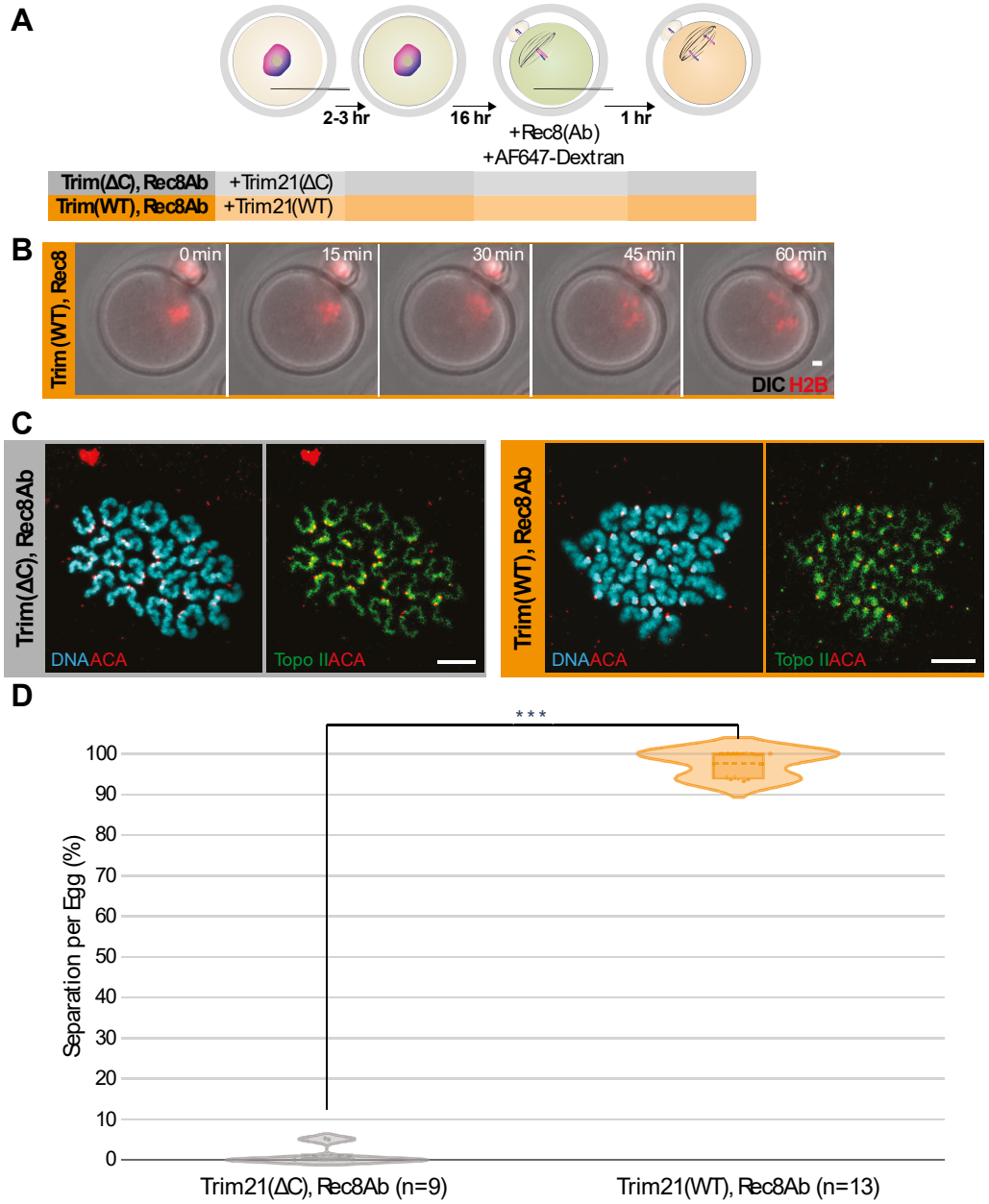

Figure 30 Depletion of Endogenous Rec8 Leads to Separation Without Activation

Endogenous Rec8 was depleted using sequential microinjections of Trim21 (at GV-stage) and anti-Rec8 antibody (at metaphase II-arrest), causing separation of dyads. ***A*** *Schematic of the experiment.* ***B*** *Images from a time-lapse experiment showing separation of chromatids as marked by fluorescent-tagged Histone 2B.* ***C*** *Example of chromosome spreads from each group showing intact dyads in the catalytically-dead Trim21(ΔC)-microinjected group and chromatids in the Trim21(WT)-microinjected group (scale bar=10 μm).* ***D*** *Violin plot showing separation with Trim21(WT) or Trim21(ΔC): boxplot shows quartiles; dashed line shows mean; and density plot is KDE.*

The experiment was then performed with metaphase II-arrested eggs that had been treated with nocodazole (Figure 31). Those that had been microinjected with wild-type Trim21 had separation (46±20%, n = 48), but this was much less than when eggs were depleted of Rec8 in the absence of nocodazole (P = 3.9 x10^{-8}, two-tailed MWU). Separation was also higher than controls that had been microinjected with Trim21(ΔC) (2±4%, n = 32; P = 2.8 x10^{-14}, two-tailed MWU).

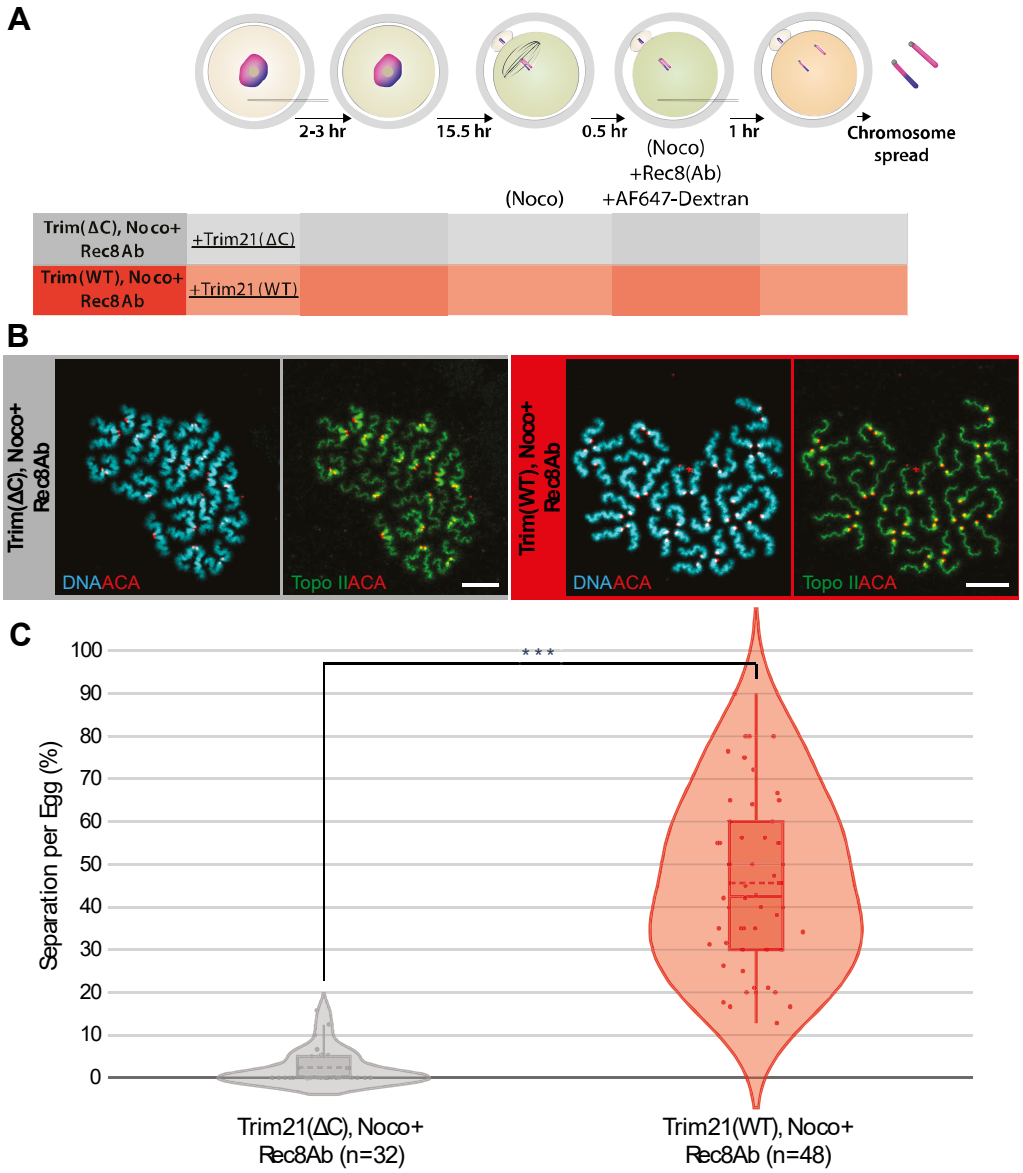

Figure 31 Removal of Endogenous Rec8 in the Presence of Nocodazole Impairs Resolution of Separated Chromatids

When endogenous Rec8 is removed in the presence of nocodazole, the almost complete levels of separation seen when endogenous Rec8 is depleted without nocodazole is impaired. ***A*** *Experimental schematic.* ***B*** *Example chromosome spreads.* ***C*** *Violin plot showing separation: boxplot shows quartiles; dashed line shows mean; and density plot is KDE.*

Finally, if tension is required for separation in a Cohesin-independent function, then it holds that washout of nocodazole, and therefore reassembly of the spindle and spindle tension, should return levels of separation back to the level before nocodazole addition. Spindle reassembly takes time, so this process was performed in the presence of MG132, a proteasome inhibitor, to prevent excess Rec8 degradation that would occur during this period (Figure 32). Again, separation was higher (P = 2.2 x10^{-10}, two-tailed MWU) (89±8%, n = 27) than controls that had been microinjected with catalytically inactive Trim21 (7±8%, n = 27).

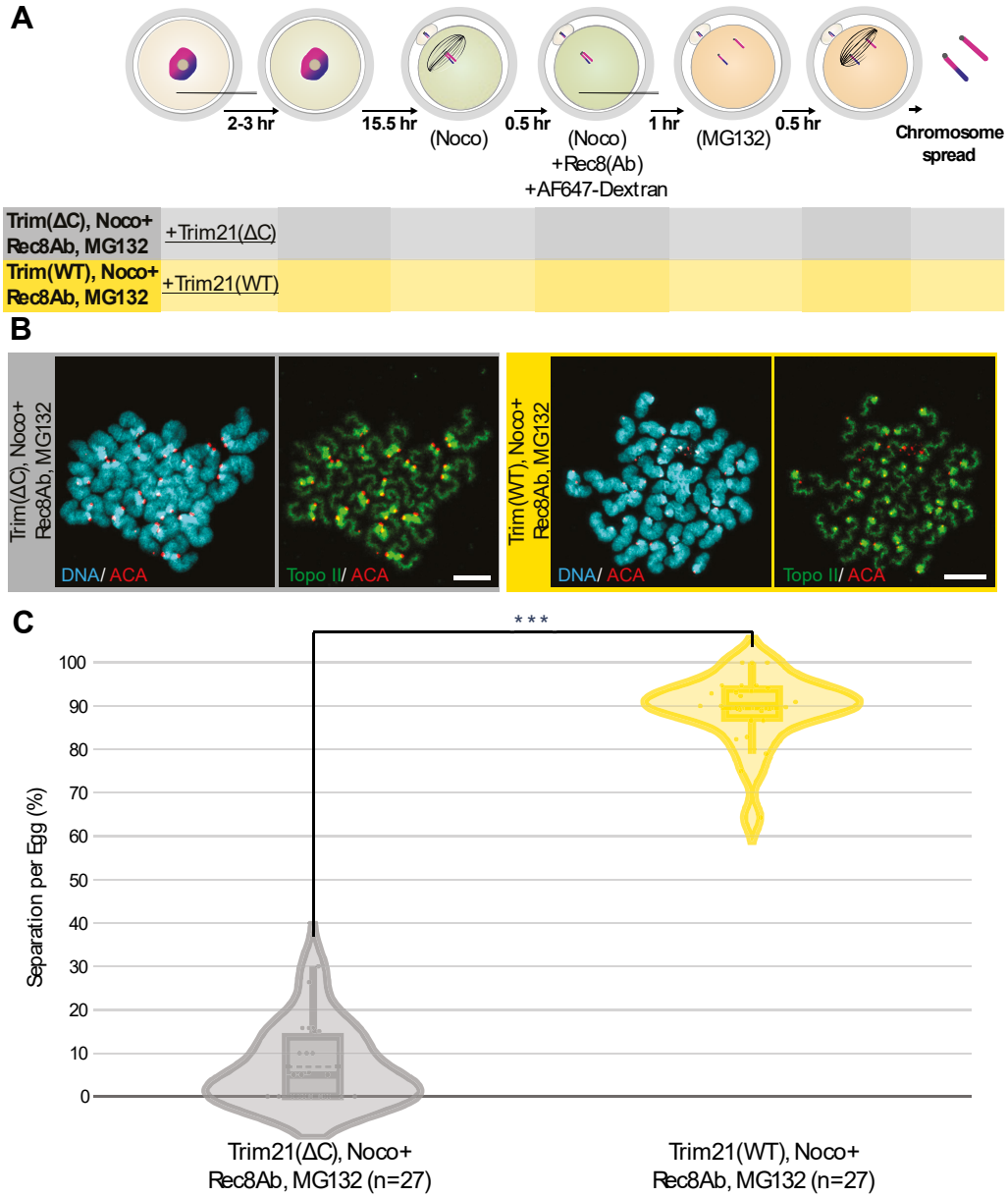

Figure 32 Separation Levels After Rec8 Depletion in the Presence of Nocodazole are Restored Following Nocodazole Washout

A *Experimental schematic (inhibitors are in brackets, microinjections are preceded by a '+', underlines show differences between groups).* ***B*** *Examples of chromosome spreads. Scale bar = 10 μm.* ***C*** *Violin plot showing separation*

levels in each group: boxplot shows quartiles; dashed line shows mean; and density plot is KDE.

Altogether, the mean attainable separation is 46±20% in the absence of a spindle. This is comparable to activation in the presence of nocodazole and reversine (P = 0.88, two-tailed MWU), and also when activation occurred in the presence of nocodazole for eggs that had been microinjected with Cdc20(MIM) (P = 0.72, two-tailed MWU).

4.6 Sgol2 Localises with Rec8 at Metaphase II-arrest

Given that deprotection can occur in the absence of spindle tension, I began looking at whether components of the yeast model, where deprotection is coordinated by the APC/C^{Cdc20}, are conserved in mouse eggs. In this model, APC/C^{Cdc20} both activates Separase through Securin destruction and deprotects through destruction of the protector, Shugoshin. Sgol2 is the mammalian orthologue involved in protection in meiosis I, but its localisation at metaphase II-arrest differs between reports (Lee et al., 2008; Chambon et al., 2013; Rattani et al., 2013). To confirm the localisation of Sgol2 at metaphase II-arrest (16 hours post-IBMX release), chromosome spreads were prepared and stained for Sgol2, Rec8 and kinetochores (ACA) (Figure 33A). Indeed, Sgol2 localised with Rec8 as well as kinetochores, confirming more recent studies about its localisation (Figure 33B,C). In fact, the intensity of Sgol2 at Rec8 was higher than that at kinetochores (P = 5.4 x10^{-29}, two-tailed MWU).

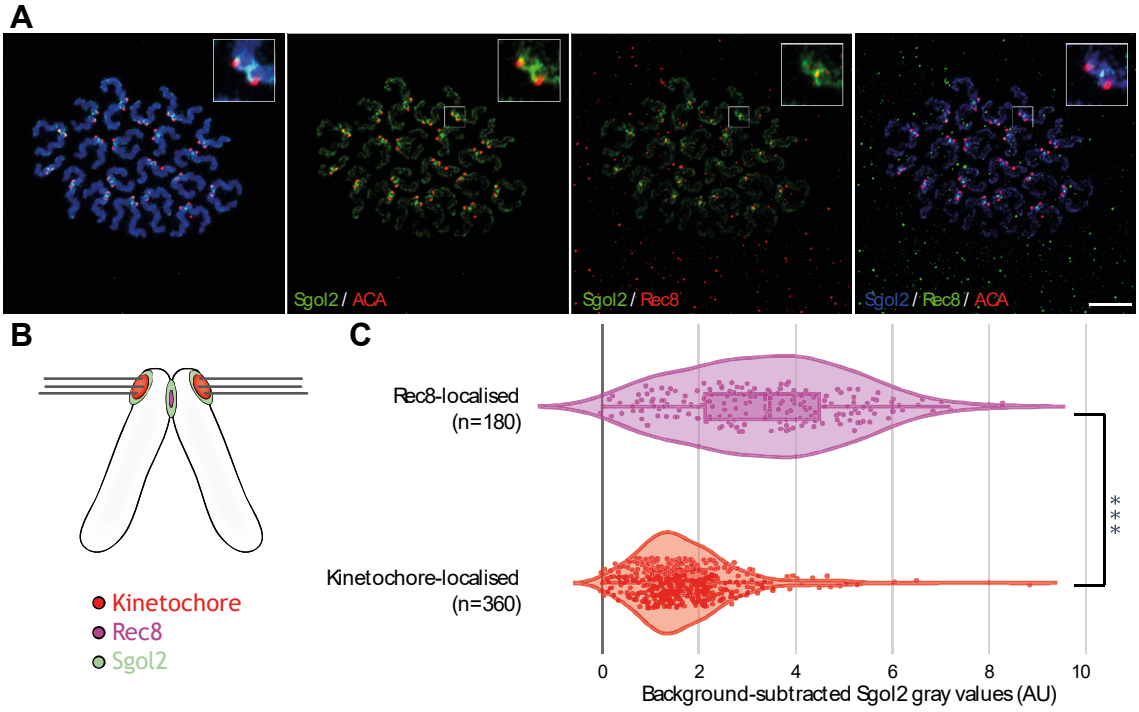

Figure 33 Sgol2 Localises with Rec8 at Metaphase II-arrest

***A** Chromosome spreads prepared of eggs 16 hours after IBMX-release, stained with DAPI (DNA); Sgol2; Kinetochores (ACA) and Rec8. Two distinct pools of Sgol2 are present: one that overlaps with Rec8; and one that overlaps with the kinetochroes. Scale bar = 10 µm. **B** Schematic summarising the localisation of Sgol2, kinetochores and Rec8 at metaphase II-arrest. **C** Violin plot showing the background-subtracted Sgol2 fluorescence intensities that localise with kinetochores and Rec8: boxplot shows quartiles; dashed line shows mean; and density plot is KDE.*

4.7 Sgol2 Decreases After Release from Metaphase II-arrest

To test whether Sgol2 decreases after resumption of meiosis II, chromosome spreads were prepared both before activation, and 1 hour after activation (Figure 34). As laser output can vary between experiments, normalisation was performed by dividing the background-subtracted Sgol2 grey values with the average background-subtracted Sgol2 intensity from metaphase II chromosome spreads imaged in each set. This showed a decrease in Sgol2 intensity (P = 2.5 x10^{-73}, two-tailed MWU). Despite the reduction in Sgol2 intensity, it could still be detected at kinetochores during anaphase II, suggesting not all Sgol2 is degraded. As the Rec8-associated Sgol2 is removed when Rec8 is cleaved in anaphase II, a comparison could not be made of the fraction that, based on localisation, is more likely to protect Cohesin.

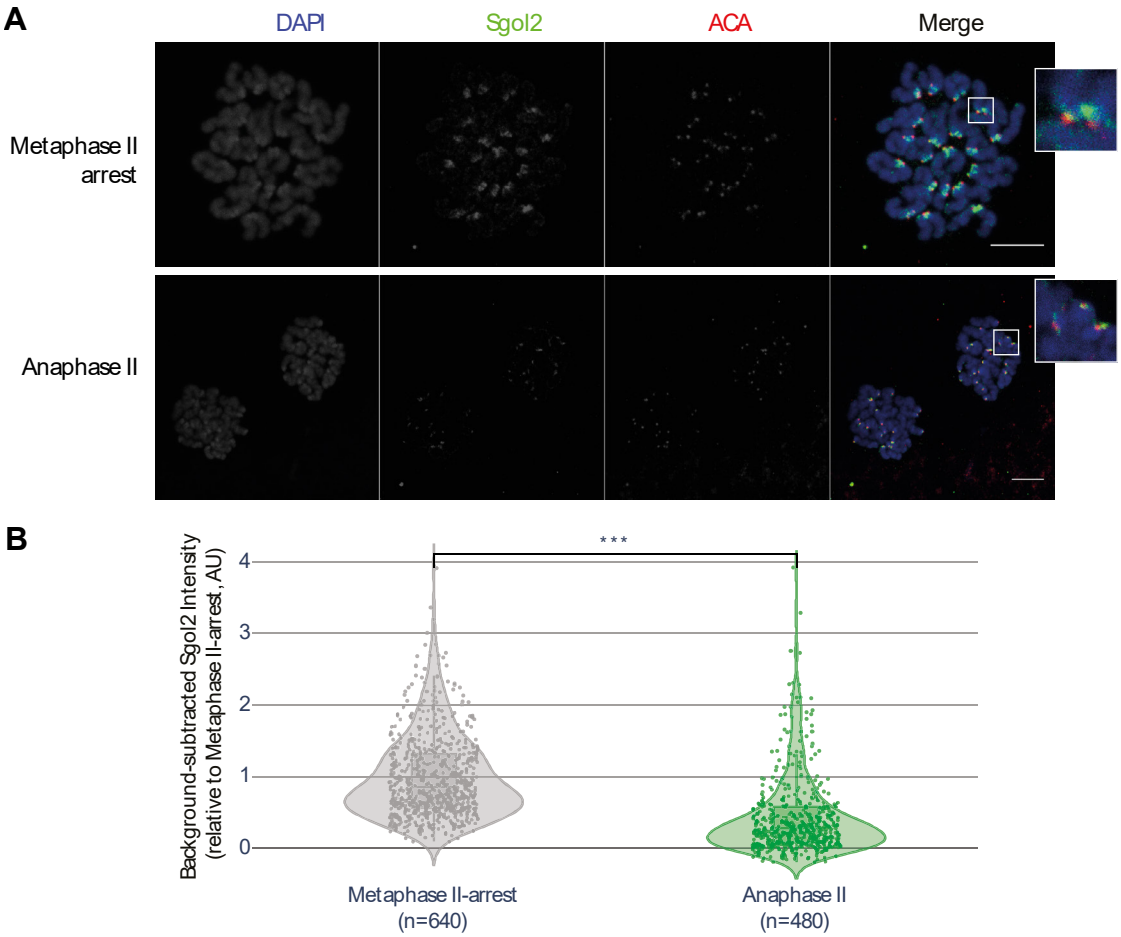

Figure 34 Sgol2 Decreases After Resumption of Meiosis II

***A** Representative images of chromosome spreads of eggs prepared at metaphase II-arrest (16 hours after IBMX-release) and anaphase II (1 hour after metaphase II-arrested eggs were activated). **B** Violin plot showing distribution of relative Sgol2 intensity at kinetochores between metaphase II-arrest and anaphase II: boxplot shows quartiles; dashed line shows mean; and density plot is KDE.*

4.8 Discussion

To test if spindle tension has any functional significance in deprotection in meiosis II, I tested the impact of removing spindle tension on deprotection. This was conducted by using the microtubule poison nocodazole to remove the spindle, and therefore spindle tension. Upon activation, eggs remain arrested due to the Spindle Assembly Checkpoint (SAC). I used two well-characterised approaches to bypass the SAC in the absence of a spindle to show that tension is not required for deprotection in meiosis II.

The first of these was the use of reversine, a potent inhibitor of Mps1 (Chen et al., 2004; Santaguida et al., 2010). Activation in the presence of nocodazole and

reversine allowed for the separation of sister chromatids, albeit not at as high levels as eggs activated in the absence of inhibitors. The use of an Mps1 inhibitor in these experiments is confounded by the fact that Mps1 has been shown to play a part in protection in oocyte meiosis I and is a key player in meiosis II in yeast (Argüello-Miranda et al., 2017; Jonak et al., 2017; El Yakoubi et al., 2017). Despite this, separation levels using an alternative method to bypass the SAC were similar. In this alternative method, rather than inhibiting Mps1, the APC/C was directly activated using a mutant form of Cdc20 that can no longer bind to the MCC and perform its function in the SAC (Izawa & Pines, 2012). When this mutant was expressed in activated eggs in the presence of nocodazole, separation could still occur, confirming that spindle tension is not required for deprotection in meiosis II.

As the levels of separation in nocodazole when the APC/C^{Cdc20} was active were not as high as separation levels that occurred when activation was performed in the presence of a spindle, I tested whether tension has an auxiliary function in deprotection or was the result of another process. To test the hypothesis tension is required for a process other than deprotection, endogenous Rec8 was removed in the presence of nocodazole. In the absence of nocodazole, this leads to a level of separation comparable to activation without inhibitors. However, there is greatly reduced separation in the presence of nocodazole, confirming that the limit on separation is due to a lack of spindle forces resolving nearby chromatids. One possible explanation for this is that decatenation is perturbed in the absence of tension. Meiosis is unique in that only one round of DNA replication precedes two rounds of chromosome segregation. Therefore catenates (sister chromatids joined by DNA bridges) that are formed in S-phase are not resolved until these divisions (Wang et al., 2008). As sister centromere separation does not occur until anaphase II, it is likely that threads at the centromere remain until this point. Indeed, inhibition of decatenation of mouse oocytes in meiosis I and -II causes severe segregation defects (Li et al., 2013). To confirm that incomplete separation was due to the lack of spindle forces in resolving separated sister chromatids, spindle tension was restored through nocodazole washout after Rec8 depletion. This brought separation back to levels comparable to removal of endogenous Rec8 in the absence of nocodazole.

I then began to interrogate if the features of the yeast model where the APC/C^{Cdc20} coordinates deprotection and cohesin Cleavage were conserved in mouse eggs. I began by staining chromosome spreads of metaphase II-arrested eggs with

Rec8 and Sgol2. This showed that, at least by confocal microscopy, these two proteins colocalise. This is an important result given that earlier reports suggested that Sgol2 did not appear between the kinetochores, where Rec8 resides, and was pertinent to the model of "deprotection by tension" (Lee et al., 2008).

In yeast, APC/C^{Cdc20} mediates degradation of Shugoshin. To investigate if this was also the case in metaphase II-arrested eggs, I stained chromosome spreads both before and after activation. Eggs in anaphase II had much less Sgol2, but Sgol2 did not completely disappear. However, the "protective" fraction of Sgol2 could not be measured as it is removed when Rec8 is cleaved by Separase. Therefore, it may be the case that the Rec8-colocalised pool of Sgol2 is regulated differently to the kinetochore pool. This would not be surprising given different kinases are at play in each pool: for example, Mps1 at the kinetochore-localised pool (El Yakoubi et al., 2017); and Aurora Kinase B and C (Kouznetsova et al., 2019) at the inter-kinetochore pool. Recent studies have also shown the kinase-regulation of Sgol2 (Rattani et al., 2017).

Chapter 5: Molecular and Computation Tools for Imaging Subcellular Components of Human Oocytes

5.1 Introduction

Previous work in human oocytes has primarily relied upon samples that are rejected for IVF treatment (collected before they've reached metaphase II-arrest) and are therefore also from fertility patients (though usually due to male-factor infertility). Meiosis I resumption and follicular growth are intertwined, and it is the administration of human Chorionic Gonadotropin (hCG) that stimulates follicular development (Herbert et al., 2015). Samples collected at 37-41 hours after hCG administration are expected to be at metaphase II-arrest (Dozortsev et al., 2004; Obeso et al., 2010; Bárcena et al., 2016), suggesting that these immature oocytes come from follicles that do not respond to hormonal stimulation.

As most of these data come from fixed samples, it is not known directly when during meiosis errors arise. Fixed material can be used to predict the source (e.g. meiosis I or II) but further resolution, such as which phase of the cell cycle is unknown. As these samples are fixed they are done without the knowledge of their developmental competence. This is particularly important for meiosis I material as it is possible that some of these oocytes would never have reached metaphase II, due to their immaturity. Recent work from Melina Schuh's lab has shown the potential of using live-cell imaging in human oocytes to gain further insight into why oocytes are prone to aneuploidy (Holubcova et al., 2015; Zielinska et al., 2015; Webster & Schuh, 2017). However, these live-cell studies used low spatial resolution to image the spindle and chromosomes, rather than investigate chromosomal and/or centromeric dynamics.

Work in mouse oocytes employing high-resolution time-lapse microscopy has demonstrated the power of monitoring centromeric dynamics to visualise chromosome segregation, including its relationship with age (Sakakibara et al., 2015). In contrast to previous human oocyte studies, this thesis uses human oocytes specifically donated for research, combined with live-cell imaging of chromosomes movements and marking of specific-chromosomes, to elucidate the pathways of how age-associated aneuploidies arise.

5.1.1 Fluorescence-Based Tracking Systems

In order to obtain high resolution data without compromising cell cycle progression, it was imperative to utilise a fluorescence-based tracking system to image the sub-cellular region of the oocyte around the chromosomes (Rabut & Ellenberg, 2004) (Figure 18). This alleviates the need to image the whole oocyte, thereby reducing phototoxicity while increasing spatial resolution. Indeed, this approach was first employed in mouse oocytes to visualise kinetochore dynamics on Zeiss confocal microscope systems (Kitajima et al., 2011), and later adapted for Leica confocal microscope systems (Lane et al., 2017).

These real-time fluorescence-based trackers work by analysing the signal of histone in real-time and feeding back to the microscope the centre of mass (Rabut & Ellenberg, 2004). However, this process relies heavily on images with strong signal:noise and assumes that there is only one object for focusing. Therefore a further modification to this approach was developed (Politi et al., 2018), where images taken by the microscope are passed to FIJI (Schindelin et al., 2012), where they are processed and objects are detected. The benefit of this object-detection approach is that it can filter out non-specific signal in its calculation of the object centre. However, it relies heavily on pre-processing (which can filter noise as well as signal) and thresholding (which is enhanced by having a larger dynamic range).

An alternative approach might be the use of template matching. Template matching is the process by which a target image is scanned for a smaller "template" and the correlation is generated across the larger image. The point with the highest correlation denotes the most likely position of the template in the image. By comparing regions between time points where changes are small, it may be possible to track a sub-region across time points, providing a way to track using image similarity rather than intensity (Sarvaiya et al., 2009).

5.1.2 Visualising Centromeres in Human Oocytes

While fluorescent-tagged CENP-C is often used to image the kinetochores (Kitajima et al., 2011), overexpression of proteins can compromise cell development. Advances in nuclease technologies such as CRISPR (Clustered Regularly Interspaced Short Palindromic Repeats) and TALENs (Transcription Activator-Like Effector Nucleases) allow modification of specific genomic sites, but can also be modified to make them catalytically dead without compromising their ability to bind specific DNA sequences (Figure 35). By attaching a fluorescent protein to these systems, specific

chromosomal sites can be seen throughout the cell cycle (Chen, Guan, et al., 2016; Ma et al., 2013).

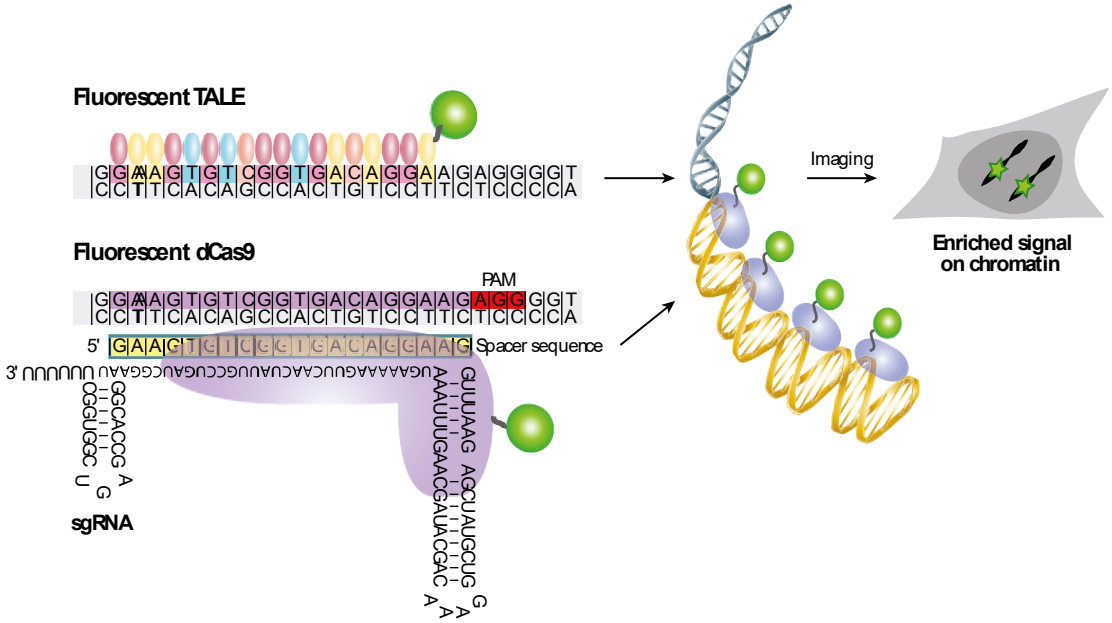

Figure 35 Fluorescent-tagging and Catalytically Disabled Programmable Nucleases Allow for Imaging Genomic Loci

Catalytically-dead, fluorescent-tagged versions of CRISPR/Cas9 and TALENs can be modified to allow visualisation of specific genomic regions. Specificity of CRISPR is conferred through a PAM sequence and an sgRNA; TALE-FPs gain specificity through modification of the TALE's RVDs (Repeat Variable Di-residue); each RVD targets a specific base in the target sequence. Figure reproduced with permission from Annual Reviews, Inc.: (Chen, Guan, et al., 2016).

CRISPR is a system used by bacteria to cleave and degrade invading DNA. In bacteria, it is made up of the Cas9 protein, CRISPR RNAs (crRNAs) and a trans-activating crRNA (tracrRNAs); the crRNAs and tracrRNAs can be fused to make a single guide RNA (sgRNA), which is more commonly used when working with mammalian cells. The specificity of CRISPR/Cas9 comes from both the Cas9 and sgRNA sequence. The Cas9 binds short motifs called PAMs (protospacer-adjacent motif), which is "NGG" (N is any nucleotide) in the most commonly used variant in mammalian cells (*Streptococcus pyogenes, S. pyogenes*) but varies amongst species of bacteria (Jiang & Doudna, 2017). The sgRNA provides the second part of specificity as the target sequence upstream of the PAM is defined by the 5' end of the sgRNA; the 3' end of the sgRNA is a scaffold recognised by Cas9. Further modification to the CRISPR system

can either enhance signal intensity or allow for multiplexing (i.e. the specific imaging of multiple chromosomal loci). As there are a variety of Cas9 proteins that bind specific secondary structures in sgRNAs, multiplexing these provides one solution to image and identify multiple chromosomes (Ma et al., 2015).

A further approach is to use the well-characterised *S. pyogenes* Cas9 and modify the sgRNA. The sgRNA contains two loops that can be further extended, as well as extending the sgRNA at the 3' end. These modifications do not appear to impact the function of the ribonucleoprotein complex. The modifications of the sgRNA include the introduction of an RNA hairpin that is recognised by another protein. Bacteriophage capping proteins such as PCP (PP7 capping protein), MCP (MS2 capping protein) and N22 (RNA binding domain of the bacteriophage protein N) recognise the PP7, MS2 and BoxB hairpins, respectively. By using a combination of these, up to seven foci can be imaged simultaneously (Ma et al., 2016). Another modification is the use of a specific sequence in the loops that are recognised by PUF (RNA binding domain of Pumilio/FBF proteins) (Cheng et al., 2016), or the use of multiple MS2 sites to enhance signal (Ma et al., 2018). Both systems combine signal enhancement with multiplexing capabilities. Finally, rather than using an sgRNA, a recent report has used the two-part tracrRNAs and crRNA to allow for multiplexing. As the crRNA is specific to the sequence of interest, it can be chemically modified at the 5' end to include a fluorophore (a fluorescent dye rather than a fluorescent protein) (Wang et al., 2019).

For sufficient signal:noise, a number of dCas9-FP:sgRNA complexes must be recruited to the same locus, therefore, either repetitive regions can be targeted using a single sgRNA, or a non-repetitive region can be targeted using a number of sgRNAs (Chen & Huang, 2014). Recent developments in confocal microscopy boost signal:noise, therefore allow imaging of two to three dCas9-FP:sgRNA complexes in one locus (Maass et al., 2018).

While using CRISPR is advantageous as only the sgRNA needs to be modified for changing the specificity of CRISPR, nuclease-dead TALENs (TALEs) have also been used for imaging genomic loci (Ma et al., 2013). However, modification of the TALE system is considerably more laborious as it requires modification of repetitive regions of DNA, which has hindered its widespread use for genomic loci though it is has been reported to provide better signal than the CRISPR system (Ren et al., 2017). Indeed, this approach has been previously applied in mouse oocytes (Miyanari et al., 2013).

The imaging of specific chromosomes is of obvious use when looking at the segregation of chromosomes that are prone to aneuploidy (Figure 36). As most of the spot tracking approaches rely on multiple foci to calculate global translation, this approach wouldn't work, and instead manual scoring of segregation patterns would be necessary. However, the number of ready-to-use sgRNAs or TALEs targeting specific and relevant chromosomes are a limiting factor (with the exception of chromosomes 15 and 18 (Ma et al., 2013)).

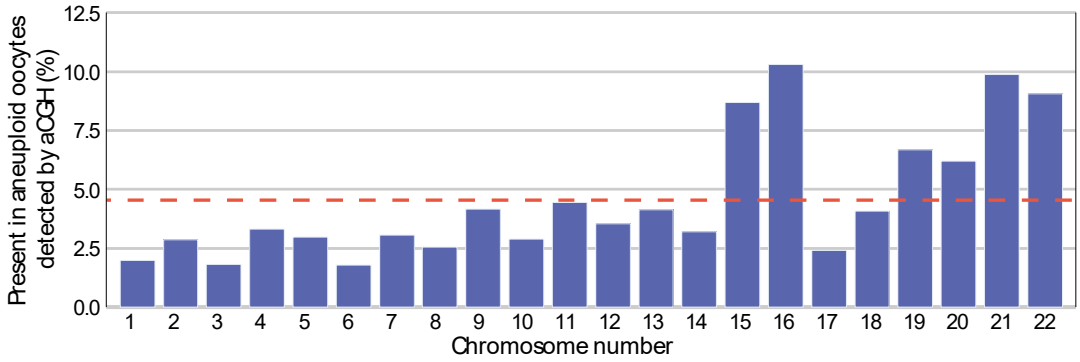

Figure 36 Aneuploidy Rates vary by Chromosome

Graph showing the proportion of each chromosome as detected by aCGH (array-Comparative Genomic Hybridisation). Dashed line shows the level of aneuploidy if all 22 autosomal chromosomes mis-segregated randomly. Data from (Fragouli et al., 2013, 2011; Handyside et al., 2012).

CRISPR/Cas9 works efficiently in mouse oocytes for genome editing, thus translating the system to human oocytes to track specific chromosomes should be feasible. By using the CRISPR/Cas9 system to analyse chromosome segregation events in human oocytes, the precise pathways to aneuploidy can be identified.

5.2 Modifying CRISPR/dCas9 for Oocytes

When experiments were first performed, the CRISPR/dCas9 system had not been used for imaging in oocytes. A previously generated plasmid pSLQ1658-dCas9-EGFP (Chen et al., 2013) was used as a base for making *in vitro* transcribed (IVT) RNA. Fully-grown GV-stage oocytes are transcriptionally silent (De La Fuente, 2006), so plasmids aren't effective for this stage. As the plasmid didn't contain a promoter compatible with commercial IVT kits (T7, T3, SP6), the dCas9-EGFP (Enhanced GFP) fragment was subcloned into a vector that does. These vectors (pRN3 (Lemaire et al., 1995) or pGEMHE (Liman et al., 1992)) also contain UTRs from the *X. laevis* ß-globin gene which enhance translation.

When this construct was microinjected into mouse oocytes along with an sgRNA targeting the higher-order telomeric repeats (TTATGG) that had been transcribed using the same kit (T7 mMessage mMachine), foci could not be seen, but a general cytoplasmic fluorescence was observed. When these oocytes were spread, however, telomeres were clearly seen – marking either end of sister chromatids (Figure 37).

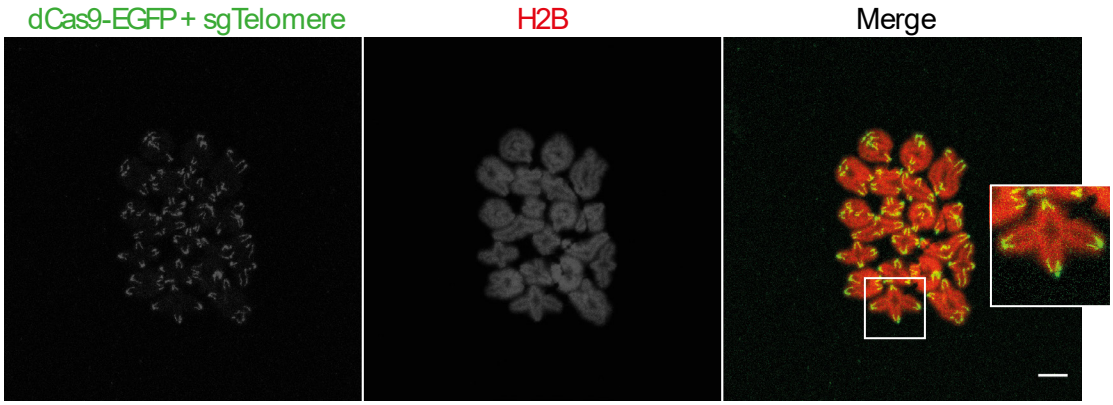

Figure 37 Nuclease-dead, Fluorescent-tagged CRISPR System Can be Used to Visualise Telomeres

Oocytes were microinjected with dCas9-EGFP and an sgRNA targeting the telomeric TTATGG repeats. Specific signal can be seen on telomeres (inset). Scale bar = 10 μm.

5.2.1 Optimisation of dCas9 to Enhance Specific Signal

The lack of specific signal in live cell was therefore most likely due to low signal:noise (SNR). To improve SNR, the concentration of dCas9-EGFP was drastically reduced from 250 ng/μl to 50 ng/μl, which allowed for the visualisation of some foci in live-cell (Figure 38). The epifluorescence system used is poor at picking up the weaker signal caused by the decrease in dCas9 concentration. As a result, future experiments were performed on confocal laser scanning microscopes (CLSM) such as the Nikon A1R microscope or Zeiss LSM880 microscope with Airyscan (Figure 38), both of which are fitted with sensitive photo-multiplier tubes (PMTs) and GaAsP (Gallium Arsenide Phosphide) PMTs.

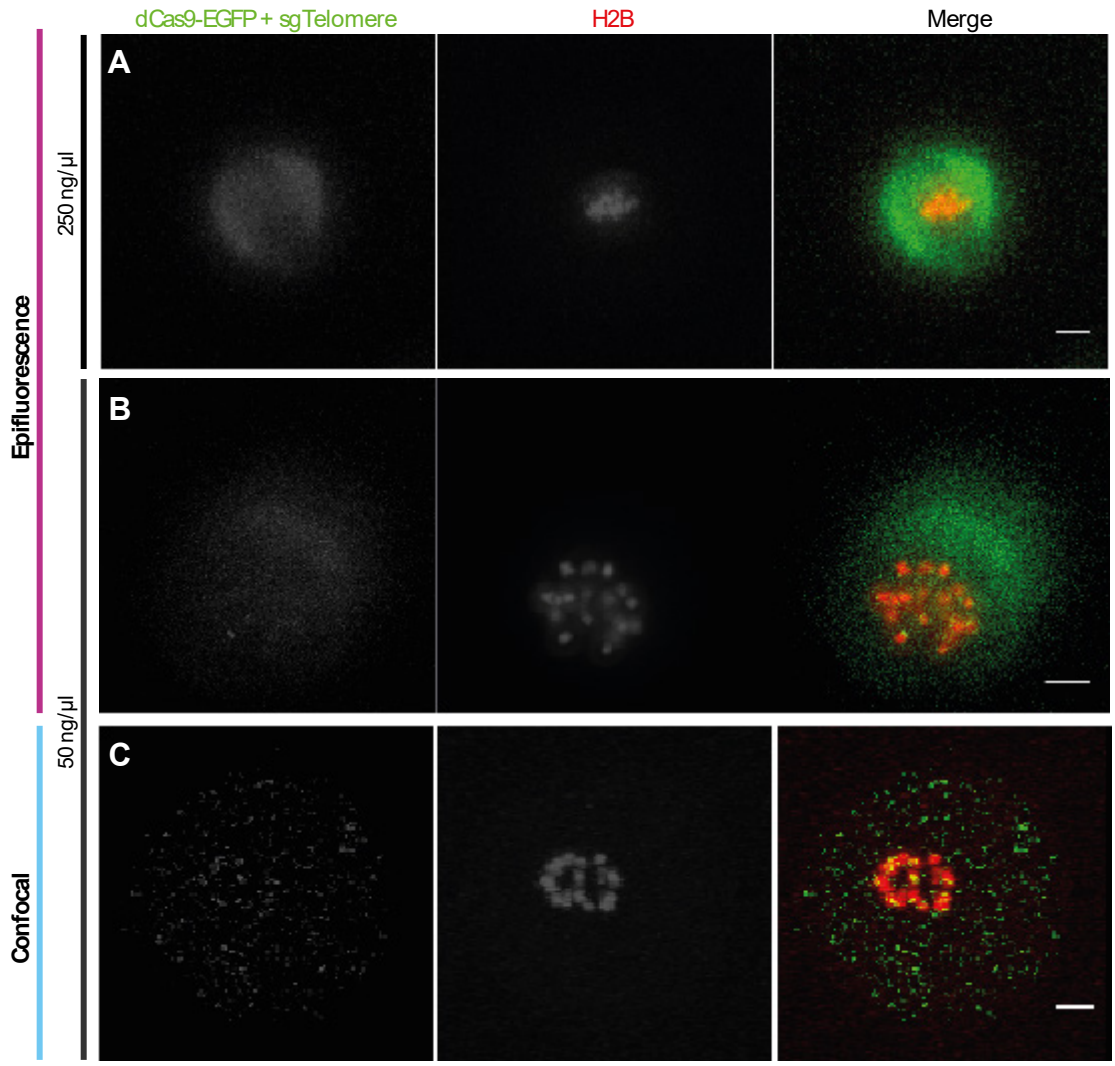

Figure 38 Titration of dCas9-EGFP Enables Imaging of Telomeric Repeats in Live Mouse Oocytes

***A** Oocyte microinjected with 250 ng/µl dCas9-EGFP+sgTelomere don't show specific signal. **B** 50 ng/µl dCas9-EGFP allows for visualisation of telomeric. **C** Specific telomeric signal, but of low-resolution, on a confocal microscope.*

The first modification was to replace the fluorescent protein of the dCas9-EGFP with mNeonGreen (Shaner et al., 2013), which is the brightest yellow/green fluorescent protein. This meant that the detector gain could be reduced, and therefore detector noise, while maintaining the same laser power.

In these initial experiments, the dCas9-EGFP construct did not correctly localise to the germinal vesicle in oocytes. In order to improve the nuclear localisation, two constructs were designed that were directed by publications using Cas9 to improve targeting efficiency of genetic modification in mouse oocytes. The first of these constructs contains a nucleoplasmin NLS on the C-terminus after the

fluorescent protein (Chang et al., 2013), and the second inserts a Flag-tag linker between the N-terminal SV40 NLS and the N-terminal end of dCas9 (Shen et al., 2014) (Table 4). When either of these constructs were microinjected without sgRNA, however, dCas9-mNeonGreen was still seen predominantly in the cytoplasm (Figure 39).

Table 4 Nuclear Localisation Sequences Used for Optimisation of dCas9

Nuclear Localisation Signal	Amino acid sequence
Bipartite SV40 NLS	KRTADGSEFESPKKKRKVE
C-myc NLS	PAAKRVKLD
Monopartite SV40 (mpSV40) NLS	PKKKRKV
mpSV40NLS-FLAG-linker	GPKKKRKVAAADYKDDDDKSRLEPGEKPYKCP-ECGKSFSQSGALTRHQRTHTR
Nucleoplasmin NLS	KRPAATKKAGQAKKKK

Though nuclear localisation of dCas9 had been performed by Chen at al. (2013) *for cell lines, dCas9 did not localise efficiently to the nucleus in oocytes. As a result, a variety of amino acid sequences were inserted into the dCas9 plasmid to optimise nuclear localisation. The names of the* ***Nuclear Localisation Signal*** *sequences are given under along with their corresponding* ***Amino acid sequence****.*

As a result, a number of other NLS sequences were investigated for their strength over nucleoplasmin NLS and the monopartite SV40 NLS (Figure 39). This led to a new construct that contained a bipartite SV40 NLS at the N-terminus and a c-myc NLS at the C-terminus. Both NLSs are thought to be considerably stronger than a monopartite SV40 NLS (Wu et al., 2009; Ray et al., 2015) (Table 4). By comparing a region in the nucleus with a region in the cytoplasm, a nuclear:cytoplasmic ratio can be calculated (Figure 39). In doing so, it revealed this new construct containing the bipartite SV40 NLS and c-myc NLS localised to the GV, with very little signal in the cytoplasm, than the original construct (P = 1.3 x10^{-2}, two-tailed MWU with Bonferroni correction for three tests). There was also greater intensity in the nucleoli as expected (Chen et al., 2013).

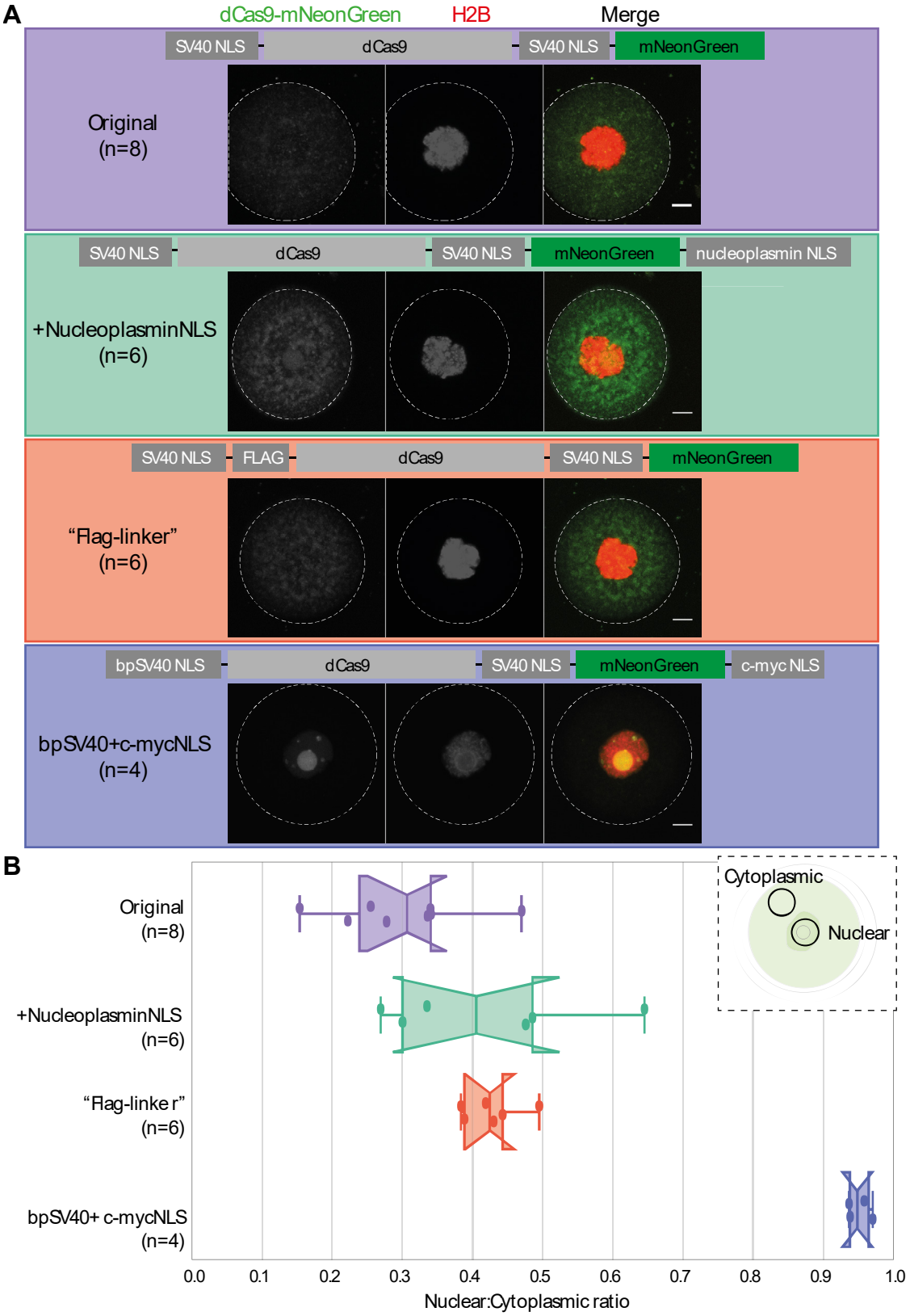

Figure 39 Optimisation of NLS Sequences for dCas9-mNeonGreen

*The original dCas9 construct was unable to localise exclusively to the nucleus in oocytes. Three constructs containing other Nuclear Localisation Sequences were used, one of which localised considerably better than the original. **A** Example images of each construct in GV-arrested oocytes (dashed lines show*

outline of oocyte). Scale bar = 10 μm. ***B*** *Boxplot showing the relative nuclear:cytoplasmic signal from oocytes in each group.*

5.2.2 Modifications to sgRNA and sgRNA Synthesis

In the earlier experiments, sgRNA was synthesised using the same kit as used for making RNA that mimics mature eukaryotic mRNAs. However, sgRNA is usually transcribed in cells using a plasmid containing a U6 promoter, which generates uncapped RNA (Jinek et al., 2012). As a result, a kit which generates uncapped RNA (MAXIscript® T7 Transcription Kit) was used. This enabled visualisation of other repeats such as the centromeric minor satellites and peri-centromeric major satellites (Figure 40). However, the yield of sgRNA was low, so a different kit (T7 Quick High Yield RNA Synthesis Kit) was used, which greatly increased the yield of sgRNA (e.g. 5-fold increase in transcribing sgTelomere, n = 2 repeats, from ~450 ng/μl to ~2600 ng/μl). A final modification to the sgRNA was the introduction of a base-flip, which stabilises the secondary structure of the sgRNA scaffold and therefore is better recognised by dCas9 (Ma et al., 2016).

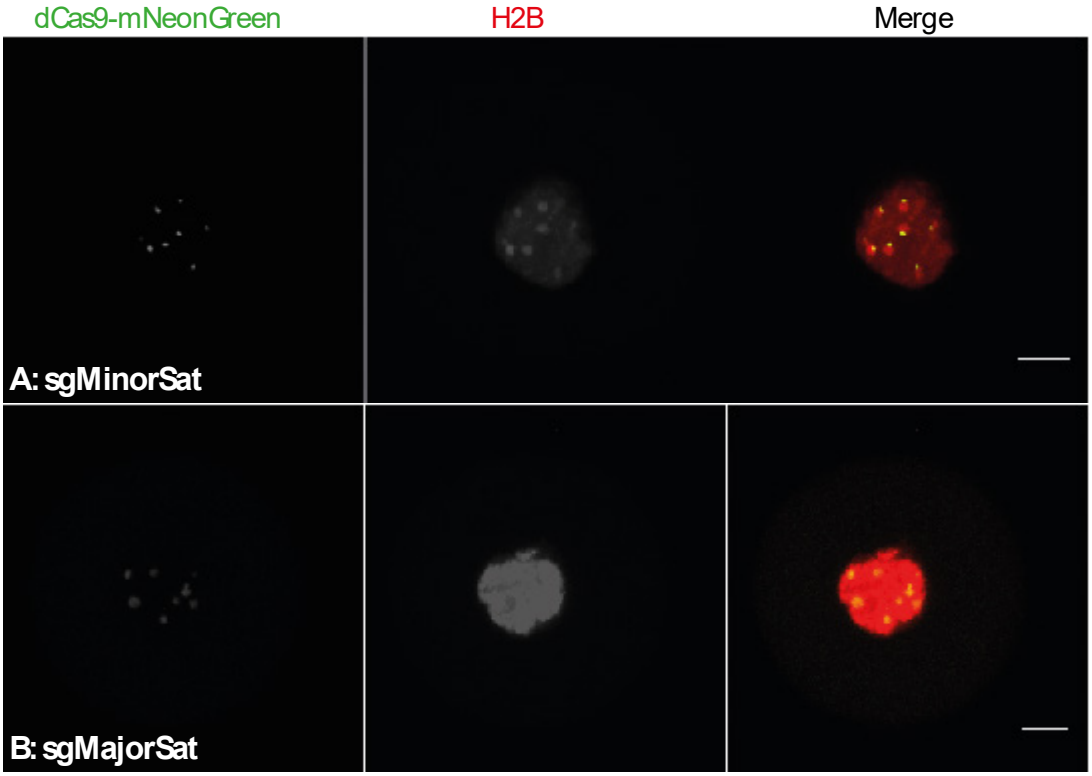

Figure 40 CRISPR/dCas9 Enables Visualisation of Structural Repeats in Mouse Oocyte Chromosomes

Panels shows live mouse oocytes showing centromeric repeats (MinorSat, ***A****) and peri-centromeric repeats (MajorSat,* ***B****). Scale bar = 10 μm.*

5.3 Finding Repeats in Mouse and Human Oocytes Amenable to CRISPR/dCas9 Tagging

5.3.1 Development of a Script to Identify Repetitive Regions for Tagging

Having demonstrated the ability of CRISPR/dCas9 to image large structural repeats, I turned to investigating the possibility of using the system to image specific chromosomes in mouse oocytes. In order to do this, I developed a Python script that used a pipeline partially adapted from Ma et al. (2015). Here, tandem repeats are first located in the reference genome using Tandem Repeat Finder (Benson, 1999), and filtered based on high conservation and their ability to work with CRISPR (i.e. containing the PAM sequence and, a 5' G or GG, etc., which is thought to improve binding (Moreno-Mateos et al., 2015)). The script also scores the sgRNAs based on an on-target score that well represents T7-transcribed sgRNAs (Moreno-Mateos et al., 2015) and U6-promoters (Doench et al., 2016). As well as on-target scores, sgRNAs are checked against other repeats for high off-targets and calculates the number of possible targets. From here, a database is generated that allows for the selection of candidate sgRNAs. A further modification was made for searching of truncated sgRNAs containing 11 nucleotides that was reported to work better than the 20 nucleotides typically used for CRISPR (Ma et al., 2016).

5.3.2 Specific Chromosome Tags in Mouse Oocytes

From the mouse genome, a candidate sgRNA was selected from near the centromere of chromosome 9. Upon microinjection with dCas9-mNeonGreen, it showed specific signal to a single chromosome (Figure 41A). Around the time of this experiment, a paper using mouse cell-lines used an sgRNA targeting the chromosome 12 gene Akap6 (Fu et al., 2016). The sgRNA sequence was used to generate an *in vitro* transcribed sgRNA, which also worked in mouse oocytes (Figure 41B).

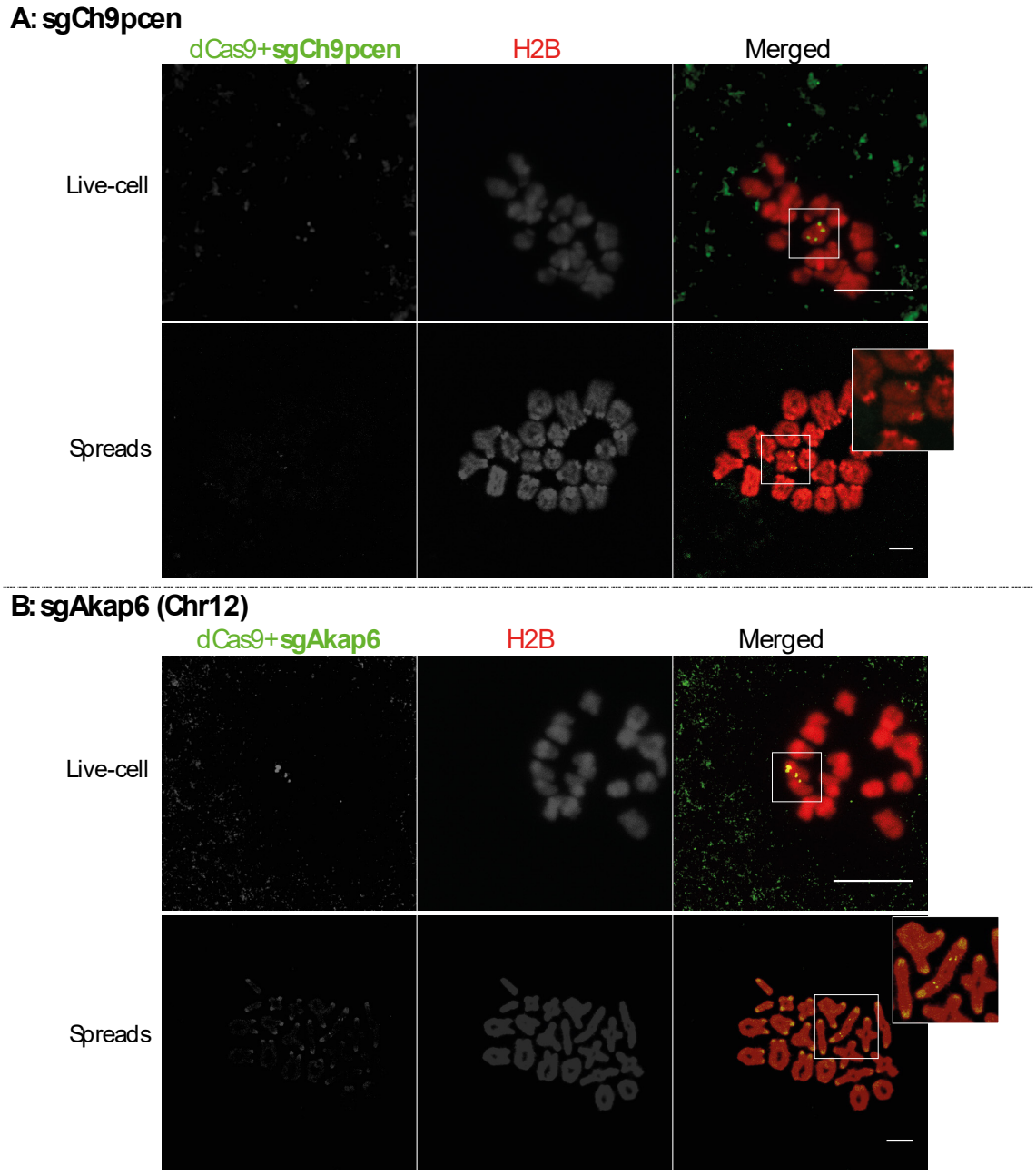

Figure 41 Chromosome-specific Markers Can be Imaged in Live-cell

Using a custom search script, a target site in the region of the peri-centromere of chromosome 9 was identified that might work with CRISPR-targeting. ***A*** *Chromosome 9 marker in a live oocyte and on chromosomes spreads prepared in meiosis I.* ***B*** *Chromosome 12 marker. Scale bar = 10 µm.*

5.4 Development of a "Centre of Mass" Tracker for NIS Elements

Imaging oocytes is difficult both because of the size of the cell and that the chromosomes move within the cell. The size of the cell means that the cell is exposed to a considerable amount of light; though the proportion of pixels collected containing analysable data are small as the chromosome mass represents a much

smaller amount of the cell. This increases phototoxicity and limits the resolution. As previously mentioned, a "Centre of Mass" tracker has been developed for Zeiss CLSMs (Rabut & Ellenberg, 2004; Kitajima et al., 2011), and another for Leica CLSMs (Lane et al., 2017), but one had yet to be developed for Nikon systems, such as the Faculty's Nikon A1R CLSM. So, the centre of mass concept was replicated for use in NIS elements.

This utilised Nikon's native NIS macro environment but delegated the task of finding the centre of mass to Python, as a native NIS solution was very slow (milliseconds in Python compared to several seconds in NIS elements). As this microscope was managed by the Faculty, *Python-Bioformats* couldn't be used as it is dependent on the installation of Java Development Kit (Linkert et al., 2010). Instead, *pims_nd2* (Wel, 2015), which uses the ND2SDK library was used (Laboratory Imaging s.r.o., 2019). This needed to be further developed as the package didn't read stage coordinates from the images. The Nikon Centre of Mass tracking macro was then used for imaging telomeres in mouse oocytes. In this initial experiment, it was suggested that the best images would be acquired using a resonant scanner, which scans the image quickly but in doing so, generates a considerable amount of noise. To counteract this, the same plane is imaged multiple times and then averaged (typically 8-16x). However, I posited that this amount of light would expose the oocyte to around the same amount of light as using a galvanometer scanner. Galvanometer scanners are slower, but more accurate, and therefore provide better quality images, even without averaging. The combination of these two changes enabled the visualisation of high-resolution dynamics of telomeres in mouse oocytes (Figure 42).

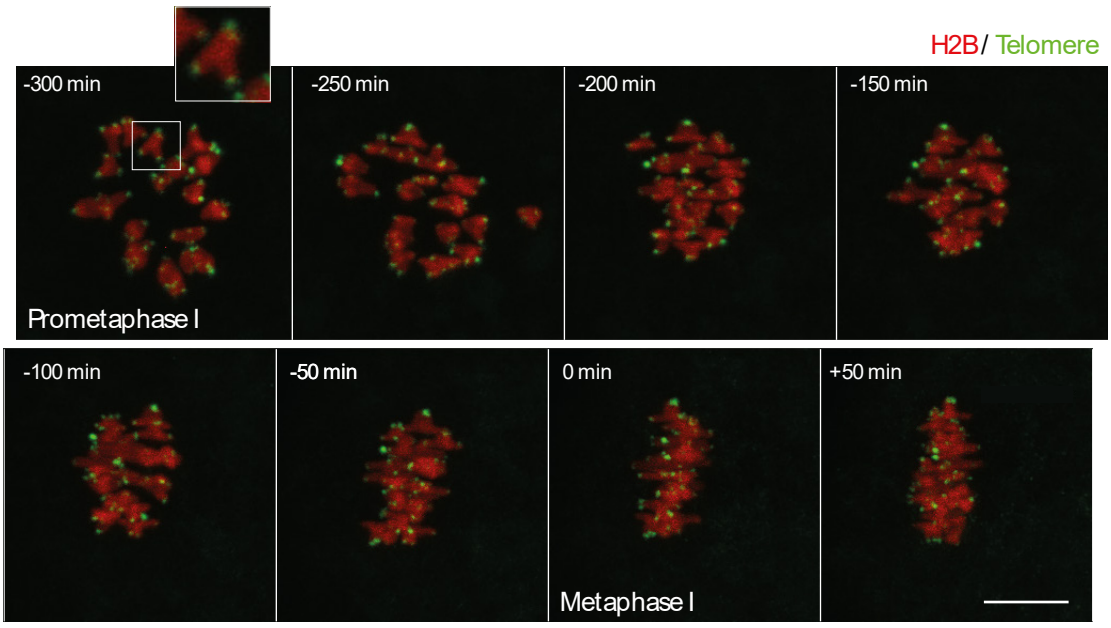

Figure 42 Time series of Telomeres in Prometaphase I to Metaphase I in Mouse Oocytes

Selected time points from a time-lapse experiment using the NIS elements autofocus macro. Oocytes were microinjected with H2B-mCherry and dCas9-mNeonGreen + sgTelomere. Inset shows a bivalent with four telomeric foci. Time shown is relative to metaphase. Scale bar = 10 µm.

5.5 Development of an Open-Source Spot Detection Script for FIJI

As previously mentioned, spot detection is fairly computationally easy, and in order to streamline the previous process (Kitajima et al., 2011), I developed an open-source script that works on top of TrackMate (Tinevez et al., 2017). TrackMate is predominantly designed for automated detection of spots and so I wanted to incorporate manual curation of spots in a user-friendly manner. As the previously described protocol for spot detection requires pre-processing in FIJI, using TrackMate, which is a plugin in FIJI, meant the pipeline would already be shortened.

As well as Gaussian and median filters, the plugin allows for in-place Difference of Gaussians filtering, which is the primary processing required for enhancing spots (Kitajima et al., 2011). As it seemed that manual detection of centromeres was the best way to get centromere coordinates, a number of processes were added to refine the user-provided points using regional centre of mass, Gaussian peak fitters or quadratic fitting schemes (Tinevez et al., 2017; Pietzsch et al., 2012). Further, it is important to keep centromeres of the same bivalent/dyad together. In order to do this, I implemented the Munkres-Kuhn algorithm for

automatic pairing (Munkres, 1957; Kuhn, 2010; Burkard et al., 2012). But again, there is also the option of manual pairing (Figure 43).

Finally, though automatic detection wasn't used, a variable Difference of Gaussians (DoG) detector was implemented. Here, a series of sigma values are computed between a range of possible sizes of blobs and successive rounds of spot detection are performed to find spots of differing sizes. As intensity decreases with higher sigma sizes, the relative threshold is decreased with each pass.

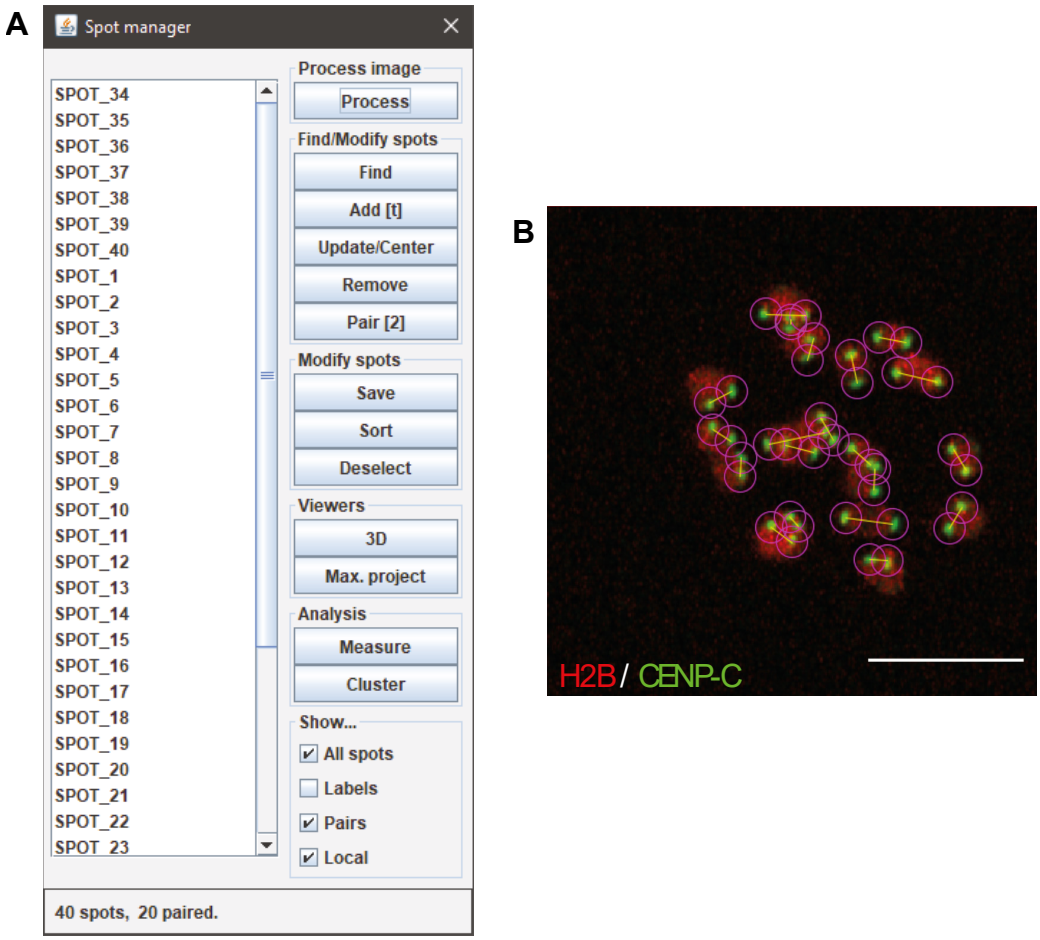

Figure 43 SpotCollectionManager: a FIJI Macro for Spot Detection and Downstream Analysis

SpotCollectionManager was designed to streamline spot detection, spot pairing and measurements. It is built on top of the open-source TrackMate plugin. ***A*** *User interface for SpotCollectionManager.* ***B*** *An example image with paired kinetochores, marked by the inner kinetochore protein CENP-C (magenta circles show spots; yellow lines show paired spots). Scale bar = 10 µm.*

5.6 Centromere Tracking Using A FIJI-based Pipeline

Upon developing *SpotCollectionManager* and optimising chromosome tracking on a Zeiss LSM880 with Airyscan using *AutoFocusScreen* (Kitajima et al., 2011), I performed a time-lapse experiment using mouse oocytes microinjected with a

centromere marker (Figure 44). After acquiring images, I used *SpotCollectionManager* to mark two spots on each bivalent. Each spot represents a sister centromere pair, based on the fluorescence from the optimised CRISPR system and an sgRNA directed to the minor satellites to mark the centromeres. These were then paired based on the presence of histone fluorescence between them. Once each time point contained forty correctly-placed spots, I used TrackMate for spot registration (Tinevez et al., 2017). As previously mentioned, this is the process of linking spots in adjacent time points to generate tracks. However, the built-in linking algorithms either assume that the motion is Brownian (i.e. random, when using the "LAP tracker") or linear (using a Kalman filter) (Jaqaman et al., 2008; Tinevez et al., 2017). Neither of these types of motion accurately describes centromeres, as speed changes throughout meiosis (Kitajima et al., 2011). Previous studies modelled the movement as autoregressive (Kitajima et al., 2011; Sakakibara et al., 2015; Kouznetsova et al., 2019), and so this was incorporated into the TrackMate-based registration process. Autoregressive motion predicts the future position of a spot based on its previous movement (Elnagar & Gupta, 1998). Further, spot registration is usually performed without the knowledge of which spots are paired. To improve accuracy, spot pairs were also taken into consideration to generate a new linking scheme that works in two broad phases. In the first phase, pairs of spots are tracked together, which prevents assignment of tracks between spots of different chromosomes. In the second phase, spot registration is then performed on spots in incomplete tracks, which are linked back to tracks from the first phase. This new registration process also utilises modules in TrakEm2 to correct images for translational movements based on the centre of spots detected (Cardona et al., 2012). The modified registration process generates complete tracks that are faithful to the user-provided pairs. It also uses the same motion model, autoregressive, as previous studies. The tracks can also be corrected using the built-in user interface of TrackMate (Tinevez et al., 2017).

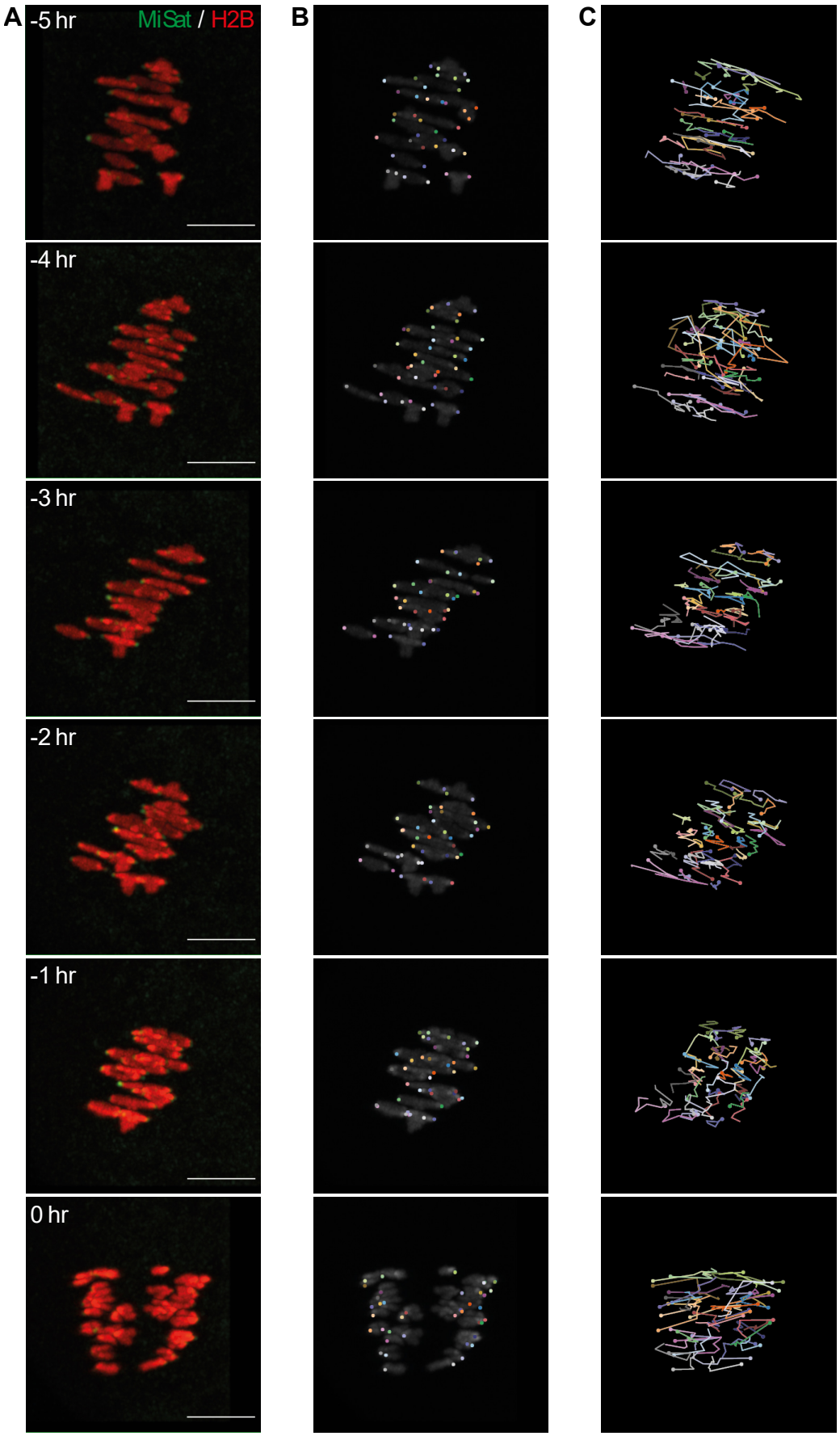

Figure 44 Centromere Tracking in Mouse Oocytes from Prometaphase I to Anaphase I

*Centromeres were marked by microinjection of the optimised CRISPR system and minor satellite sgRNA. **A** Maximum Intensity **Z**-Projection of chromosomes from prometaphase I to anaphase I showing chromosome segregation. Scale bar = 10 µm. **B** Shows the same Maximum Intensity Z-Projection, with the centromeres detected as spots. Each spot has a unique colour. **C** The tracks of centromeres showing their movement over the previous 1 hour. Tracks are coloured as in B. Times shown in A are relative to anaphase I.*

5.7 Visualisation of Human Centromeres Using Optimised CRISPR/dCas9 System

With CRISPR/dCas9 working in mouse oocytes, the system was tested in human oocytes. With the exception of telomeres, the other repeats are not conserved in the human genome. Instead, the centromeres are made up of higher order α-satellites repeats that have been shown to be targetable by CRISPR/dCas9 (Chen, Hu, et al., 2016). The same publication also showed that a subset of chromosome centromeres could be visualised by targeting ß-satellites, which are present on chromosomes 9, 13, 14, 15, 21 and 22 (Waye & Willard, 1989). sgRNAs targeting the α- and ß- satellites worked successfully when tested in human oocytes (Figure 45).

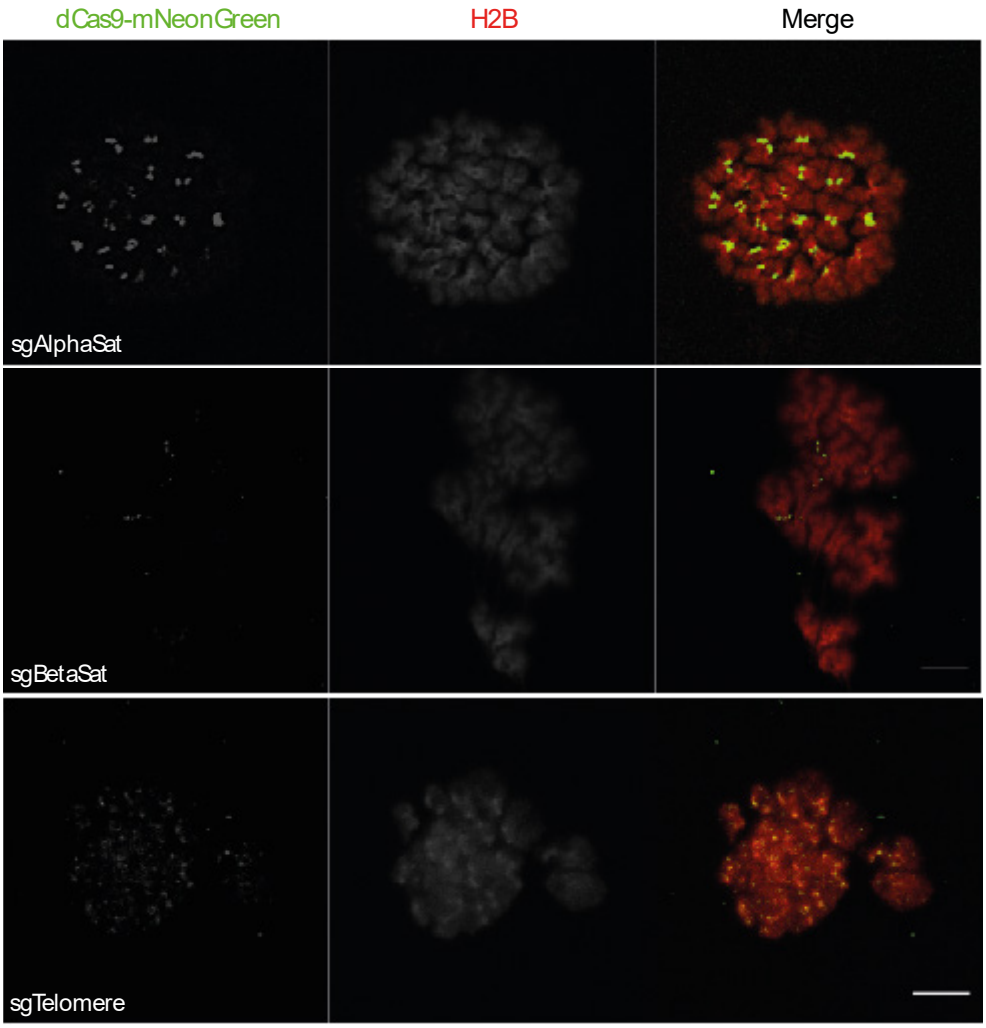

Figure 45 Optimised CRISPR Enables Visualisation of Structural Repeats in Human Oocytes

*Chromosome spreads of human oocytes that had been microinjected with the optimised CRISPR system and sgRNAs against the a-satellite repeats of all centromeres (**sgAlphaSat**), β-satellites (**sgBetaSat**, a subset of centromeres) and telomeres (**sgTelomere**). Scale bar = 10 μm.*

In part due to the difficulty in testing sgRNAs and obtaining enough human oocytes to test sgRNAs, I decided to use α-satellites rather than specific chromosome markers for the rest of the study.

5.8 Difficulty of Using "Centre of Mass" Tracking with Human Oocytes

"Centre of Mass" trackers work well for mouse oocytes as they are harvested at the GV-stage where they can be maintained at arrest for many hours, allowing for adequate protein translation. However, human oocytes were harvested at a variety of stages, where arrest cannot be maintained without the use of chemical inhibitors

(Teusel et al., 2018). In this study, the majority of oocytes were harvested after nuclear envelope break down, when incorporation of histone is impaired (Zielinska & Schuh, 2018). Further, human oocytes contain blob-like regions of high autofluorescence. Due to the paucity of material, these could not be fully characterised. However, I imaged an oocyte to understand how these autofluorescent blobs appear in different wavelengths. A single Z-plane was imaged using 6 different wavelengths without an emission filter (typically an emission filter is used to keep specific signal, but this would make it more difficult to characterise these blobs). From this it suggests that these span multiple wavelengths but are more prominent in shorter wavelengths (Figure 46). Centre of Mass tracking usually utilises the histone for tracking, so the combination of high auto-fluorescent blobs and low histone makes tracking difficulty.

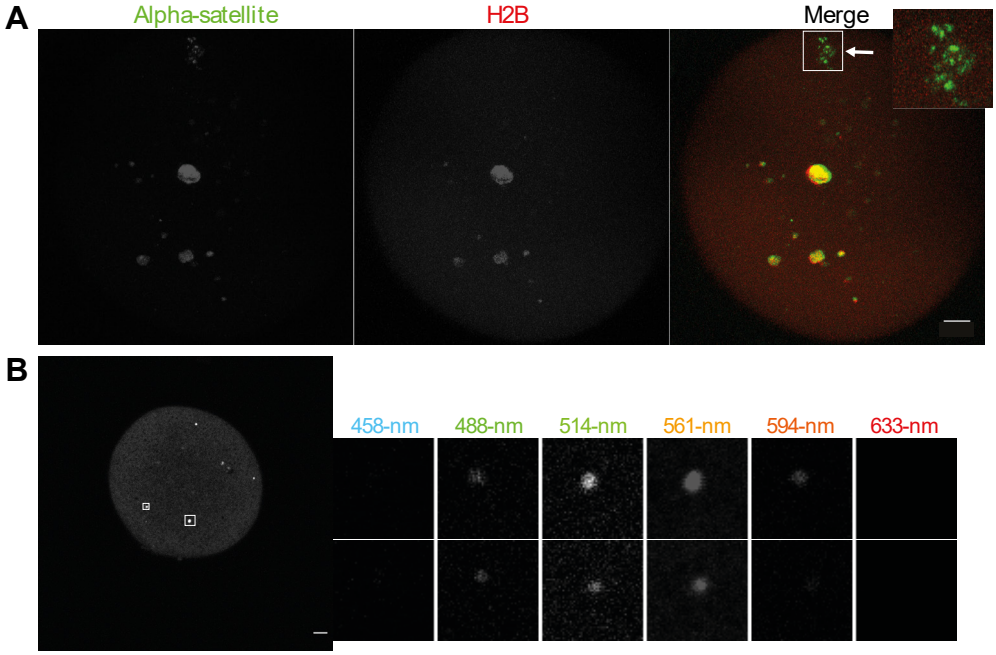

Figure 46 Autofluorescent Blobs Pose an Issue for Tracking in Human Oocytes

Example of autofluorescent blobs that make tracking difficult. ***A*** *Image of a whole oocyte taken shortly after microinjection (arrow shows chromosome mass, inset shows zoomed in chromosome mass).* ***B*** *Oocyte imaged without an emission filter, excited at a range of wavelengths showing autofluorescent blobs predominantly in lower wavelengths (large image shows merge of all channels). Scale bar = 10 μm.*

To try and alleviate this problem, I moved from using a red histone (mCherry/mScarlet (Bindels et al., 2017)) to using a monomeric far-red fluorescent

protein, miRFP670 (Shcherbakova et al., 2016). This meant that the autofluorescence was less of an issue for tracking, however the maturation time was considerably lower, making imaging difficult. A further issue was the large size of human oocytes. As the stage moved quickly, the oocyte would also move, sometimes moving the oocyte out of the field of view altogether and therefore not providing an image with anything from which to track. Predominantly due to the issues with tracking using histone, I moved to using a tracking system that was based on a more complex approach that would pre-process and segment the images before centring on a region of interest.

5.9 Modification of an Object-Detection Tracker Works Inconsistently

As mentioned in the introduction, another approach to tracking is using object detection (Politi et al., 2018). This works by passing acquired images to FIJI where they are processed to enhance the signal. To test whether this approach would be useful, I tested the object detection in images from data that had been generated thus far. This approach appeared to work even with low SNR (Figure 47). However, it became clear that using this approach on the histone signal did not work for all stages.

As α-satellite signal was visible even shortly after microinjection (~60 minutes, n = 3), I investigated how the α-satellites could be used for tracking. In order to accomplish this, I used pre-processing and segmentation, i.e. binarising the image such that positive pixels are 1 and the background is 0. As the approximate size and number of the α-satellites is known, it can be estimated what the typical number of pixels will be. So, a processing loop can be used to either reduce noise (Gaussian filter) or reduce noise and enhance edges (Gaussian Weighted Median Filter (Brocher & Wagner, 2015)). Once the thresholded pixel count is in range, a nearest-neighbour approach is used to find a cluster of foci (Ollion et al., 2013), the largest of which was selected for recentring (Figure 47).

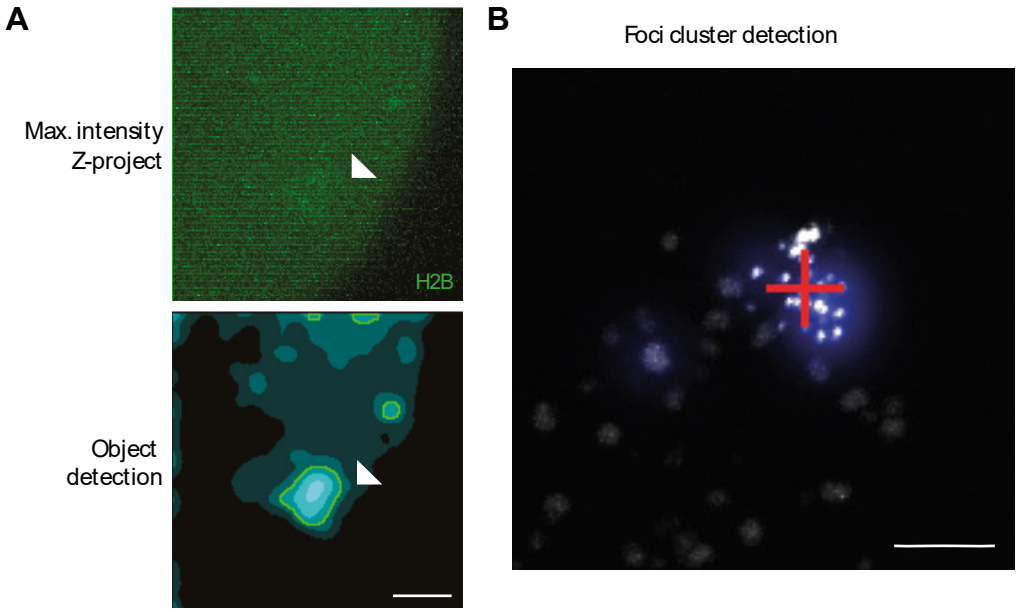

Figure 47 Using a More Complex Tracker Still Has Issues

To remedy issues with centre of mass tracking, a modified pipeline using object detection was used. ***A*** *Example of correctly segmenting even with low SNR. (Top) Image shows a maximum intensity Z-projection of the histone channel. (Bottom) Image shows the result of object detection.* ***B*** *An example of using a-satellite clusters to find chromosome mass. Cross, shows where to refocus, intensity of blue shows density of foci clusters. Scale bar = 10 μm.*

However, this did not always work. In fact, the FIJI processing script often had to be modified during an experiment, meaning the oocytes could not be imaged, and so I built a tracking system from the ground up.

5.10 Development of a Customisable Tracker Works, but with Compromised Resolution

In order to make this tracker easier to use, I borrowed concepts from the previous tracker but wanted to allow for much greater control of how objects were detected. Firstly, I modified *MyPiC (My Pipeline Constructor)* (Politi et al., 2018) so that it could send and receive HTTP (HyperText Transfer Protocol) requests, which would allow it to respond to a local Python server that communicated with the microscope. On initialisation, the Python server sends the processing, thresholding and filtering options to *MyPiC*. These options can then be configured on demand and includes many of the common image filtering options such as median, Gaussian, LoG (Laplacian of Gaussian), and DoG (Difference of Gaussians) filters as well as other processes that enhance edges (all from the Python module *scikit-image* (van der Walt

et al., 2014) and *SciPy* (Virtanen et al., 2019)). There are also options for thresholding and the same features that were used for clustering as previously mentioned (Figure 48).

Figure 48 Object Detection Can Be Enhanced Through A Customizable Approach

Customizable tracker made setting up experiments easier, but still suffered some of the same problems as the previous object detection approach. Figure shows example of a complex tracking experiment using the cluster of a-satellites to find the correct location for centring. The acquired image is filtered first using a median filter, then a Gaussian filter. The filtered image is made binary using the Otsu method. Finally, a density map is made from the detected objects and the largest density is used for centring. Scale bar = 10 µm.

While this eased the process of tracking, there were still issues. For example, tracking could not be performed if the region containing chromosomes was not in the acquired image. As a result, the resolution had to be compromised in order to give enough of a field of view to find chromosomes. However, this resolution is not sufficient for centromere tracking. An early attempt to account for oocyte translation was the use of *ITK* in the local Python server (Yaniv et al., 2018). As the oocytes rotate as well as translate, the position of chromosomes can't be predicted from their relative position to the oocyte centre and the translation detected by *ITK* was therefore inaccurate and other approaches need to be considered.

5.11 Development of a Demo Tracker Using Template Matching

While this final tracker was not used in the study, its use was tested on images that had been acquired during the optimisation of imaging. As previously described, this approach looks for image similarity rather than intensity. As the chromosome mass is identified by the researcher in the first acquisition its changed appearance in successive acquisitions can be used to find the image in the following time points. 3D cross-correlation, the back-end of this approach, is extremely slow. One possible

solution is to separate the cross-correlation into multiple 2D problems (doing XY-projections and XZ-/YZ- projections independently) as has been previously described (Matsuda et al., 2018). However, this process was modified further to account for its potential use in tracking. The sum Z-projected template is "matched" to the sum Z-projected image to give the correlation in the XY plane. This reveals a number of peaks, primarily due to the autofluorescent blobs. However, exploiting the fact that autofluorescent blobs appear similar in multiple channels, correlation accounting for autofluorescence can be penalised to further improve the accuracy. In testing this approach, the process was able to find the chromosomal region in one egg given the chromosomal region of another egg (Figure 49B). An XZ and YZ sum-projection are then made for both the template and image. The same process as before is applied to find the z-coordinate. Both XZ and YZ are used as each plane contains a different amount of information. Theoretically, they should provide the same point, but using whichever has the highest correlation also works.

An alternative approach is to exploit the fact that this template-matching approach is normalised and therefore values are between -1 and 1 (Lewis, 2001). As a result, two correlation images can be multiplied and the resulting image will contain high correlation in regions where there was high correlation in the source images (Figure 49C). By generating the correlation between the template and target image in each channel (α-satellite and histone channel separately), the result of multiplying both images creates a new image that shows the correlation along both channels. However, this still leads to spurious regions of high correlation (Figure 49C). A classic approach to improving image enhancement is to repeat a process at different scales (e.g. at half-the size of the original) (Adelson et al., 1984; Thevenaz et al., 1998). The use of this multi-scale approach has the advantage of finding matches that can be identified even at lower resolutions. The result is a much-refined process that gives more clearly defined regions of high correlation, though there are still "incorrect" regions identified. These could be further refined by checking each region for a cluster of foci in the α-satellite channel or checking the distance moved from the previous time-point, for example. Nonetheless, in these tests, this provided a novel solution to all the problems encountered in imaging human oocytes and allows for imaging with the faster maturing and brighter red fluorescent proteins attached to histone (e.g. mScarlet or mCherry), which will be important in assigning sister kinetochores to homologues during analysis.

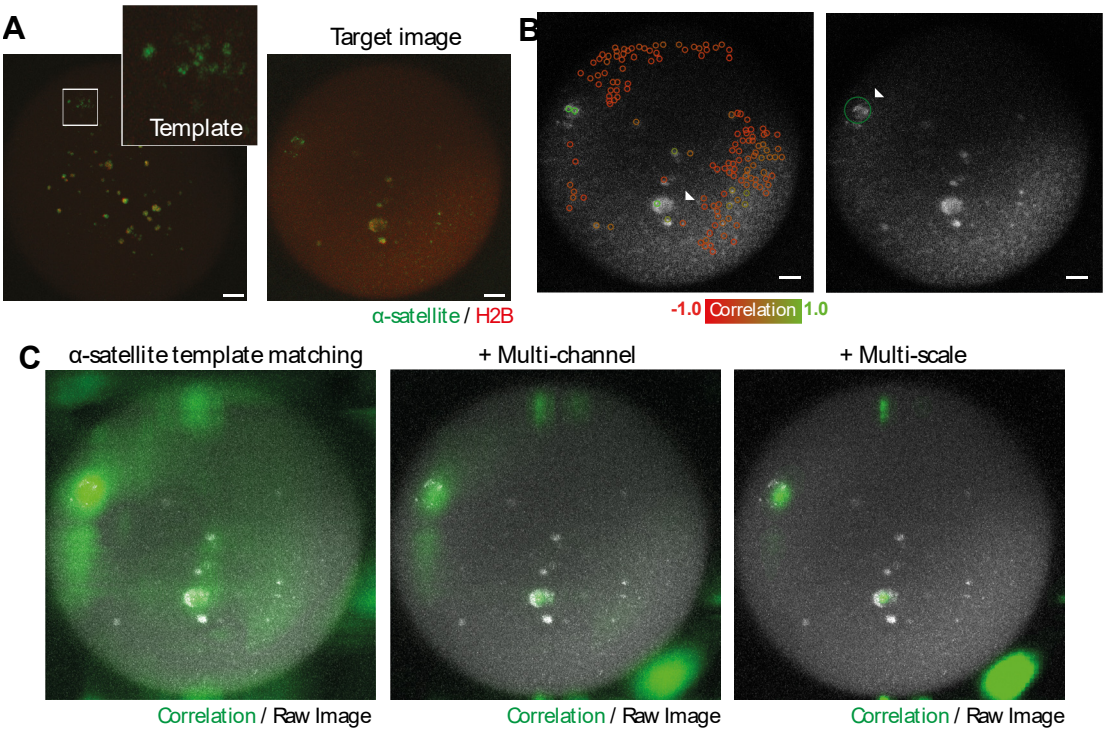

Figure 49 Template Matching Can be Used to Find Chromosome Mass in Live-cell Experiments

A *(Left) Chromosome mass identified in one oocyte was used as a template to find a chromosome mass in a different oocyte (Right).* ***B*** *(Left) The correlation between the template identified by the user and the target image is calculated and peaks are detected (either positive or negative, as shown in a scale from green to red). Arrowhead shows example of a peak of high correlation where there is autofluorescence. (Right) This can be adjusted by penalising for correlation between channels. The correct location is then found as shown by the arrowhead.* ***C*** *Shows an alternative approach of using template matching. Here, (Far-left) only the signal in the a-satellite channel is used to generate correlation between the template and target image. (Middle) The same process is then applied to the histone channel and the two images are multiplied. As the correlation is scaled between -1.0 and 1.0, this means that high correlation in both channels is shown as high in the resulting image. (Right) The template and target image are then rescaled multiple times, and the same multi-channel template matching is performed. These images are again multiplied and there are even fewer regions of "incorrect" high correlation. Scale bar = 10 μm.*

5.12 Discussion

With the exception of using CRISPR/dCas9 to visualise genomic loci, kinetochore tracking had already been utilised to monitor chromosome segregation in mouse oocytes. It was therefore expected that translating this approach into human oocytes would not be difficult. Unfortunately, this was not the case.

dCas9 and sgRNA synthesis were modified for use in GV-stage oocytes. Despite previously being optimised for nuclear localisation (Chen et al., 2013), dCas9 had to be further optimised for oocytes. One possible explanation for the difference between oocytes and cycling cells is that the latter undergo many rounds of NEBD before imaging and this may allow for import and capture into the nucleus of dCas9, giving the impression of successful nuclear localisation. The advantage of good localisation at the germinal vesical-stage is two-fold: it provides a different, and more open chromatin state for dCas9-sgRNA (Horlbeck et al., 2016) and oocytes can be arrested in this state for a controllable period of time using small-molecule inhibitors. Though the modification of dCas9 with NLSs that have been previously used to optimise CRISPR for genome editing appeared to only slightly improve localisation (Chang et al., 2013; Shen et al., 2014), one combination of NLSs (N-terminal bipartite SV40 NLS and C-terminal c-myc NLS, (Wu et al., 2009; Ray et al., 2015)) provided much greater nuclear localisation.

At the start of this work, it was not known how successful this would translate into oocytes. In order to quickly test this, sgRNAs were transcribed using the same kit as used for *in vitro* transcription, which generates RNAs that mimic mature, capped eukaryotic mRNAs (Ramanathan et al., 2016). However, sgRNAs used in mammalian cells are typically transcribed from a plasmid containing a U6 promoter and it is thought that this increases the efficiency of dCas9-sgRNA complex formation as it doesn't result in capped sgRNA. The 5' end of an sgRNA is where Watson-Crick base-pairing occurs for target searching and so *may* interfere with the homology search (Xie et al., 2017). Further, the 5' cap is also involved in nuclear export (Lewis & Izaurflde, 1997), which could reduce the activity of the dCas9-sgRNA complex. Changing to a kit that generates a high-yield of uncapped sgRNAs will likely further assist in successful visualisation genomic loci, though a comparison wasn't made.

To enable centromere tracking, I streamlined the previous pipeline for spot detection into one script that allows for manual curation and pairing. This is built heavily on previous models and approaches but differs in the greater use of manual

curation, which are usually difficult to do in other packages (such as Imaris and MATLAB-based scripts). I also modified spot registration to improve accuracy by performing the process in two phases. The first phase generates tracks from paired spots and therefore ensures that they are kept together during the registration process. This generates incomplete tracks as some spots are not paired. In the second phase, incomplete tracks are filled with the remaining spots.

The main difficulty in this project has been the imaging of human oocytes. Issues include the stage movement being translated to the oocyte and the presence of autofluorescent blobs in human oocytes. To accommodate for the autofluorescent blobs, which appear more sharply in lower wavelengths, the fluorescent tag on the histone was changed from red to far-red. However, the time needed to see histone signal was greatly extended, requiring significant modifications to the live-cell tracking scheme used in mouse oocytes. These modifications to the imaging of chromosomes eventually led to the development of a new tracking system where the image processing is done on a local Python server, using *scikit-image* as a back-end (van der Walt et al., 2014). However, this only partially resolved the problem.

A demo version of a tracker that uses template matching shows a lot of promise and may allow for the imaging of high-resolution time-lapse microscopy of human oocyte centromeres. Overall light can be further reduced in the future by preceding the template matching stage with the capture of a low-zoom single plane to recentre the oocyte in XY. This recentring also helps to reduce the problem of oocyte movement on the microscope. As the image used for template matching is a Z-stack, this image can also be used to refine the cell centre for the next time point. The final high-resolution image can also be used to refine the centre of the chromosomes for the next time point, creating a feedback loop that traverses throughout the experiment.

Chapter 6: Using Live-cell Microscopy to Understand the Impact of Ageing in Human Oocytes

6.1 Introduction

Data from studies comparing oocytes from younger and older women note the increased presence of separated sister chromatids in meiosis II (Fragouli et al., 2010; Handyside et al., 2012; Fragouli et al., 2013). These were first observed by chromosomes spreads (Angell, 1991) and then by array-Comparative Genome Hybridisation (aCGH) (Ottolini et al., 2015). However, some of this work is likely to underrepresent the ageing effect as the use of DNA sequencing can only be used to detect gain or loss of chromosomes and chromatids, but not separation; the latter would be seen as "euploid" as the correct amount of DNA is present. Recent work in mouse oocytes, using high-resolution time-lapse microscopy, has shown that the majority of these are generated by hyper-stretching of bivalents in prometaphase I by spindle forces that lead to premature resolution of bivalents into dyads (Sakakibara et al., 2015). These dyads then realign on the metaphase I spindle and undergo a metaphase II-like division. Other live-cell work suggests that the presence of separated chromatids in meiosis II is not due to this form of missegregation, but from dyads separating prematurely shortly after anaphase I (Yun et al., 2014). Due in part to the paucity of human oocytes available to research, the amount of live-cell data generated has been low. Previous data, based on oocytes unsuitable for IVF treatment, looked at the change of spindle morphology over time and showed that spindle microtubules are nucleated from kinetochores themselves (Holubcova et al., 2015; Mogessie et al., 2018). The authors show that human oocytes spend a large part of prometaphase I with multipolar spindles, that only become bipolar very near metaphase I. These data were generated without using chromosome tracking, and thus the resolution would have been too low to see centromeres.

While my original aim was to look at segregation defects over time, the spatial resolution was compromised to allow the generation of some data for tracking. The resolution, however, still allows for the scoring of alignment defects at metaphase I and -II, as misaligned chromosomes are easily discernible from those that are aligned based on their distance.

Previous work in mouse oocytes has shown that, as well as an increase in aneuploidy due to advanced age, there is also an increase in misalignment at

metaphase I and -II (Liu & Keefe, 2008; Lister et al., 2010; Chiang et al., 2010; Nakagawa & FitzHarris, 2017; Yun et al., 2014). Consistent with this, misalignment has been reported in meiosis I in human oocytes as seen from lower resolution studies (Battaglia et al., 1996; Volarcik et al., 1998). Metaphase is typically defined as the time in the cell cycle when chromosomes are correctly aligned on the spindle (Orr & Maiato, 2019). Studies in model organisms show that the depletion of key Cohesin components increase misalignment of chromosomes in metaphase in mitosis (Sonoda et al., 2001; Kenney & Heald, 2006), providing a possible link between the age-associated decrease in Cohesin and age-associated increase in misalignment in metaphase I and –II. Lagging chromosomes during anaphase are a further predictor of aneuploidy (Cimini et al., 2001; Thompson & Compton, 2008), though this has been suggested to not be the case in mitosis (Thompson & Compton, 2011). Cohesin is cleaved by Separase in a synchronous manner (Yaakov et al., 2012), and therefore a delay in cleavage is unlikely to explain the presence of laggards. Instead, it is thought that lagging in anaphase is predominantly due to attachments of the laggard to both spindle poles (Cimini et al., 2001). Given the association of aneuploidy with misalignment at metaphase I and -II, I used the α-satellite system optimised in Chapter 5, to investigate misalignment of chromosomes in human oocytes with increased resolution.

6.2 Cell Cycle Defects are Most Common in Oocytes Harvested at GV-stage

Studies in human oocytes often use oocytes that are unsuitable for IVF treatment as they are too immature, which means some of these are still at the GV-stage at collection. As a result, events can easily be timed to a single reference point, the breakdown of the nuclear envelope (NEBD, or GVBD in oocytes). That oocytes are still at the GV-stage ~37 hours after administration of hCG may suggest that the oocyte has come from a follicle that has not responded normally to the hormonal cue. To obtain a population of oocytes maturing from follicles that respond normally to hCG administration, oocytes were harvested for the work in thesis at an earlier stage (18.5-37 hours after hCG administration) from donors with an age range of 19-44 (median: 33.5) years. Out of the 53 samples, only 12 (23%) were harvested at the GV-stage, the remainder were harvested after GVBD and were predominantly in meiosis I at the start of experiments (74%). Using the available time-lapse data that had been collected, cell cycle stages were scored (Figure 50).

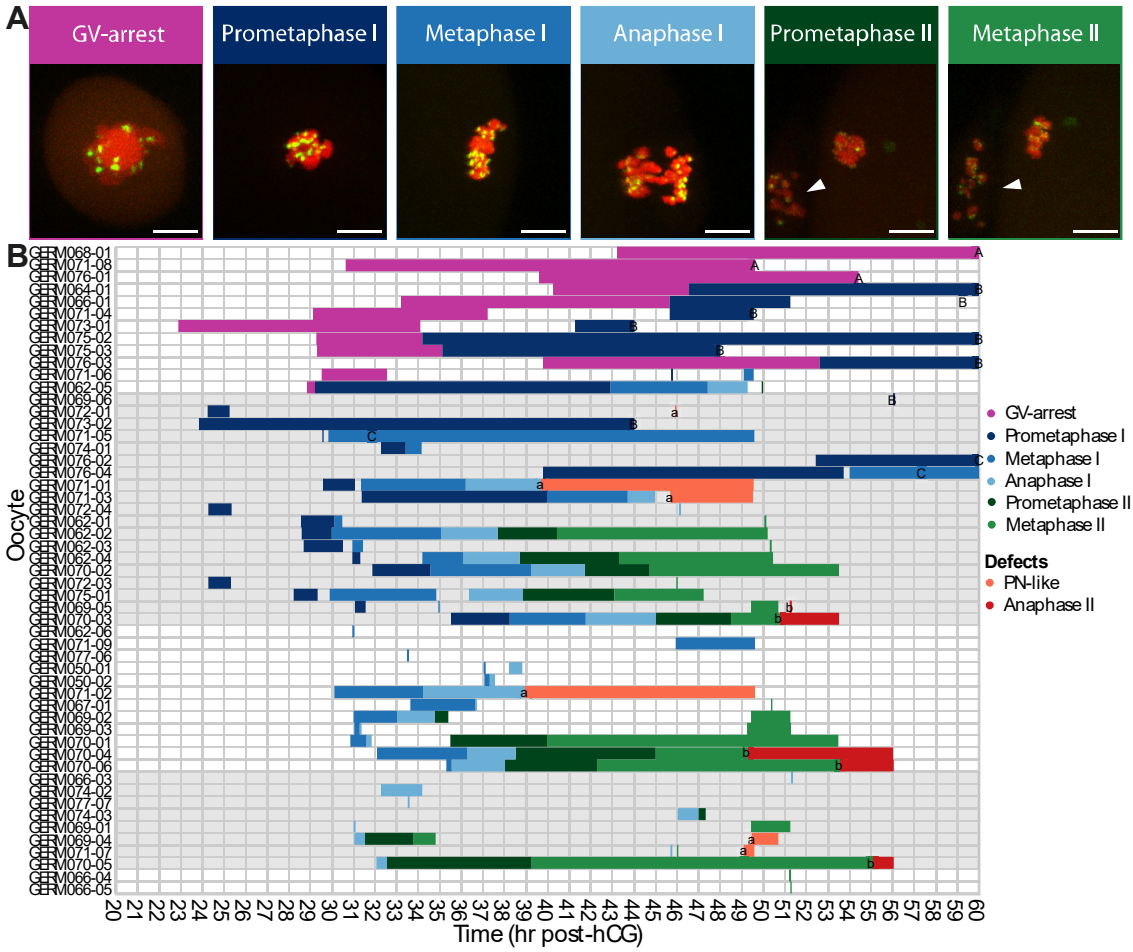

Figure 50 Cell Cycle Progression of All Oocytes Analysed

*All images from oocytes were scored and the time points mapped to the time hCG was administered. **A** Example of each stage scored (arrowhead shows polar body chromosomes, scale bar = 10 µm). **B** Gantt chart showing cell cycle events over time post-hCG, sorted by stage at the start of experiment (grey areas separate groups that started at the same stage); Defects are (A) Fails to undergo GVBD (B) Fails to reach metaphase I (C) Fails to undergo anaphase I (a) Formed PN-like structure (b) Spontaneously resumes meiosis II. Gaps in the Gantt chart represent periods when tracking failed or imaging was not performed.*

From this, it is obvious that there are number of recurring defects (A-C in Figure 50). Most of these defects (10/15, 67%) come from oocytes that were harvested at the GV-stage, while 5/15 (33%) oocytes with defects were harvested after GVBD. Nonetheless, this equates to 12% of oocytes that have defects when harvested after GV-stage, which is less than those harvested at GV-stage (P = 9.1 x10^{-6}, Fisher's exact test). Five oocytes spontaneously resumed meiosis II

and underwent anaphase II; and six were unable to reform the meiosis II spindle after undergoing anaphase I (see Discussion for possible explanations).

6.3 Timing of Key Cell-Cycle Events is not Perturbed by Experimental Set-up

In order to get the most accurate picture of cell-cycle timings, oocytes that failed to advance to anaphase I were excluded from the rest of the analysis, leaving 41 samples. Looking at the proportion of cells at each stage over time shows general synchrony between oocytes from the time of hCG administration (Figure 51A).

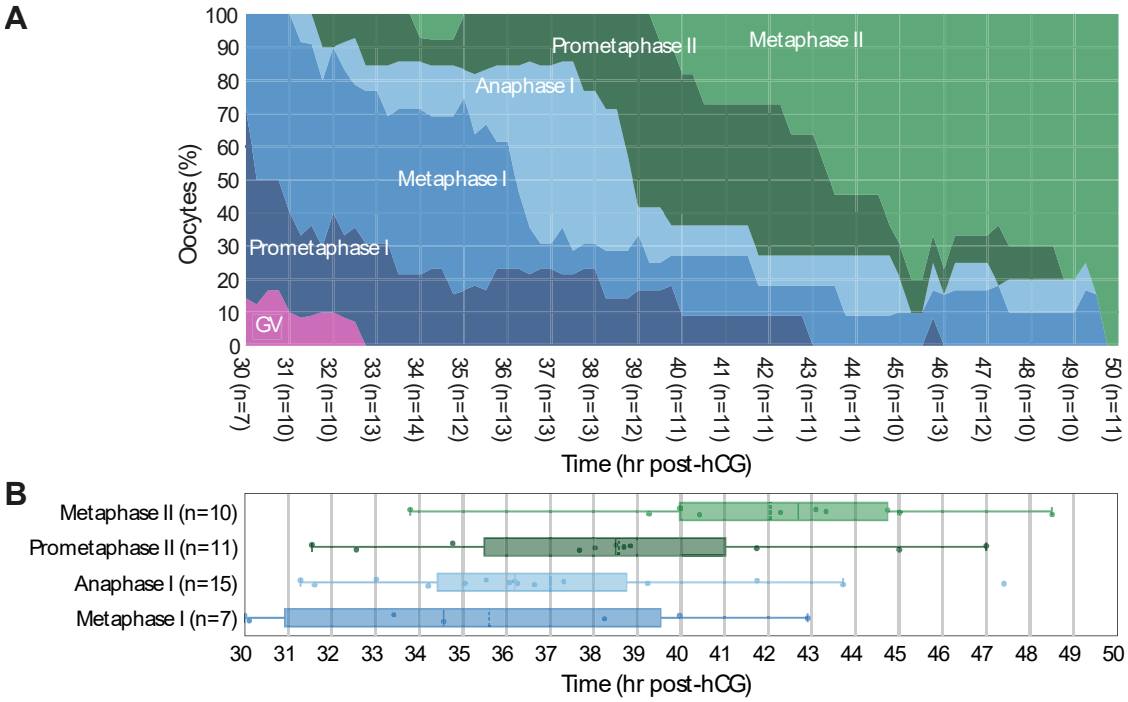

Figure 51 Progression of Human Oocytes Through Meiosis

*The cell cycle events of all the oocytes were mapped to time after hCG administration to assess the synchrony of oocytes. **A** An area graph showing the proportion of oocytes at each stage at 15 minute intervals, post hCG administration, excluding oocytes that failed to undergo anaphase I. n numbers show the number of oocytes scored at that time point. **B** A boxplot showing the time of cell-cycle transitions.*

As not all the samples were tracked between transitions from one cell cycle stage to another, I further filtered the data to only get the time points when cell cycle transitions had been observed (Figure 51B). This showed some variation, which is not surprising considering the variation of the oocytes at the time of collection. Overall, these times were comparable to those from a recently published live-cell dataset (Holubcova et al., 2015) (P = 1.0 for Metaphase I, P = 0.81 for Anaphase I, P = 0.39 for Prometaphase II, P = 0.83 for Metaphase II, two-tailed t-test from mean

and standard deviation; all means are relative to the mean time of Metaphase I for each dataset), suggesting that the experimental set-up did not perturb the cells any more than this live-cell study.

6.4 Age-Associated Increase in Misalignment at Metaphase I

Using *SpotCollectionManager*, I went on to analyse abnormalities from younger and older donors. As previously mentioned, compromises in resolution prevent the exact counting of centromeres, especially when they are close together or large. Therefore, there is often either an overestimation or underestimation of centromere counts. Two previous reports in human oocytes investigating kinetochores at high resolution noted that sister kinetochores become more distant with advanced age (Patel et al., 2015; Zielinska et al., 2015), both looking at fixed oocytes. Due to the reduced resolution, determination of sister centromere distances could not be reliably performed on the acquired images. Instead, I focused on misalignment at metaphase I and -II, which allowed for this analysis to be performed quantitatively and in an unbiased manner.

To understand the extent of misalignment, I compared all centromere distances from the estimated metaphase plate (Jaqaman et al., 2010). A metaphase plate estimate can be performed quite simply as the spindle axis (the longest axis of the spindle) is in the same direction as spindle tension on sister kinetochore pairs (Figure 52A) (Kitajima et al., 2011). In performing this analysis, it showed that there is an increase in displacement from the metaphase plate that is associated with advanced age (P = 6.8 x10^{-4}, two-tailed MWU) (Figure 52B). Based on previous qualitative studies (Liu & Keefe, 2008; Lister et al., 2010; Chiang et al., 2010; Nakagawa & FitzHarris, 2017; Yun et al., 2014), such a dramatic increase is surprising, as the major contributor is the presence of a few misaligned chromosomes. To test whether the presence of such outliers are age-associated, I pooled the displacement measurements from both young and old oocytes and defined outliers (above 3.36 µm from the metaphase I plate) using Tukey's fences (Tukey, 1977). 0 out of 8 oocytes from younger donors contained outliers compared to 7 out of 9 oocytes from older donors (P = 2.3 x10^{-3}, Fisher's exact test) (Figure 52D). The number of outlying chromosomes was low, between 1 and 3, and therefore the overall significant change in displacement with age is somewhat surprising (Figure 52E). One possible explanation is that even those chromosomes in older oocytes that align closer to the metaphase plate are not as tightly aligned as in younger oocytes.

To test for this, I repeated the displacement analysis, this time excluding outliers. This showed that there is still an increase even in those chromosomes that are not outlying (P = 1.5 x10^{-2}, two-tailed MWU) (Figure 52F).

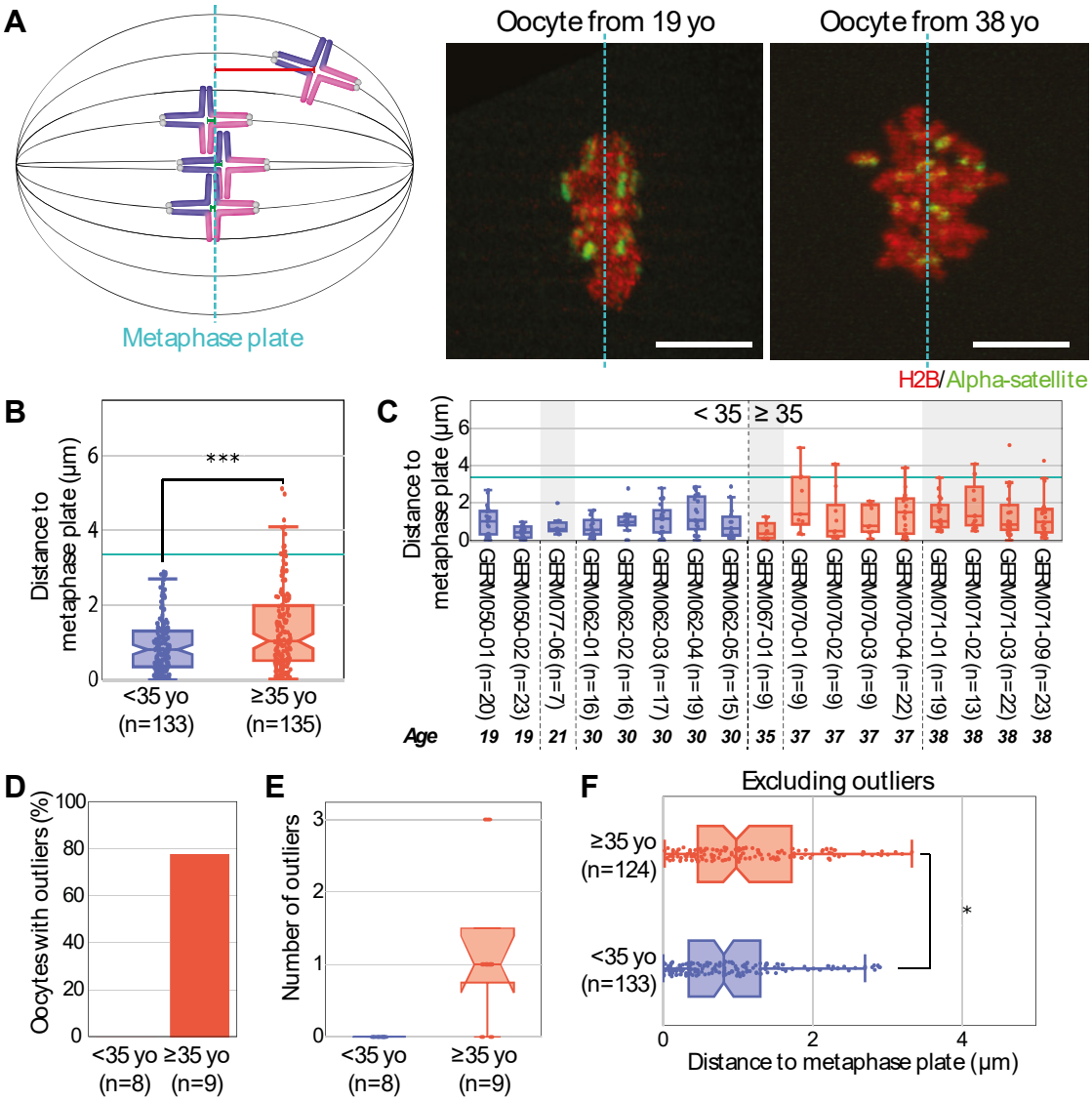

Figure 52 An Increase in Displacement to the Metaphase I Plate is Associated with Age

Oocytes of older women had a higher displacement compared to the estimated metaphase plate. ***A*** *Schematic showing how measurements are calculated and an example of an oocyte from a younger and older donor. Scale bar = 10 µm.* ***B*** *Boxplot showing an age-associated increase with displacement from the metaphase I plate. Green line marks the boundary of outliers.* ***C*** *Boxplot showing displacements per oocyte (younger on the left of dashed grey line; older on the right). Light grey boxes separate donors and green line shows the boundary of outliers.* ***D*** *Bar chart showing the proportion of oocytes containing outlying chromosomes, grouped by age.* ***E*** *A box plot showing the number of outliers per age group.* ***F*** *A box plot showing the displacement from the*

metaphase plate excluding outliers, showing that there is still a difference in those that align closer to the metaphase I plate.

6.5 Age-Associated Increase in Misalignment at Metaphase II

Following anaphase I, eggs arrest at metaphase II on a new metaphase plate. I performed the same analysis as in metaphase I to see if displacement increased in an age-dependent manner. Similar to the metaphase I analysis, the overall distances to the metaphase plate also increase (P = 3.5 x10^{-9}, two-tailed MWU) in an age-dependent (Figure 53). I calculated Tukey's fences and found that outliers occurred above 4.96 μm. 0 out of 7 of the younger eggs contained outliers, compared to 5 out of 12 of older eggs (P = 0.10, Fisher's exact test, the lack of statistical significance may be due to the low and unequal number of samples in each group). The number of outlying chromosomes is also small, ranging again from 1 to 3. When outliers are removed, there is still an overall increase in displacement from the metaphase II plate (P = 3.5 x10^{-8}, two-tailed MWU).

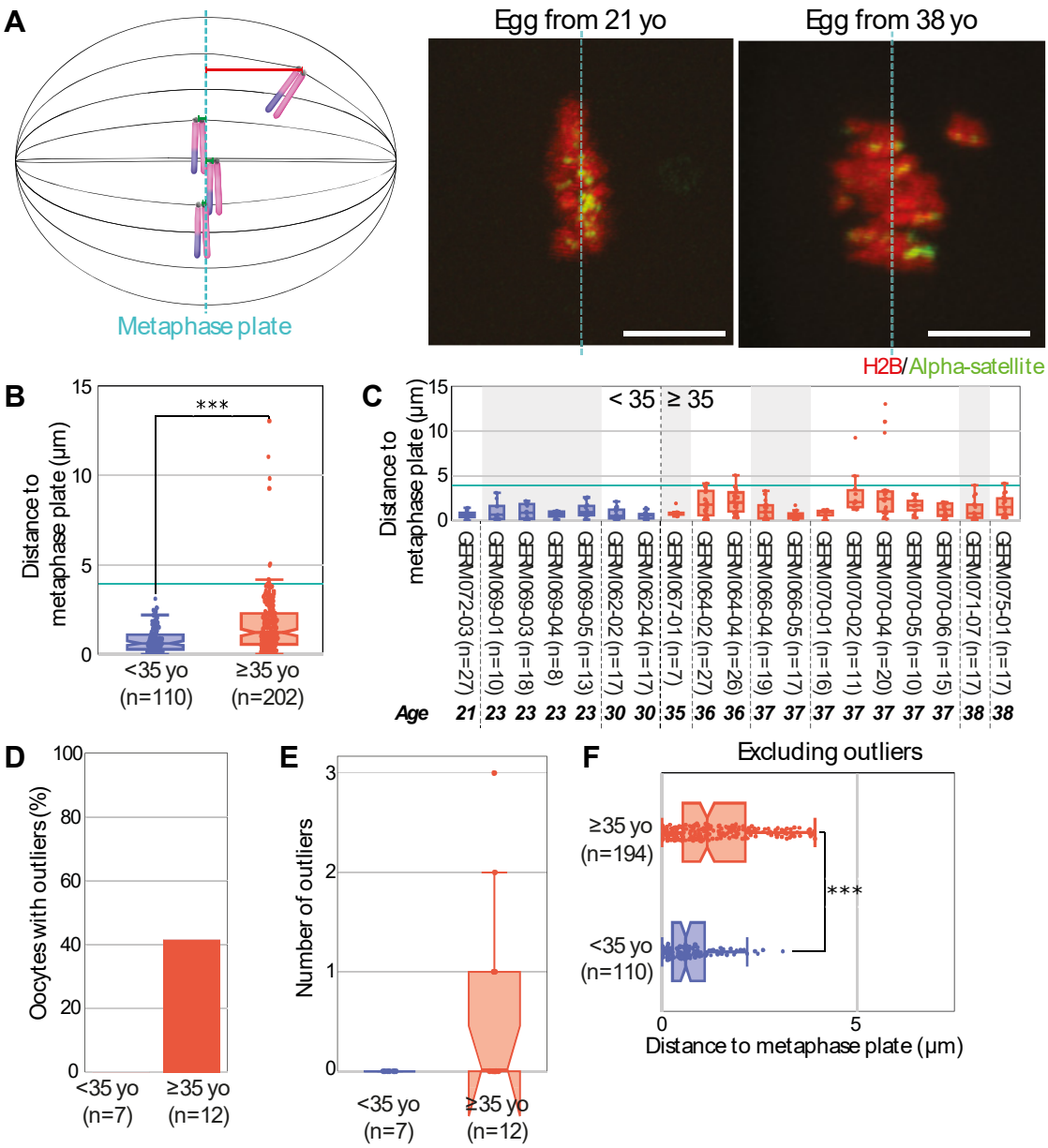

Figure 53 Displacement to Metaphase Plate is Also Increased at Metaphase II in an Age-Dependent Manner

As was the case with misalignment in metaphase I, there is also an increase in displacement at metaphase II. ***A*** *Experimental schematic and examples of eggs. Scale bar = 10 µm.* ***B*** *Boxplot showing an age-associated increase with displacement from the metaphase II plate. Green line shows limit for outliers.* ***C*** *Displacement to metaphase II plate per egg. Green line shows limit for outliers; dashed grey line separates young and older donors; grey boxes separate individual donors.* ***D*** *A bar chart showing the proportion of eggs containing outlying chromosomes grouped by age.* ***E*** *A box plot showing the number of outlying chromosomes per egg.* ***F*** *Shows that there is an overall age-dependent increase in displacement to the metaphase II plate, after excluding outlying chromosomes.*

6.6 Eggs Resume Meiosis II upon Activation by Calcium Ionophore

To test whether eggs could also be analysed after resumption of meiosis II, I treated metaphase II-arrested eggs with calcium ionophore, A23187, to activate them (Nakagawa et al., 2001). 7 out of 11 eggs (64%) successfully activated and were observed to undergo anaphase II around 1.6±0.2 hours (mean ± standard deviation) after activation (Figure 54).

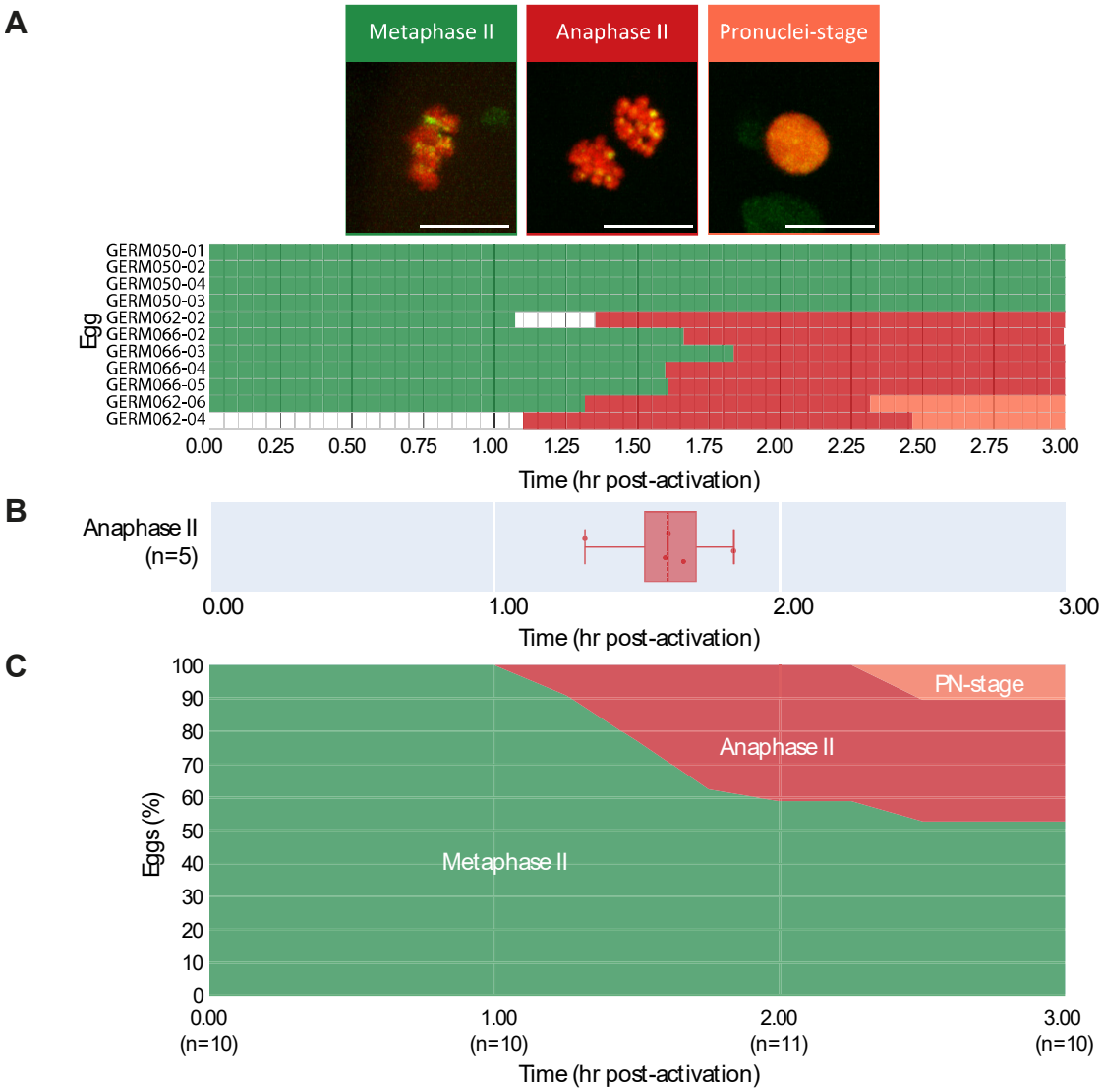

Figure 54 In Vitro Matured Human Eggs Successfully Undergo Anaphase II After Activation

After eggs had been imaged in meiosis I and arrested in metaphase II, they were activated with calcium ionophore to artificially resume meiosis II. ***A*** *A Gantt chart showing the progress of each egg after activation. Legend is above the Gantt chart, showing examples of each stage.* ***B*** *A box plot showing the time of the metaphase II to anaphase II transition.* ***C*** *An area graph showing the proportion of eggs at each stage over time.*

6.7 Measuring Lagging Chromosomes During Anaphase

Displacement measurements at metaphase have been previously performed by estimating a metaphase plate and calculating distances between this and kinetochores/centromeres (described in 3.10.10). However, lagging chromosomes in anaphase cannot be as easily quantified, though they may be a predictor of aneuploidy (Liu & Keefe, 2008; Lister et al., 2010; Chiang et al., 2010; Nakagawa & FitzHarris, 2017; Yun et al., 2014). In metaphase, the spindle axis can be approximated as tension between kinetochore pairs (or pairs of sister kinetochores in meiosis I) is in the same direction as the spindle axis. However, in anaphase, it is not known which kinetochore belongs to which chromosome, and therefore the direction of tension cannot be inferred in the same way. As a result, I modified spindle axis estimation for use in anaphase using a k-means clustering approach. k-means clustering is an approach which, given a user-specified number of clusters, will take spot locations and group them such that the mean of each cluster is the smallest (Lloyd, 1982), e.g. 2 clusters can be used to represent each bulk of separating chromatids. A line that passes through the centre of these two clusters approximates the spindle axis (Strang, 2016). Rather than using the midpoint between the two clusters, measurements are made from each chromosome to the front of the cluster that the chromosome belongs to (herein referred to as "anaphase fronts", Figure 55A). This better represents the movement of chromatids, and at least partially take accounts of the extent of anaphase. If measurements are made from the midpoint then chromosomes analysed later in anaphase, when chromosomes have moved further from the midpoint, would appear to be lagging compared to those that are earlier in anaphase. Performing this analysis in anaphase II, suggested that there is an increase in lagging with age (P = 2.3 x10^{-5}, two-tailed MWU) (Figure 55). However, there was only one donor in each age group, and so this result should be treated as preliminary. This analysis could not be performed in anaphase I due to low number of oocytes from older women that could be analysed for centromeres.

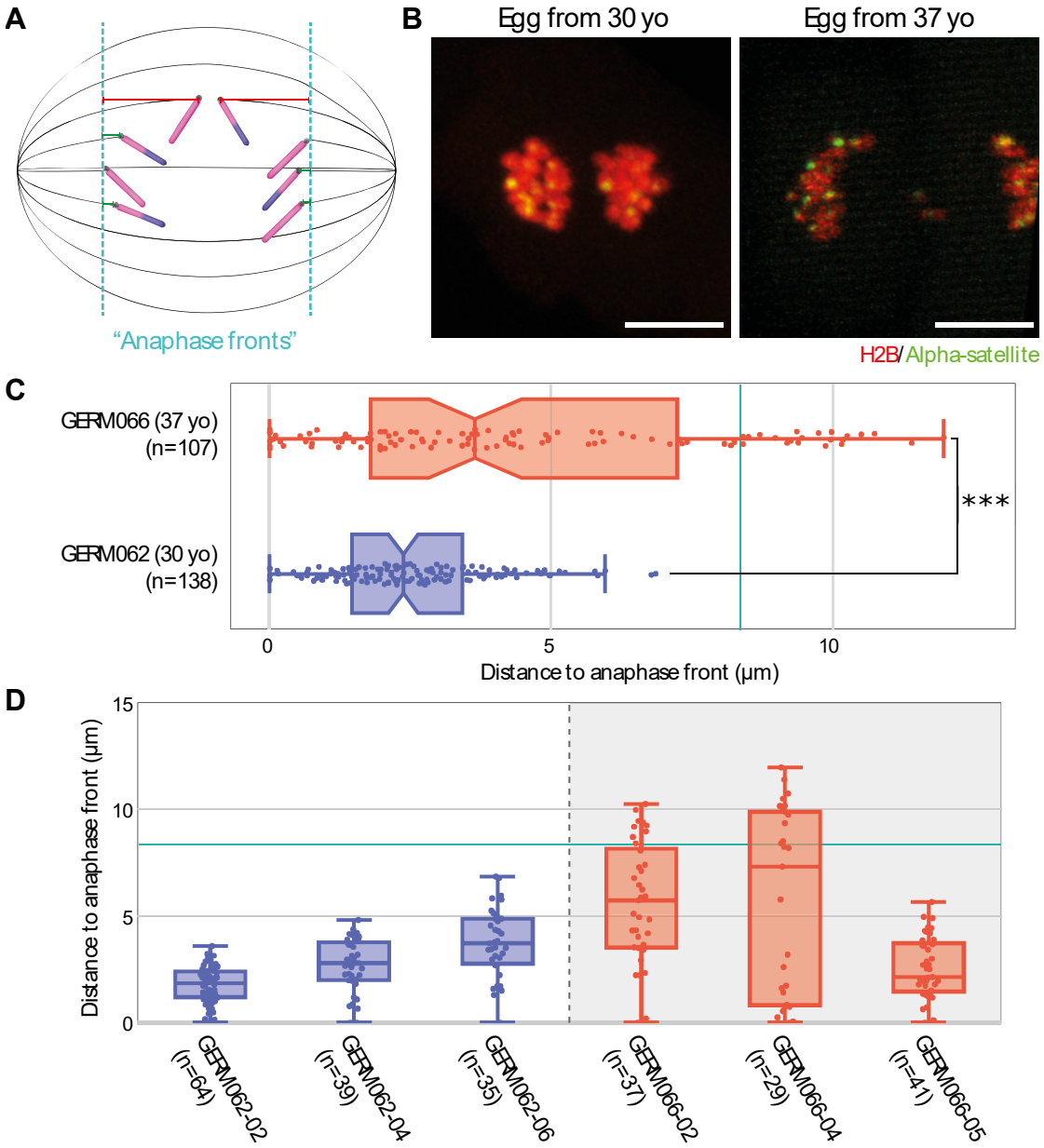

Figure 55 An Increase in Laggards in Anaphase II Might be Age-Associated

A *A schematic showing how measurements are made by measuring centromeres to the front of all centromeres.* ***B*** *Eggs undergoing anaphase II from a younger and an older donor. Scale bar = 10 µm.* ***C*** *A box plot showing the distance of kinetochores from the "anaphase fronts", grouped by egg.* ***D*** *Distances to anaphase front per egg.*

6.8 Discussion

Fifty-three oocytes were collected from thirteen donors to determine whether the techniques developed in Chapter 5 can be applied to detect differences in chromosome alignment from younger and older oocytes. Due to compromises in

resolution, I instead focused on changes in displacement from the metaphase plate at metaphase I and -II.

Most of the samples that successfully progressed in this experiment came from oocytes that were harvested after GVBD. This is in comparison to previous work which used oocytes that remained at the GV-stage even for many hours after hCG administration, when they would be expected to be at metaphase II arrest (Dozortsev et al., 2004; Obeso et al., 2010; Bárcena et al., 2016). As oocytes harvested at the GV-stage were more likely to fail to reach anaphase I, this may suggest that oocytes collected at the GV-stage are unable to progress normally through meiosis. It may also be the result of *in vitro* maturation of oocytes outside of the follicle at this early stage, or a combination of the two. As all-but-one of the oocytes that were collected at the GV-stage had defects, only the one oocyte that progressed beyond anaphase I was included for further analysis.

There were a number of recurring defects in the oocytes used in this study. For example, some of the oocytes spontaneously activated and resumed meiosis II. However, this defect was not relevant to this study as it typically occurred late into the experiment. Such oocytes were typically harvested at a later time post-hCG administration (24-26 hours), consistent with results in mouse that show that extending the time of collection after hCG administration results in a greater proportion of eggs that spontaneously activate (Xu et al., 1997; Abbott et al., 1998), though this was still less than the time point of egg collection for ICSI (Dozortsev et al., 2004; Obeso et al., 2010; Bárcena et al., 2016). Another defect was the presence of PN-like structures that appeared shortly after anaphase I, instead of reassembly of the meiosis II spindle. Such defects have been previously described in mouse eggs that have been depleted of Emi2, a protein involved in the regulation of metaphase II-arrest (Madgwick et al., 2006).

Of those samples that appeared to progress normally, it appears that the timing of cell cycle events is fairly synchronous. There is some variation, however, which is not surprising considering that oocytes are at different stages when they are collected. The timings are comparable to a recent live-cell study in human oocytes (Holubcova et al., 2015), suggesting that this experimental system did not have a major negative effect on the oocytes, at least in comparison to this study. However, it cannot be ruled out that there is some impact of either overexpression of markers or imaging by microscopy. Unpublished data from the lab, based on un-injected oocytes fixed between 20 and 40 hours post-hCG administration,

suggests that the majority of oocytes undergo anaphase I by 34 hours post-hCG administration (Hedquist-Hall and Lister, unpublished data). Importantly oocytes from Holubcova et al. (2015), had been harvested at the GV-stage, and thus the similarity in timings may be surprising, considering that, in my hands, such oocytes do not progress well. However, only oocytes that progressed normally were included in Holubcova et al. (2015) and, it has been shown that, although oocytes of older mice are more prone to aneuploidy, there is very little difference in the actual timings of anaphase I (Lister et al., 2010; Nabti et al., 2017).

To specifically test for age-associated differences, I used *SpotCollectionManager* to determine the distances of centromere to the metaphase plate in meiosis I and –II. Using these data, I have shown that at both metaphase I and metaphase II, the overall displacement from the metaphase plate is increased with advanced age. This is in line with previous reports in human oocytes (Volarcik et al., 1998) that used qualitative approaches to assess the degree of misalignment in human oocytes. However, these previous reports suggest that the misaligned chromosomes are few in number and therefore I tested whether this was the case from displacement distances. I identified outliers and showed that these were absent in oocytes of younger women, but not in those of older women; this was true for both metaphase I and -II. The actual number of outlying chromosomes is fairly low, ranging from 1 to 3. A further advantage of the increased resolution is the ability to analyse those chromosomes that appear closer to the metaphase plate. I excluded the outliers and showed that even those chromosomes that are more properly aligned are still further displaced in oocytes of older women than those of younger women. Metaphase is marked by the correct alignment of chromosomes to a metaphase plate, and therefore this age-associated increase misalignment is best understood by considering the forces that bring chromosomes into alignment. The two primary forces are that generated by spindle attachments to kinetochores and the counteracting force from Cohesin between sister kinetochores (Musacchio & Salmon, 2007). As Cohesin is reduced in an aged dependent manner (Chiang et al., 2010; Lister et al., 2010), this imbalance of forces likely results in misalignment. Indeed, depletion of Cohesin factors in mitosis results in misalignment at metaphase (Sonoda et al., 2001; Kenney & Heald, 2006). Further, the identity of outliers, whether they are chromosomes or chromatids, will be important in understanding the age-associated increase in displacement. Chromatids will move freely, unless attached

to both spindle poles, and will therefore have a greater displacement from the metaphase plate as there is no counteracting force from Cohesin. Given that there is an age-associated increase in prematurely separated chromatids (Angell, 1991; Fragouli et al., 2011, 2013; Handyside, 2012), this is another possible explanation for the increase in displacement to the metaphase plate with age. Importantly, prematurely separated chromatids have been suggested to appear either as meiosis I spindle is forming in prometaphase (Sakakibara et al., 2015), or as the meiosis II spindle reforms shortly after anaphase I (Yun et al., 2014). As a result, segregation defects arise as the spindle begins to form attachments to the kinetochores. Error correction results in attachments being generated and broken in multiple rounds until correct attachments have formed. In an aged oocyte, this is resisted by much less Cohesin than in young oocytes. In mitosis, extended metaphase arrest results in the removal of Cohesin as the force generated by the spindle-kinetochore attachments overpowers the inter-kinetochore Cohesin, in a process called "cohesion fatigue" (Daum et al., 2011; Stevens et al., 2011). Though my results suggest that metaphase I is not extended, that there is less Cohesin resisting attachments from spindle fibres, could explain why chromatids separate. Further, prometaphase and metaphase in mammalian meiosis are both considerably longer than in mitosis and therefore kinetochores are likely to undergo many more rounds of attachments. However, an important distinction is that cohesion fatigue in mitosis occurs in metaphase, whereas prematurely separated chromatids in meiosis appear to be caused in the lead-up to metaphase.

The importance of these results showing an age-related increase in displacements to the metaphase I and -II plates will be further enhanced by understanding how these increased displacements translate to segregation defects. This can, of course, be tested with higher spatial and temporal resolution as is proposed in Chapter 5.

I also tested the ability of eggs that had been used in these experiments to resume meiosis II upon stimulation by the calcium ionophore A23187. This led to successful activation in the majority of eggs, as seen by the presence of separating chromatids. Though only 6 activated eggs could be further analysed (3 from a younger donor, and 3 from an older donor), it enabled the generation of an analytical tool that can calculate the displacement of chromosomes or chromatids during

anaphase. Using this tool in anaphase II, showed that the presence of lagging chromatids appeared to increase with age. One possible reason for this will be the presence of “merotelic” attachments (Kouznetsova et al., 2014). These are spindle attachments to single kinetochores from both spindle poles, which prevent the timely migration of chromatids in anaphase II. A caveat to these data are that they are performed as single time points. Recent data suggests that correction can also occur after metaphase (Kouznetsova et al., 2019), again stressing the importance of performing higher resolution time-lapse studies.

In conclusion, there are quite clear changes to the alignment of chromosomes with age, but whether this has a direct impact on aneuploidy is yet to be uncovered. Further experiments that allow for the reconstruction of centromere dynamics will allow for these findings to be understood in the context of how maternal age is related to an increase risk of aneuploidy.

Chapter 7: Conclusions and Future Directions

The overall aim of this thesis was to investigate the determinants of faithful chromosome segregation in mammalian meiosis. To achieve this, I investigated the regulation of deprotection of Cohesin in meiosis II using a mouse model and assessed chromosome alignment in human oocytes through live-cell microscopy of centromeres.

7.1 Regulation of Cohesin Removal in Meiosis II

Upon follicle stimulation after puberty, oocytes are relieved from prophase I arrest and continue into meiosis II only to arrest again at metaphase II-arrest (Mehlmann, 2005; Herbert et al., 2015). This arrest can last several hours as the egg awaits fertilisation from sperm. Given the context of the aged oocyte, and the impact of Cohesin deterioration, this extended period can exacerbate an already dire situation. The spindle forces in metaphase II are given an extended period to further compromise the remaining centromeric Cohesin, potentially leading to the generation of separated chromatids.

Protection of centromeric Cohesin in meiosis I is a critical process that ensures faithful segregation in meiosis II (Kitajima et al., 2004). However, the mechanisms by which this is relinquished in meiosis II have only been partially described by a small number of models (Lee et al., 2008; Chambon et al., 2013; Argüello-Miranda et al., 2017; Herbert & Toth, 2017). The first of which is the "deprotection by tension" model and the second is through I2PP2A inhibition of PP2A that inhibits PP2A in meiosis II but not in meiosis I. I explain in 4.1.3 why this latter model is unlikely to be true and why the findings are likely confounded by I2PP2A being a histone chaperone (Higgins & Herbert, 2013; Krishnan et al., 2017; Qu et al., 2019), and by its interaction with Sgol2 (Qu et al., 2019). Most likely, I2PP2A is not relevant for deprotection.

7.1.1 Tension is not Required for Deprotection of Cohesin in Meiosis II

As a result, I focused on the deprotection by tension model. Given that *in vivo* matured eggs are not as capable as *in vitro* matured eggs to maintain CSF-arrest (Xu et al., 1997; Abbott et al., 1998), I tested whether *in vitro* matured eggs could be activated. Microinjection of an APC/C^{Cdc20} reporter, fluorescent-tagged Securin, showed that the APC/C^{Cdc20} did become active and resulted in the degradation of Securin upon activation. This was further confirmed by analysing chromosome spreads after activation that showed activated eggs had fully separated chromatids.

The next step was to find a method to remove spindle tension, which can be accomplished by using a spindle poison: absence of a spindle means there is no tension. However, the absence of attachments causes SAC arrest, i.e. inhibition of the APC/C^{Cdc20} through formation of the MCC (Chang et al., 2004). Therefore, two methods to bypass this arrest were used to investigate whether sister separation could occur in the absence of spindle tension: inhibition of the master SAC-kinase Mps1, using reversine (Chen et al., 2004; Santaguida et al., 2010), and a mutant form of Cdc20 that can activate the APC even during SAC arrest (Sironi et al., 2001).

Activation in the presence of nocodazole prevented Securin degradation. But, activation in the presence of both nocodazole and reversine allowed for APC/C^{Cdc20} activity, showing that this was a feasible approach. Upon inspecting chromosome spreads, separation was almost absent in eggs that had been activated in the presence of nocodazole, but there was ~50% separation in those activated with nocodazole and reversine. This showed that deprotection did not require tension, but separation was rarely complete, unlike in controls that had been activated without inhibitors. Given that Mps1 has been implicated in protection in mouse oocyte meiosis I (El Yakoubi et al., 2017), and in yeast meiosis II (Argüello-Miranda et al., 2017), it was important to test an alternative approach to confirm these results.

Cdc20(MIM) contains a single amino acid substitution that prevents its binding to the MCC, but still allows binding to the APC/C (Izawa & Pines, 2012). When wild-type Cdc20 was over-expressed, Securin did not degrade upon activation in the presence of nocodazole. However, Securin was degraded when Cdc20(MIM) was over-expressed. This manifested as ~50% of separation as seen by chromosome spreads, in stark contrast to predominantly no separation in eggs microinjected with Cdc20(WT) and activated in the presence of nocodazole.

Both approaches, either using reversine or Cdc20(MIM) when eggs were activated in the presence of nocodazole, provided similar levels of separation, but neither gave the level of separation, ~100%, as was the case with activation in the presence of a spindle. While this may suggest that tension is still somehow required, it may speak to the possibility that another tension-dependent process is compromised. To test between these possibilities, I removed endogenous Rec8 using the TrimAway system (Clift et al., 2017, 2018), which leads to high levels of separation in the presence of a spindle, but separation is again ~50% when this experiment was performed in nocodazole treated eggs. As these experiments are

performed without activation, this suggests that the lower levels of separation are not related to the APC/C or deprotection. To further confirm this, I washed out nocodazole to allow for regeneration of the spindle and therefore tension. This led to a level of separation comparable to controls. Tension is not only important for bi-orientation of sister kinetochores but is also involved in decatenation (Wang et al., 2008). During DNA-replication, chromatids become entangled with ultrafine threads called catenates that link chromosomes together. The removal of these threads requires Topoisomerase II (Topo II) (Lima & Mondragón, 1994), which itself relies on spindle tension to mediate excision and repair of these catenates. When Topo II is inhibited in oocyte meiosis I and -II (Li et al., 2013), faithful chromosome segregation is compromised.

While a clear picture has been generated about the lack of a requirement of tension for deprotection, whether or not catenation explains the lower separation levels is yet to be determined. As the centromeres only experience tension in meiosis II, Topo II activity in meiosis I is unlikely to resolve these catenates and therefore further work could characterise the role of catenation in my results. This can either be performed by antibody staining of BLM or PICH (Nielsen et al., 2015), for example. However, initial tests of three PICH and BLM antibodies showed they do not work on mouse egg chromosome spreads. An alternative approach is to repeat the nocodazole washout experiment in the presence of a Topo II inhibitor, such as ICRF-193 (Iwai et al., 1997; Li et al., 2013). If Topo II-dependent decatenation is required, then it would be expected that separation would fall to ~50% again after Rec8 depletion in the presence of nocodazole, accounting for the other half of chromatids that did not appear to separate. An alternative approach would be to activate eggs in the presence of a Topo II inhibitor. If decatenation is the explanation for the lower levels of separation, then again it would be expected that separation would be ~50% as catenates would prevent chromatids segregating normally.

Finally, given that Emi2, the APC/C inhibitor at CSF-arrest, is degraded upon activation (Isoda et al., 2011), this work also shows that CSF-arrest and SAC arrest work independently of each other at metaphase II-arrest.

7.1.2 Deprotection Mediated by APC/C^{Cdc20}?

Given that I2PP2A is unlikely to play a role in deprotection and tension is not required, there is clearly a gap in knowledge regarding how deprotection in meiosis II occurs. A recent model in yeast (Argüello-Miranda et al., 2017; Jonak et al., 2017),

proposed an alternative system whereby the APC/C^{Cdc20} performs a myriad of functions both to deprotect Cohesin and also to activate Separase through Securin destruction. This model of deprotection mediated by the APC/C^{Cdc20} is particularly attractive as it implies sustained protection up until anaphase II, which itself needs to be tested.

As has been mentioned, there is some suggestion from the literature that protection is required as artificially activating Separase through microinjection of Securin antibody leads to a reduction in Rec8 – presumably Rec8 not involved in cohesive Cohesin – but not separation (Huo et al., 2006). However, an important control will be the ability to measure the activity of Separase in such an experiment (Agircan & Schiebel, 2014).

Many of the key molecular components of the yeast model are conserved in mammals, such as Shugoshin, Mps1 and Casein Kinase 1. Of these, I started to look at Sgol2, the mammalian orthologue of Shugoshin that protects centromeric Cohesin in meiosis I (Gutiérrez-Caballero et al., 2012). Reports differ in its localisation during metaphase II-arrest, but I co-stained Sgol2 and Rec8 and showed that they do indeed colocalise between the kinetochores. There is also another pool of Sgol2 at each kinetochore. Upon activation, I showed that Sgol2 decreases, but doesn't always completely disappear, as is the case in anaphase I (Ding et al., 2018). While this may suggest that Sgol2 does not play a part in deprotection, the relevant fraction of Sgol2, that which binds Rec8, disappears due to Separase-mediated cleavage. Therefore, it will be important to test whether Sgol2 that localises with Rec8 disappears in an APC/C^{Cdc20}-mediated manner. That the kinetochore fraction is stabilised could be due to Sgol2's interaction with a number of other kinases at the kinetochore (Rattani et al., 2013), that prevents its immediate degradation. Securin contains a D-box, which is recognised by the APC/C^{Cdc20} and leads to its degradation upon anaphase onset (Zur & Brandeis, 2001). However, mutation of this D-box stabilises the protein in anaphase. This mutant, Securin(Dm), allows for the investigation of APC/C^{Cdc20}-mediated proteolysis in anaphase II in the absence of Separase cleavage (Hagting et al., 2002). Staining chromosome spreads of eggs that have been microinjected with Securin(Dm) and activated, with an anti-Sgol2 antibody will show whether this Cohesin-located fraction is degraded differently to that of the kinetochore.

Alternatively, it is possible that Sgol1 rather than Sgol2 is involved in protection after anaphase I. A recent report suggests that protection needs to be

maintained shortly after anaphase I and implicated Pias1, a SUMO E3-ligase (Ding et al., 2018). However, the target of sumoylation was not identified. Given that Sgol2 reaches undetectable levels, at least by fluorescence microscopy, it is possible that other candidates can be considered for protection, though a direct role of the APC/C^{Cdc20} in Sgol1 destruction has not been established (Fu et al., 2007; Karamysheva et al., 2009). Given that Cdk1-Cyclin B1 is involved in Sgol1's recruitment to Cohesin (Liu, Jia, et al., 2013; Liu, Rankin, et al., 2013), destruction of Cyclin B1 itself may be sufficient for removal of Sgol1 from Cohesin. Nonetheless, establishing a system to activate Separase in the absence of APC/C^{Cdc20}, will allow the elucidation of (a) whether protection is active and (b) which Shugoshin might be involved protection. The latter by depleting endogenous Shugoshins, e.g. through the TrimAway system (Clift et al., 2018, 2017).

Mps1 plays a crucial role in the APC/C^{Cdc20}-mediated model of deprotection in yeast meiosis II and is also important for protection in meiosis I (El Yakoubi et al., 2017). El Yakoubi et al. (2017) show that Mps1 appears to be localised to kinetochores in metaphase II-arrest, but not at where Cohesin might reside (though this is based on low numbers). Given that Mps1 is involved in the SAC response, a specific localisation to Cohesin would be unexpected. However, it could also function by priming kinetochore-associated Shugoshin for its function in protection. The regulation of Mps1 is itself dependent on a number of kinases, including itself (Koch et al., 2019). Recent studies show that Cdk1-Cyclin B1 is also involved in its localisation to the kinetochores (Alfonso-Pérez et al., 2019; Hayward et al., 2019), again providing an APC/C^{Cdc20}-mediated route to its involvement outside of direct degradation.

Given that the molecular components of deprotection are also present in meiosis I, it will be important to understand the differences in regulation between these two divisions. In anaphase I, Sgol2 degrades to undetectable levels (Ding et al., 2018), suggesting that its degradation maybe mediated by the APC/C^{Cdc20}, though this has yet to be tested. It does contain a number of putative D-box motifs (RxxL) (ProViz & Davey Lab, 2019b), and mutation of these would enhance our understanding of deprotection in meiosis I. Aurora Kinase B is known to be involved in the removal of Sgol2 from the arms in meiosis I, providing an alternative route of regulation (Rattani et al., 2017).

In budding yeast, Casein Kinase 1 (CK1) performs separate functions in meiosis I and -II, and each are crucial for faithful segregation in meiosis. In meiosis I,

Monopolin recruits CK1 to the kinetochores so that sister kinetochores are oriented to the same spindle pole (Petronczki et al., 2006). However in meiosis II, CK1 leads to the degradation of Shugoshin and Mps1 (Argüello-Miranda et al., 2017; Jonak et al., 2017), proteins important for protection of centromeric Cohesin in meiosis I. While key sub-units of Monopolin are degraded in anaphase I (Matos et al., 2008), which prevents mono-orientation in meiosis II, how CK1 does not have an impact on Shugoshin and Mps1 in meiosis I is an interesting question in and of itself.

Taken together, the exact mechanisms of how deprotection is performed in mammalian eggs are still unclear but are not regulated by spindle tension. Testing the requirements of deprotection and its molecular players will be of particular importance to understanding the maternal age effect, as eggs arrest for several hours in metaphase II with a lowly active but persistent APC/C^{Cdc20}, and little centromeric Cohesin to counteract spindle forces.

7.2 Live-Cell Imaging of Human Oocytes

While the initial aim of the human oocyte study was to track centromeres through meiosis I and -II, it became clear that live-cell imaging of human oocytes was not a trivial task. It required the development of several molecular and computation tools and, while it is now close to being functional, still requires some development. However, the data generated during the optimisation revealed that chromosomes of older women's oocytes are misaligned to get a greater extent than younger women's in metaphase I, and also in metaphase II.

Work in mouse oocytes showed the utility of tracking centromeres in order to gain insights into chromosome dynamics, including in the context of ageing (Kitajima et al., 2011; Yun et al., 2014; Sakakibara et al., 2015). Studies investigating kinetochore dynamics require the microinjection of a fluorescent-tagged kinetochore protein and histone protein to track development from GV-arrest. In order to accomplish this in human oocytes, several modifications were made: as oocytes were typically not harvested at the GV-stage, histone integration was weak (Zielinska & Schuh, 2018); too high levels of kinetochore proteins can cause biological artefacts such as SAC arrest, which is more likely to manifest in the extended meiosis in human oocytes; human oocytes differ in size, and generate problems unique to themselves.

7.2.1 Development of Molecular Tools to Image Centromeres

To remedy the problem of overexpression of kinetochore proteins, I used the CRISPR system to tag centromeres of human oocyte chromosomes (Chen et al., 2013; Chen, Guan, et al., 2016; Chen, Hu, et al., 2016). The use of CRISPR for visualising genomic loci has been shown to have minimal effect on cell cycle progression (Stanyte et al., 2018). While transferring the fluorescent-tagged dCas9 protein to an *in vitro* transcription plasmid was easy, the optimisation took longer. Firstly, this protein did not localise exclusively to the nucleus and therefore had to be further optimised. This was done by modifying one of the NLSs at the N-terminus and adding an extra NLS at the C-terminus. Each of these is thought to be better at nuclear localisation than the two existing monopartite SV40 NLSs found in the plasmid (Wu et al., 2009; Ray et al., 2015). That this optimisation was required was unexpected as dCas9 had been optimised by the original authors (Chen et al., 2013). This likely represents differences between using cycling cell lines and prophase-arrested oocytes. Considering the frequent use of CRISPR/Cas9 for modifying zygotes it is likely that this will enhance CRISPR efficiency, though this was not tested. Further modifications included the optimisation of sgRNA synthesis for *in vitro* transcription by comparing two commercial kits, and also the introduction of a base-flip to enhance its structures (Ma et al., 2016).

The differences between using CRISPR/dCas9 in oocytes and cycling cell lines became an issue again when attempting to optimise chromosome-specific markers. While this task would have been difficult in any case, as the paucity of human oocytes make it difficult to test sgRNAs, this was further complicated by the differences in efficiencies of sgRNAs that are *in vitro* transcribed and those that are plasmid transcribed (Moreno-Mateos et al., 2015). As oocytes are not transcriptionally active (Song & Wessel, 2005; De La Fuente, 2006), the only choice was microinjection of *in vitro* generated sgRNAs. Nonetheless, a number of sgRNAs that had been published were easily translated into mouse and human oocytes. A chromosome-specific sgRNA was designed for mouse oocytes to putatively target chromosome 9. The latter was performed to judge the feasibility of monitoring specific chromosomes in human oocytes (e.g. those prone to aneuploidy: 15, 16, 18, 21 and 22). However, screening sgRNAs was difficult and as there is a difference between sgRNAs in oocytes and cell-lines, cell-lines could not be used for screening. Instead, α-satellites were used, which mark all centromeres.

In the future, specific chromosomes could be marked using correlative microscopy i.e. use Fluorescence *In Situ* Hybridisation and Whole Chromosome Painting at the end of an experiment and then relating the chromosome tracks to specific chromosomes. However, the chromosome decondensation between meiosis I and -II makes following centromeres through both divisions difficult (Yun et al., 2014). Here, the marking of specific chromosomes becomes a lot more powerful. One approach to mark multiple specific chromosomes is by modifying sgRNAs (Cheng et al., 2016; Ma et al., 2016, 2018). This can be by introducing an RNA hairpin that is recognised by a protein, the latter of which is tagged with a fluorescent protein (Ma et al., 2016); introducing a sequence into the sgRNA that is recognised by another fluorescent-tagged protein (Cheng et al., 2016); or using the split crRNA and tracrRNAs and chemically modifying the crRNA with a fluorescent dye (Wang et al., 2019). In terms of introducing hairpins into the sgRNA scaffold, I was able to successfully test each pair of hairpin and hairpin-recognising protein partners. However, multiplexing was difficult. The specific RNA-binding proteins also needed NLS optimisation (data not shown). Another approach is to introduce a specific sequence into the sgRNA that is recognised by an RNA-binding protein (Cheng et al., 2016). As hairpins are secondary structures specific to bacteriophages, the proteins that recognise them are unlikely to have an effect on endogenous RNAs. This is contrary to introducing a short RNA sequence, as any short sequence is likely to be present in endogenous RNAs and therefore may interfere with the translation of these proteins. The final approach of using fluorescent-tagged crRNAs is a good approach, as these are typically modified with fluorescent dyes rather than proteins, and therefore translation and maturation time isn't an issue, and are typically very bright. An alternate approach to using CRISPR is to use a nuclease-dead TALEN system. Fluorescent-tagged, nuclease-dead TALENs have already been used to mark chromosomes 15 and 18 (Ma et al., 2013), which are of particular interest as they frequently mis-segregate.

7.2.2 Development of Computation Tools to Track Chromosomes

In order to image chromosomes in live-cell at high resolution, the microscope needs to be able to refocus in the sub-volume around the chromosomes. The previous approach to tracking in real-time has been using the centre of mass of histone fluorescence for mouse oocytes (Kitajima et al., 2011). However, histone incorporation is weak when RNA encoding fluorescent-tagged histone is

microinjected after nuclear envelope breakdown (Zielinska & Schuh, 2018), where most of the human oocytes in this study were collect. This problem was worsened by the fact that human oocytes contain autofluorescent blobs that would alter the centre of mass of the image towards themselves. To counter this, I used an object detection approach (Politi et al., 2018), which filters the signal for objects that are most likely to be the chromosome mass. As the signal was usually weak, this still worked inefficiently. As a result, I replaced the object detection approach with an approach that uses clusters of α-satellite signals to find the chromosome mass. This worked a lot better as α-satellites were tagged with mNeonGreen which could be seen much sooner after microinjection; and the typical size and number of the fluorescent blobs were unlikely to confuse this approach. To accomplish this, a larger sub-region had to be used for tracking in order to ensure that all of the α-satellites would be caught. This compromise in resolution meant that not all centromeres could be resolved.

Thus, finally, a novel approach was generated using template matching (Lindeberg, 2015). This looks for similarities of a sub-region of a previous time point in the current time point and accounts for autofluorescent blobs by reducing the chance of centring on sub-regions that appear similar between channels. In a test scenario using two different oocytes, this functioned successfully. However, future work will include modifying this to be integrated into the microscope tracking workflow. This also needs to be modified to allow for sub-pixel resolution, especially in the Z-axis which typically has a considerably lower resolution than the X- or Y-axes. A further modification will be the ability to find the cell bounds and use this to calculate the relative chromosome position in real-time compared to the cell-centre. This allows for the potential detection of anaphase: spot detection can be performed in real-time and k-means clustering (an approach to group objects by a feature, such as distances to a putative centre (Lloyd, 1982)) can be used to detect whether there are separate clusters of centromeres. A safety measure would be that a line that passes through the centre of these two clusters, which approximates the longest axis of the spindle, should also pass close to the centre of the cell. As one cluster will remain in the oocyte and the other will be extruded to the first polar body, a line that passes between these will likely also extend near the centre of the oocyte itself. k-means clustering requires the knowledge of how many clusters to expect, but this can be automated using the gap statistic (Tibshirani et al., 2001).

Using this, it should be able to prevent the tracking of the polar body at the loss of tracking the oocyte chromosomes.

Finally, spot detection was modified. In the original publication, this was performed by pre-processing in FIJI (Schindelin et al., 2012), followed by spot detection in Imaris, and then further work in Java (Kitajima et al., 2011). To streamline this process and reduce the overall financial cost, this whole process was performed in FIJI, which is free and open-source. Pre-processing is typically a Difference of Gaussians function (Kitajima et al., 2011), but to make this easier, it can be done just before spot detection in FIJI. Spot detection is then itself performed using TrackMate (Tinevez et al., 2017). A key part of this spot detection was the inclusion of features that make it easier to manually curate spots. This is typically difficult in other packages (including TrackMate itself) as these packages are designed to allow for the loss of some spots, though this is obviously not the case for centromere tracking. The centromeres can also be paired in the same step, and all of this can be performed in a user-friendly interface on most computers systems for free. Spot registration was also modified using TrackMate to make it more accurate (Tinevez et al., 2017). As the spot detection script allows for pairing, spot registration was performed to ensure that paired spots stayed together while generating tracks.

Altogether, the foundations have been laid to be able to track chromosomes in human oocytes. One outstanding challenge is the movement of human oocytes. This could be fixed by physically restricting them using a silicone insert containing wells, or it may be possible to do this computationally, using object detection and centring.

7.2.3 Human Oocytes Resume Meiosis I Synchronously upon Hormonal Stimulation

Only 12 out of the 53 oocytes used in this work were at the GV-stage at the start of the experiment. This meant that timing cell cycle events from the traditional landmark of GVBD was not possible. Of the 12 oocytes that were harvested at the GV-stage, only 1 appeared to progress through anaphase I successfully. Using the remaining oocytes, and the single GV-stage oocyte that appeared to progress normally, I mapped meiosis I and –II events to the time hCG was administered. In doing so, it showed that most oocytes appear to progress in a fairly synchronous

manner. These times were in line with that of a published dataset of human oocytes (Holubcova et al., 2015). This shows that the imaging and microinjection of fluorescent-tagged markers appeared to have minimal negative impact on the progression of oocytes through meiosis, though some negative impact of the experimental setup cannot be excluded.

7.2.4 Misalignment of Chromosomes in Metaphase I and -II

While the images acquired could not be used for centromere tracking, they could be used to assess the degree of misalignment during metaphase I and -II. As misaligned chromosomes appear away from the main bulk of chromosomes, they can be quite easily measured, even if not all centromeres can be counted due to the limited resolution. In using spot detection, I modified a previous approach to estimate the axes of the spindle. The previous approach searched for three axes: a spindle axis that goes between the "poles", and two that go through the metaphase plate. Misaligned chromosomes will rotate these in a way which does not represent the true axes and therefore a different approach was taken. Tension between kinetochores is approximately in the same direction as the spindle poles and therefore can be used to generate an estimate of the spindle axis. The angle of each chromosome pair can then be compared to this initial estimate and removed from the estimate if the angle is an outlier. Using linear algebra, a plane that represents the metaphase plate can be fitted at the centre of all centromeres, and distances to this can be calculated (Anton & Rorres, 2013; Strang, 2016).

By applying this approach, I was able to show that there is an age-associated increase in misaligned chromosomes in metaphase I and in metaphase II. While previous studies have shown this to be the case in aged mouse oocytes (Liu & Keefe, 2008; Lister et al., 2010; Chiang et al., 2010; Nakagawa & FitzHarris, 2017; Yun et al., 2014), high-resolution studies have not been performed in human oocyte/eggs until now. This enhanced approach also showed that even the chromosomes that are more correctly aligned to the metaphase plate are also further away from the metaphase plate in the oocytes of older women compared to younger women, both in metaphase I and metaphase II. As previous mouse oocyte studies suggest that the presence of misaligned chromosomes give rise to aneuploidy, this is likely to be a useful predictor. However, mouse oocyte studies also show that segregation errors can arise from bivalents that prematurely separate into dyads and realign on the metaphase I plate (Sakakibara et al., 2015). These are likely to be missed by this

analysis as they would have a normal displacement from the estimated metaphase plate. Nonetheless, the association with age for the presence of these malformities is clear. As Cohesin is reduced in an age-dependent manner (Chiang et al., 2010; Lister et al., 2010), and Cohesin depletion has been previously shown to result in an increase in misalignment (Sonoda et al., 2001; Kenney & Heald, 2006), it provides a possible molecular explanation for the age-associated increase in displacement. A further reason is the presence of prematurely separated sister chromatids, which are also increased in an age-dependent manner (Fragouli et al., 2010, 2013; Handyside et al., 2012). Unless these chromatids are attached to both spindle poles, they can move freely and are therefore likely to be further away from the estimated metaphase plate.

Whether this increase in displacement leads to aneuploidy can only be further studied by performing high-resolution time-lapse microscopy to track centromeres throughout the entirety of meiosis I and even into meiosis II.

With respect to imaging of meiosis II, I have shown that eggs that have been used for these time-lapse experiments are able to resume meiosis II and undergo anaphase II upon activation by the calcium ionophore A23187. Images from egg activations experiments were used to generate a tool to measure how well chromatids segregate together in anaphase II, which will be beneficial for future time-lapse and fixed cell studies. The groundwork for generating high-resolution centromere tracking data in human oocytes has been laid out by these developments and is likely to provide novel insights into how chromosome missegregation leads to aneuploidy in oocytes of older women.

References

Abbott, A.L., Xu, Z., Kopf, G.S., Ducibella, T. & Schultz, R.M. (1998) In Vitro Culture Retards Spontaneous Activation of Cell Cycle Progression and Cortical Granule Exocytosis That Normally Occur in In Vivo Unfertilized Mouse Eggs. *Biology of Reproduction*. 59 (6), 1515–1521.

Adelson, E.H., Burt, P.J., Anderson, C.H., Ogden, J.M. & Bergen, J.R. (1984) Pyramid methods in image processing. RCA Engineer p.33–41.

Agircan, F.G. & Schiebel, E. (2014) Sensors at Centrosomes Reveal Determinants of Local Separase Activity Jonathan M. G. Higgins (ed.). *PLoS Genetics*. 10 (10), e1004672.

Albertini, D.F. & Carabatsos, M.J. (1998) Comparative aspects of meiotic cell cycle control in mammals. *Journal of Molecular Medicine*. 76 (12), 795–799.

Alfonso-Pérez, T., Hayward, D., Holder, J., Gruneberg, U. & Barr, F.A. (2019) MAD1-dependent recruitment of CDK1-CCNB1 to kinetochores promotes spindle checkpoint signaling. *The Journal of Cell Biology*. 218 (4), 1108–1117.

Angell, R.R. (1991) Predivision in human oocytes at meiosis I: a mechanism for trisomy formation in man. *Hum Genet*. 86 (4), 383–387.

Anton, H. & Rorres, C. (2013) *Elementary Linear Algebra*. 11th edition. Wiley.

Anton, T., Bultmann, S., Leonhardt, H. & Markaki, Y. (2014) Visualization of specific DNA sequences in living mouse embryonic stem cells with a programmable fluorescent CRISPR/Cas system. *Nucleus*. 5 (2), 163–172.

Argüello-Miranda, O., Zagoriy, I., Mengoli, V., Rojas, J., Jonak, K., Oz, T., Graf, P. & Zachariae, W. (2017) Casein Kinase 1 Coordinates Cohesin Cleavage, Gametogenesis, and Exit from M Phase in Meiosis II. *Developmental Cell*. 40 (1), 37–52.

Arivis ag (2019) *Tracking & Lineage*. [Online] [online]. Available from: https://www.arivis.com/en/imaging-science/tracking-lineage (Accessed 22 November 2019).

Armond, J.W., Harry, E.F., McAinsh, A.D. & Burroughs, N.J. (2015) Inferring the Forces Controlling Metaphase Kinetochore Oscillations by Reverse Engineering System Dynamics Alexandre V Morozov (ed.). *PLOS Computational Biology*. 11 (11), e1004607.

Armond, J.W., Vladimirou, E., McAinsh, A.D. & Burroughs, N.J. (2016) KiT: a MATLAB package for kinetochore tracking. *Bioinformatics*. 32 (12), 1917–1919.

van Assen, H.C., Egmont-Petersen, M. & Reiber, J.H.C. (2002) Accurate object localization in gray level images using the center of gravity measure: accuracy versus precision. *IEEE Transactions on Image Processing*. 11 (12), 1379–1384.

Bacia, K., Petrášek, Z. & Schwille, P. (2012) Correcting for spectral cross-talk in dual-color fluorescence cross-correlation spectroscopy. *ChemPhysChem*. 13 (5), 1221–1231.

Baker, S.M., Plug, A.W., Prolla, T.A., Bronner, C.E., Harris, A.C., Yao, X., Christie, D.M., Monell, C., Arnheim, N., Bradley, A., Ashley, T. & Liskay, R.M. (1996) Involvement of mouse Mlh1 in DNA mismatch repair and meiotic crossing over. *Nature Genetics*. 13 (3), 336–342.

Balaji J (2014) *Time Series Analyzer*. [Online] [online]. Available from: https://imagej.nih.gov/ij/plugins/time-series.html (Accessed 19 November 2019).

Bárcena, P., Rodríguez, M., Obradors, A., Vernaeve, V. & Vassena, R. (2016) Should we worry about the clock? Relationship between time to ICSI and reproductive outcomes in cycles with fresh and vitrified oocytes. *Advanced Access publication on April*. 31 (6), 1182–1191.

Battaglia, D.E.E., Goodwin, P., Klein, N.A.A. & Soules, M.R.R. (1996) Fertilization and early embryology: Influence of maternal age on meiotic spindle assembly oocytes from naturally cycling women. *Human Reproduction*. 11 (10), 2217–2222.

Benson, G. (1999) Tandem repeats finder: a program to analyze DNA sequences. *Nucleic Acids Research*. 27 (2), 573–580.

Bertoli, C., Skotheim, J.M. & de Bruin, R.A.M.M. (2013) Control of cell cycle transcription during G1 and S phases. *Nature reviews. Molecular cell biology*. 14 (8), 518–528.

Bhakdi, S. & Thaicharoen, P. (2018) Easy Employment and Crosstalk-Free Detection of Seven Fluorophores in a Widefield Fluorescence Microscope. *Methods and Protocols*. 1 (2), 20.

Bindels, D.S., Haarbosch, L., van Weeren, L., Postma, M., Wiese, K.E., Mastop, M., Aumonier, S., Gotthard, G., Royant, A., Hink, M.A. & Gadella, T.W.J. (2017) mScarlet: a bright monomeric red fluorescent protein for cellular imaging. *Nature Methods*. 14 (1), 53–56.

Bishop, J.D., Schuniacher, J.M. & Schumacher, J.M. (2002) Phosphorylation of the Carboxyl Terminus of Inner Centromere Protein (INCENP) by the Aurora B Kinase Stimulates Aurora B Kinase Activity. *Journal of Biological Chemistry*. 277 (31), 27577–27580.

Brocher, J. & Wagner, T. (2015) *BioVoxxel Toolbox*. [Online] [online]. Available from: https://imagej.net/BioVoxxel_Toolbox (Accessed 19 November 2019).

Bugge, M., Collins, A., Petersen, M.B., Fisher, J., Brandt, C., Michael Hertz, J., Tranebjaerg, L., de Lozier-Blanchet, C., Nicolaides, P., Brøndum-Nielsen, K., Morton, N. & Mikkelsen, M. (1998) Non-disjunction of chromosome 18. *Human Molecular Genetics*. 7 (4), 661–669.

Burkard, R., Dell'Amico, M. & Martello, S. (2012) *Assignment Problems*. 2nd edition. Society for Industrial and Applied Mathematics.

Burroughs, N.J., Harry, E.F. & McAinsh, A.D. (2015) Super-resolution kinetochore tracking reveals the mechanisms of human sister kinetochore directional

switching. *eLife*. 4e09500.

Cardona, A., Saalfeld, S., Schindelin, J., Arganda-Carreras, I., Preibisch, S., Longair, M., Tomancak, P., Hartenstein, V. & Douglas, R.J. (2012) TrakEM2 Software for Neural Circuit Reconstruction Aravinthan Samuel (ed.). *PLoS ONE*. 7 (6), e38011.

Carl Zeiss Microscopy GmbH (2017) *Definite Focus.2*. [Online] [online]. Available from: https://www.zeiss.com/microscopy/int/products/light-microscopes/axio-observer-for-biology/definite-focus.html (Accessed 19 November 2019).

Carl Zeiss Microscopy GmbH (2019) *ZEN*. [Online] [online]. Available from: https://www.zeiss.com/microscopy/int/products/microscope-software/zen.html (Accessed 19 November 2019).

Chambon, J.-P., Touati, S.A., Berneau, S., Cladière, D., Hebras, C., Groeme, R., McDougall, A. & Wassmann, K. (2013) The PP2A Inhibitor I2PP2A Is Essential for Sister Chromatid Segregation in Oocyte Meiosis II. *Current Biology*. 23 (6), 485–490.

Chang, H.-Y.Y., Levasseur, M. & Jones, K.T. (2004) Degradation of APCcdc20 and APCcdh1 substrates during the second meiotic division in mouse eggs. *Journal of cell science*. 117 (Pt 26), 6289–96.

Chang, H.Y., Minahan, K., Merriman, J.A. & Jones, K.T. (2009) Calmodulin-dependent protein kinase gamma 3 (CamKIIγ3) mediates the cell cycle resumption of metaphase II eggs in mouse. *Development*. 136 (24), 4077–4081.

Chang, N., Sun, C., Gao, L., Zhu, D., Xu, X., Zhu, X., Xiong, J.-W. & Xi, J.J. (2013) Genome editing with RNA-guided Cas9 nuclease in Zebrafish embryos. *Cell Research*. 23 (4), 465–472.

Chen, B., Gilbert, L.A., Cimini, B.A., Schnitzbauer, J., Zhang, W., Li, G.-W., Park, J., Blackburn, E.H., Weissman, J.S., Qi, L.S. & Huang, B. (2013) Dynamic imaging of genomic loci in living human cells by an optimized CRISPR/Cas system. *Cell*. 155 (7), 1479–1491.

Chen, B., Guan, J. & Huang, B. (2016) Imaging Specific Genomic DNA in Living Cells. *Annual Review of Biophysics*. 45 (1), 1–23.

Chen, B., Hu, J., Almeida, R., Liu, H., Balakrishnan, S., Covill-Cooke, C., Lim, W.A. & Huang, B. (2016) Expanding the CRISPR imaging toolset with Staphylococcus aureus Cas9 for simultaneous imaging of multiple genomic loci. *Nucleic Acids Research*. 44 (8), e75.

Chen, B. & Huang, B. (2014) 'Imaging Genomic Elements in Living Cells Using CRISPR/Cas9', in *Methods in enzymology*. [Online]. pp. 337–354.

Chen, S., Zhang, Q., Wu, X., Schultz, P.G. & Ding, S. (2004) Dedifferentiation of Lineage-Committed Cells by a Small Molecule. *Journal of the American Chemical Society*. 126 (2), 410–411.

Cheng, A.W., Jillette, N., Lee, P., Plaskon, D., Fujiwara, Y., Wang, W., Taghbalout, A. & Wang, H. (2016) Casilio: a versatile CRISPR-Cas9-Pumilio hybrid for gene

regulation and genomic labeling. *Cell research*. 26 (2), 254–257.

Chian, R.-C., Lim, J.-H. & Tan, S.-L. (2004) State of the art in in-vitro oocyte maturation. *Current Opinion in Obstetrics and Gynecology*. 16 (3), 211–219.

Chiang, T., Duncan, F.E., Schindler, K., Schultz, R.M. & Lampson, M. a (2010) Evidence that weakened centromere cohesion is a leading cause of age-related aneuploidy in oocytes. *Current biology : CB*. 20 (17), 1522–1528.

Chiang, T., Schultz, R.M. & Lampson, M.A. (2012) Meiotic origins of maternal age-related aneuploidy. *Biology of reproduction*. 86 (1), 1–7.

Ciliberto, A. & Hauf, S. (2017) Micromanaging checkpoint proteins. *eLife*. 6.

Cimini, D., Howell, B., Maddox, P., Khodjakov, A., Degrassi, F. & Salmon, E.D. (2001) Merotelic kinetochore orientation is a major mechanism of aneuploidy in mitotic mammalian tissue cells. *Journal of Cell Biology*. 152 (3), 517–527.

Ciosk, R., Shirayama, M., Shevchenko, Anna, Tanaka, T., Toth, A., Shevchenko, Andrej & Nasmyth, K. (2000) Cohesin's Binding to Chromosomes Depends on a Separate Complex Consisting of Scc2 and Scc4 Proteins. *Molecular Cell*. 5 (2), 243–254.

Claxton, N.S., Fellers, T.J. & Davidson, M.W. (2006) 'Laser Scanning Confocal Microscopy', in *Encyclopedia of Medical Devices and Instrumentation*. [Online]. Hoboken, NJ, USA: John Wiley & Sons, Inc. p.

Clift, D., McEwan, W.A., Labzin, L.I., Konieczny, V., Mogessie, B., James, L.C. & Schuh, M. (2017) A Method for the Acute and Rapid Degradation of Endogenous Proteins. *Cell*. 171 (7), 1692-1706.e18.

Clift, D., So, C., McEwan, W.A., James, L.C. & Schuh, M. (2018) Acute and rapid degradation of endogenous proteins by Trim-Away. *Nature Protocols*. 13 (10), 2149–2175.

Cole, R.W., Jinadasa, T. & Brown, C.M. (2011) Measuring and interpreting point spread functions to determine confocal microscope resolution and ensure quality control. *Nature Protocols*. 6 (12), 1929–1941.

Conklin, E.G. (1915) Why Polar Bodies do not Develop. *Proceedings of the National Academy of Sciences of the United States of America*. 1 (9), 491–496.

Corbett, K.D. & Harrison, S.C. (2012) Molecular Architecture of the Yeast Monopolin Complex. *Cell Reports*. 1 (6), 583–589.

Corbett, K.D., Yip, C.K., Ee, L.-S., Walz, T., Amon, A. & Harrison, S.C. (2010) The monopolin complex crosslinks kinetochore components to regulate chromosome-microtubule attachments. *Cell*. 142 (4), 556–567.

Das, C., Tyler, J.K. & Churchill, M.E.A. (2010) The histone shuffle: Histone chaperones in an energetic dance. Trends in Biochemical Sciences 35 (9) p.476–489.

Daum, J.R., Potapova, T.A., Sivakumar, S., Daniel, J.J., Flynn, J.N., Rankin, S. &

Gorbsky, G.J. (2011) Cohesion fatigue induces chromatid separation in cells delayed at metaphase. *Current biology : CB*. 21 (12), 1018–1024.

Davey, N.E. & Morgan, D.O. (2016) Building a Regulatory Network with Short Linear Sequence Motifs: Lessons from the Degrons of the Anaphase-Promoting Complex. *Molecular Cell*. 64 (1), 12–23.

Deng, W., Shi, X., Tjian, R., Lionnet, T. & Singer, R.H. (2015) CASFISH: CRISPR/Cas9-mediated in situ labeling of genomic loci in fixed cells. *Proceedings of the National Academy of Sciences*. 112 (38), 11870–11875.

Ding, Y., Kaido, M., Llano, E., Pendas, A.M. & Kitajima, T.S. (2018) The Post-anaphase SUMO Pathway Ensures the Maintenance of Centromeric Cohesion through Meiosis I-II Transition in Mammalian Oocytes. *Current Biology*. 28 (10), 1661–1669.

Doench, J.G., Fusi, N., Sullender, M., Hegde, M., Vaimberg, E.W., Donovan, K.F., Smith, I., Tothova, Z., Wilen, C., Orchard, R., Virgin, H.W., Listgarten, J. & Root, D.E. (2016) Optimized sgRNA design to maximize activity and minimize off-target effects of CRISPR-Cas9. *Nature Biotechnology*. 34 (2), 184–191.

Domingo-Sananes, M.R., Kapuy, O., Hunt, T. & Novak, B. (2011) Switches and latches: a biochemical tug-of-war between the kinases and phosphatases that control mitosis. *Philosophical Transactions of the Royal Society B: Biological Sciences*. 366 (1584), 3584–3594.

Down, J.L. (1887) Lettsomian Lectures on Some of the Mental Affections of Childhood and Youth. *British medical journal*. 1 (1362), 256–9.

Dozortsev, D., Nagy, P., Abdelmassih, S., Oliveira, F., Brasil, A., Abdelmassih, V., Diamond, M. & Abdelmassih, R. (2004) The optimal time for intracytoplasmic sperm injection in the human is from 37 to 41 hours after administration of human chorionic gonadotropin. *Fertility and Sterility*. 82 (6), 1492–1496.

Duncan, F.E., Hornick, J.E., Lampson, M.A., Schultz, R.M., Shea, L.D. & Woodruff, T.K. (2012) Chromosome cohesion decreases in human eggs with advanced maternal age. *Aging Cell*. 11 (6), 1121–1124.

Dupré, A., Haccard, O. & Jessus, C. (2011) Mos in the oocyte: how to use MAPK independently of growth factors and transcription to control meiotic divisions. *Journal of signal transduction*. 2011350412.

Earnshaw, W.C. & Heck, M.M.S. (1985) Localization of topoisomerase II in mitotic chromosomes. *Journal of Cell Biology*. 100 (5), 1716–1725.

Edwards, J.H., Harnden, D.G., Cameron, A.H., Crosse, V.M. & Wolf, O.H. (1960) A NEW TRISOMIC SYNDROME. *The Lancet*. 275 (7128), 787–790.

Eitoku, M., Sato, L., Senda, T. & Horikoshi, M. (2008) Histone chaperones: 30 Years from isolation to elucidation of the mechanisms of nucleosome assembly and disassembly. Cellular and Molecular Life Sciences 65 (3) p.414–444.

Elnagar, A. & Gupta, K. (1998) Motion prediction of moving objects based on autoregressive model. *IEEE Transactions on Systems, Man, and Cybernetics Part*

A:Systems and Humans. 28 (6), 803–810.

Emanuele, M.J., Lan, W., Jwa, M., Miller, S.A., Chan, C.S.M. & Stukenberg, P.T. (2008) Aurora B kinase and protein phosphatase 1 have opposing roles in modulating kinetochore assembly. *Journal of Cell Biology*. 181 (2), 241–254.

Eppig, J.J. (2018) Reproduction: Oocytes Call, Granulosa Cells Connect. *Current Biology*. 28 (8), R354–R356.

Fattaey, A. & Booher, R.N. (1997) 'Myt1: a Wee1-type kinase that phosphorylates Cdc2 on residue Thr14', in *Progress in Cell Cycle Research*. [Online]. Boston, MA: Springer US. pp. 233–240.

Featherstone, C. & Jackson, S.P. (1999) DNA double-strand break repair. *Current Biology*. 9 (20), R759–R761.

Fisher, J.M., Harvey, J.F., Morton, N.E. & Jacobs, P. a (1995) Trisomy 18: studies of the parent and cell division of origin and the effect of aberrant recombination on nondisjunction. *American journal of human genetics*. 56 (3), 669–675.

Flemming, W. (1882) Zellsubstanz, Kern und Zelltheilung [Cell substance, nucleus and cell division]. *FCW Vogel, Leipzig, Germany). German*.

Foss, S., Watkinson, R., Sandlie, I., James, L.C. & Andersen, J.T. (2015) TRIM21: A cytosolic Fc receptor with broad antibody isotype specificity. *Immunological Reviews*. 268 (1), 328–339.

Fragouli, E., Alfarawati, S., Goodall, N.N., Sánchez-García, J.F., Colls, P. & Wells, D. (2011) The cytogenetics of polar bodies: Insights into female meiosis and the diagnosis of aneuploidy. *Molecular Human Reproduction*. 17 (5), 286–295.

Fragouli, E., Alfarawati, S., Spath, K., Jaroudi, S., Sarasa, J., Enciso, M. & Wells, D. (2013) The origin and impact of embryonic aneuploidy. *Human Genetics*. 132 (9), 1001–1013.

Fragouli, E., Katz-Jaffe, M., Alfarawati, S., Stevens, J., Colls, P., Goodall, N.N., Tormasi, S., Gutierrez-Mateo, C., Prates, R., Schoolcraft, W.B., Munne, S. & Wells, D. (2010) Comprehensive chromosome screening of polar bodies and blastocysts from couples experiencing repeated implantation failure. *Fertility and Sterility*. 94 (3), 875–887.

Frommer, W.B., Davidson, M.W. & Campbell, R.E. (2009) Genetically encoded biosensors based on engineered fluorescent proteins. *Chemical Society Reviews*. 38 (10), 2833–2841.

Fu, G., Hua, S., Ward, T., Ding, X., Yang, Y., Guo, Z. & Yao, X. (2007) D-box is required for the degradation of human Shugoshin and chromosome alignment. *Biochemical and Biophysical Research Communications*. 357 (3), 672–678.

Fu, Y., Rocha, P.P., Luo, V.M., Raviram, R., Deng, Y., Mazzoni, E.O. & Skok, J.A. (2016) CRISPR-dCas9 and sgRNA scaffolds enable dual-colour live imaging of satellite sequences and repeat-enriched individual loci. *Nature Communications*. 7 (1), 11707.

Gandhi, R., Gillespie, P.J. & Hirano, T. (2006) Human Wapl Is a Cohesin-Binding Protein that Promotes Sister-Chromatid Resolution in Mitotic Prophase. *Current Biology*. 16 (24), 2406–2417.

Ghauharali & Brakenhoff (2000) Fluorescence photobleaching-based image standardization for fluorescence microscopy. *Journal of Microscopy*. 198 (2), 88–100.

Golan, A., Yudkovsky, Y. & Hershko, A. (2002) The cyclin-ubiquitin ligase activity of cyclosome/APC is jointly activated by protein kinases Cdk1-cyclin B and Plk. *Journal of Biological Chemistry*. 277 (18), 15552–15557.

Gómez, R., Valdeolmillos, A., Parra, M.T., Viera, A., Carreiro, C., Roncal, F., Rufas, J.S., Barbero, J.L., Suja, J.A., Gomez, R., Valdeolmillos, A., Parra, M.T., Viera, A., Carreiro, C., Roncal, F., Rufas, J.S., Barbero, J.L. & Suja, J.A. (2007) Mammalian SGO2 appears at the inner centromere domain and redistributes depending on tension across centromeres during meiosis II and mitosis. *EMBO Rep*. 8 (2), 173–180.

Gougeon, A. (1996) Regulation of Ovarian Follicular Development in Primates: Facts and Hypotheses. *Endocrine Reviews*. 17 (2), 121–155.

Gould, K.L., Moreno, S., Tonks, N.K. & Nurse, P. (1990) Complementation of the mitotic activator, p80cdc25, by a human protein-tyrosine phosphatase. *Science*. 250 (4987), 1573–1576.

Grey, C., Baudat, F. & de Massy, B. (2018) PRDM9, a driver of the genetic map Paula E. Cohen (ed.). *PLOS Genetics*. 14 (8), e1007479.

Grimison, B., Liu, J., Lewellyn, A.L. & Maller, J.L. (2006) Metaphase Arrest by Cyclin E-Cdk2 Requires the Spindle-Checkpoint Kinase Mps1. *Current Biology*. 16 (19), 1968–1973.

Gutiérrez-Caballero, C., Cebollero, L.R., Pendás, A.M., Gutié Rrez-Caballero, C., Cebollero, L.R. & Pendá, A.M. (2012) Shugoshins: From protectors of cohesion to versatile adaptors at the centromere. *Trends in Genetics*. 28 (7), 351–360.

Haarhuis, J.H.I., Elbatsh, A.M.O. & Rowland, B.D. (2014) Cohesin and its regulation: on the logic of X-shaped chromosomes. *Developmental cell*. 31 (1), 7–18.

Hadjantonakis, A.-K. & Papaioannou, V.E. (2004) Dynamic in vivo imaging and cell tracking using a histone fluorescent protein fusion in mice. *BMC biotechnology*. 4 (1), 33.

Hagting, A., Den Elzen, N., Vodermaier, H.C., Waizenegger, I.C., Peters, J.M. & Pines, J. (2002) Human securin proteolysis is controlled by the spindle checkpoint and reveals when the APC/C switches from activation by Cdc20 to Cdh1. *Journal of Cell Biology*. 157 (7), 1125–1137.

Han, B.-S. & Gao, J.-L. (2013) Effects of chemical combinations on the parthenogenetic activation of mouse oocytes. *Experimental and Therapeutic Medicine*. 5 (5), 1281–1288.

Handel, M.A. & Schimenti, J.C. (2010) Genetics of mammalian meiosis: regulation,

dynamics and impact on fertility. *Nature reviews. Genetics*. 11 (2), 124–136.

Handyside, A.H. (2012) Molecular origin of female meiotic aneuploidies. *Biochimica et Biophysica Acta (BBA) - Molecular Basis of Disease*. 1822 (12), 1913–1920.

Handyside, A.H., Montag, M., Magli, M.C., Repping, S., Harper, J., Schmutzler, A., Vesela, K., Gianaroli, L. & Geraedts, J. (2012) Multiple meiotic errors caused by predivision of chromatids in women of advanced maternal age undergoing in vitro fertilisation. *European Journal of Human Genetics*. 20 (7), 742–747.

Hansen, D. V., Tung, J.J. & Jackson, P.K. (2006) CaMKII and Polo-like kinase 1 sequentially phosphorylate the cytostatic factor Emi2/XErp1 to trigger its destruction and meiotic exit. *Proceedings of the National Academy of Sciences of the United States of America*. 103 (3), 608–613.

Hassold, T., Merrill, M., Adkins, K., Freeman, S. & Sherman, S. (1995) Recombination and maternal age-dependent nondisjunction: Molecular studies of trisomy 16. *American Journal of Human Genetics*. 57 (4), 867–874.

Hassold, T.J., Pettay, D., Freeman, S.B., Grantham, M. & Takaesu, N. (1991) Molecular studies of non-disjunction in trisomy 16. *Journal of Medical Genetics*. 28 (3), 159–162.

Hayward, D., Alfonso-Pérez, T., Cundell, M.J., Hopkins, M., Holder, J., Bancroft, J., Hutter, L.H., Novak, B., Barr, F.A. & Gruneberg, U. (2019) CDK1-CCNB1 creates a spindle checkpoint–permissive state by enabling MPS1 kinetochore localization. *The Journal of Cell Biology*. 218 (4), 1182–1199.

Herbert, M., Kalleas, D., Cooney, D., Lamb, M. & Lister, L. (2015) Meiosis and Maternal Aging: Insights from Aneuploid Oocytes and Trisomy Births. *Cold Spring Harbor Perspectives in Biology*. 7 (4), a017970.

Herbert, M. & Toth, A. (2017) How Meiosis Creates the Single-Copy Genome. *Developmental Cell*. 40 (1), 3–4.

Hermans-Borgmeyer, I. (2013) *Mercury-and Fluorinert®-free piezo-assisted transfer of ES cells into mouse embryos using the Eppendorf PiezoXpert®*.

Hertz, E.P.T.P.T., Kruse, T., Davey, N.E.E.N.E., López-Méndez, B., Sigurðsson, J.O.O., Montoya, G., Olsen, J.V. V, Nilsson, J., Arroyo, J.D., Lee, G.M., Hahn, W.C., Bollen, M., Peti, W., Ragusa, M.J., Beullens, M., Brunet, A., Bonni, A., Zigmond, M.J., Lin, M.Z., et al. (2016) A Conserved Motif Provides Binding Specificity to the PP2A-B56 Phosphatase. *Molecular Cell*. 63 (4), 686–695.

Higgins, J.M.G. & Herbert, M. (2013) Nucleosome assembly proteins get SET to defeat the guardian of chromosome cohesion. *PLoS genetics*. 9 (9), e1003829.

Hochegger, H., Klotzbücher, A., Kirk, J., Howell, M., le Guellec, K., Fletcher, K., Duncan, T., Sohail, M. & Hunt, T. (2001) New B-type cyclin synthesis is required between meiosis I and II during Xenopus oocyte maturation. *Development (Cambridge, England)*. 128 (19), 3795–3807.

Hochegger, H., Takeda, S. & Hunt, T. (2008) Cyclin-dependent kinases and cell-cycle transitions: does one fit all? *Nature Reviews Molecular Cell Biology*. 9 (11), 910–

916.

Hodges, C.A. & Hunt, P.A. (2002) Simultaneous analysis of chromosomes and chromosome-associated proteins in mammalian oocytes and embryos. *Chromosoma*. 111 (3), 165–169.

Holubcova, Z., Blayney, M., Elder, K. & Schuh, M. (2015) Error-prone chromosome-mediated spindle assembly favors chromosome segregation defects in human oocytes. *Science*. 348 (6239), 1143–1147.

Homer, Hayden A, McDougall, A., Levasseur, M., Murdoch, A.P. & Herbert, M. (2005) Mad2 is required for inhibiting securin and cyclin B degradation following spindle depolymerisation in meiosis I mouse oocytes. *Reproduction*. 130 (6), 829–843.

Homer, Hayden A., McDougall, A., Levasseur, M., Yallop, K., Murdoch, A.P. & Herbert, M. (2005) Mad2 prevents aneuploidy and premature proteolysis of cyclin B and securin during meiosis I in mouse oocytes. *Genes & development*. 19 (2), 202–207.

Horlbeck, M.A., Witkowsky, L.B., Guglielmi, B., Replogle, J.M., Gilbert, L.A., Villalta, J.E., Torigoe, S.E., Tjian, R. & Weissman, J.S. (2016) Nucleosomes impede Cas9 access to DNA in vivo and in vitro. *eLife*. 52767–2771.

Huang, H., Feng, J., Famulski, J., Rattner, J.B., Liu, S.T., Kao, G.D., Muschel, R., Chan, G.K.T. & Yen, T.J. (2007) Tripin/hSgo2 recruits MCAK to the inner centromere to correct defective kinetochore attachments. *The Journal of cell biology*. 177 (3), 413–424.

Hübner, M.R., Eckersley-Maslin, M.A. & Spector, D.L. (2013) Chromatin organization and transcriptional regulation. *Current Opinion in Genetics & Development*. 23 (2), 89–95.

Huff, J. (2015) The Airyscan detector from ZEISS: confocal imaging with improved signal-to-noise ratio and super-resolution. *Nature Methods*. 12 (12), i–ii.

Hunter, N. (2015) Meiotic Recombination: The Essence of Heredity. *Cold Spring Harbor Perspectives in Biology*. 7 (12), a016618.

Huo, L.-J., Zhong, Z.-S., Liang, C.-G., Wang, Q., Yin, S., Ai, J.-S., Yu, L.-Z., Chen, D.-Y., Schatten, H. & Sun, Q.-Y. (2006) Degradation of securin in mouse and pig oocytes is dependent on ubiquitin-proteasome pathway and is required for proteolysis of the cohesion subunit, Rec8, at the metaphase-to-anaphase transition. *Frontiers in bioscience : a journal and virtual library*. 11 (1), 2193–2202.

Hutchins, J.R.A., Dikovskaya, D. & Clarke, P.R. (2003) Regulation of Cdc2/cyclin B activation in Xenopus egg extracts via inhibitory phosphorylation of Cdc25c phosphatase by Ca 2+/calmodium-dependent kinase II. *Molecular Biology of the Cell*. 14 (10), 4003–4014.

Icha, J., Weber, M., Waters, J.C. & Norden, C. (2017) Phototoxicity in live fluorescence microscopy, and how to avoid it. *BioEssays*. 39 (8), 1700003.

Inoue, D., Ohe, M., Kanemori, Y., Nobui, T. & Sagata, N. (2007) A direct link of the

Mos–MAPK pathway to Erp1/Emi2 in meiotic arrest of Xenopus laevis eggs. *Nature*. 446 (7139), 1100–1104.

Isoda, M., Sako, K., Suzuki, K., Nishino, K., Nakajo, N., Ohe, M., Ezaki, T., Kanemori, Y., Inoue, D., Ueno, H. & Sagata, N. (2011) Dynamic regulation of Emi2 by Emi2-bound Cdk1/Plk1/CK1 and PP2A-B56 in meiotic arrest of Xenopus eggs. *Developmental cell*. 21 (3), 506–519.

Iwai, M., Hara, A., Andoh, T. & Ishida, R. (1997) ICRF-193, a catalytic inhibitor of DNA topoisomerase II, delays the cell cycle progression from metaphase, but not from anaphase to the G1 phase in mammalian cells. *FEBS Letters*. 406 (3), 267–270.

Izawa, D. & Pines, J. (2012) Mad2 and the APC/C compete for the same site on Cdc20 to ensure proper chromosome segregation. *Journal of Cell Biology*. 199 (1), 27–37.

Jaqaman, K., King, E.M., Amaro, A.C., Winter, J.R., Dorn, J.F., Elliott, H.L., Mchedlishvili, N., McClelland, S.E., Porter, I.M., Posch, M., Toso, A., Danuser, G., McAinsh, A.D., Meraldi, P. & Swedlow, J.R. (2010) Kinetochore alignment within the metaphase plate is regulated by centromere stiffness and microtubule depolymerases. *Journal of Cell Biology*. 188 (5), 665–679.

Jaqaman, K., Loerke, D., Mettlen, M., Kuwata, H., Grinstein, S., Schmid, S.L. & Danuser, G. (2008) Robust single-particle tracking in live-cell time-lapse sequences. *Nature Methods*. 5 (8), 695–702.

Ji, Z., Gao, H., Jia, L., Li, B. & Yu, H. (2017) A sequential multi-target Mps1 phosphorylation cascade promotes spindle checkpoint signaling. *eLife*. 61–3.

Jia, J.-L., Han, Y.-H., Kim, H.-C., Ahn, M., Kwon, J.-W., Luo, Y., Gunasekaran, P., Lee, S.-J., Lee, K.S., Kyu Bang, J., Kim, N.-H. & Namgoong, S. (2015) Structural basis for recognition of Emi2 by Polo-like kinase 1 and development of peptidomimetics blocking oocyte maturation and fertilization. *Scientific Reports*. 5 (1), 14626.

Jia, L., Li, B., Warrington, R.T., Hao, X., Wang, S. & Yu, H. (2011) Defining pathways of spindle checkpoint silencing: Functional redundancy between Cdc20 ubiquitination and p31 comet. *Molecular Biology of the Cell*. 22 (22), 4227–4235.

Jiang, F. & Doudna, J.A. (2017) CRISPR–Cas9 Structures and Mechanisms. *Annual Review of Biophysics*. 46 (1), 505–529.

Jinek, M., Chylinski, K., Fonfara, I., Hauer, M., Doudna, J.A. & Charpentier, E. (2012) A Programmable Dual-RNA-Guided DNA Endonuclease in Adaptive Bacterial Immunity. *Science*. 337 (6096), 816–821.

Jonak, K., Zagoriy, I., Oz, T., Graf, P., Rojas, J., Mengoli, V. & Zachariae, W. (2017) APC/C-Cdc20 mediates deprotection of centromeric cohesin at meiosis II in yeast. *Cell Cycle*. 1–8.

Jonkman, J. & Brown, C.M. (2015) Any way you slice it—A comparison of confocal microscopy techniques. *Journal of Biomolecular Techniques*. 26 (2), 54–65.

Karabinova, P., Kubelka, M. & Susor, A. (2011) Proteasomal degradation of ubiquitinated proteins in oocyte meiosis and fertilization in mammals. *Cell and Tissue Research*. 346 (1), 1–9.

Karamysheva, Z., Diaz-Martinez, L.A., Crow, S.E., Li, B. & Yu, H. (2009) Multiple anaphase-promoting complex/cyclosome degrons mediate the degradation of human Sgo1. *The Journal of biological chemistry*. 284 (3), 1772–1780.

Katis, V.L., Lipp, J.J., Imre, R., Bogdanova, A., Okaz, E., Habermann, B., Mechtler, K., Nasmyth, K. & Zachariae, W. (2010) Rec8 phosphorylation by casein kinase 1 and Cdc7-Dbf4 kinase regulates cohesin cleavage by separase during meiosis. *Developmental cell*. 18 (3), 397–409.

Kawashima, S.A., Yamagishi, Y., Honda, T., Lshiguro, K.I., Watanabe, Y., Ishiguro, K. & Watanabe, Y. (2010) Phosphorylation of H2A by Bub1 prevents chromosomal instability through localizing shugoshin. *Science*. 327 (5962), 172–177.

Kenney, R.D. & Heald, R. (2006) Essential roles for cohesin in kinetochore and spindle function in Xenopus egg extracts. *Journal of Cell Science*. 119 (24), 5057–5066.

Kim, J., Ishiguro, K.-I.I., Nambu, A., Akiyoshi, B., Yokobayashi, S., Kagami, A., Ishiguro, T., Pendas, A.M., Takeda, N., Sakakibara, Y., Kitajima, T.S., Tanno, Y., Sakuno, T. & Watanabe, Y. (2014) Meikin is a conserved regulator of meiosis-I-specific kinetochore function. *Nature*. 517 (7535), 466–471.

Kishigami, S. & Wakayama, T. (2007) Efficient strontium-induced activation of mouse oocytes in standard culture media by chelating calcium. *The Journal of reproduction and development*. 53 (6), 1207–1215.

Kitajima, T. & EMBL Colleagues (2011) *Tracking Kinetochores Throughout Meiosis Using Imaris*. [Online] [online]. Available from: https://imaris.oxinst.com/learning/view/article/tracking-kinetochores-throughout-meiosis (Accessed 22 November 2019).

Kitajima, T.S., Kawashima, S.A. & Watanabe, Y. (2004) The conserved kinetochore protein shugoshin protects centromeric cohesion during meiosis. *Nature*. 427 (6974), 510–517.

Kitajima, T.S., Miyazaki, Y., Yamamoto, M. & Watanabe, Y. (2003) Rec8 cleavage by separase is required for meiotic nuclear divisions in fission yeast. *EMBO Journal*. 22 (20), 5643–5653.

Kitajima, T.S., Ohsugi, M. & Ellenberg, J. (2011) Complete kinetochore tracking reveals error-prone homologous chromosome biorientation in mammalian oocytes. *Cell*. 146 (4), 568–581.

Kitajima, T.S., Sakuno, T., Ishiguro, K., Iemura, S., Natsume, T., Kawashima, S.A. & Watanabe, Y. (2006) Shugoshin collaborates with protein phosphatase 2A to protect cohesin. *Nature*. 441 (7089), 46–52.

Koch, L.B., Opoku, K.N., Deng, Y., Barber, A., Littleton, A.J., London, N., Biggins, S. & Asbury, C.L. (2019) Autophosphorylation is sufficient to release Mps1 kinase from native kinetochores. *Proceedings of the National Academy of Sciences*. 116

(35), 17355–17360.

Kornbluth, S. & Fissore, R. (2015) Vertebrate Reproduction. *Cold Spring Harbor Perspectives in Biology*. 7 (10), a006064.

Kouznetsova, A., Hernández-Hernández, A. & Höög, C. (2014) Merotelic attachments allow alignment and stabilization of chromatids in meiosis II oocytes. *Nature Communications*. 5 (1), 4409.

Kouznetsova, A., Kitajima, T.S., Brismar, H. & Höög, C. (2019) Post-metaphase correction of aberrant kinetochore-microtubule attachments in mammalian eggs. *EMBO reports*. 20 (8), e47905.

Krishnan, S., Smits, A.H., Vermeulen, M. & Reinberg, D. (2017) Phospho-H1 Decorates the Inter-chromatid Axis and Is Evicted along with Shugoshin by SET during Mitosis. *Molecular Cell*. 67 (4), 579-593.e6.

Kruse, T., Biedenkopf, N., Hertz, E.P.T., Dietzel, E., Stalmann, G., López-Méndez, B., Davey, N.E., Nilsson, J. & Becker, S. (2018) The Ebola Virus Nucleoprotein Recruits the Host PP2A-B56 Phosphatase to Activate Transcriptional Support Activity of VP30. *Molecular Cell*. 69 (1), 136-145.e6.

Kuhn, H.W. (2010) 'The Hungarian Method for the Assignment Problem', in *50 Years of Integer Programming 1958-2008*. [Online]. Berlin, Heidelberg: Springer Berlin Heidelberg. pp. 29–47.

Kuliev, A., Zlatopolsky, Z., Kirillova, I., Spivakova, J. & Cieslak Janzen, J. (2011) Meiosis errors in over 20,000 oocytes studied in the practice of preimplantation aneuploidy testing. *Reproductive BioMedicine Online*. 22 (1), 2–8.

Kumada, K., Nakamura, T., Nagao, K., Funabiki, H., Nakagawa, T. & Yanagida, M. (1998) Cut1 is loaded onto the spindle by binding to Cut2 and promotes anaphase spindle movement upon Cut2 proteolysis. *Current Biology*. 8 (11), 633–641.

De La Fuente, R. (2006) Chromatin modifications in the germinal vesicle (GV) of mammalian oocytes. *Developmental Biology*. 292 (1), 1–12.

Laboratory Imaging s.r.o. (2019) *ND2 SDK*. [Online] [online]. Available from: https://www.nd2sdk.com/ (Accessed 19 November 2019).

Lam, I. & Keeney, S. (2015) Mechanism and Regulation of Meiotic Recombination Initiation. *Cold Spring Harbor Perspectives in Biology*. 7 (1), a016634.

Lamb, N.E., Feingold, E., Savage, A., Avramopoulos, D., Freeman, S., Gu, Y., Hallberg, A., Hersey, J., Karadima, G., Pettay, D., Saker, D., Shen, J., Taft, L., Mikkelsen, M., Petersen, M.B., Hassold, T. & Sherman, S.L. (1997) Characterization of susceptible chiasma configurations that increase the risk for maternal nondisjunction of chromosome 21. *Human Molecular Genetics*. 6 (9), 1391–1399.

Lamb, N.E., Freeman, S.B., Savage-Austin, A., Pettay, D., Taft, L., Hersey, J., Gu, Y., Shen, J., Saker, D., May, K.M., Avramopoulos, D., Petersen, M.B., Hallberg, A., Mikkelsen, M., Hassold, T.J. & Sherman, S.L. (1996) Susceptible chiasmate configurations of chromosome 21 predispose to non- disjunction in both

maternal meiosis I and meiosis II. *Nature Genetics*. 14 (4), 400–405.

Lamb, N.E., Yu, K., Shaffer, J., Feingold, E. & Sherman, S.L. (2005) Association between maternal age and meiotic recombination for trisomy 21. *American journal of human genetics*. 76 (1), 91–99.

Lambie, E.J. & Shirleen Roeder, G. (1988) A yeast acts in (Cis) to inhibit meiotic gene conversion of adjacent sequences. *Cell*. 52 (6), 863–873.

Lampson, M.A. & Cheeseman, I.M. (2011) Sensing centromere tension: Aurora B and the regulation of kinetochore function. *Trends in Cell Biology*. 21 (3), 133–140.

Lane, S.I.R., Crouch, S. & Jones, K.T. (2017) '*Imaging Chromosome Separation in Mouse Oocytes by Responsive 3D Confocal Timelapse Microscopy*', in [Online]. Humana Press, New York, NY. pp. 245–254.

Lee, J., Kitajima, T.S., Tanno, Y., Yoshida, K., Morita, T., Miyano, T., Miyake, M. & Watanabe, Y. (2008) Unified mode of centromeric protection by shugoshin in mammalian oocytes and somatic cells. *Nature cell biology*. 10 (1), 42–52.

Lemaire, P., Garrett, N. & Gurdon, J.. (1995) Expression cloning of Siamois, a xenopus homeobox gene expressed in dorsal-vegetal cells of blastulae and able to induce a complete secondary axis. *Cell*. 81 (1), 85–94.

Lewis, J.D. & Izaurflde, E. (1997) The Role of the Cap Structure in RNA Processing and Nuclear Export. *European Journal of Biochemistry*. 247 (2), 461–469.

Lewis, J.P. (2001) Fast Normalized Cross-Correlation. *Proceedings of Vision Interface*. 10120–123.

Li, X.-M., Yu, C., Wang, Z.-W., Zhang, Y.-L., Liu, X.-M., Zhou, D., Sun, Q.-Y. & Fan, H.-Y. (2013) DNA topoisomerase II is dispensable for oocyte meiotic resumption but is essential for meiotic chromosome condensation and separation in mice. *Biology of reproduction*. 89 (5), 118.

Li, X. & Nicklas, R.B. (1997) Tension-sensitive kinetochore phosphorylation and the chromosome distribution checkpoint in praying mantid spermatocytes. *Journal of cell science*. 110 (Pt 5 (5), 537–45.

Lima, C.D. & Mondragón, A. (1994) Mechanism of type II DNA topoisomerases: a tale of two gates. *Structure*. 2 (6), 559–560.

Liman, E.R., Tytgat, J. & Hess, P. (1992) Subunit stoichiometry of a mammalian K+ channel determined by construction of multimeric cDNAs. *Neuron*. 9 (5), 861–871.

Lindeberg, T. (1993) Detecting salient blob-like image structures and their scales with a scale-space primal sketch: A method for focus-of-attention. *International Journal of Computer Vision*. 11 (3), 283–318.

Lindeberg, T. (2015) Image Matching Using Generalized Scale-Space Interest Points. *Journal of Mathematical Imaging and Vision*. 52 (1), 3–36.

Lindeberg, T. (1994) *Scale-Space Theory in Computer Vision*. Springer US.

Linkert, M., Rueden, C.T., Allan, C., Burel, J.-M., Moore, W., Patterson, A., Loranger, B., Moore, J., Neves, C., MacDonald, D., Tarkowska, A., Sticco, C., Hill, E., Rossner, M., Eliceiri, K.W. & Swedlow, J.R. (2010) Metadata matters: access to image data in the real world. *The Journal of Cell Biology*. 189 (5), 777–782.

Lister, L.M., Kouznetsova, A., Hyslop, L.A., Kalleas, D., Pace, S.L., Barel, J.C., Nathan, A., Floros, V., Adelfalk, C., Watanabe, Y., Jessberger, R., Kirkwood, T.B., Höög, C. & Herbert, M. (2010) Age-related meiotic segregation errors in mammalian oocytes are preceded by depletion of cohesin and Sgo2. *Current biology : CB*. 20 (17), 1511–1521.

Liu, H., Jia, L. & Yu, H. (2013) Phospho-H2A and cohesin specify distinct tension-regulated Sgo1 pools at kinetochores and inner centromeres. *Current biology : CB*. 23 (19), 1927–1933.

Liu, H., Qu, Q., Warrington, R., Rice, A., Cheng, N. & Yu, H. (2015) Mitotic Transcription Installs Sgo1 at Centromeres to Coordinate Chromosome Segregation. *Molecular Cell*. 59 (3), 426–436.

Liu, H., Rankin, S. & Yu, H. (2013) Phosphorylation-enabled binding of SGO1-PP2A to cohesin protects sororin and centromeric cohesion during mitosis. *Nature cell biology*. 15 (1), 40–49.

Liu, L. & Keefe, D.L. (2008) Defective cohesin is associated with age-dependent misaligned chromosomes in oocytes. *Reproductive BioMedicine Online*. 16 (1), 103–112.

Liu, Y.-J., Liu, C., Chang, Z., Wadas, B., Brower, C.S., Song, Z.-H., Xu, Z.-L., Shang, Y.-L., Liu, W.-X., Wang, L.-N., Dong, W., Varshavsky, A., Hu, R.-G. & Li, W. (2016) Degradation of the Separase-cleaved Rec8, a Meiotic Cohesin Subunit, by the N-end Rule Pathway. *Journal of Biological Chemistry*. 291 (14), 7426–7438.

Llano, E., Gómez, R., Gutiérrez-Caballero, C., Herrán, Y., Sánchez-Martín, M., Vázquez-Quiñones, L., Hernández, T., de Alava, E., Cuadrado, A., Barbero, J.L., Suja, J.A., Pendás, A.M., Gutiéerrez-Caballero, C., Herrán, Y., Sánchez-Martín, M., Vázquez-Quiñones, L., Hernández, T., De Álava, E., Cuadrado, A., et al. (2008) Shugoshin-2 is essential for the completion of meiosis but not for mitotic cell division in mice. *Genes & development*. 22 (17), 2400–2413.

Lloyd, S.P. (1982) Least Squares Quantization in PCM. *IEEE Transactions on Information Theory*. 28 (2), 129–137.

Losada, A. (2014) Cohesin in cancer: Chromosome segregation and beyond. *Nature Reviews Cancer*. 14 (6), 389–393.

Lyons, N.A. & Morgan, D.O. (2011) Cdk1-Dependent Destruction of Eco1 Prevents Cohesion Establishment after S Phase. *Molecular Cell*. 42 (3), 378–389.

Ma, H., Naseri, A., Reyes-Gutierrez, P., Wolfe, S.A., Zhang, S. & Pederson, T. (2015) Multicolor CRISPR labeling of chromosomal loci in human cells. *Proceedings of the National Academy of Sciences*. 112 (10), 3002–3007.

Ma, H., Reyes-Gutierrez, P. & Pederson, T. (2013) Visualization of repetitive DNA sequences in human chromosomes with transcription activator-like effectors. *Proceedings of the National Academy of Sciences of the United States of America*. 110 (52), 21048–21053.

Ma, H., Tu, L.-C., Naseri, A., Chung, Y.-C., Grunwald, D., Zhang, S. & Pederson, T. (2018) CRISPR-Sirius: RNA scaffolds for signal amplification in genome imaging. *Nature Methods*. 15 (11), 928–931.

Ma, H., Tu, L.-C., Naseri, A., Huisman, M., Zhang, S., Grunwald, D. & Pederson, T. (2016) Multiplexed labeling of genomic loci with dCas9 and engineered sgRNAs using CRISPRainbow. *Nature Biotechnology*. 34 (5), 528–530.

Maass, P.G., Barutcu, A.R., Shechner, D.M., Weiner, C.L., Melé, M. & Rinn, J.L. (2018) Spatiotemporal allele organization by allele-specific CRISPR live-cell imaging (SNP-CLING). *Nature Structural & Molecular Biology*. 25 (2), 176–184.

Madgwick, S., Hansen, D. V, Levasseur, M., Jackson, P.K. & Jones, K.T. (2006) Mouse Emi2 is required to enter meiosis II by reestablishing cyclin B1 during interkinesis. *The Journal of cell biology*. 174 (6), 791–801.

Madgwick, S. & Jones, K.T. (2007) How eggs arrest at metaphase II: MPF stabilisation plus APC/C inhibition equals Cytostatic Factor. *Cell division*. 2 (1), 4.

Maguire, M.P. (1985) Evidence on the nature and complexity of the mechanism of chiasma maintenance in maize. *Genetical Research*. 45 (1), 37–49.

Maguire, M.P. (1974) The need for a chiasma binder. Journal of Theoretical Biology 48 (2) p.485–487.

Marangos, P. & Carroll, J. (2008) Securin regulates entry into M-phase by modulating the stability of cyclin B. *Nature Cell Biology*. 10 (4), 445–451.

Maresca, T.J. & Salmon, E.D. (2009) Intrakinetochore stretch is associated with changes in kinetochore phosphorylation and spindle assembly checkpoint activity. *Journal of Cell Biology*. 184 (3), 373–381.

Marr, D. & Hildreth, E. (1980) Theory of edge detection. *Proceedings of the Royal Society of London - Biological Sciences*. 207 (1167), 187–217.

Masui, Y. & Markert, C.L. (1971) Cytoplasmic control of nuclear behavior during meiotic maturation of frog oocytes. *Journal of Experimental Zoology*. 177 (2), 129–145.

Matos, J., Lipp, J.J., Bogdanova, A., Guillot, S., Okaz, E., Junqueira, M., Shevchenko, A. & Zachariae, W. (2008) Dbf4-Dependent Cdc7 Kinase Links DNA Replication to the Segregation of Homologous Chromosomes in Meiosis I. *Cell*. 135 (4), 662–678.

Matsuda, A., Schermelleh, L., Hirano, Y., Haraguchi, T. & Hiraoka, Y. (2018) Accurate and fiducial-marker-free correction for three-dimensional chromatic shift in biological fluorescence microscopy. *Scientific Reports*. 8 (1), 7583.

Mattiroli, F. & Sixma, T.K. (2014) Lysine-targeting specificity in ubiquitin and

ubiquitin-like modification pathways. *Nature Structural & Molecular Biology*. 21 (4), 308–316.

McGuinness, B.E., Anger, M., Kouznetsova, A., Gil-Bernabé, A.M., Helmhart, W., Kudo, N.R., Wuensche, A., Taylor, S., Hoog, C., Novak, B. & Nasmyth, K. (2009) Regulation of APC/C Activity in Oocytes by a Bub1-Dependent Spindle Assembly Checkpoint. *Current Biology*. 19 (5), 369–380.

McReynolds, T. & Blythe, D. (2005) 'Image Processing Techniques', in *Advanced Graphics Programming Using OpenGL*. [Online]. Elsevier. pp. 211–245.

Mehlmann, L.M. (2005) Stops and starts in mammalian oocytes: recent advances in understanding the regulation of meiotic arrest and oocyte maturation. *Reproduction*. 130 (6), 791–799.

Michaelis, C., Ciosk, R. & Nasmyth, K. (1997) Cohesins: Chromosomal Proteins that Prevent Premature Separation of Sister Chromatids. *Cell*. 91 (1), 35–45.

Miyagaki, Y., Kanemori, Y. & Baba, T. (2011) Possible involvement of mitogen- and stress-activated protein kinase 1, MSK1, in metaphase-II arrest through phosphorylation of EMI2 in mouse oocytes. *Developmental Biology*. 359 (1), 73–81.

Miyanari, Y., Ziegler-Birling, C. & Torres-Padilla, M.-E. (2013) Live visualization of chromatin dynamics with fluorescent TALEs. *Nature structural & molecular biology*. 20 (11), 1321–1324.

Mochida, S., Rata, S., Hino, H., Nagai, T. & Novák, B. (2016) Two Bistable Switches Govern M Phase Entry. *Current Biology*. 26 (24), 3361–3367.

Mogessie, B., Scheffler, K. & Schuh, M. (2018) *Assembly and Positioning of the Oocyte Meiotic Spindle*. 34 (1), 381–403.

Molecular Devices (2011) *MetaMorph*. [Online] [online]. Available from: https://www.moleculardevices.com/products/cellular-imaging-systems/acquisition-and-analysis-software/metamorph-microscopy#gref (Accessed 19 November 2019).

Moore, D. & Orr-Weaver, T. (1997) 'Chromosome Segregation during Meiosis: Building an Unambivalent Bivalent', in *Current Topics in Developmental Biology Volume 37*. [Online]. Elsevier. pp. 263–299.

Moreno-Mateos, M.A., Vejnar, C.E., Beaudoin, J.-D., Fernandez, J.P., Mis, E.K., Khokha, M.K. & Giraldez, A.J. (2015) CRISPRscan: designing highly efficient sgRNAs for CRISPR-Cas9 targeting in vivo. *Nature Methods*. 12 (10), 982–988.

Moroi, Y., Peebles, C., Fritzler, M.J., Steigerwald, J. & Tant, E.M. (1980) Autoantibody to centromere (kinetochore) in scleroderma sera. Medical Sciences 77 (3).

Moshkin, Y.M., Doyen, C.M., Kan, T.-W., Chalkley, G.E., Sap, K., Bezstarosti, K., Demmers, J.A., Ozgur, Z., van Ijcken, W.F.J. & Verrijzer, C.P. (2013) Histone Chaperone NAP1 Mediates Sister Chromatid Resolution by Counteracting Protein Phosphatase 2A Beth A Sullivan (ed.). *PLoS Genetics*. 9 (9), e1003719.

Müller, H., Moroni, M.C., Vigo, E., Petersen, B.O., Bartek, J. & Helin, K. (1997) Induction of S-phase entry by E2F transcription factors depends on their nuclear localization. *Molecular and Cellular Biology*. 17 (9), 5508–5520.

Munkres, J. (1957) Algorithms for the Assignment and Transportation Problems. *Journal of the Society for Industrial and Applied Mathematics*. 5 (1), 32–38.

Musacchio, A. (2015a) Closing the Mad2 cycle. *eLife*. 4 (May), 1–3.

Musacchio, A. (2015b) The Molecular Biology of Spindle Assembly Checkpoint Signaling Dynamics. *Current Biology*. 25 (20), R1002–R1018.

Musacchio, A. & Desai, A. (2017) A Molecular View of Kinetochore Assembly and Function. *Biology*. 6 (1), 5.

Musacchio, A. & Salmon, E.D. (2007) The spindle-assembly checkpoint in space and time. *Nature reviews. Molecular cell biology*. 8 (5), 379–393.

Nabti, I., Grimes, R., Sarna, H., Marangos, P. & Carroll, J. (2017) Maternal age-dependent APC/C-mediated decrease in securin causes premature sister chromatid separation in meiosis II. *Nature Communications*. 8 (1), 15346.

Nabti, I., Reis, A., Levasseur, M., Stemmann, O. & Jones, K.T. (2008) Securin and not CDK1/cyclin B1 regulates sister chromatid disjunction during meiosis II in mouse eggs. *Developmental Biology*. 321 (2), 379–386.

Nagaoka, S.I., Hassold, T.J. & Hunt, P.A. (2012) Human aneuploidy: mechanisms and new insights into an age-old problem. *Nature reviews. Genetics*. 13 (7), 493–504.

Nakagawa, K., Yamano, S., Moride, N., Yamashita, M., Yoshizawa, M. & Aono, T. (2001) Effect of activation with Ca ionophore A23187 and puromycin on the development of human oocytes that failed to fertilize after intracytoplasmic sperm injection. *Fertility and Sterility*. 76 (1), 148–152.

Nakagawa, S. & FitzHarris, G. (2017) Intrinsically Defective Microtubule Dynamics Contribute to Age-Related Chromosome Segregation Errors in Mouse Oocyte Meiosis-I. *Current Biology*. 27 (7), 1040–1047.

Namgoong, S. & Kim, N.-H. (2018) Meiotic spindle formation in mammalian oocytes: implications for human infertility†. *Biology of Reproduction*. 98 (2), 153–161.

Nasmyth, K. (2015) A meiotic mystery: How sister kinetochores avoid being pulled in opposite directions during the first division. *BioEssays*. 37 (6), 657–665.

Nielsen, C.F., Huttner, D., Bizard, A.H., Hirano, S., Li, T.N., Palmai-Pallag, T., Bjerregaard, V.A., Liu, Y., Nigg, E.A., Wang, L.H.C. & Hickson, I.D. (2015) PICH promotes sister chromatid disjunction and co-operates with topoisomerase II in mitosis. *Nature Communications*. 6.

Nigg, E.A. (2001) Mitotic kinases as regulators of cell division and its checkpoints. *Nature Reviews Molecular Cell Biology*. 2 (1), 21–32.

Nikon Instruments Inc. (2013) *NIS-Elements*. [Online] [online]. Available from:

https://www.microscope.healthcare.nikon.com/products/software/nis-elements (Accessed 19 November 2019).

Nishiyama, T., Ladurner, R., Schmitz, J., Kreidl, E., Schleiffer, A., Bhaskara, V., Bando, M., Shirahige, K., Hyman, A.A., Mechtler, K. & Peters, J.-M. (2010) Sororin mediates sister chromatid cohesion by antagonizing Wapl. *Cell*. 143 (5), 737–749.

Nurse, P. & Thuriaux, P. (1980) Regulatory genes controlling mitosis in the fission yeast Schizosaccharomyces pombe. *Genetics*. 96 (3), 627–37.

Obara, B., Byun, J., Fedorov, D. & Manjunath, B.S. (2007) *Automatic Nuclei Detection and Dataflow in Bisquik System*.

Obeso, I., Rosales, J., García, G., Santos, R.M.D., Galache, P.M.D. & Patrizio, P. (2010) Optimal time for ICSI after hCG administration and oocyte incubation period. *Fertility and Sterility*. 94 (4), S253.

Ohe, M., Kawamura, Y., Ueno, H., Inoue, D., Kanemori, Y., Senoo, C., Isoda, M., Nakajo, N. & Sagata, N. (2010) Emi2 inhibition of the anaphase-promoting complex/cyclosome absolutely requires Emi2 binding via the C-terminal RL tail. *Molecular Biology of the Cell*. 21 (6), 905–913.

Oliver, T.R., Feingold, E., Yu, K., Cheung, V., Tinker, S., Yadav-Shah, M., Masse, N. & Sherman, S.L. (2008) New Insights into Human Nondisjunction of Chromosome 21 in Oocytes R. Scott Hawley (ed.). *PLoS Genetics*. 4 (3), e1000033.

Oliver, T.R., Tinker, S.W., Allen, E.G., Hollis, N., Locke, A.E., Bean, L.J.H., Chowdhury, R., Begum, F., Marazita, M., Cheung, V., Feingold, E. & Sherman, S.L. (2012) Altered patterns of multiple recombinant events are associated with nondisjunction of chromosome 21. *Human genetics*. 131 (7), 1039–1046.

Ollion, J., Cochennec, J., Loll, F., Escudé, C. & Boudier, T. (2013) TANGO: A generic tool for high-throughput 3D image analysis for studying nuclear organization. *Bioinformatics*. 29 (14), 1840–1841.

Orr, B. & Maiato, H. (2019) No chromosome left behind: The importance of metaphase alignment for mitotic fidelity. *Journal of Cell Biology*. 218 (4), 1086–1088.

Orth, M., Mayer, B., Rehm, K., Rothweiler, U., Heidmann, D., Holak, T.A., Stemmann, O., Aravind, L., Koonin, E. V, Brar, G.A., Kiburz, B.M., Zhang, Y., Kim, J.E., White, F., Amon, A., Chen, R.H., Brady, D.M., Smith, D., Murray, A.W., et al. (2011) Shugoshin is a Mad1/Cdc20-like interactor of Mad2. *The EMBO journal*. 30 (14), 2868–2880.

Ottolini, C.S., Newnham, L.J., Capalbo, A., Natesan, S.A., Joshi, H.A., Cimadomo, D., Griffin, D.K., Sage, K., Summers, M.C., Thornhill, A.R., Housworth, E., Herbert, A.D., Rienzi, L., Ubaldi, F.M., Handyside, A.H. & Hoffmann, E.R. (2015) Genome-wide maps of recombination and chromosome segregation in human oocytes and embryos show selection for maternal recombination rates. *Nature Genetics*. 47 (7), 727–735.

Pachis, S.T. & Kops, G.J.P.L. (2018) Leader of the SAC: molecular mechanisms of Mps1/TTK regulation in mitosis. *Open biology*. 8 (8), 180109.

Page, S.L. & Hawley, R.S. (2004) The Genetics and Molecular Biology of the Synaptonemal Complex. *Annual Review of Cell and Developmental Biology*. 20 (1), 525–558.

Patel, J., Tan, S.L., Hartshorne, G.M., McAinsh, A.D., Chan, G.K., Liu, S.-T., Yen, T.J., Chiang, T., Duncan, F.E., Schindler, K., Schultz, R.M., Lampson, M.A., Corbett, K.D., Yip, C.K., Ee, L.-S., Walz, T., Amon, A., Harrison, S.C., Duncan, F.E., et al. (2015) Unique geometry of sister kinetochores in human oocytes during meiosis I may explain maternal age-associated increases in chromosomal abnormalities. *Biology open*. 5 (2), 178–184.

Peters, J.-M. (2006) The anaphase promoting complex/cyclosome: a machine designed to destroy. *Nature Reviews Molecular Cell Biology*. 7 (9), 644–656.

Peters, J.-M. & Nishiyama, T. (2012) Sister Chromatid Cohesion. *Cold Spring Harbor Perspectives in Biology*. 4 (11), a011130–a011130.

Petronczki, M., Matos, J., Mori, S., Gregan, J., Bogdanova, A., Schwickart, M., Mechtler, K., Shirahige, K., Zachariae, W. & Nasmyth, K. (2006) Monopolar attachment of sister kinetochores at meiosis I requires casein kinase 1. *Cell*. 126 (6), 1049–1064.

Petronczki, M., Siomos, M.F. & Nasmyth, K. (2003) Un Ménage à Quatre. *Cell*. 112 (4), 423–440.

Petry, S. (2016) Mechanisms of Mitotic Spindle Assembly. *Annual Review of Biochemistry*. 85 (1), 659–683.

Pietzsch, T., Preibisch, S., Tomančák, P. & Saalfeld, S. (2012) Imglib2-generic image processing in Java. *Bioinformatics*. 28 (22), 3009–3011.

Politi, A.Z., Cai, Y., Walther, N., Hossain, M.J., Koch, B., Wachsmuth, M. & Ellenberg, J. (2018) Quantitative mapping of fluorescently tagged cellular proteins using FCS-calibrated four-dimensional imaging. *Nature Protocols*. 13 (6), 1445–1464.

ProViz & Davey Lab (2019a) *SET - Set - Q9EQU5*. [Online] [online]. Available from: http://proviz.ucd.ie/proviz.php?uniprot_acc=Q9EQU5&tools=pp2a (Accessed 19 November 2019).

ProViz & Davey Lab (2019b) *Shugoshin 2 - Sgo2 - Q7TSY8*. [Online] [online]. Available from: http://proviz.ucd.ie/proviz.php?uniprot_acc=Q7TSY8&tools=degradation (Accessed 25 November 2019).

Qi, S.-T., Wang, Z.-B., Huang, L., Liang, L.-F., Xian, Y.-X., Ouyang, Y.-C., Hou, Y., Sun, Q.-Y. & Wang, W.-H. (2015) Casein kinase 1 (α, δ and ε) localize at the spindle poles, but may not be essential for mammalian oocyte meiotic progression. *Cell Cycle*. 14 (11), 1675–1685.

Qi, S.-T., Wang, Z.-B., Ouyang, Y.-C., Zhang, Q.-H., Hu, M.-W., Huang, X., Ge, Z., Guo, L., Wang, Y.-P., Hou, Y., Schatten, H. & Sun, Q.-Y. (2013) Overexpression

of SETβ, a protein localizing to centromeres, causes precocious separation of chromatids during the first meiosis of mouse oocytes. *Journal of Cell Science*. 126 (7), 1595–1603.

Qu, Q., Zhang, Q., Yang, L., Chen, Y. & Liu, H. (2019) SET binding to Sgo1 inhibits Sgo1–cohesin interactions and promotes chromosome segregation. *The Journal of Cell Biology*. 218 (8), 2514–2528.

Rabut, G. & Ellenberg, J. (2004) Automatic real-time three-dimensional cell tracking by fluorescence microscopy. *Journal of microscopy*. 216 (Pt 2), 131–7.

Ramanathan, A., Robb, G.B. & Chan, S.H. (2016) mRNA capping: Biological functions and applications. *Nucleic Acids Research*. 44 (16), 7511–7526.

Rattani, A., Ballesteros Mejia, R., Roberts, K., Roig, M.B., Godwin, J., Hopkins, M., Eguren, M., Sanchez-Pulido, L., Okaz, E., Ogushi, S., Wolna, M., Metson, J., Pendás, A.M., Malumbres, M., Novák, B., Herbert, M. & Nasmyth, K. (2017) APC/C Cdh1 Enables Removal of Shugoshin-2 from the Arms of Bivalent Chromosomes by Moderating Cyclin-Dependent Kinase Activity. *Current Biology*. 1462–1476.

Rattani, A., Wolna, M., Ploquin, M., Helmhart, W., Morrone, S., Mayer, B., Godwin, J., Xu, W., Stemmann, O., Pendas, A. & Nasmyth, K. (2013) Sgol2 provides a regulatory platform that coordinates essential cell cycle processes during meiosis I in oocytes. *eLife*. 2e01133.

Ray, M., Tang, R., Jiang, Z. & Rotello, V.M. (2015) Quantitative Tracking of Protein Trafficking to the Nucleus Using Cytosolic Protein Delivery by Nanoparticle-Stabilized Nanocapsules. *Bioconjugate Chemistry*. 26 (6), 1004–1007.

Ren, R., Deng, L., Xue, Y., Suzuki, K., Zhang, Weiqi, Yu, Y., Wu, J., Sun, L., Gong, X., Luan, H., Yang, F., Ju, Z., Ren, X., Wang, S., Tang, H., Geng, L., Zhang, Weizhou, Li, J., Qiao, J., et al. (2017) Visualization of aging-associated chromatin alterations with an engineered TALE system. *Cell Research*. 27 (4), 483–504.

Richards, J.S. & Pangas, S.A. (2010) The ovary: basic biology and clinical implications. *Journal of Clinical Investigation*. 120 (4), 963–972.

Riedel, C.G., Katis, V.L., Katou, Y., Mori, S., Itoh, T., Helmhart, W., Gálová, M., Petronczki, M., Gregan, J., Cetin, B., Mudrak, I., Ogris, E., Mechtler, K., Pelletier, L., Buchholz, F., Shirahige, K. & Nasmyth, K. (2006) Protein phosphatase 2A protects centromeric sister chromatid cohesion during meiosis I. *Nature*. 441 (7089), 53–61.

Rieder, C.L., Schultz, A., Cole, R. & Sluder, G. (1994) Anaphase onset in vertebrate somatic cells is controlled by a checkpoint that monitors sister kinetochore attachment to the spindle. *Journal of Cell Biology*. 127 (5), 1301–1310.

Rietdorf, J. & Stelzer, E.H.K. (2006) 'Special optical elements', in *Handbook of Biological Confocal Microscopy: Third Edition*. [Online]. Springer US. pp. 43–58.

Rottenfusser, R., Wilson, E.E., Davidson, M.W. & Carl Zeiss Microscopy GmbH (2006)

Numerical Aperture and Resolution. [Online] [online]. Available from: https://www.zeiss.com/microscopy/int/solutions/reference/basic-microscopy/numerical-aperture-and-resolution.html (Accessed 22 November 2019).

Sakakibara, Y., Hashimoto, S., Nakaoka, Y., Kouznetsova, A., Höög, C. & Kitajima, T.S. (2015) Bivalent separation into univalents precedes age-related meiosis I errors in oocytes. *Nature Communications*. 6 (1), 7550.

Santaguida, S., Tighe, A., D'Alise, A.M., Taylor, S.S. & Musacchio, A. (2010) Dissecting the role of MPS1 in chromosome biorientation and the spindle checkpoint through the small molecule inhibitor reversine. *The Journal of cell biology*. 190 (1), 73–87.

Sarvaiya, J.N., Patnaik, S. & Bombaywala, S. (2009) 'Image registration by template matching using normalized cross-correlation', in *ACT 2009 - International Conference on Advances in Computing, Control and Telecommunication Technologies*. [Online]. 2009 pp. 819–822.

Savva, G.M., Walker, K. & Morris, J.K. (2010) The maternal age-specific live birth prevalence of trisomies 13 and 18 compared to trisomy 21 (Down syndrome). *Prenatal diagnosis*. 30 (1), 57–64.

Schermelleh, L., Heintzmann, R. & Leonhardt, H. (2010) A guide to super-resolution fluorescence microscopy. *The Journal of Cell Biology*. 190 (2), 165–175.

Schindelin, J., Arganda-Carreras, I., Frise, E., Kaynig, V., Longair, M., Pietzsch, T., Preibisch, S., Rueden, C., Saalfeld, S., Schmid, B., Tinevez, J.-Y., White, D.J., Hartenstein, V., Eliceiri, K., Tomancak, P. & Cardona, A. (2012) Fiji: an open-source platform for biological-image analysis. *Nature Methods*. 9 (7), 676–682.

Schuh, M. & Ellenberg, J. (2007) Self-organization of MTOCs replaces centrosome function during acentrosomal spindle assembly in live mouse oocytes. *Cell*. 130 (3), 484–498.

Schultz, R.M., Montgomery, R.R. & Belanoff, J.R. (1983) Regulation of mouse oocyte meiotic maturation: Implication of a decrease in oocyte cAMP and protein dephosphorylation in commitment to resume meiosis. *Developmental Biology*. 97 (2), 264–273.

Schwab, M., Lutum, A.S. & Seufert, W. (1997) Yeast Hct1 is a regulator of Cib2 cyclin proteolysis. *Cell*. 90 (4), 683–693.

Shaner, N.C., Lambert, G.G., Chammas, A., Ni, Y., Cranfill, P.J., Baird, M.A., Sell, B.R., Allen, J.R., Day, R.N., Israelsson, M., Davidson, M.W. & Wang, J. (2013) A bright monomeric green fluorescent protein derived from Branchiostoma lanceolatum. *Nature methods*. 10 (5), 407–409.

Shcherbakova, D.M., Baloban, M., Emelyanov, A. V., Brenowitz, M., Guo, P. & Verkhusha, V. V. (2016) Bright monomeric near-infrared fluorescent proteins as tags and biosensors for multiscale imaging. *Nature Communications*. 7 (1), 12405.

Shen, B., Zhang, W., Zhang, J., Zhou, J., Wang, J., Chen, L., Wang, L., Hodgkins, A., Iyer, V., Huang, X. & Skarnes, W.C. (2014) Efficient genome modification by CRISPR-Cas9 nickase with minimal off-target effects. *Nature methods*. 11 (4), 399–402.

Sherwood, R., Takahashi, T.S. & Jallepalli, P. V (2010) Sister acts: coordinating DNA replication and cohesion establishment. *Genes & development*. 24 (24), 2723–2731.

Shoji, S., Muto, Y., Ikeda, M., He, F., Tsuda, K., Ohsawa, N., Akasaka, R., Terada, T., Wakiyama, M., Shirouzu, M. & Yokoyama, S. (2014) The zinc-binding region (ZBR) fragment of Emi2 can inhibit APC/C by targeting its association with the coactivator Cdc20 and UBE2C-mediated ubiquitylation. *FEBS Open Bio*. 4 (1), 689–703.

Shoji, S., Yoshida, N., Amanai, M., Ohgishi, M., Fukui, T., Fujimoto, S., Nakano, Y., Kajikawa, E. & Perry, A.C.F. (2006) Mammalian Emi2 mediates cytostatic arrest and transduces the signal for meiotic exit via Cdc20. *EMBO Journal*. 25 (4), 834–845.

Sirlin, J.L. & Edwards, R.G. (1959) Timing of DNA synthesis in ovarian oocyte nuclei and pronuclei of the mouse. *Experimental Cell Research*. 18 (1), 190–194.

Sironi, L., Melixetian, M., Faretta, M., Prosperini, E., Helin, K. & Musacchio, A. (2001) Mad2 binding to Mad1 and Cdc20, rather than oligomerization, is required for the spindle checkpoint. *EMBO Journal*. 20 (22), 6371–6382.

Skibbens, R. V, Corson, L.B., Koshland, D. & Hieter, P. (1999) Ctf7p is essential for sister chromatid cohesion and links mitotic chromosome structure to the DNA replication machinery. *Genes & development*. 13 (3), 307–19.

Slupe, A.M., Merrill, R.A. & Strack, S. (2011) Determinants for Substrate Specificity of Protein Phosphatase 2A. *Enzyme Research*. 2011 (C), 1–8.

Smith, L.D. & Ecker, R.E. (1971) The interaction of steroids with Rana pipiens oocytes in the induction of maturation. *Developmental Biology*. 25 (2), 232–247.

Song, J.L. & Wessel, G.M. (2005) How to make an egg: transcriptional regulation in oocytes. *Differentiation; research in biological diversity*. 73 (1), 1–17.

Sonoda, E., Matsusaka, T., Morrison, C., Vagnarelli, P., Hoshi, O., Ushiki, T., Nojima, K., Fukagawa, T., Waizenegger, I.C., Peters, J.M., Earnshaw, W.C. & Takeda, S. (2001) Scc1/Rad21/Mcd1 Is Required for Sister Chromatid Cohesion and Kinetochore Function in Vertebrate Cells. *Developmental Cell*. 1 (6), 759–770.

Spring, K.R., Russ, J.C., Parry-Hil, M.J., Fellers, T.J. & Davidson, M.W. (2016) *Difference of Gaussians Edge Enhancement*. [Online] [online]. Available from: https://micro.magnet.fsu.edu/primer/java/digitalimaging/processing/diffgaussians/index.html (Accessed 24 November 2019).

Stanyte, R., Nuebler, J., Blaukopf, C., Hoefler, R., Stocsits, R., Peters, J.-M. & Gerlich, D.W. (2018) Dynamics of sister chromatid resolution during cell cycle progression. *The Journal of Cell Biology*. 217 (6), 1985–2004.

Stearns, T. (2001) Centrosome duplication. a centriolar pas de deux. *Cell*. 105 (4), 417–420.

Stemmann, O., Zou, H., Gerber, S.A., Gygi, S.P. & Kirschner, M.W. (2001) Dual Inhibition of Sister Chromatid Separation at Metaphase. *Cell*. 107 (6), 715–726.

von Stetina, J.R. & Orr-Weaver, T.L. (2011) Developmental control of oocyte maturation and egg activation in metazoan models. *Cold Spring Harbor Perspectives in Biology*. 3 (10), 1–19.

Stevens, D., Gassmann, R., Oegema, K. & Desai, A. (2011) Uncoordinated Loss of Chromatid Cohesion Is a Common Outcome of Extended Metaphase Arrest Daniela Cimini (ed.). *PLoS ONE*. 6 (8), e22969.

Strang, G. (2016) *Introduction to Linear Algebra*. Wellesley-Cambridge Press.

Sudakin, V., Ganoth, D., Dahan, A., Heller, H., Hershko, J., Luca, F.C., Ruderman, J. V. & Hershko, A. (1995) The cyclosome, a large complex containing cyclin-selective ubiquitin ligase activity, targets cyclins for destruction at the end of mitosis. *Molecular Biology of the Cell*. 6 (2), 185–198.

Susiarjo, M., Rubio, C. & Hunt, P. (2009) Analyzing mammalian female meiosis. *Methods in molecular biology (Clifton, N.J.)*. 558339–354.

Suzuki, T., Suzuki, E., Yoshida, N., Kubo, A., Li, H., Okuda, E., Amanai, M. & Perry, A.C.F. (2010) Mouse Emi2 as a distinctive regulatory hub in second meiotic metaphase. *Development*. 137 (19), 3281–3291.

Swain, J.E. (2012) Is there an optimal pH for culture media used in clinical IVF? *Human Reproduction Update*. 18 (3), 333–339.

Swain, J.E. (2010) Optimizing the culture environment in the IVF laboratory: impact of pH and buffer capacity on gamete and embryo quality. *Reproductive BioMedicine Online*. 21 (1), 6–16.

Terret, M.E., Wassmann, K., Waizenegger, I., Maro, B., Peters, J.-M. & Verlhac, M.-H. (2003) The Meiosis I-to-Meiosis II Transition in Mouse Oocytes Requires Separase Activity. *Current Biology*. 13 (20), 1797–1802.

Teusel, F., Henschke, L. & Mayer, T.U. (2018) 'Small molecule tools in mitosis research', in *Methods in Cell BiologyTeusel, Franziska Henschke, Lars Mayer, Thomas U.* 1st edition [Online]. Elsevier Inc. pp. 137–155.

Thevenaz, P., Ruttimann, U.E. & Unser, M. (1998) A pyramid approach to subpixel registration based on intensity. *IEEE Transactions on Image Processing*. 7 (1), 27–41.

Thompson, S.L. & Compton, D.A. (2011) Chromosome missegregation in human cells arises through specific types of kinetochore-microtubule attachment errors. *Proceedings of the National Academy of Sciences of the United States of America*. 108 (44), 17974–17978.

Thompson, S.L. & Compton, D.A. (2008) Examining the link between chromosomal instability and aneuploidy in human cells. *Journal of Cell Biology*. 180 (4), 665–

672.

Thornton, B.R. & Toczyski, D.P. (2003) Securin and B-cyclin/CDK are the only essential targets of the APC. *Nature Cell Biology*. 5 (12), 1090–1094.

Tibshirani, R., Walther, G. & Hastie, T. (2001) Estimating the number of clusters in a data set via the gap statistic. *Journal of the Royal Statistical Society: Series B (Statistical Methodology)*. 63 (2), 411–423.

Tinevez, J.Y., Perry, N., Schindelin, J., Hoopes, G.M., Reynolds, G.D., Laplantine, E., Bednarek, S.Y., Shorte, S.L. & Eliceiri, K.W. (2017) TrackMate: An open and extensible platform for single-particle tracking. *Methods*. 11580–90.

Tsutsumi, M., Fujiwara, R., Nishizawa, H., Ito, M., Kogo, H., Inagaki, H., Ohye, T., Kato, T., Fujii, T. & Kurahashi, H. (2014) Age-related decrease of meiotic cohesins in human oocytes. Qinghua Shi (ed.). *PloS one*. 9 (5), e96710.

Tukey, J.W. (1977) *Exploratory Data Analysis*. Addison-Wesley series in behavioral science. Addison-Wesley Publishing Company.

Tunquist, B.J. (2003) Under arrest: cytostatic factor (CSF)-mediated metaphase arrest in vertebrate eggs. *Genes & Development*. 17 (6), 683–710.

Uhlmann, F. (2011) Cohesin subunit Rad21L, the new kid on the block has new ideas. *EMBO Reports*. 12 (3), 183–184.

Uhlmann, F. & Nasmyth, K. (1998) Cohesion between sister chromatids must be established during DNA replication. *Current Biology*. 8 (20), 1095–1102.

Uhlmann, F., Wernic, D., Poupart, M.-A.A., Koonin, E. V. & Nasmyth, K. (2000) Cleavage of Cohesin by the CD Clan Protease Separin Triggers Anaphase in Yeast. *Cell*. 103 (3), 375–386.

Virtanen, P., Gommers, R., Oliphant, T.E., Haberland, M., Reddy, T., Cournapeau, D., Burovski, E., Peterson, P., Weckesser, W., Bright, J., van der Walt, S.J., Brett, M., Wilson, J., Millman, K.J., Mayorov, N., Nelson, A.R.J., Jones, E., Kern, R., Larson, E., et al. (2019) *SciPy 1.0--Fundamental Algorithms for Scientific Computing in Python*.

Vitrolife Sweden AB (2017) *Vitrolife G-Series™ 2 Manual 9.0*.

Vladimirou, E., Mchedlishvili, N., Gasic, I., Armond, J.W., Samora, C.P., Meraldi, P. & McAinsh, A.D. (2013) Nonautonomous Movement of Chromosomes in Mitosis. *Developmental Cell*. 27 (1), 60–71.

Volarcik, K., Sheean, L., Goldfarb, J., Woods, L., Abdul-Karim, F.W. & Hunt, P. (1998) The meiotic competence of in-vitro matured human oocytes is influenced by donor age: Evidence that folliculogenesis is compromised in the reproductively aged ovary. *Human Reproduction*. 13 (1), 154–160.

Wagner, R. & Barry, M. (1836) Some Remarks and Inquiries Concerning the Germinal Vesicle (Vesicula Germinativa.). *Edinburgh medical and surgical journal*. 45 (127), 423–426.

Wallace, W.H.B. & Kelsey, T.W. (2010) Human Ovarian Reserve from Conception to the Menopause Virginia J. Vitzthum (ed.). *PLoS ONE*. 5 (1), e8772.

Van Der Walt, S., Colbert, S.C. & Varoquaux, G. (2011) The NumPy array: A structure for efficient numerical computation. *Computing in Science and Engineering*. 13 (2), 22–30.

van der Walt, S., Schönberger, J.L., Nunez-Iglesias, J., Boulogne, F., Warner, J.D., Yager, N., Gouillart, E. & Yu, T. (2014) scikit-image: image processing in Python. *PeerJ*. 2 (1), e453.

Wang, H., Nakamura, M., Abbott, T.R., Zhao, D., Luo, K., Yu, C., Nguyen, C.M., Lo, A., Daley, T.P., La Russa, M., Liu, Y. & Qi, L.S. (2019) CRISPR-mediated live imaging of genome editing and transcription. *Science*. 365 (6459), 1301–1305.

Wang, L.H.C., Schwarzbraun, T., Speicher, M.R. & Nigg, E.A. (2008) Persistence of DNA threads in human anaphase cells suggests late completion of sister chromatid decatenation. *Chromosoma*. 117 (2), 123–135.

Wang, S., Zickler, D., Kleckner, N. & Zhang, L. (2015) Meiotic crossover patterns: Obligatory crossover, interference and homeostasis in a single process. *Cell Cycle*. 14 (3), 305–314.

Watanabe, Y., Yokobayashi, S., Yamamoto, M. & Nurse, P. (2001) Pre-meiotic S phase is linked to reductional chromosome segregation and recombination. *Nature*. 409 (6818), 359–363.

Waye, J.S. & Willard, H.F. (1989) Human ß satellite DNA: Genomic organization and sequence definition of a class of highly repetitive tandem DNA. *Proceedings of the National Academy of Sciences of the United States of America*. 86 (16), 6250–6254.

Webster, A. & Schuh, M. (2017) Mechanisms of Aneuploidy in Human Eggs. *Trends in Cell Biology*. 27 (1), 55–68.

Wel, C. van der (2015) *pims_nd2 : A reader for Nikon .ND2*. [Online] [online]. Available from: https://github.com/soft-matter/pims_nd2 (Accessed 19 November 2019).

Williams, C.J. & Erickson, G.F. (2000) *Morphology and Physiology of the Ovary*.

Wu, C.-G., Chen, H., Guo, F., Yadav, V.K., Mcilwain, S.J., Rowse, M., Choudhary, A., Lin, Z., Li, Y., Gu, T., Zheng, A., Xu, Q., Lee, W., Resch, E., Johnson, B., Day, J., Ge, Y., Ong, I.M., Burkard, M.E., et al. (2017) PP2A-B′ holoenzyme substrate recognition, regulation and role in cytokinesis. *Cell Discovery*. 317027.

Wu, J., Corbett, A.H. & Berland, K.M. (2009) The intracellular mobility of nuclear import receptors and NLS cargoes. *Biophysical journal*. 96 (9), 3840–3849.

Wu, J.Q., Hansen, D. V., Guo, Y., Wang, M.Z., Tang, W., Freel, C.D., Tung, J.J., Jackson, P.K. & Kornbluth, S. (2007) Control of Emi2 activity and stability through Mos-mediated recruitment of PP2A. *Proceedings of the National Academy of Sciences of the United States of America*. 104 (42), 16564–16569.

Xie, C., Chen, Y.-L., Wang, D.-F., Wang, Y.-L., Zhang, T.-P., Li, H., Liang, F., Zhao, Y. & Zhang, G.-Y. (2017) SgRNA Expression of CRIPSR-Cas9 System Based on MiRNA Polycistrons as a Versatile Tool to Manipulate Multiple and Tissue-Specific Genome Editing. *Scientific Reports*. 7 (1), 5795.

Xu, Z., Abbott, A., Kopf, G.S., Schultz, R.M. & Ducibella, T. (1997) Spontaneous Activation of Ovulated Mouse Eggs: Time-dependent Effects on M-phase Exit, Cortical Granule Exocytosis, Maternal Messenger Ribonucleic Acid Recruitment, and Inositol 1,4,5-trisphosphate Sensitivity1. *Biology of Reproduction*. 57 (4), 743–750.

Xu, Z., Cetin, B., Anger, M., Cho, U.S., Helmhart, W., Nasmyth, K. & Xu, W. (2009) Structure and function of the PP2A-shugoshin interaction. *Molecular cell*. 35 (4), 426–441.

Yaakov, G., Thorn, K. & Morgan, D.O. (2012) Separase biosensor reveals that cohesin cleavage timing depends on phosphatase PP2A(Cdc55) regulation. *Developmental cell*. 23 (1), 124–136.

El Yakoubi, W., Buffin, E., Cladière, D., Gryaznova, Y., Berenguer, I., Touati, S.A., Gómez, R., Suja, J.A., van Deursen, J.M. & Wassmann, K. (2017) Mps1 kinase-dependent Sgo2 centromere localisation mediates cohesin protection in mouse oocyte meiosis I. *Nature Communications*. 8 (1), 694.

Yamano, H., Gannon, J., Mahbubani, H. & Hunt, T. (2004) Cell Cycle-Regulated Recognition of the Destruction Box of Cyclin B by the APC/C in Xenopus Egg Extracts. *Molecular Cell*. 13 (1), 137–147.

Yaniv, Z., Lowekamp, B.C., Johnson, H.J. & Beare, R. (2018) SimpleITK Image-Analysis Notebooks: a Collaborative Environment for Education and Reproducible Research. *Journal of Digital Imaging*. 31 (3), 290–303.

Yoshida, N. & Perry, A.C. (2007) Piezo-actuated mouse intracytoplasmic sperm injection (ICSI). *Nat Protoc*. 2 (2), 296–304.

Yun, Y., Lane, S.I.R. & Jones, K.T. (2014) Premature dyad separation in meiosis II is the major segregation error with maternal age in mouse oocytes. *Development*. 141 (1), 199–208.

Zielinska, A.P., Holubcova, Z., Blayney, M., Elder, K. & Schuh, M. (2015) Sister kinetochore splitting and precocious disintegration of bivalents could explain the maternal age effect. *eLife*. 4e11389.

Zielinska, A.P. & Schuh, M. (2018) 'A microscopy-based approach for studying meiosis in live and fixed human oocytes', in *Methods in Cell Biology*. 1st edition [Online]. Elsevier Inc. pp. 315–333.

Zur, A. & Brandeis, M. (2001) Securin degradation is mediated by fzy and fzr, and is required for complete chromatid separation but not for cytokinesis. *EMBO Journal*. 20 (4), 792–801.

Appendix A: List of Papers Published and Manuscripts in Preparation

- A manuscript is being prepared related to Chapter 4, a collaboration with Wolfgang Zachariae's group.
- Hyslop, L.A., Blakeley, P., Craven, L., Richardson, J., Fogarty, N.M.E., Fragouli, E., **Lamb, M.**, Wamaitha, S.E., Prathalingam, N., Zhang, Q., O'Keefe, H., Takeda, Y., Arizzi, L., Alfarawati, S., Tuppen, H.A., Irving, L., Kalleas, D., Choudhary, M., Wells, D., et al. (2016) Towards clinical application of pronuclear transfer to prevent mitochondrial DNA disease. *Nature*. 534 (7607), 383–386.
- Herbert, M., Kalleas, D., Cooney, D., **Lamb, M.** & Lister, L. (2015) Meiosis and Maternal Aging: Insights from Aneuploid Oocytes and Trisomy Births. *Cold Spring Harbor Perspectives in Biology*. 7 (4), a017970.

Appendix B: Repository for *SpotCollectionManager*

SpotCollectionManager is a FIJI macro and runs with minimal dependencies and therefore should work on a vanilla FIJI download (available at fiji.sc), as long as the TrackMate plugin has been installed (installation instructions can be found at imagej.net/TrackMate). Code for *SpotCollectionManager* can be found here:

- https://gist.github.com/mahdilamb/c5ca38fa31756d0b6bc538e575bf8e12 (SpotCollectionManager)
- https://gist.github.com/mahdilamb/64b1996f88333f23dee2e010b113f1a1 (HelperFunctions)